The Impact of Distinct Bone Morphogenetic Proteins on Self-Renewal and Differentiation of Human Embryonic and Induced Pluripotent Stem Cells

DISSERTATION

Submitted in fulfillment of the requirements
for the award of the degree of

Doctor of Science (Dr. rer. nat.)

to the
Department of Biology, Chemistry and Pharmacy
of the Freie Universität Berlin

by

Björn Lichtner

Germany

2014

The research work for this dissertation was performed from January 2010 to September 2013 under the supervision of Prof. Dr. James Adjaye at the Max-Planck-Institute for Molecular Genetics in Berlin, Germany. The dissertation was submitted in May 2014 to the Department of Biology, Chemistry and Pharmacy and in December 2015 to the library of the Freie Universität Berlin, Germany.

1st Reviewer: Prof. Dr. Hans Lehrach
                 Max-Planck-Institute for Molecular Genetics

2nd Reviewer: Prof. Dr. Petra Knaus
                 Freie Universität Berlin

Date of disputation: 8th December 2014

Meinen Großeltern Irma und Matthias Lichtner

Acknowledgements

Firstly, I would like to express my deep gratitude to Prof. Dr. James Adjaye for accepting me as a PhD student into his "Molecular Embryology and Aging" group at the Max-Planck-Institute for Molecular Genetics (MPIMG) in Berlin. He made it possible for me to perform research in this exciting area of human pluripotent stem cells. I am very grateful to him for his excellent supervision, advice, constant support and encouragement over the last few years.

I am very grateful to Prof. Dr. Hans Lehrach from the MPIMG for being the first reviewer of my dissertation. Thanks to his support and approval it was possible for me to conduct my PhD work at this institute.

The annual scientific mentoring committee meetings with Prof. Dr. Petra Knaus as part of the doctoral program of the Berlin-Brandenburg School for Regenerative Therapies (BSRT) are greatly appreciated. I am also very grateful to her for being the second supervisor of my dissertation as a representative of the Freie Universität Berlin. Prof. Knaus and her group had already introduced me to TGF-β superfamily signaling during my university studies of biochemistry.

I would like to thank all my colleagues and peers of the MPIMG and the BSRT for their warm welcome and all their support. It was a pleasure to work with them and I will always remember the great times we have shared.

Prof. Dr. Rolf-Dieter Wegner (Center for Prenatal Diagnosis and Human Genetics, Berlin) and Prof. Dr. Karl Sperling (Institute of Medical Genetics and Human Genetics, Charité, Berlin) kindly agreed to provide our group with chorionic villi cells. I very much appreciate the lively discussions I have had with Prof. Wegner.

For the planning and offering of valuable interdisciplinary trainings, social events and activities I would like to express my great appreciation to the coordinators of the three graduate schools BSRT, Dahlem Research School (DRS) and Humboldt Graduate School in Berlin.

I also wish to acknowledge the financial support which I received from the BSRT, Max Planck Society and DRS. Additionally, I would like to express my sincere gratitude to Prof. Dr. Volker A. Erdmann (Freie Universität Berlin) and Prof. Yoav I. Henis, PhD (Tel Aviv University), who had supported my application to the BSRT for the international doctoral program.

Finally, I would like to thank my family – my mother Anna-Maria, brother Torsten, stepfather Horst as well as my green iguana Kassiopeia – who were always there for me during the ups and downs of the last few years.

Table of Contents

List of Figures

List of Tables

Abbreviations

Plural forms of abbreviations (except irregular nouns) have a lowercase 's' added to the end.

General

Abbreviation	Full name / description
1x	1-fold optical magnification or 1 cycle (depending on the context)
1X	1-fold concentrated
6-well	one well of a 6-well tissue culture plate
A_{xxx}	absorbance at XXX nm wavelength
AVG	average
bFGF	basic fibroblast growth factor
BMP	bone morphogenetic protein
BSA	bovine serum albumin
C_t	threshold cycle
CC	cellular component
cDNA	complementary deoxyribonucleic acid
CM	conditioned medium
cRNA	complementary ribonucleic acid
CV	chorionic villi
ddH2O	double-distilled water
DNA	deoxyribonucleic acid
EB	embryoid body
ECM	extracellular matrix
ELISA	enzyme-linked immunosorbent assay
EMT	epithelial-to-mesenchymal transition
EVT	extravillous cytotrophoblast / extravillous cytotrophoblast cell
FBS	fetal bovine serum
GDF	growth differentiation factor
GFP	green fluorescent protein
hCG	human chorionic gonadotropin
HCl	hydrochloric acid
hECC	human embryonal carcinoma cell
HERV	human endogenous retrovirus
hESC	human embryonic stem cell
hiPSC	human induced pluripotent stem cell
HLA-G	human leukocyte antigen G
ICM	inner cell mass
IgG / IgM	immunoglobulin G / immunoglobulin M
IVF	*in vitro* fertilization
MAPK	mitogen-activated protein kinase
MEF	mouse embryonic fibroblast
MEF-CM	mouse embryonic fibroblast - conditioned medium
MHC	major histocompatibility complex
MMP	matrix metalloproteinase
mRNA	messenger ribonucleic acid
n/a	not applicable

Abbreviation	Full name / description
OD$_{XXX}$	optical density at XXX nm wavelength
P / P$_{Det}$ / P$_{Diff}$	P-value / detection P-value / differential P-value
Passage X	passage number X of an *in vitro* cell culture
PBS	phosphate-buffered saline
PCR	polymerase chain reaction
PFA	paraformaldehyde
PGC	primordial germ cell
Real-time qPCR	real-time quantitative polymerase chain reaction
RNA	ribonucleic acid
rpm	revolutions per minute
rRNA	ribosomal ribonucleic acid
SCT	syncytiotrophoblast / syncytiotrophoblast cell
SDS-PAGE	sodium dodecyl sulfate - polyacrylamide gel electrophoresis
SE	standard error
STDEV	standard deviation
STR	short tandem repeat
TF	transcription factor
TGF-β	transforming growth factor-beta
UV	ultraviolet
w/o	without
× g	times gravity

Nucleic acid and protein sequences

Nucleic acids		Proteins		
Base	1-Letter code	Amino acid	3-Letter code	1-Letter code
Adenine	A	Alanine	Ala	A
Cytosine	C	Arginine	Arg	R
Guanine	G	Asparagine	Asn	N
Thymine	T	Aspartic acid	Asp	D
Uracil	U	Cysteine	Cys	C
		Glutamic acid	Glu	E
		Glutamine	Gln	Q
		Glycine	Gly	G
		Histidine	His	H
		Isoleucine	Ile	I
		Leucine	Leu	L
		Lysine	Lys	K
		Methionine	Met	M
		Phenylalanine	Phe	F
		Proline	Pro	P
		Serine	Ser	S
		Threonine	Thr	T
		Tryptophan	Trp	W
		Tyrosine	Tyr	Y
		Valine	Val	V

Semantics

Physical and chemical quantities

Physical or chemical quantity				Unit	
Time				s	seconds
				min	minutes
				h	hours
				d	days
Size	**Length**	general		m	meters
		proteins		aa	amino acids
		nucleic acids	double-stranded	bp	base pairs
			single-stranded	nt	nucleotides
	Space	area		m²	square meters
		volume		m³	cubic meters
				l	liters
Amount of substance				mol	moles (1 mol = 6.022×10^{23})
Mass	general			g	grams
	molecular weight (MW)	general		g/mol	grams per mol
		proteins		Da	Daltons (1 Da = 1 g/mol)
Concentration	molar (amount per volume)			M	molar (1 M = 1 mol/l)
	mass (weight per volume; w/v)			g/l	grams per liter (1 % = 10 g/l)
	volume (volume per volume; v/v)			ml/l	milliliter per liter (1 % = 10 ml/l)
Temperature				°C	degrees Celsius (1 °C = 1 Kelvin)
Electricity	current			A	Amperes
	voltage			V	Volts
	field strength			V/m	Volts per meter
Energy	general			cal	calories (1 cal = 4.184 Joules)
	Gibbs free energy			cal/mol	calories per mol
Enzyme activity				U	units

Unit prefixes

Prefix		Factor	
k	kilo	10^3	1,000
c	centi	10^{-2}	0.01
m	milli	10^{-3}	0.001
μ	micro	10^{-6}	0.000 001
n	nano	10^{-9}	0.000 000 001
p	pico	10^{-12}	0.000 000 000 001
a	atto	10^{-18}	0.000 000 000 000 000 001

Abstract (English)

Bone Morphogenetic Proteins (BMPs) are a large and evolutionarily highly conserved family of biologically active cytokines that belong to the Transforming Growth Factor-beta (TGF-β) superfamily. They act as agonists of cell surface receptors and exert pleiotropic functions during all stages of life in multicellular animals. With respect to human pluripotent stem cells, it has been shown that BMPs can induce differentiation into embryonic (mesoderm, endoderm, germ cells) and extraembryonic (primitive endoderm, trophoblast) lineages. To date, BMP4 has served as the "standard BMP" for model studies related to these cells, although the BMP family consists of more than 20 members. Therefore, this research project aimed at investigating the potential effects of distinct BMPs on human embryonic stem cells (hESCs) and human induced pluripotent stem cells (hiPSCs). BMP5, BMP10 and BMP13 were chosen, since these proteins represent members of different BMP subgroups based on sequence homology, and are known for their different physiological roles *in vivo*.

The results showed – in agreement with previous BMP4 model studies – that all three ligands trigger these cells to differentiate into derivatives of the trophoblast lineage in the absence of exogenous Basic Fibroblast Growth Factor (bFGF). However, the individual BMPs exhibited differences in the kinetics of induced differentiation as a consequence of receptor complexity existing for BMP signaling, with BMP10 being the most potent ligand. hESCs (derived from pre-implantation blastocysts) and hiPSCs (generated by reprogramming of somatic cells) shared comparable expression patterns of BMP-related TGF-β superfamily type-I and type-II receptor subtypes. This could explain the same properties with respect to ligand potency and activation of SMAD-dependent (via SMAD1/5/8) and SMAD-independent (via MAPK p38) signal transduction pathways between both types of pluripotent stem cells. The adaptation of receptor expression profile occurred during the reprogramming process of somatic cells to hiPSCs. The tested BMPs had both unique and shared target genes, such as *CDX2*, *DLX3*, *DLX5*, *GATA2*, *GATA3*, *HAND1*, *ID2*, *MSX2* and *TFAP2A*, known to be associated with the emergence of trophoblast cells. BMP stimulation activated in hESCs the expression of the BMP antagonist Noggin as a negative feedback mechanism to restrict extensive BMP action. Unlike BMP4, BMP10 is resistant to inhibition by Noggin.

In summary, this work has shed light on the induction of trophoblast differentiation in human pluripotent stem cells by individual BMP family members. Comparative global gene expression analyses and signal transduction studies revealed the molecular mechanisms which lead for distinct ligands to a collective differentiation fate. Moreover, several over- and underrepresented signaling, metabolic and other pathways as well as cellular components were identified during the course of BMP-mediated trophoblast differentiation. These provide insights into the biochemical and morphological processes that might mimic human placentation *in vitro*. Recombinant BMPs, especially BMP4, are used as cell fate inducers in many differentiation protocols applying more stringent culture conditions based on human pluripotent stem cells. In this regard, the present work has unveiled three additional cytokines that can be implemented into protocols for the directed differentiation of hESCs/hiPSCs to derive clinically relevant cell types for future regenerative therapies.

Abstract (Deutsch)

Knochenmorphogenetische Proteine (englisch: *Bone Morphogenetic Proteins*, BMPs) bilden eine große und evolutionär stark konservierte Familie biologisch aktiver Zytokine, die zur Transformierenden Wachstumsfaktor-beta - Superfamilie (englisch: *Transforming Growth Factor-beta*, TGF-β) gehören. Sie wirken als Agonisten von Zelloberflächenrezeptoren und üben pleiotrope Funktionen in allen Lebensphasen von multizellulären Tieren aus. In Bezug auf humane pluripotente Stammzellen wurde gezeigt, dass BMPs eine Differenzierung zu embryonalen (Mesoderm, Endoderm, Keimzellen) und extraembryonalen (primitives Endoderm, Trophoblast) Abstammungslinien induzieren können. Das bis heute in entsprechenden Modellstudien üblicherweise verwendete BMP ist BMP4, obwohl die BMP-Familie aus über 20 Mitgliedern besteht. Deshalb wurden in diesem Forschungsprojekt die potenziellen Effekte untersucht, die verschiedenartige BMPs auf humane embryonale Stammzellen (hESCs) und humane induzierte pluripotente Stammzellen (hiPSCs) ausüben. Hierfür wurden BMP5, BMP10 und BMP13 ausgewählt, weil diese Proteine aufgrund ihrer Sequenzhomologie Mitglieder verschiedener BMP-Untergruppen repräsentieren, und für ihre unterschiedlichen physiologischen Funktionen *in vivo* bekannt sind.

Die Ergebnisse zeigten – in Übereinstimmung mit bisherigen BMP4-Modellstudien – dass alle drei Liganden in Abwesenheit von exogenem Basischen Fibroblastenwachstumsfaktor (bFGF) eine Differenzierung dieser Zellen zu Derivaten der Trophoblastlinie auslösen. Jedoch wurden Unterschiede in der Kinetik der induzierten Differenzierung zwischen den individuellen BMPs festgestellt, die eine Konsequenz der für BMP-Signaltransduktion existierenden Rezeptorkomplexität sind, wobei BMP10 der stärkste Ligand war. hESCs (aus Blastozysten im Präimplantationsstadium isoliert) und hiPSCs (durch Reprogrammierung somatischer Zellen erzeugt) wiesen vergleichbare Expressionsmuster an Unterarten von BMP-zugehörigen Typ-I- und Typ-II-Rezeptoren der TGF-β-Superfamilie auf. Dies könnte die gleichen Eigenschaften hinsichtlich der Wirkungsstärke der Liganden und der Aktivierung von SMAD-abhängigen (via SMAD1/5/8) und SMAD-unabhängigen (via MAPK p38) Signaltransduktionswegen zwischen beiden Arten von pluripotenten Stammzellen erklären. Die Anpassung des Rezeptorexpressionsprofils fand während des Vorgangs der Reprogrammierung von somatischen Zellen zu hiPSCs statt. Die getesteten BMPs hatten sowohl einzigartige als auch gemeinsame Zielgene, wie zum Beispiel *CDX2*, *DLX3*, *DLX5*, *GATA2*, *GATA3*, *HAND1*, *ID2*, *MSX2* und *TFAP2A*, die bekanntermaßen mit der Entstehung von Trophoblastzellen in Verbindung stehen. BMP-Stimulation aktivierte in hESCs die Expression des BMP-Antagonisten Noggin als einen negativen Rückkopplungsmechanismus, um extensive BMP-Signalwirkung einzuschränken. Im Gegensatz zu BMP4 ist BMP10 resistent gegen Inhibition durch Noggin.

Zusammenfassend hat diese Arbeit die Wissenslücke über die Induktion von Trophoblastdifferenzierung in humanen pluripotenten Stammzellen durch individuelle BMP-Familienmitglieder geschlossen. Vergleichende globale Genexpressionsanalysen und Signaltransduktionsstudien deckten die molekularen Mechanismen auf, welche für verschiedenartige Liganden zu einem kollektiven Differenzierungsschicksal führen. Darüber

hinaus wurden im Verlauf der BMP-vermittelten Trophoblastdifferenzierung mehrere über- und unterrepräsentierte Signal-, Stoffwechsel- und andere *Pathways* sowie zelluläre Bestandteile identifiziert. Diese geben Einblicke in die biochemischen und morphologischen Prozesse, die humane Plazentation *in vitro* imitieren könnten. Rekombinante BMPs, vor allem BMP4, sind Bestandteil vieler Differenzierungsprotokolle, mit denen unter strengen Zellkulturbedingungen die Spezialisierung von humanen pluripotenten Stammzellen zu bestimmten gewünschten Zelltypen erreicht wird. In diesem Zusammenhang hat die vorliegende Arbeit drei weitere Zytokine aufgedeckt, die in Protokolle für die zielgerichtete Differenzierung von hESCs/hiPSCs implementiert werden können, um klinisch relevante Zelltypen für zukünftige regenerative Therapien herzustellen.

1   Introduction

1.1   Human embryonic development

1.1.1   Embryogenesis (from fertilization to gastrulation)

1.1.1.1   Pre-implantation embryo

The cell fusion between oocyte and sperm marks the onset of a new life. This event is called fertilization and takes place *in vivo* in the oviduct near the ovary. The resulting diploid zygote moves along the oviduct to the uterus. During this 3–4 days long journey (Figure 1-1A), the zygote undergoes few cell divisions until it reaches an 8-cell stage, the morula. The cells of the morula, called blastomeres, perform a morphological change known as compaction, which is the initiation of the first cell lineage specialization event in life (Adjaye et al., 2005): The outer blastomeres form **trophectoderm** (alias **trophoblast**) and the interior blastomeres form the **inner cell mass** (**ICM**). The decision between both cell differentiation fates is supposed to be a result of reciprocal interaction between the transcription factors CDX2 (favoring trophoblast) and OCT4 (favoring ICM) (Niwa et al., 2005; Babaie et al., 2007), but the exact underlying molecular mechanisms are still unclear. The resulting **blastocyst** marks the next stage of embryogenesis. It contains the outer trophoblast cell layer, the interior ICM cell cluster, and a fluid-filled cavity, the blastocoel. Around day 7 post-fertilization, the blastocyst comprises a few hundred cells and adheres to the endometrium of the uterine wall for implantation. The cells of the ICM will constitute the embryo, whereas the trophoblast cells will establish the extraembryonic placenta.

1.1.1.2   Post-implantation embryo

The next cell lineage specialization event of the post-implantation embryo is the formation of the three germ layers (ectoderm, mesoderm and endoderm). This very critical developmental step is called gastrulation. It starts around day 14 when epiblast cells of the former ICM undergo epithelial-to-mesenchymal transition (EMT), a process also known to be involved in metastasis of tumor cells (Baum et al., 2008). EMT is characterized by downregulation of the cell adhesion protein E-Cadherin to lose the characteristics of epithelial cells and upregulation of Vimentin to acquire the characteristics of mesenchymal cells. Epiblast cells undergoing EMT lose cell-cell contact and migrate inward through the **primitive streak** to form mesoderm and endoderm, whereas the remaining outer epiblast cells form ectoderm (Figure 1-1B). Besides other factors and signaling pathways, the transcription factors T (Brachyury) and MIXL1 are involved in primitive streak initiation (Tam and Loebel, 2007). Together, these three embryonic germ layers will constitute all tissues and organs of the future fetus. This is due to critically regulated temporal and spatial gene expression and cell signaling during organogenesis of the embryo. Cells of the **ectoderm** (the outer germ layer) give rise to e.g. skin epidermis, nervous tissues and sense organs. Cells of the **mesoderm** (the middle germ layer) develop into e.g. the musculoskeletal system, cardiovascular system, lymphatic
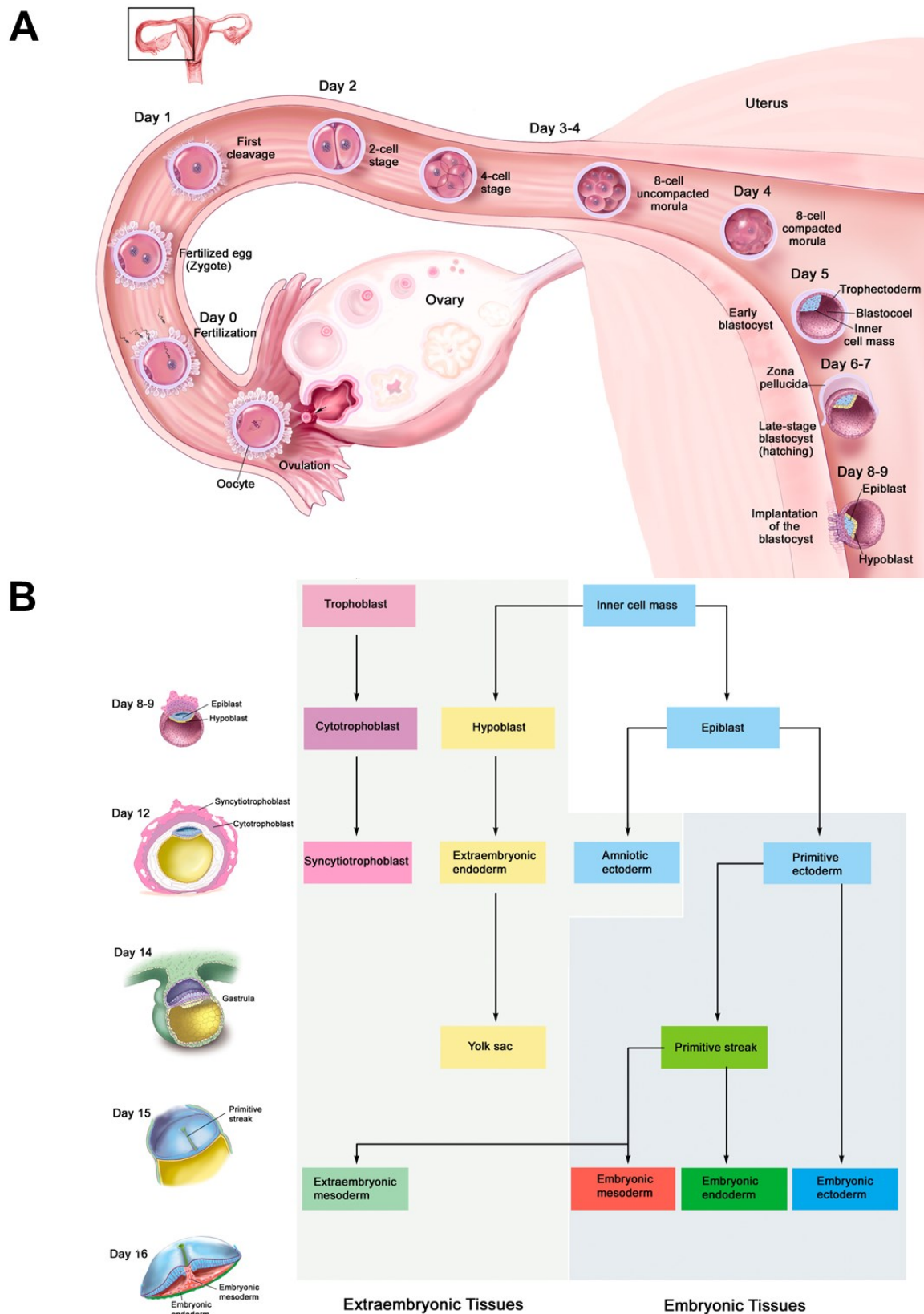
Figure 1-1   Human embryonic development from fertilization to gastrulation.
(A) Fertilization of the oocyte and movement of the developing embryo towards the uterus for implantation.
(B) Formation of the three embryonic germ layers (ectoderm, mesoderm and endoderm). Detailed information on each illustrated stage and on subsequent developmental steps can be found in the book of Bruce M. Carlson about human developmental biology (Carlson, 2012). (Illustrations modified from © 2001 Terese Winslow with kind permission from the artist; http://www.teresewinslow.com.)

system, kidneys and gonads. Cells of the **endoderm** (the inner germ layer) evolve into e.g. liver, pancreas, lungs, thyroid, gastrointestinal tract and urinary bladder. The development of the haploid **gametes** (oocytes or sperm) within the germline, whose destiny is exclusively restricted to reproduction, takes place in a niche apart from the somatic tissues (Lehmann, 2012).

1.1.2 Placentation

1.1.2.1 Placenta and chorionic villi (CV)

Successful pregnancy requires the anchoring of the embryo to the uterine wall and its access to the maternal blood circulation via the **placenta**. This extraembryonic organ is a characteristic of higher mammals (Eutheria, Placentalia), but homologous or analogous structures can also be found at varying levels of development in other animals, including invertebrates. In humans, its anatomical and functional units are the **chorionic villi** (**CV**), which are tree-like structures that sprout at the blastocyst's implantation site out of the chorion. The chorion is the outer of the four extraembryonic membranes that surround the developing embryo (amnion, chorion, yolk sac and allantois). It consists of an outer layer of trophoblast and an inner layer of somatic extraembryonic mesoderm tissue. Initially, CV are entirely composed of trophoblast tissue (primary CV). At later stages, they additionally include an inner core of somatic extraembryonic mesoderm (secondary CV), which is finally vascularized by umbilical blood vessels that grow into it (tertiary CV). The latter two features make tissue biopsies of placental CV a suitable source for prenatal diagnosis to determine chromosomal or genetic disorders in the fetus (chorionic villus sampling (Wegner and Stumm, 2011)).

1.1.2.2 Villous and extravillous trophoblast differentiation pathway

The various functions of the placenta are accomplished by two possible differentiation fates of the trophectoderm-derived **villous cytotrophoblasts** within CV, which are progenitor cells and of epithelial nature (reviewed by Red-Horse et al., 2004; Lunghi et al., 2007).

1.) Differentiation to **multinucleated syncytiotrophoblasts** (**SCTs**):

Villous cytotrophoblast cells fuse to form a continuous monolayer of multinucleated syncytiotrophoblasts (SCTs), which entirely covers the surface of CV. In the case of CV branches that float freely in the intervillous space, known as **floating villi** (Figure 1-2), this polarized epithelial layer is in direct contact with the maternal blood flow. It serves as a selective barrier for the exchange of nutrients, metabolites and respiratory gases between the maternal and fetal blood circuit, with an additional endocrine function to maintain pregnancy and support fetal growth. For these purposes, SCTs contain many different active transporters within their maternal- and fetal-facing membranes (reviewed by Knipp et al., 1999), proteins that are involved in the homeostasis of elements (e.g. calcium for skeleton mineralization (Lafond and Simoneau, 2006)), and produce and release hormones such as hCG and progesterone (reviewed by Malassiné and Cronier, 2002). A special feature of SCT development is the involvement of envelope glycoprotein genes (*env*) from evolutionarily preserved human endogenous retrovirus (HERV) proviral elements in mediation of the cell fusion between

mononuclear villous cytotrophoblasts (de Parseval and Heidmann, 2005). Multinucleated SCTs are mitotically inactive and subjected to a continuous conversion process, in which SCTs are replaced by the subjacent layer of differentiating villous cytotrophoblasts, and extruded as apoptotic material into the maternal blood circulation (Huppertz and Kingdom, 2004).

2.) Differentiation to **invasive extravillous cytotrophoblasts** (**EVTs**):

Branches of CV which are directly in contact with the uterine wall are called **anchoring villi** (Figure 1-2). Villous cytotrophoblasts in anchoring villi form cell columns through proliferation. At the distal sites, these mononuclear cells turn into a fully invasive phenotype by undergoing an EMT-like transition. They break through the covering SCT epithelium and detach from the villus as extravillous cytotrophoblast cells (EVTs) to invade the decidua and remodel its blood vessels. This extravillous differentiation pathway serves to physically attach the fetus to the mother and to establish access to her vascular infrastructure. Unlike cancer cells, EVTs are transiently invasive and only migrate to the proximal third of the myometrium, and are mitotically inactive. The invasiveness of EVTs is mediated by their ability to secrete several types of protease enzymes for degradation of the extracellular matrix (ECM) of the surrounding uterine tissue. The concomitant expression of corresponding protease inhibitors and other factors by EVTs and uterine cells regulates the invasiveness of EVTs in an autocrine and paracrine way (Bischof et al., 2000). Maternal immune tolerance of the fetal semi-allograft is achieved by substitution of classical MHC class-I and class-II molecules by Human Leukocyte Antigen G (HLA-G), a non-classical MHC class-I molecule, on the surface of EVTs. The absence of the classical molecules prevents the recognition of EVTs by maternal T lymphocytes, and the presence of HLA-G shields EVTs from an attack by natural killer cells (Pazmany et al., 1996). As a successful strategy for endovascular invasion, EVTs finally transform their adhesion receptor phenotype so as to resemble the vascular endothelial cells they replace (Zhou et al., 1997), an impressive process referred to as "pseudo-vasculogenesis" or "vascular mimicry".

The development of the placenta is critically regulated and must conform to the requirements of the rapidly growing fetus. Dysfunctions in any of both trophoblast differentiation pathways are associated with a wide range of pregnancy complications. Among them are spontaneous abortion and preterm birth, intrauterine growth restriction, preeclampsia and choriocarcinoma (Lunghi et al., 2007; Red-Horse et al., 2004). Some genes which impact on placental and fetal growth were found to be regulated – beyond the classical Mendelian inheritance – by genomic imprinting, and are only transcribed from the maternal allele (growth restricting factors) or paternal allele (growth promoting factors). This led to the "parental conflict hypothesis" (Moore and Haig, 1991; Constância et al., 2002).
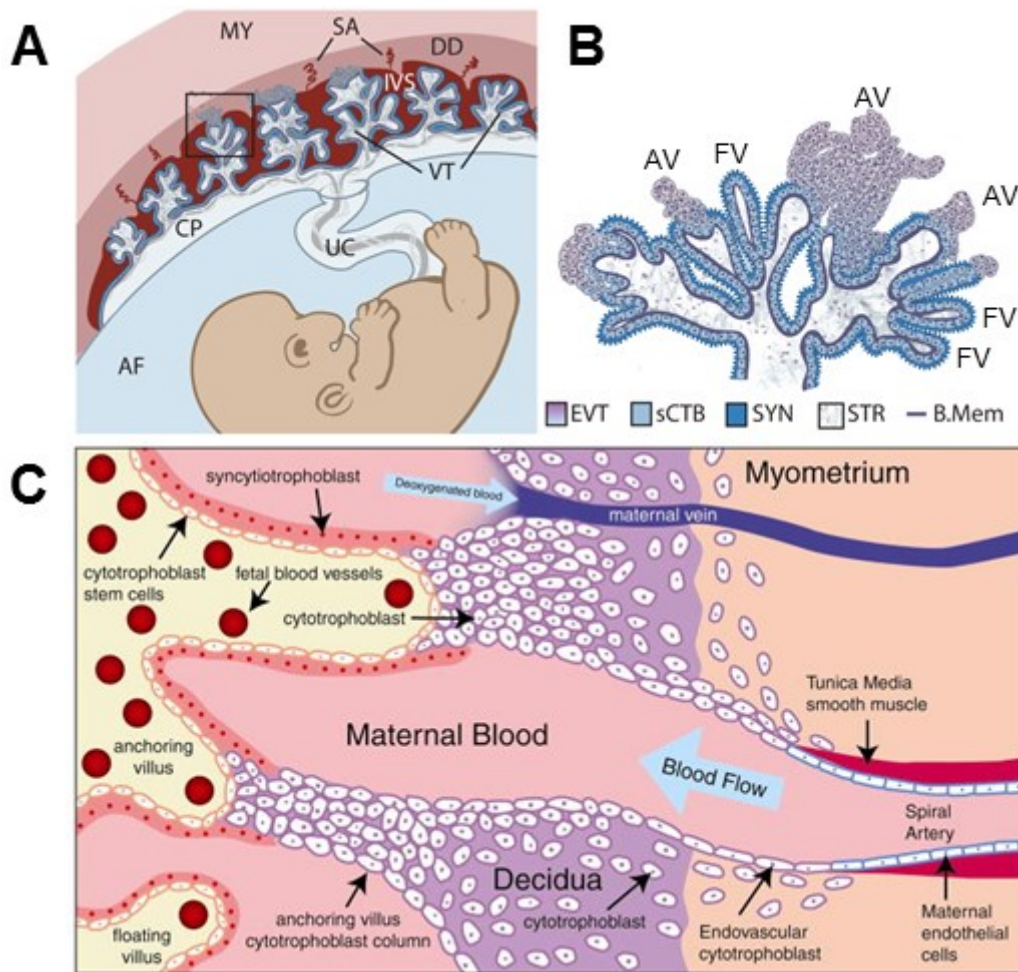
Figure 1-2   Placenta and its chorionic villi subunits with syncytiotrophoblasts and extravillous cytotrophoblasts at the maternal-fetal interface.
(A) Structure and orientation of fetus and placenta in uterus at around 6 weeks of gestation. Maternal structures: DD = decidua (endometrium, uterine lining during pregnancy), IVS = intervillous space filled with maternal blood, MY = myometrium, SA = spiral arteries; fetal structures: AF = amniotic fluid, CP = chorionic plate, UC = umbilical cord, VT = villous tree. **(B)** Structure of villous tree (boxed area in panel A) with anchoring villi (AV) and floating villi (FV). EVT = invasive extravillous cytotrophoblasts, sCTB = subsyncytial villous cytotrophoblasts (prior to cell fusion), SYN = multinucleated syncytiotrophoblasts, STR = stroma with fetal capillaries, B.Mem = basement membrane. **(C)** Specializing trophoblast cells of AV and FV at the maternal-fetal interface. (Illustrations modified from Robbins et al., 2010 (panel A and B) and Lam et al., 2005 (panel C).)

1.2 Human pluripotent stem cells

1.2.1 Human embryonic stem cells (hESCs)

1.2.1.1 Derivation and characteristics

Human embryonic stem cells (**hESCs**) are isolated from the ICM of pre-implantation embryos, generated by *in vitro* fertilization (IVF), at the blastocyst stage (Thomson et al., 1998). They possess the capacity of unlimited **self-renewal** *in vitro* if kept under culture conditions that support their undifferentiated state, and can therefore be regarded as being immortal. In addition, hESCs are **pluripotent**, i.e. they are able to differentiate into any cell type of the human body. In addition to derivatives of the three somatic germ layers (Reubinoff et al., 2000) and

5

the germline (Clark et al., 2004a), hESCs were also shown to be able to specialize to derivatives of the extraembryonic trophoblast (Gerami-Naini et al., 2004). This seems to be a paradox, given the fact that ICM cells represent the fraction of former morula cells that had avoided trophoblast differentiation during embryogenesis.

1.2.1.2 Significance for basic research and medicine

The derivation of the first hESC lines by James A. Thomson in 1998, almost 20 years after the derivation of mouse ESCs, had a widespread impact on biomedical research. hESCs offered the possibility to investigate the basic molecular events of early human development. They became an alternative to the less eligible human embryonal carcinoma cells (hECCs), which had been serving as model system for many years. Due to their differentiation capacity, hESCs offered a new source for regenerative therapies involving cell transplants. Within recent years, data from many studies worldwide have provided insights into the gene regulatory networks and signaling pathways that are required to maintain the undifferentiated and pluripotent state of hESCs, as well as into the external stimuli that are required to induce their *in vitro* differentiation to obtain specific cell types.

1.2.2 Human induced pluripotent stem cells (hiPSCs)

1.2.2.1 Derivation and characteristics

Human induced pluripotent stem cells (**hiPSCs**) are generated by "reprogramming" of differentiated somatic cells back to a hESC-like ground state. Previous approaches of reprogramming included somatic cell nuclear transfer into enucleated zygotes (cloning) of frogs (Gurdon et al., 1958) or forced fusion of somatic cells with hESCs (Cowan et al., 2005). In 2007, the group of Shinya Yamanaka demonstrated that adult human cells can be reprogrammed back to a naïve state, called hiPSCs, via forced reactivation of selected genes that are naturally silenced during early embryonic development upon initiation of gastrulation. After successful attempts in the mouse model, they retrovirally transduced the cDNA of the four transcription factors OCT4, SOX2, KLF4 and c-MYC into the genome of human skin fibroblasts (Takahashi et al., 2007). Around the same time, Thomson's group showed that pluripotency in these cells can be induced by lentiviral transduction of OCT4, SOX2, NANOG and LIN28 (Yu et al., 2007). This breakthrough led to a scienticif paradigm shift, as stem cell differentiation was believed to be a unidirectional, irreversible process. In the meantime, hiPSCs have been derived from nearly all cell types, whereat the number of required reprogramming factors could often be reduced. In order to avoid the disadvantages of transgene integrations, other delivery strategies for these factors such as via episomal plasmids, mRNAs or recombinant proteins have been successfully applied. Various small chemical molecules have been identified to support the reprogramming process (reviewed by Tavernier et al., 2013). hiPSCs turned out to resemble hESCs in many aspects, including morphology, growth properties, gene expression, epigenetic signature and pluripotency. In the mouse model it could be shown that iPS cells fulfill the two most stringent *in vivo* pluripotency criteria: The proof of germline transmission, as assessed by experiments involving chimera (Okita et al., 2007), and the proof of

contribution to a whole embryo, as assessed by tetraploid complementation (Kang et al., 2009). Both tests cannot be realized in the human model due to ethical issues.

1.2.2.2 Significance for basic research and medicine

With respect to biomedical research, hiPSCs offer great advantages compared to hESCs. Firstly, their creation is free of any ethical concerns, since it does not require the destruction of a human embryo. Secondly, since every individual can be a donor for cells to be reprogrammed, hiPSCs open up possibilities that have never existed before: They can be used for personalized medicine (cell-based regenerative therapies without risk of immune rejection; *in vitro* drug efficacy and tolerability tests) as well as to create cellular model systems to study diseases and their potential treatments (reviewed by Drews et al., 2012 and Okano et al., 2013). For their discovery of cloning and iPS cells, Sir John B. Gurdon and Shinya Yamanaka were jointly awarded the Nobel Prize in Physiology or Medicine in 2012.

1.3 Bone Morphogenetic Proteins (BMPs) as part of the Transforming Growth Factor-beta (TGF-β) superfamily

1.3.1 Physiological functions of TGF-β superfamily signaling

Ligands of the **Transforming Growth Factor-beta** (**TGF-β**) superfamily are biologically active cytokines that bind to receptors on the cell surface to induce signals which finally lead to cellular responses. They are present within a broad range of multicellular animals (from nematodes to humans), evolutionarily highly conserved, and involved in the regulation of numerous pivotal biological processes. These include cell fate determination (differentiation, programmed cell death), cell proliferation, adhesion and migration (Schmierer and Hill, 2007). The ligands exert their functions during all stages of life, ranging from early embryonic patterning by formation of morphogen gradients to adult tissue homeostasis and regeneration (reviewed by Wu and Hill, 2009). Since malfunctions in TGF-β superfamily signaling can be lethal or result in malformations and serious diseases (reviewed by Gordon and Blobe, 2008), it is critically regulated on all possible levels (reviewed by Moustakas and Heldin, 2009).

1.3.2 Ligand members

The core members of ligands in mammals include genes for 3 isoforms of **TGF-β**, 4 **Activin-β** chains, the protein **Nodal** and about 20 **Bone Morphogenetic Proteins** (**BMPs**) and related **Growth Differentiation Factors** (**GDFs**) (Figure 1-3). All agonists are synthesized as dimeric pre-pro-proteins, and the monomers share a cystine knot motif as a structural hallmark (Schmierer and Hill, 2007). BMPs represent a large subfamily of cytokines within the TGF-β superfamily. Originally discovered by their ability to induce bone formation, they were given the name "Bone Morphogenetic Proteins". Meanwhile it has become clear that BMPs exert pleiotropic functions which affect the whole organism, thus the name "Body Morphogenetic Proteins" has been suggested to be more adequate (Wagner et al., 2010). BMPs are usually

secreted as mature proteins into the extracellular space after proteolytic cleavage of their inactive precursor forms. Homodimers are the prevalent form, but also heterodimeric ligands exist *in vitro* and *in vivo*, which were described to be more potent activators of signaling than their corresponding homodimers (Sieber et al., 2009).
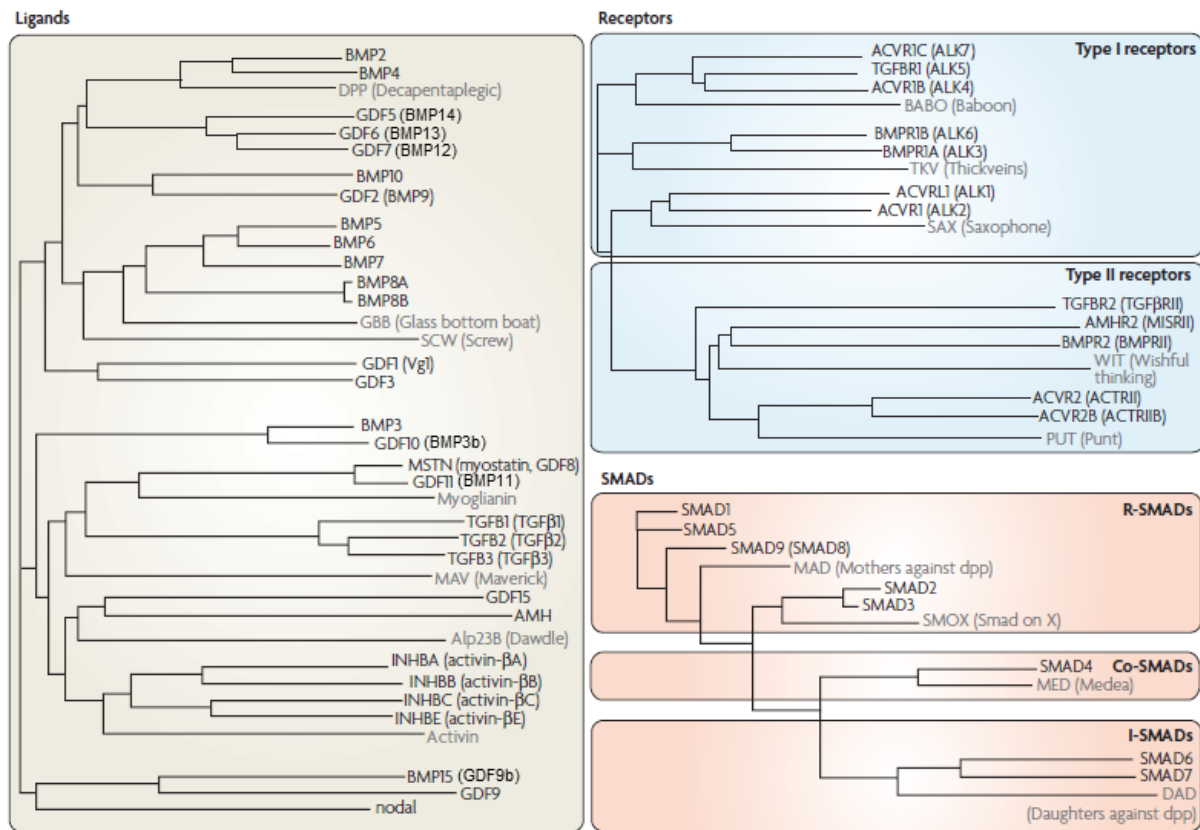
Figure 1-3 **Ligands, receptors and SMADs of the Transforming Growth Factor-beta (TGF-β) superfamily.** Phylogenetic trees derived from protein alignments (black: proteins in humans; grey: protein orthologs in the fruit fly *Drosophila melanogaster*). For the ligands, the putative mature, fully processed forms were used for alignments. Protein symbols are given with alternative names in parentheses. Abbreviations: ACVR = Activin Receptor, ALK = Activin Receptor-like Kinase, BMP = Bone Morphogenetic Protein, BMPR = Bone Morphogenetic Protein Receptor, GDF = Growth Differentiation Factor, Co-SMAD = Common-mediator SMAD, I-SMAD = Inhibitory SMAD, R-SMAD = Receptor-regulated SMAD, TGF = Transforming Growth Factor, TGFBR = Transforming Growth Factor-beta Receptor. (Figure modified from Schmierer and Hill, 2007.)

1.3.3 Receptor activation and intracellular signal transduction

Ligands of the TGF-β superfamily signal through serine/threonine kinase transmembrane receptors. Two functional classes of **receptors** exist: **Type-I** and **type-II** (Figure 1-3).

Canonical TGF-β superfamily signaling in mammalian cells acts via **SMAD proteins** (Figure 1-3) and takes place as follows (Schmierer and Hill, 2007) (Figure 1-4): Binding of the dimeric ligand to the extracellular domain of receptors causes the formation of a heterotetrameric active receptor complex, consisting of one dimer of type-II receptors, one dimer of type-I receptors, and the bound ligand. The constitutively active intracellular kinase domain of type-II receptors then phosphorylates the type-I receptors within a strictly conserved N-terminal domain, the GS-box. This leads to a conformational change and the activation of

the intracellular kinase domain of type-I receptors, and enables the recruitment of receptor-regulated SMADS (R-SMADs) which act as intracellular signal transducers. After phosphorylation of R-SMADs by the kinase of type-I receptors at their C-terminal SSXS-motif, two of these R-SMADs are enabled to associate and to form an active heterotrimeric complex together with one SMAD4. This protein complex translocates to the nucleus where the SMADs bind in cooperation with other proteins to specific promoters and activate the transcription of target genes.

The abovementioned signal transduction can be split into two branches downstream of type-I receptors: Signaling via the R-SMADs SMAD2 and SMAD3 or signaling via SMAD1, SMAD5 and SMAD8. Both pathways are linked together via SMAD4, also called common-mediator SMAD (Co-SMAD), for which the R-SMADs compete to bind. In general, with few exceptions, TGF-βs, Activins and Nodal signal via SMAD2/3 (activated through type-I receptors ALK4, ALK5 and ALK7), and BMPs and related GDFs via SMAD1/5/8 (activated through type-I receptors ALK1, ALK2, ALK3 and ALK6).
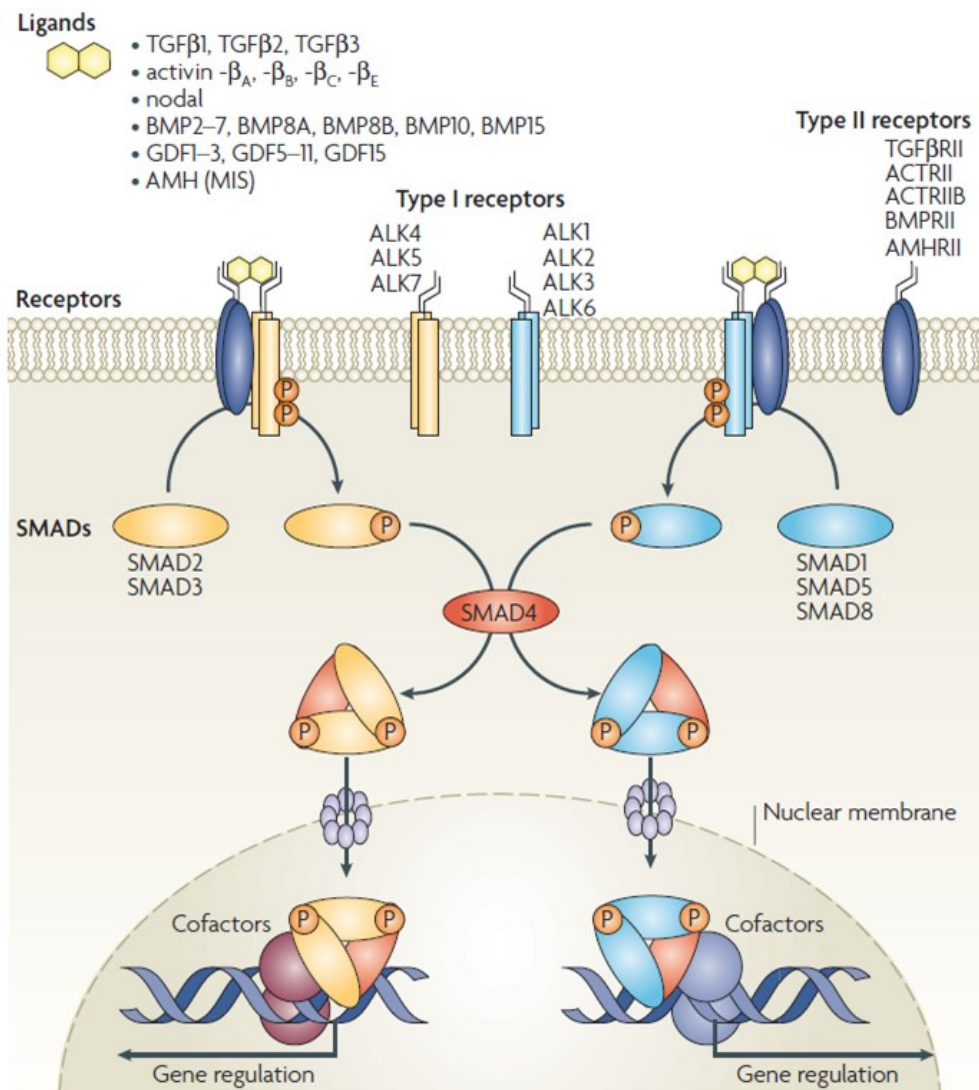
Figure 1-4   Canonical TGF-β superfamily signaling pathways in mammalian cells.
See text for description. Left side: TGF-β/Activin/Nodal branch (acting via SMAD2/3), right side: BMP/GDF branch (acting via SMAD1/5/8). (Figure modified from Schmierer and Hill, 2007.)

1.3.4 Complexity of BMP signaling

Although much more individual ligands exist compared to the number of receptors through which they signal, BMPs are able to induce different and specific signals that result in different cell effects. This is possible due to the numerous potential combinations between type-I and -II receptors of the heterotetrameric receptor complex (Gilboa et al., 2000; Nickel et al., 2009):

Besides the canonical signaling via SMADs, BMPs can also signal via SMAD-independent pathways, including different mitogen-activated protein kinase (MAPK) pathways (via ERK1/2, p38 or SAPK/JNK) and signaling via Akt (also known as Protein Kinase B) (Gallea et al., 2001; Guicheux et al., 2003; Gamell et al., 2008; Boergermann et al., 2010). The mode of receptor oligomerization is decided by various factors, such as ligand-receptor affinities and the expression levels of individual receptors on the cell surface (Sieber et al., 2009). BMP type-I and type-II receptors can be present at the plasma membrane as monomers and as homomeric and heteromeric complexes that can be stable or transient (Marom at al., 2011; reviewed by Ehrlich et al., 2011). They can exist in preformed hetero-oligomeric complexes already prior to ligand binding, or be recruited into hetero-oligomeric complexes after ligand binding, which can decide between SMAD-dependent and SMAD-independent signaling (Nohe et al., 2002; Hassel et al., 2003). Moreover, BMP receptors were proven to be able to take different endocytosis routes, depending on the membrane domains in which they are localized (e.g. lipid rafts). This influences the type of activated signaling pathway (SMAD versus non-SMAD), too (Hartung et al., 2006; reviewed by Sieber et al., 2009).

1.4 BMPs in the context of human pluripotent stem cells

1.4.1 Known effects

TGF-β superfamily signaling is involved in the control of a wide range of early cell fate decisions in hESCs (Greber et al., 2008). To maintain the undifferentiated state, **SMAD2/3** signaling needs to be active and **SMAD1/5/8** signaling to be repressed (James et al., 2005) (in the following referred to as **Activin/Nodal branch** and **BMP/GDF branch**, respectively). Though, inhibition of BMP signaling induces neuroectoderm differentiation (Pera et al., 2004; Itsykson et al., 2005), and treatment with Activin A leads to definitive endoderm differentiation (Brown et al., 2011). This indicates divergent roles for both pathways and implies that a certain balance between both competing branches is a key in maintaining the undifferentiated phenotype.

BMP-mediated signaling is known to induce diverse differentiation fates in hESCs, and in this context, to integrate inputs from other extrinsic signals (reviewed by Li and Chen, 2013). Since the initial study of Xu et al. in 2002 (Xu et al., 2002), BMP-driven hESC differentiation has been the focus of several investigations. The obtained cellular phenotypes after *in vitro* treatment of hESCs with recombinant proteins comprised several lineages, including:

- Trophoblast (by BMP2, BMP4, BMP7, GDF5 (alias BMP14) (Xu et al., 2002); BMP4 (Zhang et al., 2008); BMP2, BMP6, BMP2/6 heterodimers (Valera et al., 2010));

- extraembryonic endoderm (by BMP2, BMP7, BMP2/7 heterodimers (Pera et al., 2004); BMP4 (Zhang et al., 2008));
- mesoderm (by BMP4 (Zhang et al., 2008));
- mesendoderm and definitive endoderm (by BMP2, BMP6, BMP2/6 heterodimers (Valera et al., 2010)); and
- germ cells (by BMP4, BMP7, BMP8b (Kee et al., 2006)).

The large discrepancies in differentiation outcome and poor reproducibility of results can be explained due to variations in experimental conditions (cell culture media composition, presence or absence of xenogeneic feeder cells, duration of exposure to BMPs, adherent or embryoid body-based differentiation, etc.).

Most recent model studies using BMP4 revealed that the cellular fate following BMP stimulation critically depends on whether **Basic Fibroblast Growth Factor (bFGF)**, a standard supplement of many cell culture media for human pluripotent stem cells to support their self-renewal (McDevitt and Palecek, 2008), is present or absent during the treatment. It is now widely accepted by the scientific community that BMP4 treatment in the presence of exogenous bFGF induces hESCs to differentiate into primitive streak and its derivatives mesoderm and endoderm (Yu et al., 2011), and in its absence to the trophoblast lineage (Yu et al., 2011; Amita et al., 2013). The differentiation kinetics towards trophoblast is accelerated under normoxic compared to hypoxic culture conditions and slowed down in the presence of bFGF (Das et al., 2007). Recent experiments from our group demonstrated that inhibition of autocrine bFGF signaling is a key in directing BMP4-mediated hESC differentiation to syncytiotrophoblasts (Sudheer et al., 2012).

However, in 2011 a study challenged the well-recognized trophoblast identity of the BMP4-driven differentiated hESCs in general by claiming that they would resemble a phenotype of (extra-)embryonic mesoderm (Bernardo et al., 2011). This has led to a controversial debate (Greber, 2011) which persists to this day (Roberts et al., 2014).

1.4.2 Questions raised

The majority of model studies investigating the effect of BMP-mediated signaling on hESCs has been carried out using BMP4 as "standard ligand" for stimulation of these cells. This is surprising for two reasons: Firstly, the large family of BMPs consists of about 20 members that are divided into several subgroups depending on sequence homology (Figure 1-3). Secondly, these cytokines are known for their enormous diversity in biological functions *in vivo* (Wagner et al., 2010). Studies with other progenitor and mature cells as model system have shown that the response of cells to BMPs can differ significantly: Individual BMP family members could induce different cell fates within a given cell line (Berasi et al., 2011; Brederlau et al., 2002), but were also able to functionally compensate for each other both *in vitro* and *in vivo* (Solloway and Robertson, 1999; Cheng et al., 2003; Ricard et al., 2012). It is even possible that one and the same cell type shows distinct responses between mature ligands sharing over 90 % sequence identity (e.g. BMP6 versus BMP7 (Solloway and Robertson, 1999; Takeda et al., 2012; Huse et al., 2011)), while others respond identically to ligands sharing only 60 % sequence identity (e.g. BMP2 or BMP4 versus BMP7 (Solloway and Robertson, 1999; Cheng et al., 2003; Larman et al., 2012)). It is obviously evident that

there exists a gap in the knowledge and understanding of the function of individual ligands with regard to the directed differentiation of human pluripotent stem cells.

Moreover, the majority of model studies concerning BMPs and human pluripotent stem cells has been conducted using hESCs. Although there is growing evidence that hiPSCs – as reprogrammed somatic cells – are relying on the same signaling pathways controlling pluripotency and early cell fate decisions like hESCs from embryonic origins (Vallier et al., 2009a), in-depth studies investigating BMP signaling in hiPSCs remain to be done.

1.4.3   BMP5, BMP10 and BMP13 as to date untested ligands

BMP5, BMP10 and BMP13 are up to now members of untested BMPs, both in case of hESCs and hiPSCs. All three cytokines are known to carry out diverse physiological roles, which are briefly summarized below:

–   **BMP5:** BMP5 contributes to limb development, bone morphogenesis (Bessa et al., 2008a) and is involved in the development of several soft tissues (lungs, liver, ureter, bladder, intestines (King et al., 1994), kidney (Bramlage et al., 2011), nervous system (Beck et al., 2001)). Homozygous loss-off-function mutations in *Bmp5* are associated with a viable short ear mouse phenotype that displays defects in skeletal development and soft tissues. BMP5 and its subgroup member BMP7 can functionally compensate for one another during murine development (Solloway and Robertson, 1999).

–   **BMP10:** BMP10 is insofar a special ligand as its expression and function seem to be restricted to specific parts of the developing heart (Neuhaus et al., 1999; Chen et al., 2004; Zhang et al., 2011; Huang et al., 2012). A rare exception is its involvement in postnatal vascular remodeling of the retina, at which BMP10 can functionally replace its subgroup member BMP9 (Ricard et al., 2012). Noteworthy, BMP9 is unable to substitute for BMP10 in cardiac development, which confirms the exclusive function of BMP10 (Chen et al., 2013a). BMP10-deficient knockout mice (*Bmp10$^{-/-}$*) die due to lethal cardiac defects before birth. A functional BMP10-specific receptor in the heart has not yet been identified.

–   **BMP13:** BMP13 (also known as GDF6) is expressed in a variety of tissues such as cartilage, tendon, intestines, skeletal muscle and placenta. It appears to be a vertebrate-specific protein (reviewed by Williams et al., 2008). BMP13 is involved in skull joint development during skeletal segmentation and supports cartilage formation, chondrocyte development and hypertrophy (but unlike BMP5 not cell proliferation (Mailhot et al., 2008)). BMP13 plays a role in eye development, tendon, ligament and connective tissue formation and healing. In mesenchymal stem cells, BMP13 does not support osteogenesis unlike many other BMPs, but instead induces tendon-like tissue (Berasi et al., 2011).

In addition, all three ligands represent members of distinct BMP subgroups (Figure 1-3). Sequence alignment of the mature ligands (Figure 1-5) reveals a homology of 46 % for BMP5:BMP10, 42 % for BMP5:BMP13 and 53 % for BMP10:BMP13. All these properties qualify them as ideal BMP candidates for hESC/hiPSC-related investigations.

```
            1-10       11-20      21-30      31-40      41-50      51-60
BMP5        AANKRKNQNR NKSSSHQDSS RMSSVGDYNT SEQKQACKKH ELYVSFRDLG WQDWIIAPEG   376
BMP10       ---------- ---------- ---------- NAKGNYCKRT PLYIDFKEIG WDSWIIAPPG   346
BMP13       ---------- --------TA FASRHGKRHG KKSRLRCSKK PLHVNFKELG WDDWIIAPLE   377
                                             .  .    *.:    *::.*:::* *:.*****

            61-70      71-80      81-90      91-100     101-110    111-120
BMP5        YAAFYCDGEC SFPLNAHMNA TNHAIVQTLV HLMFPDHVPK PCCAPTKLNA ISVLYFDDSS   436
BMP10       YEAYECRGVC NYPLAEHLTP TKHAIIQALV HLKNSQKASK ACCVPTKLEP ISILYLDKGV   406
BMP13       YEAYHCEGVC DFPLRSHLEP TNHAIIQTLM NSMDPGSTPP SCCVPTKLTP ISILYIDAGN   437
            * *: * * * .:** *:   *:***:*:*: .        .      **.**** **:**:* .

            121-130    131-138
BMP5        NVILKKYRNM VVRSCGCH    454 (138 aa)
BMP10       VTYKFKYEGM AVSECGCR    424 (108 aa)
BMP13       NVVYKQYEDM VVESCGCR    455 (120 aa)
            .  :*. *  .* .***:
```

Figure 1-5   Sequence alignment of BMP5, BMP10 and BMP13 (mature ligands).
The N-terminal signal- and pro-peptide were omitted from the alignment. The numbers on the right refer to the amino acid residue of the protein entry stored in the UniProt resource database (Chapter 2.13, accession numbers in Table 2-8). Lengths of the mature polypeptides are given in parentheses. Residues shared by individual BMP pairs are highlighted in green, blue and orange. Red color and an asterisk (*) indicate positions which have a single, fully conserved residue (consensus sequence); a colon (:) indicates conservation between groups of strongly similar properties (scoring > 0.5 in the Gonnet PAM 250 matrix); a period (.) indicates conservation between groups of weakly similar properties (scoring ≤ 0.5). The highly conserved cysteines are shaded in grey. These include the six cysteines forming the three disulfide bonds of the cystine knot as typical structural motif of BMP monomers (light grey; bonds between positions 37/103, 66/135, 70/137) and the cysteine contributing to the interchain disulfide bond between monomers of dimeric ligands (dark grey). Homology was calculated based on the overlapping sequence regions of BMP pairs.

1.5   Aim of this PhD work

Based on the raised questions concerning the effects of BMPs on human pluripotent stem cells, the objectives of the present study were:

I.   To comparatively test whether BMP5, BMP10 and BMP13 induce differentiation of hESCs under chemically-defined conditions in the absence of exogenous bFGF; and if so, to which cell lineage.

II. To identify similarities and differences in early cellular responses with respect to signal transduction downstream of BMP receptors and genome-wide transcriptional changes.

III. To investigate how comparable hiPSCs are to hESCs with respect to their signaling properties and differentiation capabilities upon stimulation with the distinct BMPs.

IV. Finally, to derive a hypothesis regarding the mechanism of action of individual ligands on the regulation of self-renewal and pluripotency of hESCs and hiPSCs.

2 Materials

All materials were stored according to the recommended conditions of the manufacturers. These may include a certain temperature range, protection from light and preparation of small aliquots. Companies are listed together with the country in which their headquarters is located.

2.1 Inorganic and organic chemicals

Basic chemicals were of analytical grade (purity ≥ 99 %), unless stated otherwise.

Table 2-1   List of inorganic and organic chemicals.
In alphabetical order.

Chemical	Company	Catalog #
Acetic acid (96 %)	Merck, Germany	1.00062.2500
Acrylamide/bis-acrylamide (30 % / 0.8 %; 37.5:1)	Carl Roth, Germany	3029.1
Agarose, standard	Carl Roth, Germany	3810.3
Agarose, low range ultra	Bio-Rad, USA	161-3106
Ammonium peroxydisulfate (APS)	Carl Roth, Germany	9592.3
Ampicillin sodium salt	Carl Roth, Germany	HP62.1
B-27® Supplement minus vitamin A (50X), liquid	Gibco/Invitrogen, USA	12587-010
Bacto™ agar	Becton Dickinson, USA	214030
Bacto™ tryptone	Becton Dickinson, USA	211705
Bacto™ yeast extract	Becton Dickinson, USA	288620
Boric acid (H_3BO_3)	Merck, Germany	1.00165.0500
Bovine serum albumin (BSA), lyophilized powder	Sigma-Aldrich, USA	A3059-50G
Bovine serum albumin (BSA), solution (30 % in DPBS; cell culture / GMP grade)	Sigma-Aldrich, USA	A9576
Bromophenol blue sodium salt	Sigma-Aldrich, USA	B5525-5G
Calcium chloride dihydrate ($CaCl_2 \bullet 2H_2O$)	Sigma-Aldrich, USA	C7902-500G
Chang Medium® B (liquid basal) and C (lyophilized supplement)	Irvine Scientific, USA	T101-019
DAPI (4',6-diamidino-2-phenylindole dihydrochloride)	Invitrogen, USA	D1306
Dimethylformamide	Sigma-Aldrich, USA	D4551
Dimethyl sulphoxide (DMSO)	Sigma-Aldrich, USA	D2650
Disodium hydrogen phosphate dihydrate ($Na_2HPO_4 \bullet 2H_2O$)	Merck, Germany	1.06580.1000
Dithiothreitol (DTT) (1.25 M solution)	New England Biolabs, USA	B7703S
DMEM Dulbecco's Modified Eagle Medium (1X) [+] 4.5 g/l glucose, [+] L-glutamine, [+] pyruvate	Gibco/Invitrogen, USA	41966-029
DMEM/F-12 (1:1) (1X) Dulbecco's Modified Eagle Medium / Ham's F-12 Nutrient Mixture [+] L-glutamine, [+] 15 mM HEPES	Gibco/Invitrogen, USA	31330-038
DNase I set (1500 Kunitz units)	Qiagen, Germany	79254
dNTP mix (deoxyribonucleotide triphosphates) (25 mM dATP, dCTP, dGTP and dTTP)	Jena Bioscience, Germany	NU-1023S
DPBS Dulbecco's Phosphate Buffered Saline (1X) [−] $CaCl_2$, [−] $MgCl_2$	Gibco/Invitrogen, USA	14190-094
Ethanol	Merck, Germany	1.00983.2500

Chemical	Company	Catalog #
Ethidium bromide (EtBr) solution (~ 1 % in H_2O)	Sigma-Aldrich, USA	46067
Ethylenediaminetetraacetic acid (EDTA) tetrasodium salt dihydrate	Sigma-Aldrich, USA	E6511
FACSFlow™ buffer	BD Biosciences, USA	342003
Fetal bovine serum (FBS)	Biochrom, Germany	S 0115
Fetal bovine serum, embryonic stem cell-qualified (ES-FBS)	Gibco/Invitrogen, USA	10439-016
Gelatin from bovine skin, type B (gel strength ~ 225 g Bloom)	Sigma-Aldrich, USA	G9382
Glycerol (87 %)	Merck, Germany	1.04094.1000
Glycine	Merck, Germany	1.04201.1000
HEPES, free acid	Calbiochem, USA	391338
Hexadimethrine bromide (Polybrene®)	Sigma-Aldrich, USA	107689
Hydrochloric acid (HCl) (fuming 37 %)	Merck, Germany	1.00317.2500
HyperLadder™ V DNA ladder (25–500 bp; 192 ng/µl)	Bioline, Germany	BIO-33031
IMDM Iscove's Modified Dulbecco's Medium (1X) [+] L-glutamine, [+] 25 mM HEPES	Gibco/Invitrogen, USA	21980-032
Isopropanol	Merck, Germany	1.09634.2500
KnockOut™ DMEM [+] 4.5 g/l D-glucose, [+] sodium pyruvate, [−] L-glutamine	Gibco/Invitrogen, USA	10829-018
KnockOut™ Serum Replacement	Gibco/Invitrogen, USA	10828-028
L-glutamine (200 mM in 0.85 % NaCl solution; 100X)	Lonza, Switzerland	BE17-605F
Matrigel™ basement membrane matrix, growth factor reduced; source: Engelbreth-Holm-Swarm (EHS) mouse sarcoma (~ 10 mg/ml)	BD Biosciences, USA	356231
2-mercaptoethanol (β-mercaptoethanol) (pure)	Sigma-Aldrich, USA	M7522
2-mercaptoethanol (50 mM in DPBS; 500X)	Gibco/Invitrogen, USA	31350-010
Methanol	Merck, Germany	1.06009.2500
Minimum Essential Medium (MEM) Alpha (1X) [+] GlutaMAX™, [+] ribonucleosides, [+] deoxyribonucleosides	Gibco/Invitrogen, USA	32571-028
Mitomycin C from *Streptomyces caespitosus* (per vial: 2 mg + 48 mg NaCl)	Sigma-Aldrich, USA	M0503
M-MLV reaction buffer (5X)	USB/Affymetrix, USA	71505
M-MLV reverse transcriptase (200 units/µl)	USB/Affymetrix, USA	78306
N-2 Supplement (100X), liquid	Gibco/Invitrogen, USA	17502-048
NEBuffer 3 (10X)	New England Biolabs, USA	B7003S
NEBuffer 4 (10X)	New England Biolabs, USA	B7004S
Non-essential amino acids (10 mM; 100X)	Lonza, Switzerland	BE13-114E
*Not*I restriction enzyme (10,000 U/ml)	New England Biolabs, USA	R0189
PageRuler™ prestained protein ladder (10–170 kDa)	Fermentas, USA	SM0671
Paraformaldehyde (PFA) (16 % aqueous solution; EM grade)	Electron Microscopy Sciences, USA	15710
Penicillin/streptomycin (each 10,000 U/ml; 100X)	Lonza, Switzerland	DE17-602E
Perfect Plus™ 1 kb DNA ladder (0.25–10 kbp; 100 ng/µl)	Roboklon, Germany	E3131-01
Phosphatase inhibitor cocktail tablets PhosSTOP	Roche, Switzerland	4906845001
Phusion® HF buffer (5X)	Finnzymes, Finland	F-518L
Phusion® Hot Start II high-fidelity DNA polymerase (2 U/µl)	Finnzymes, Finland	F-549S
Ponceau S	Sigma-Aldrich, USA	P3504
Potassium chloride (KCl)	Merck, Germany	1.04936.1000

Chemical	Company	Catalog #
Potassium dihydrogen phosphate (KH_2PO_4)	Merck, Germany	1.04873.1000
Protease inhibitor cocktail tablets cOmplete Mini, EDTA-free	Roche, Switzerland	11836170001
Random primers (oligodeoxyribonucleotides, mostly hexamers; 3 µg/µl)	Invitrogen, USA	58875
RNaseZap® spray	Ambion/Invitrogen, USA	AM9782
Skim milk powder (non-fat dry milk powder)	Gedimex, Belgium	SKIM 23
Sodium chloride (NaCl)	Merck, Germany	1.06404.1000
Sodium deoxycholate	Sigma-Aldrich, USA	D6750-100G
Sodium dodecyl sulfate (SDS)	Bio-Rad, USA	161-0301
Sodium hydroxide (NaOH)	Merck, Germany	1.06498.1000
Sodium pyruvate (100 mM; 100X)	Gibco/Invitrogen, USA	11360-039
SYBR® Green PCR master mix (2X)	Applied Biosystems, USA	4309155
Tetramethylethylenediamine (TEMED)	Carl Roth, Germany	2367.3
Titanium™ Taq DNA polymerase (50X)	Clontech, USA	639208
Tris(hydroxymethyl)aminomethane (Tris base)	Merck, Germany	1.08382.0500
Triton® X-100	Sigma-Aldrich, USA	T8532-100ML
Trypan blue solution (0.4 %)	Sigma-Aldrich, USA	T8154
Trypsin-EDTA (0.05 %; 1X)	Gibco/Invitrogen, USA	25300-054
Tween® 20	Sigma-Aldrich, USA	P1379-500ML
Valproic acid (VPA) sodium salt	Calbiochem, USA	676380-5GM
Water, double-distilled (ddH2O)	Prepared at the Max-Planck-Institute	n/a
Water for injection (WFI; cell culture grade)	Gibco/Invitrogen, USA	A12873-01
Water, ultrapure (LiChrosolv®; HPLC grade)	Merck, Germany	1.15333.2500
*Xho*I restriction enzyme (20,000 U/ml)	New England Biolabs, USA	R0146
X-ray film developer G 153, component A & B	Agfa, Belgium	HT536
X-ray film rapid fixer G 354	Agfa, Belgium	2828Q

2.2 Kits

Table 2-2   List of kits.
In alphabetical order.

Kit	Company	Catalog #
Alkaline Phosphatase Detection Kit	Millipore, USA	SCR004
Amersham™ ECL™ Prime Western Blotting Detection Reagent Kit	GE Healthcare, UK	RPN2232
Human Chorionic Gonadotropin (HCG) ELISA Kit	BQ Kits, USA	BQ 047F
HumanHT-12 v4.0 Expression BeadChip Kit	Illumina, USA	BD-103-0604
HumanRef-8 v3.0 Expression BeadChip Kit	Illumina, USA	BD-102-0603
Illumina® TotalPrep™ RNA Amplification Kit	Ambion/Invitrogen, USA	AMIL1791
NucleoBond® Xtra Maxi EF Kit	Macherey-Nagel, Germany	740424.50
Pierce® BCA Protein Assay Kit	Thermo Scientific, USA	23227
PureLink® Genomic DNA Mini Kit (including RNAse A and Proteinase K)	Invitrogen, USA	K1820-02
RNeasy® Mini Kit	Qiagen, Germany	74106
Senescence β-Galactosidase Staining Kit	Cell Signaling Technology, USA	9860
TRAPEZE® RT Telomerase Detection Kit	Chemicon/Millipore, USA	S7710

2.3 Antibodies

Table 2-3   List of primary antibodies.
In alphabetical order.

Human antigen	Immunogen used for antibody production	Host species	Antibody isotype	Clonality[1]	Company	Catalog # (Batch)	Application[2] IC	WB
Akt (pan)	Synthetic peptide at the C-terminal sequence of mouse Akt	Rabbit	IgG	C67E7	Cell Signaling, USA	4691 (Ref: 11/2010, Lot: 11)		x
phospho-Akt (Ser473)	Synthetic phosphopeptide corresponding to residues surrounding Ser473 of mouse Akt	Mouse	IgG2b	587F11	Cell Signaling, USA	4051 (Ref: 08/2010, Lot: 13)		x
Brachyury	*E.coli*-derived recombinant human Brachyury (amino acids 2–202)	Goat	IgG	polyclonal	R&D Systems, USA	AF2085	x	
Cytokeratin-7	Ovarian carcinoma cell line OTN 11	Mouse	IgG1, κ	OV-TL 12/30	Dako, Denmark	M7018	x	x
E-Cadherin	Synthetic peptide corresponding to the sequence surrounding residue 780 of human E-Cadherin	Rabbit	IgG	24E10	Cell Signaling, USA	3195	x	
ERK1/2 (p44/42)	Synthetic peptide (KLH-coupled) derived from the sequence of p42 MAPK	Mouse	IgG1	L34F12	Cell Signaling, USA	4696 (Ref: 08/2010, Lot: 6)		x
phospho-ERK1/2 (p44/42) (Thr202/Tyr204)	Synthetic phosphopeptide (KLH-coupled) corresponding to residues surrounding Thr202/Tyr204 of human p44 MAPK	Rabbit	IgG	D13.14.4E	Cell Signaling, USA	4370 (Ref: 07/2010, Lot: 6)		x
α-Fetoprotein (AFP)	AFP (amino acids 500–610) partial recombinant protein with GST tag	Mouse	IgG, κ	1G7	Sigma-Aldrich, USA	WH0000174M1	x	
FOXA2 (HNF-3β)	*E.coli*-derived recombinant human HNF-3β (amino acids 242–457)	Goat	IgG	polyclonal	R&D Systems, USA	AF2400	x	
GAPDH	Purified rabbit muscle Glyceraldehyde-3-Phosphate Dehydrogenase (whole molecule)	Mouse	IgG1	6C5	Ambion, USA	AM4300		x
β-hCG	Purified human native protein (full length)	Mouse	IgG1	HCG-60	Abcam, UK	ab763	x	
KLF4 (GKLF)	Epitope corresponding to amino acids 1–180 mapping at the N-terminus of GKLF of human origin	Rabbit	IgG	polyclonal	Santa Cruz, USA	sc-20691	x	
LIN28	*E.coli*-derived human LIN28 GST fusion protein (amino acids 1–209)	Rabbit	IgG	polyclonal	Proteintech, UK	11724-1-AP	x	

Human antigen	Immunogen used for antibody production	Host species	Antibody isotype	Clonality[1]	Company	Catalog # (Batch)	Application[2] IC	WB
c-MYC	Epitope corresponding to amino acids 1−262 of c-MYC of human origin	Rabbit	IgG	polyclonal	Santa Cruz, USA	sc-764	x	
NANOG	*E.coli*-derived recombinant human NANOG (Trp153−Val305)	Goat	IgG	polyclonal	R&D Systems, USA	AF1997	x	x
Nestin	Fusion protein corresponding to human Nestin	Mouse	IgG1	10C2	Millipore, USA	MAB5326	x	
OCT4	Amino acids 1−134 of OCT4 of human origin	Mouse	IgG2b	C-10	Santa Cruz, USA	sc-5279	x	x
p38	Synthetic peptide (KLH-coupled) derived from the sequence of human p38 MAPK	Rabbit	not specified	polyclonal	Cell Signaling, USA	9212 (Ref: 06/2009, Lot: 16)		x
phospho-p38 (Thr180/Tyr182)	Synthetic phosphopeptide corresponding to residues surrounding Thr180/Tyr182 of human p38 MAPK	Rabbit	IgG	D3F9	Cell Signaling, USA	4511 (Ref: 01/2011, Lot: 5)		x
PAX6	Peptide (QVPGSEPDMSQYWPRLQ) derived from the C-terminus of mouse PAX6	Rabbit	not specified	polyclonal	Covance, USA	PRB-278P	x	
SAPK/JNK	Human JNK2/MBP fusion protein	Rabbit	IgG	56G8	Cell Signaling, USA	9258 (Ref: 08/2010, Lot: 7)		x
phospho-SAPK/JNK (Thr183/Tyr185)	Synthetic phosphopeptide (KLH-coupled) corresponding to residues surrounding Thr183/Tyr185 of human SAPK/JNK	Rabbit	IgG	81E11	Cell Signaling, USA	4668 (Ref: 01/2011, Lot: 7)		x
SMAD1	Synthetic peptide corresponding to residues surrounding Ser190 of human SMAD1	Rabbit	not specified	polyclonal	Cell Signaling, USA	9743 (Ref: 12/2010, Lot: 2)		x
phospho-SMAD1/5 (Ser463/465)	Synthetic phosphopeptide (KLH-coupled) corresponding to residues surrounding Ser463/465 of human SMAD5	Rabbit	IgG	41D10	Cell Signaling, USA	9516 (Ref: 05/2011, Lot: 2)		x
α-Smooth Muscle Actin	N-terminal synthetic decapeptide of α-Smooth Muscle Actin	Mouse	IgG2a, κ	1A4	Dako, Denmark	M0851	x	
SOX2	Peptide mapping near the C-terminus of SOX2 of human origin	Goat	IgG	polyclonal	Santa Cruz, USA	sc-17320	x	
SOX17	*E.coli*-derived recombinant human SOX17 (amino acids 177−414)	Goat	IgG	polyclonal	R&D Systems, USA	AF1924	x	
SSEA-4	Human embryonal carcinoma cell line 2102Ep	Mouse	IgG3, κ	MC-813-70	Millipore, USA	90231	x	

Human antigen	Immunogen used for antibody production	Host species	Antibody isotype	Clonality[1]	Company	Catalog # (Batch)	Application[2]	
							IC	WB
Syncytin-1	Amino acids 33–312 mapping near the N-terminus of Syncytin (HERV-W gene) of human origin	Rabbit	IgG	polyclonal	Santa Cruz, USA	sc-50369	x	
TRA-1-60	Human embryonal carcinoma cell line 2102Ep	Mouse	IgM	TRA-1-60	Millipore, USA	90232	x	
TRA-1-81	Human embryonal carcinoma cell line 2102Ep	Mouse	IgM	TRA-1-81	Millipore, USA	90233	x	
Tubulin Beta-3 Chain (βIII-Tubulin)	Synthetic peptide corresponding to the C-terminal sequence of human βIII-Tubulin coupled to BSA	Mouse	IgG2b	SDL.3D10	Sigma-Aldrich	T8660	x	

[1] For monoclonal antibodies: The name of the B cell hybridoma clone is mentioned below.

[2] Antibody application for this PhD work: IC = immunocytochemistry, WB = western immunoblot.

The specificity of antibodies directed against phosphorylated (p-) species of protein kinases was confirmed by means of positive (+) and negative (−) control cell extracts (all purchased from Cell Signaling, USA):

- p-Akt: Total cell extracts from Jurkat cells, serum starved overnight and then treated with calyculin A (+) or with 50 µM LY294002 (−) for 1 h (#9273; Ref: 03/2011, Lot: 19).
- p-ERK1/2: Total cell extracts from Jurkat cells treated with TPA at 200 nM for 10 min (+) or with U0126 (Mek1/2 inhibitor) at 10 µM for 1 h (−) (#9194; Ref: 06/2011, Lot: 6).
- p-p38: Total cell extracts from C-6 glioma cells treated with anisomycin (+) or untreated (−) (#9213; Ref: 10/2011, Lot: 41).
- p-SAPK/JNK: Total cell extracts from 293 cells treated with UV light (+) or untreated (−) (#9253; Ref: 01/2011, Lot: 38).

Table 2-4   List of secondary antibodies.

Antigen	Host species	Antibody labeling	Antibody conjugate	Company	Catalog #	Application[1]	
						IC	WB
Goat IgG (Fc fragment)	Rabbit	n/a	Horseradish peroxidase	Calbiochem, USA	401504		x
Goat IgG (H+L)	Chicken	red-fluorescent Alexa Fluor® 594	n/a	Invitrogen, USA	A-21468	x	
Goat IgG (H+L)	Donkey	green-fluorescent Alexa Fluor® 488	n/a	Invitrogen, USA	A-11055	x	
Mouse IgG	Sheep	n/a	Horseradish peroxidase	GE Healthcare, UK	NA9310		x
Mouse IgG (H+L)	Chicken	red-fluorescent Alexa Fluor® 594	n/a	Invitrogen, USA	A-21201	x	
Mouse IgG (H+L)	Goat	green-fluorescent Alexa Fluor® 488	n/a	Invitrogen, USA	A-11001	x	
Mouse IgG (H+L)	Goat	red-fluorescent Alexa Fluor® 594	n/a	Invitrogen, USA	A-11005	x	
Rabbit IgG	Goat	n/a	Horseradish peroxidase	Calbiochem, USA	DC03L		x
Rabbit IgG (H+L)	Chicken	red-fluorescent Alexa Fluor® 594	n/a	Invitrogen, USA	A-21442	x	
Rabbit IgG (H+L)	Donkey	green-fluorescent Alexa Fluor® 488	n/a	Invitrogen, USA	A-21206	x	
Rabbit IgG (H+L)	Goat	orange-fluorescent Alexa Fluor® 546	n/a	Invitrogen, USA	A-11010	x	

---

[1] Antibody application for this PhD work: IC = immunocytochemistry, WB = western immunoblot.

2.4 Plasmids

All plasmids were amplified in *Escherichia coli* (*E.coli*) bacteria and then purified (Chapter 3.6.1). The identity of the four plasmids encoding the reprogramming factors (human OCT4, SOX2, KLF4 and c-MYC) was confirmed by diagnostic restriction enzyme digestion (Chapter 3.6.2).

Table 2-5   List of plasmids.

Plasmid	Company / Institute	Encoded proteins for retroviral vector production	Bacterial antibiotic resistance gene	Diagnostic restriction enzyme digestion	
				Restriction enzyme	Expected DNA fragments[1] [bp]
pMXs-hOCT3/4[2]	Addgene, USA[3]; #17217	human OCT4	*ampR*	*Xho*I	5700 → 4930 + 400 + 370
pMXs-hSOX2[2]	Addgene, USA[3]; #17218	human SOX2	*ampR*	*Not*I	5560 → 4500 + 1060
pMXs-hKLF4[2]	Addgene, USA[3]; #17219	human KLF4	*ampR*	*Not*I	6020 → 4500 + 1520
pMXs-hc-MYC[2]	Addgene, USA[3]; #17220	human c-MYC	*ampR*	*Not*I	5920 → 4500 + 1420
pLIB-EGFP	Clontech, USA	Enhanced Green Fluorescent Protein (eGFP)	*ampR*		
Packaging plasmid		retroviral Gag-Pol (core structural proteins and enzymes from Moloney murine leukemia virus (M-MLV))	*ampR*		
Envelope plasmid		retroviral VSV-G (envelope glycoprotein from vesicular stomatitis virus (VSV))	*ampR*		

[1] Lengths were calculated according to the individual plasmid maps under assumption of a 100 % complete digestion.

[2] Transfer vector plasmids encoding the four reprogramming factors were generated by the Yamanaka lab (Kyoto University, Japan; Takahashi et al., 2007). They consist of the pMXs vector backbone generated by Toshio Kitamura (University of Tokyo, Japan; Kitamura et al., 2003) with open reading frames of human OCT4, SOX2, KLF4 and c-MYC cloned into.

[3] Addgene is a non-profit plasmid repository that collects, stores and distributes plasmids worldwide for use in scientific research (http://www.addgene.org).

2.5 Primers

Primers were purchased from either Eurofins MWG Operon (Germany) or BioTeZ (Germany). Lyophilized primers were resuspended in ultrapure water (HPLC grade) to generate stock solutions of 100 µM. Based on those stock solutions, working solutions containing 5 µM forward and 5 µM reverse primer were prepared for all individual primer pairs. Stock and working solutions were stored at −20 °C.

Table 2-6   List of primers for PCR of human genomic DNA.

Primer pair		Sequence (5′ → 3′)	Length [bp]	% GC	T_m [°C][1]	Product length [bp]
For STR analysis of cell lines[2]:						
D7S796	forward	TTTTGGTATTGGCCATCCTA	20	40.0	51.5	variable
	reverse	GAAAGGAACAGAGAGACAGGG	21	52.4	54.8	
D10S1214	forward	ATTGCCCCAAAACTTTTTTG	20	35.0	50.2	variable
	reverse	TTGAAGACCAGTCTGGGAAG	20	50.0	54.1	
D17S1290	forward	GCAACAGAGCAAGACTGTC	19	52.6	53.8	variable
	reverse	GGAAACAGTTAAATGGCCAA	20	40.0	51.2	
D21S2055	forward	AACAGAACCAATAGGCTATCTATC	24	37.5	52.0	variable
	reverse	TACAGTAAATCACTTGGTAGGAGA	24	37.5	52.8	
For sex determination of cell lines[3]:						
AMEL	forward	CCCTGGGCTCTGTAAAGAATAGTG	24	50.0	57.0	X chromosome (*AMELX* gene): 106 bp
	reverse	ATCAGAGCTTAAACTGGGAAGCTG	24	45.8	57.0	Y chromosome (*AMELY* gene): 112 bp
SRY	forward	ATAAGTATCGACCTCGTCGGAA	22	45.5	55.0	X chromosome: n/a
	reverse	GCACTTCGCTGCAGAGTACCGA	22	59.1	61.5	Y chromosome (*SRY* gene): 93 bp

---

[1] Melting temperature (T_m) of primers was calculated using OligoAnalyzer 3.1 (Table 2-16) based on the default settings of the software.

[2] Primer reference: Park et al., 2008.

[3] Primer references: Mannucci et al., 1994 (AMEL); Santos et al., 1998 (SRY).

Table 2-7 List of primers for real-time qPCR of human cDNA.
In alphabetical order. Criteria for primer design and validation are described in Chapter 3.8.1.4.

Gene	Primer	Sequence (5′ → 3′)	Length [bp]	% GC	T_m [°C][1]	Transcript	Accession number mRNA RefSeq[2]	Strand on template	Start	Stop	Product length [bp]	Exon junction location on mRNA[3]	Intron size [bp] and intron location on genomic DNA[4]
ACTA2	forward reverse	GCGTGGCTATTCCTTCGTTACT CACAGTTTCTCCTTGATGTCCC	22 22	50.0 50.0	57.1 55.6	variant 1	NM_001141945.1	plus minus	1066 1131	1087 1110	66	n/a	1530 (41505450–41503919 on NT_030059.13)
						variant 2	NM_001613.2	plus minus	707 772	728 751			
AFP	forward reverse	CTTCTTTGGGCTGCTCGCTA CTGTTGCTGCCTTTGTTTGGAA	20 22	55.0 45.5	57.6 56.7		NM_001134.1	plus minus	582 672	601 651	91	662/663	n/a
CD34	forward reverse	TGGCTGTCTTGGGCATCACT GGTTCCAGCTCCAGCCTTTC	20 20	55.0 60.0	59.3 58.5	variant 2	NM_001773.2	plus minus	1160 1241	1179 1222	82	1230/1231	n/a
CDX2	forward reverse	GGCAGCCAAGTGAAAACCAG CGGATGGTGATGTAGCGACT	20 20	55.0 55.0	57.1 56.8		NM_001265.4	plus minus	706 815	725 796	110	715/716	n/a
CGA	forward reverse	ATCCCACTCCACTAAGGTCCA AGTCATCAAGACAGCACTTGGT	21 22	52.4 45.5	57.4 56.4	variant 1	NM_001252383.1	plus minus	417 615	437 594	199	n/a	416 (25915802–25915385 on NT_007299.13)
						variant 2	NM_000735.3	plus minus	324 522	344 501			
CGB genes	forward reverse	GTGCATCACCGTCAACACCA CACATCGCGGTAGTTGCACA	20 20	55.0 55.0	58.2 58.1	CGB gene	NM_000737.3	plus minus	500 611	519 592	112	n/a	235 (21794911–21794675 on NT_011109.16)
						CGB1 gene	NM_033377.1	plus minus	352 463	371 444			235 (21807611–21807375 on NT_011109.16)
						CGB2 gene	NM_033378.1	plus minus	352 463	371 444			235 (21804146–21804382 on NT_011109.16)
						CGB5 gene	NM_033043.1	plus minus	500 611	519 592			235 (21816219–21816455 on NT_011109.16)
						CGB7 gene	NM_033142.1	plus minus	500 611	519 592			235 (21826316–21826080 on NT_011109.16)
						CGB8 gene	NM_033183.2	plus minus	507 618	526 599			235 (21819680–21819444 on NT_011109.16)
DAZL	forward	CCTGCCGCCATCATGTCTAC	20	60.0	58.2	variant 2	NM_001351.3	plus	283	302	97	297/298	n/a

Gene	Primer	Sequence (5′ → 3′)	Length [bp]	% GC	T_m [°C][1]	Transcript	Accession number mRNA RefSeq[2]	Strand on template	Start	Stop	Product length [bp]	Exon junction location on mRNA[3]	Intron size [bp] and intron location on genomic DNA[4]
	reverse	CTTGGCTGGTTGCAGCTGAT	20	55.0	58.5			minus	379	360			
FLK1	forward	TCCCTGCCGTGTTGAAGAGTT	21	52.4	58.9		NM_002253.2	plus	5196	5216	118	n/a	n/a
	reverse	CATTGAACCTCCCGCATTCA	20	50.0	55.6			minus	5313	5294			
FOXA2	forward	GTATGCTGGGAGCGGTGAA	19	57.9	57.5	variant 1	NM_021784.4	plus	202	220	96	n/a	1037 (22504830−22503792 on NT_011387.8)
	reverse	TCATGTTGCTCACGGAGGAG	20	55.0	57.0			minus	297	278			
						variant 2	NM_153675.2	plus	189	207			
								minus	284	265			
GAPDH	forward	CTGGTAAAGTGGATATTGTTGCCAT	25	40.0	55.5	variant 1	NM_002046.4	plus	248	272	81	303/304	n/a
	reverse	TGGAATCATATTGGAACATGTAAACC	26	34.6	53.7			minus	328	303			
						variant 2	NM_001256799.1	plus	272	296	81	327/328	n/a
								minus	352	327			
GATA4	forward	GCCCGACACCCCAATCTC	18	66.7	58.6		NM_002052.3	plus	1152	1169	122	n/a	39990 (4041788−4081779 on NT_077531.4)
	reverse	GCGTTGCACAGATAGTGACC	20	55.0	56.2			minus	1273	1254			
GATA6	forward	TGTGCGTTCATGGAGAAGATCA	22	45.5	56.4		NM_005257.4	plus	2473	2494	83	n/a	n/a
	reverse	TTTGATAAGAGACCTCATGAACCGACT	27	40.7	57.5			minus	2555	2529			
GCM1	forward	TCTCTTCACCTACGCCTCTCATC	23	52.2	57.7		NM_003643.3	plus	1376	1398	101	n/a	n/a
	reverse	GATCCAAACCCAAGTATGTCATTTC	25	40.0	54.2			minus	1476	1452			
HAND1	forward	AGGCTGAACTCAAGAAGGCG	20	55.0	57.5		NM_004821.2	plus	744	763	120	n/a	1555 (15019953−15018397 on NT_029289.11)
	reverse	CGGTGCGTCCTTTAATCCTCT	21	52.4	57.0			minus	863	843			
HERV-FRD	forward	TTTGTCTCCTCTCGCCTTCAG	21	52.4	56.7		NM_207582.2	plus	2010	2030	140	n/a	n/a
	reverse	AGGATTTCGCCTCTGTCGTG	20	55.0	57.2			minus	2149	2130			
HERV-W	forward	CTGGCATTGGCGGTATCACA	20	55.0	57.9	variant 1	NM_014590.3	plus	2047	2066	182	n/a	n/a
	reverse	TCCCCCTCTTTCAGCGGTTA	20	55.0	58.2			minus	2228	2209			
						variant 2	NM_001130925.1	plus	1765	1784			
								minus	1946	1927			
HLA-G	forward	GAAAAGGAGGGAGCTACTCTC	21	52.38	54.3		NM_002127.5	plus	1194	1214	103	n/a	357 (29738187−29738545 on NT_007592.15)
	reverse	CAAAGAGGAGTCAGGGTTCTTG	22	50.0	55.3			minus	1296	1275			
KRT7	forward	AGATCGCCACCTACCGCAAG	20	60.0	59.6		NM_005556.3	plus	1290	1309	74	n/a	2544 (14782722−14785267 on NT_029419.12)
	reverse	ATTCACGGCTCCCACTCCAT	20	55.0	58.8			minus	1363	1344			

Gene	Primer	Sequence (5′ → 3′)	Length [bp]	% GC	T_m [°C][1]	Transcript	Accession number mRNA RefSeq[2]	Strand on template	Start	Stop	Product length [bp]	Exon junction location on mRNA[3]	Intron size [bp] and intron location on genomic DNA[4]
MIXL1	forward reverse	TACCCCGACATCCACTTGC AATCTCCGGCCTAGCCAAAG	19 20	57.9 55.0	57.2 57.2		NM_031944.1	plus minus	328 471	346 452	144	n/a	1432 (19929554–19930987 on NT_167186.1)
NANOG	forward reverse	CCTGTGATTTGTGGGCCTG GACAGTCTCCGTGTGAGGCAT	19 21	57.9 57.1	56.5 59.1		NM_024865.2	plus minus	292 369	310 349	78	367/368	n/a
NES	forward reverse	CTCAGCTTTCAGGACCCCAA GAGCAAAGATCCAAGACGCC	20 20	55.0 55.0	57.1 56.3		NM_006617.1	plus minus	1103 1177	1122 1158	75	1115/1116	n/a
OCT4 (*POU5F1*)	forward reverse	GTGGAGGAAGCTGACAACAA ATTCTCCAGGTTGCCTCTCA	20 20	50.0 50.0	55.2 55.8	variant 1	NM_002701.4	plus minus	676 795	695 776	120	n/a	284 (31073348–31073063 on NT_007592.15)
						variant 2	NM_203289.4	plus minus	1008 1127	1027 1108			
						variant 3	NM_001173531.1	plus minus	522 641	541 622			
PAX6	forward reverse	CCTATGCCCAGCTTCACCAT ATAACTCCGCCCATTCACCG	20 20	55.0 55.0	57.4 57.4	variant 1	NM_000280.4	plus minus	1546 1662	1565 1643	117	n/a	2577 (31754986–31752408 on NT_009237.18)
						variant 2	NM_001604.5	plus minus	1490 1606	1509 1587			
						variant 3	NM_001127612.1	plus minus	1460 1576	1479 1557			
						variant 4	NM_001258462.1	plus minus	1502 1618	1521 1599			
						variant 5	NM_001258463.1	plus minus	1440 1556	1459 1537			
						variant 6	NM_001258464.1	plus minus	1448 1564	1467 1545			
						variant 7	NM_001258465.1	plus minus	1434 1550	1453 1531			
SOX7	forward reverse	TGCCCACTTCATGCAACTCC AGGTACCCTGGGTCTTTGGTCA	20 22	55.0 54.5	58.2 60.0		NM_031439.2	plus minus	2308 2417	2327 2396	110	n/a	n/a
SOX17	forward reverse	CAAGATGCTGGGCAAGTCG CTCTGCCTCCTCCACGAAG	19 19	57.9 63.2	56.6 57.4		NM_022454.3	plus minus	501 570	519 552	70	511/512	n/a

Gene	Primer	Sequence (5′ → 3′)	Length [bp]	% GC	T_m [°C][1]	Transcript	Accession number mRNA RefSeq[2]	Strand on template	Start	Stop	Product length [bp]	Exon junction location on mRNA[3]	Intron size [bp] and intron location on genomic DNA[4]
SYCP3	forward reverse	AGCAGTGGGATTTAGATATGCAGA TGTTTTCAATCTCTGGCTCTGAAC	24 24	41.7 41.7	55.9 55.4	variant 1	NM_001177949.1	plus minus	540 661	563 638	122	n/a	1908 (64270659–64268750 on NT_029419.12)
						variant 2	NM_153694.4	plus minus	536 657	559 634			
						variant 3	NM_001177948.1	plus minus	525 646	548 623			
T	forward reverse	CCTCGAATCCACATAGTGAGAGT GCTGTGATCTCCTCGTTCTGAT	23 22	47.8 50.0	55.8 56.5	variant 1	NM_003181.3	plus minus	1021 1133	1043 1112	113	1125/1126	n/a
						variant 2	NM_001270484.1	plus minus	928 1040	950 1019	113	1032/1033	
VASA	forward reverse	GGATGTTCCTGCATGGTTGGA GTGCTCTTGCCCTTTCTGGTA	21 21	52.4 52.4	57.7 57.3	variant 1	NM_024415.2	plus minus	2094 2207	2114 2187	114	2196/2197	n/a
						variant 2	NM_001142549.1	plus minus	1992 2105	2012 2085	114	2094/2095	
						variant 3	NM_001166533.1	plus minus	2034 2147	2054 2127	114	2136/2137	
						variant 4	NM_001166534.1	plus minus	1593 1706	1613 1686	114	1695/1696	

[1] Melting temperature (T_m) of primers was calculated using OligoAnalyzer 3.1 (Table 2-16) based on the default settings of the software.

[2] Accession number for the human mRNA Reference Sequence (RefSeq) stored in the RefSeq collection database of the National Center for Biotechnology Information (NCBI) (Table 2-17).

[3] For primers annealing on exon junctions: The location of the exon junction on the human mRNA RefSeq is mentioned below.

[4] For intron-spanning primers: The size of the intron and its location on the human genomic DNA RefSeq stored in NCBI's RefSeq collection database is mentioned below.

2.6 Recombinant human proteins

Table 2-8   List of recombinant human proteins.
In alphabetical order.

Protein	Company	Catalog # (Lot #)	Source[1]	Accession number[2]	Region and length [aa][3]	MW [kDa][4]	Purity[5]
bFGF (FGF2)	Peprotech, USA	100-18B	*E.coli*	P09038	Ala135–Ser288 (154)	17.1	> 95 %
BMP4	R&D Systems, USA	314-BP-010 (BEM6511041)	NS0	P12644	Ser293–Arg408 (116)	13.1	> 95 %
BMP5	R&D Systems, USA	615-BMC-020 (SXV0209062, SXV0310081, SXV0310111)	CHO	P22003	Ala317–His454 (138)	15.6	> 95 %
BMP6	Peprotech, USA	120-06 (0609461-1 (F1009))	HEK293	P22004	Val397–His513 (117)	13.1	> 95 %
BMP7	Peprotech, USA	120-03 (0307S264 (H4210), 0711264 (G1811))	CHO	P18075	Ala316–His431 (116)	13.1	> 98 %
BMP10	R&D Systems, USA	2926-BP-025 (QAL0211021)	CHO	O95393	Asn317–Arg424 (108)	12.2	> 97 %
BMP13 (GDF6)	Peprotech, USA	120-04 (0104272 (E054))	*E.coli*	Q6KF10	Thr336–Arg455 (120)	13.6	> 95 %

[1] Expression systems: NS0 = murine myeloma cell line, CHO = Chinese hamster ovary cell line, HEK293 = human embryonic kidney cells, *E.coli* = *Escherichia coli* bacteria. The mature protein forms of bFGF and BMP13 do not contain post-translational modifications such as glycosylations, whose absence due to production in non-eukaryotic cells would impair their biological activity.

[2] Accession number for the protein entry stored in the Universal Protein (UniProt) resource database (Table 2-17).

[3] Region (N- → C-terminus) and length of the recombinant human proteins correspond to their natural (wild-type) biologically active mature forms which lack the signal- and pro-peptide as result of proteolytic cleavage of the inactive precursors. Native BMPs are disulfide-linked homodimers.

[4] Average molecular weight (MW) of the mature polypeptide chain (monomer) was determined using the Compute pI/Mw tool (Table 2-16) based on the default settings of the software.

[5] Purity and biological activity of the recombinant human proteins were certified via established standard assays by the Quality Control of the companies.

Reconstitution and storage of recombinant human proteins:

Lyophilized proteins were reconstituted under aseptic conditions according to the instructions of the manufacturers: bFGF (1 mg per vial) was first resuspended at 1 mg/ml in 0.2 µm sterile-filtered 5 mM Tris-Cl (pH 7.6) and then further diluted to 8 µg/ml in DPBS (cell culture grade) supplemented with 1 % BSA (cell culture / GMP grade) as a carrier protein. BMP4 (10 µg per vial), BMP5 (20 µg per vial) and BMP10 (25 µg per vial) were resuspended at 10 µg/ml in water for injection (WFI; cell culture grade) containing 4 mM HCl and 0.1 % BSA. BMP6 and BMP7 (both 10 µg per vial) were first resuspended at 100 µg/ml in WFI and

then further diluted to 10 µg/ml in DPBS supplemented with 0.1 % BSA. BMP13 (50 µg per vial) was first resuspended at 200 µg/ml in WFI supplemented with 50 µg BSA carrier protein per µg BMP protein and then further diluted to 100 µg/ml in DPBS containing 0.1 % BSA. Small aliquots of 40–120 µl protein solution (bFGF: 500 µl) were prepared to avoid repeated freeze-thaw cycles, immediately snap-frozen in liquid nitrogen and then stored at −80 °C.

2.7 Buffer and staining solutions

Only home-made buffer and staining solutions are described here. All commercially purchased solutions are listed in Table 2-1. The solutions were prepared using ddH2O as solvent and stored at room temperature, unless stated otherwise.

Table 2-9   List of compositions of buffer and staining solutions.
In alphabetical order. Component details can be found in Table 2-1 (chemicals).

Solution	Composition	Prepared stock concentrate	1X working concentration	Comments
Blocking buffer (1X) (for immunocytochemistry)	FBS in PBS-T buffer		10 % (v/v) FBS in 1X PBS-T buffer	Stored at −20 °C.
Blocking buffer (1X) (for western immunoblotting)	Skim milk powder in TBS-T buffer		5 % (w/v) skim milk powder in 1X TBS-T buffer	Always freshly prepared.
Blotting buffer (1X)	Glycine Tris base Methanol		200 mM 25 mM 15 % (v/v)	Always freshly prepared.
Blue DNA/RNA sample loading buffer (6X)	Glycerol EDTA Bromophenol blue	30 % (v/v) 60 mM 0.25 % (w/v)	5 % (v/v) 10 mM 0.04 % (w/v)	
Blue protein sample loading buffer (3X)	Tris-Cl buffer (pH 6.8) SDS Glycerol Bromophenol blue DTT (1.25 M stock solution)	187.5 mM 6 % (w/v) 30 % (v/v) 0.03 % (w/v) 10 % (v/v)	62.5 mM 2 % (w/v) 10 % (v/v) 0.01 % (w/v) 3.33 % (v/v)	Buffer w/o DTT stored at room temperature. DTT stock solution stored at −20 °C and added immediately before use.
DAPI staining solution (50,000X)	DAPI dissolved in dimethyl-formamide and further diluted in PBS buffer	10 mg DAPI in 2 ml dimethyl-formamide	Stock concentrate diluted to 100 ng/ml in PBS buffer	Stock concentrate stored in aliquots at −20 °C protected from light. 1X staining solution stored at 4 °C protected from light.
HBS (2X) HEPES-buffered saline	NaCl HEPES $Na_2HPO_4 \bullet 2H_2O$	281 mM 100 mM 1.5 mM	140.5 mM 50 mM 0.75 mM	pH 7.12 Stored at −20 °C.
Paraformaldehyde fixing buffer (1X)	PFA in PBS buffer		4 % (w/v) PFA in 1X PBS buffer	Stored at 4 °C.
PBS (10X) Phosphate-buffered saline	NaCl KCl $Na_2HPO_4 \bullet 2H_2O$ KH_2PO_4	1.37 M 27 mM 100 mM 20 mM	137 mM 2.7 mM 10 mM 2 mM	pH 7.4
PBS-T (1X)	Triton® X-100 in PBS buffer		0.1 % (v/v) Triton® X-100 in 1X PBS buffer	
Phosphatase inhibitor cocktail (10X)	Phosphatase inhibitor cocktail tablet PhosSTOP in RIPA lysis buffer	1 tablet in 1 ml RIPA lysis buffer	1 tablet per 10 ml RIPA lysis buffer	Stock concentrate stored in aliquots at −20 °C.
Ponceau S staining solution (1X)	Ponceau S Acetic acid		0.5 % (w/v) 3 % (v/v)	Stored protected from light. Can be reused many times.

Solution	Composition	Prepared stock concentrate	1X working concentration	Comments
Protease inhibitor cocktail (25X)	Protease inhibitor cocktail tablet cOmplete Mini (EDTA-free) in RIPA lysis buffer	1 tablet in 2 ml RIPA lysis buffer	1 tablet per 50 ml RIPA lysis buffer	Stock concentrate stored in aliquots at −20 °C.
RIPA lysis buffer (1X) Radioimmunoprecipitation assay lysis buffer (+ protease and phosphatase inhibitors)	Tris-Cl buffer (pH 7.6)		50 mM	Pure lysis buffer stored at 4 °C. Inhibitor cocktails added immediately prior to usage.
	NaCl		150 mM	
	SDS		0.1 % (w/v)	
	Triton® X-100		1 % (v/v)	
	Sodium deoxycholate		0.5 % (w/v)	
	Protease inhibitor cocktail (25X)		1/25 (v/v)	
	Phosphatase inhibiotor cocktail (10X)		1/10 (v/v)	
SB buffer (20X) Sodium borate buffer	H_3BO_3	800 mM	40 mM	pH 8.0
	NaOH	200 mM	10 mM	
SDS-PAGE running buffer (10X)	Glycine	2 M	200 mM	
	Tris base	250 mM	25 mM	
	SDS	1 % (w/v)	0.1 % (w/v)	
TAE buffer (50X) Tris-acetate-EDTA buffer	Tris base	2 M	40 mM	pH 8.0
	Acetic acid	1 M	20 mM	
	EDTA	50 mM	1 mM	
TBS (10X) Tris-buffered saline	Tris-Cl buffer (pH 7.6)	200 mM	20 mM	
	NaCl	1.37 M	137 mM	
TBS-T (1X)	Tween® 20 in TBS buffer		0.1 % (v/v) Tween® 20 in 1X TBS buffer	
Tris-Cl buffers (0.5 M / pH 6.8) (1.0 M / pH 7.6) (1.5 M / pH 8.8)	Tris base, HCl	individual	individual	Tris base was dissolved in ddH2O at the desired concentration. pH value was adjusted by stepwise addition of smoking HCl under control of a properly pre-calibrated pH meter at room temperature while mixing using a magnetic stirrer. The mixture was finally adjusted to the desired volume by ddH2O.

2.8 Cell culture media

Cell culture media for eukaryotic cell culture were 0.2 µm sterile-filtered using Filtropur V vacuum filtration units. Prepared media were stored at 4 °C and used within 10 days or aliquoted and stored at −20 °C or −80 °C for up to 3 months.

Table 2-10   List of compositions of cell culture media for eukaryotic cells.
In alphabetical order. Component details can be found in Table 2-1 (chemicals).

Medium	Components	Volumes	Final concentrations of supplements
Chang medium	MEM Alpha (1X)	ad 500 ml	
	ES-FBS	75 ml	15 % (v/v)
	Penicillin/streptomycin (10,000 U/ml)	5 ml	100 U/ml
	L-glutamine (200 mM)	5 ml	2 mM
	Chang® B (liquid basal)	90 ml	18 % (v/v)
	Chang® C (lyophilized supplement, dissolved in 10 ml water for injection)	10 ml	2 % (v/v)

Medium	Components	Volumes	Final concentrations of supplements
DMEM medium	DMEM (1X)	ad 500 ml	
	FBS	50 ml	10 % (v/v)
	Penicillin/streptomycin (10,000 U/ml)	5 ml	100 U/ml
	L-glutamine (200 mM)	5 ml	2 mM
	Non-essential amino acids (10 mM)	5 ml	0.1 mM
Freeze media	Freeze Chang medium:		
	Chang medium	ad 10 ml	
	ES-FBS	4.5 ml	51.75 % (v/v)
	DMSO	1 ml	10 % (v/v)
	Freeze DMEM medium:		
	DMEM medium	ad 10 ml	
	FBS	4.5 ml	49.5 % (v/v)
	DMSO	1 ml	10 % (v/v)
	Freeze hESC medium:		
	hESC medium	ad 10 ml	
	KnockOut™ Serum Replacement	4.5 ml	54 % (v/v)
	DMSO	1 ml	10 % (v/v)
hESC medium	KnockOut™ DMEM	ad 500 ml	
	KnockOut™ Serum Replacement	100 ml	20 % (v/v)
	Penicillin/streptomycin (10,000 U/ml)	5 ml	100 U/ml
	L-glutamine (200 mM)	5 ml	2 mM
	Non-essential amino acids (10 mM)	5 ml	0.1 mM
	Sodium pyruvate (100 mM)	5 ml	1 mM
	2-mercaptoethanol (50 mM in DPBS)	1 ml	0.1 mM
	Recombinant human bFGF (8 µg/ml) (Table 2-8)	500 µl	8 ng/ml
Iscove's medium	IMDM (1X)	ad 500 ml	
	FBS	50 ml	10 % (v/v)
	Penicillin/streptomycin (10,000 U/ml)	5 ml	100 U/ml
	L-glutamine (200 mM)	5 ml	2 mM
MEF-conditioned medium (MEF-CM)	= hESC medium pre-conditioned on mitotically inactivated mouse embryonic fibroblasts (MEFs) (as described in Chapter 3.1.2.8)		
N2B27 medium	DMEM/F-12 (1X)	ad 500 ml	
	N-2 Supplement (100X), liquid	5 ml	1X
	B-27® Supplement minus vitamin A (50X), liquid	10 ml	1X
	Penicillin/streptomycin (10,000 U/ml)	5 ml	100 U/ml
	L-glutamine (200 mM)	5 ml	2 mM
	Non-essential amino acids (10 mM)	5 ml	0.1 mM
	2-mercaptoethanol (50 mM in DPBS)	1 ml	0.1 mM
	BSA (30 % in DPBS; cell culture / GMP grade)	800 µl	0.5 mg/ml

Table 2-11   List of compositions of cell culture media for prokaryotic cells.
Component details can be found in Table 2-1 (chemicals).

Medium	Components	Amounts	Final concentrations of supplements
LB medium (pure)[1] Lysogeny broth medium	ddH2O	ad 1 l	
	Bacto™ yeast extract	5 g	0.5 % (w/v)
	Bacto™ tryptone	10 g	1 % (w/v)
	NaCl	10 g	1 % (w/v)

Medium	Components	Amounts	Final concentrations of supplements
LB medium (with selective antibiotic)	Ampicillin (50 mg/ml)[2] in LB medium[3]	1/1000 (v/v)	50 µg/ml
LB agar medium (with selective antibiotic)[4]	LB medium (w/o selective antibiotic)	ad 250 ml	
	Bacto™ agar	3.75 g	1.5 % (w/v)
	Ampicillin (50 mg/ml)[2]	250 µl	50 µg/ml

[1] pH ~ 7.0, then autoclaved.

[2] Ampicillin stock solutions (50 mg/ml in ddH2O; 1000X) were stored in aliquots at −20 °C.

[3] Since ampicillin is heat-sensitive and instable once dissolved, it was added into the LB medium post-autoclaving at room temperature immediately before use.

[4] Preparation of LB agar plates for bacterial growth: LB medium with agar was heated in a microwave until the agar was completely dissolved. Ampicillin was supplemented once the LB agar had cooled down to around 45 °C. The mixture was poured into petri dishes (filling height approx. 5 mm) for polymerization. The dishes were sealed and stored at 4 °C for maximum 1 week.

2.9 Cell lines

Ethics statement:

- Primary human chorionic villi cells were obtained after written informed consent. The utilization of these cells was approved by the Ethics Commission of the Charité – Universitätsmedizin Berlin, Germany.

- Human embryonic stem cell lines H1 and H9 were derived by James A. Thomson (Thomson et al., 1998) at the University of Wisconsin, USA, from redundant human embryos that had been produced by IVF. Both imported cell lines were derived in 1998, which is before the cut-off date of 1st May 2007 as per the currently valid German laws ("Embryonenschutzgesetz" (ESchG) and "Stammzellgesetz" (StZG)). The use of hESCs by our laboratory for research purposes was approved by the Robert-Koch-Institute, Berlin, Germany.

- All work involving living animals for production of mouse embryonic fibroblasts was carried out by qualified personnel.

Table 2-12   List of eukaryotic cell lines.

Cell line	Tissue source	Obtained from
Chorionic villi cells (CV cells)	Chorionic villus sampling during routine prenatal diagnosis (Wegner and Stumm, 2011); no chromosomal abnormalities were detected	Institut für Medizinische Genetik und Humangenetik Prof. Dr. Karl Sperling Charité – Campus Virchow-Klinikum Augustenburger Platz 1 13353 Berlin, Germany http://genetik.charite.de Zentrum für Pränataldiagnostik und Humangenetik Prof. Dr. Rolf-Dieter Wegner Kurfürstendamm 199 10719 Berlin, Germany http://www.kudamm-199.de

Cell line	Tissue source	Obtained from
HEK-293T	Human embryonic kidney	ATCC, USA[1] http://www.atcc.org
hESC line H1	ICM of human male pre-implantation embryo at blastocyst stage	WiCell Research Institute, USA[2] http://www.wicell.org
hESC line H9	ICM of human female pre-implantation embryo at blastocyst stage	
hiPSC lines iPS1 and iPS2	Derived by reprogramming of CV cells via retroviral transduction of human OCT4, SOX2, KLF4 and c-MYC (Chapter 3.2); both hiPSC lines are genetic clones which were derived from the same CV cell line	Generated in the course of this PhD project (Chapter 4.1)
Mouse embryonic fibroblasts (MEFs)	Fibroblasts of mouse embryos of pregnant female mice at day 13 or day 14 post-coitum[3]	Prepared at the Max-Planck-Institute

[1] The American Type Culture Collection (ATCC) is a global non-profit bioresource center.

[2] The WiCell Research Institute is a non-profit organization that distributes human stem cell lines worldwide.

[3] Mouse strain CF-1® (Harlan Laboratories, USA). MEFs were isolated and prepared as demonstrated in this video published by our laboratory (Jozefczuk et al., 2012).

Table 2-13   List of prokaryotic cell lines.

Cell line	Company
Escherichia coli (*E.coli*) bacteria (strain TOP10; premade chemically competent cells)	Invitrogen, USA

2.10 Technical equipment

Table 2-14   List of technical equipment.

Equipment	Company
Centrifuges	
Centrifuge 5417 C	Eppendorf, Germany
Centrifuge 5810 R	Eppendorf, Germany
Savant SpeedVac concentrator centrifuge SVC100H with refrigerated vapor trap RVT400	Thermo Scientific, USA
SORVALL® RC-5 superspeed centrifuge with fixed-angle rotor type GS-3	Du Pont Instruments, USA
Avanti® J-25 high-speed centrifuge with fixed-angle rotor type JA-12	Beckman Coulter, USA
Beckman L7 ultracentrifuge with swinging-bucket rotor type SW-28	Beckman Coulter, USA
Electrophoresis and electroblotting systems	
Horizontal electrophoresis system	Fisherbrand, UK
Mini-PROTEAN® vertical electrophoresis 2-gel system (including 15-well-combs, glass plates, casting stands and casting frames)	Bio-Rad, USA

Equipment	Company
Mini Trans-Blot® electroblotting system (including cassettes and fiber pads)	Bio-Rad, USA
PowerPac™ 300 power supply for electrophoresis & blotting	Bio-Rad, USA
Microscopes and cameras	
Inverted phase-contrast microscope Olympus CK2	Olympus, Japan
Stereo microscope Leica MZ9.5 with cold light source KL 1500 LCD	Leica Microsystems, Germany
Fluorescence microscope Axiovert 200M with camera AxioCam MRm	Zeiss, Germany
Digital camera PowerShot A650 IS	Canon, Japan
PCR machines	
Thermal cycler DNA Engine Dyad® (96-well blocks)	Bio-Rad, USA
7900HT Fast Real-Time PCR System (384- and 96-well blocks)	Applied Biosystems, USA
Pipettes	
PIPETBOY (for 2–50 ml serological pipette tips)	Integra Biosciences, Germany
PIPETMAN Classic™ (P2, P20, P200, P1000; 0.1–1000 µl)	Gilson, USA
PIPETMAN M (P200M)	Gilson, USA
Multi-channel pipette DISCOVERY (12 channel; P200)	Abimed, Germany
Shaker and mixer	
Vortex-Genie 2® vortexer	Scientific Industries, USA
Magnetic stirrer IKA-Combimag REO	IKA / Janke & Kunkel, Germany
Rotating table G10 Gyrotory Shaker	New Brunswick Scientific, USA
Tilting table Rocky®	LTF Labortechnik, Germany
Spectrophotometers	
NanoDrop® 2000 spectrophotometer	Thermo Scientific, USA
SpectraMax® 250 microplate spectrophotometer	Molecular Devices, USA
Temperature control devices	
Liquid nitrogen tanks (−196 °C storage)	Linde, Germany
Ultra low freezer -86C (−80 °C storage; non-defrosting)	Forma Scientific, USA
Freezer (−20 °C storage; non-defrosting)	Bosch, Germany
Fridge (4 °C storage)	Bosch, Germany
ThermoStat Plus (24 × 1.5 ml block) (−5 °C to 99 °C)	Eppendorf, Germany
Water bath with circulation pump Julabo SW 20 (20 °C to 99 °C)	Julabo, Germany
Tissue culture hoods and incubators	
HERAguard® HPH 9 laminar flow clean bench	Heraeus, Germany
HERAsafe® HSP 12 laminar flow clean bench	Heraeus, Germany
Innova® CO-170 CO_2 incubator	New Brunswick Scientific, USA
Other	
AlphaImager™ gel imaging system	Alpha Innotech, USA
Bioruptor® sonication device (12 × 0.5 ml tube holder)	Diagenode, USA
Flow cytometer FACSCalibur™	BD Biosciences, USA
Microwave Privileg 1026	Quelle, Germany
pH meter MP220	Mettler Toledo, Switzerland
Precision balance BP 2100 S	Sartorius, Germany
X-ray film developing machine CURIX 60	Agfa, Belgium

2.11 Consumables and disposables

If necessary, materials were autoclaved at the institute prior to usage or were purchased as gamma-sterilized or DNA/RNA/DNase/RNase-free.

Table 2-15   List of consumables and disposables.
In alphabetical order.

Consumable / Disposable	Company
Cell scrapers and cell spatulas (cell lifters)	TPP, Switzerland
Centrifuge bottles with sealing cap, polypropylene; 500 ml	Beckman Coulter, USA
Centrifuge tubes, polyallomer; 25 × 89 mm	Beckman Coulter, USA
Clear optical reaction plates with optical adhesive films; 96 wells, 384 wells	Applied Biosystems, USA
Conical tubes; 15 ml, 50 ml	Sarstedt, Germany
Cryo 1°C freezing container Nalgene® "Mr. Frosty"	Thermo Scientific, USA
Cryo.s™ freezing tubes with screw cap; 2 ml	Greiner Bio One, Germany
Erlenmeyer flasks; 2 liter	Schott Duran, Germany
Film cassette BAS 2325	Fujifilm, Japan
Filtropur V vacuum filtration units; 0.2 µm pore size, 500 ml	Sarstedt, Germany
Gloves, powder-free textured green nitrile with aloe vera internal coating; M, L	Blossom / Mexpo International, USA
Graduated cylinders FORTUNA®; 1000 ml	Poulten & Graf, Germany
Hypodermic needles BD Microlance™; 19 gauge	Becton Dickinson, USA
Laboratory glass bottles Duran®; 250 ml, 500 ml, 1000 ml	Schott Duran, Germany
Lumi-Film chemiluminescent detection films	Roche, Switzerland
Neubauer chamber (hemocytometer) with 20 × 20 mm coverslips	Marienfeld, Germany
Nitrocellulose membrane Amersham Hybond™; 0.45 µm pore size	GE Healthcare, UK
Parafilm® M	Pechiney Plastic Packaging, USA
Pasteur pipettes, glass; 150 mm	VWR International, Germany
PCR tube strips with lids; 8 × 0.2 ml	Sarstedt, Germany
Petri dishes; 92 × 16 mm	Sarstedt, Germany
Pipette tips, standard; P2, P20/200, P1000 (white, yellow, blue)	Sarstedt, Germany
Pipette tips, with filter; P2, P20, P200, P1000	Biozym Scientific, Germany
Pipette tips, Diamond D200	Gilson, USA
Reaction tubes; 0.5 ml, 1.5 ml, 2.0 ml	Sarstedt, Germany
Round-bottom tubes BD Falcon™, polystyrene; 12 × 75 mm	Becton Dickinson, USA
Serological pipette tips; 2 ml, 5 ml, 10 ml, 25 ml, 50 ml	Sarstedt, Germany
Syringe-driven filters Acrodisc® (Supor® membrane, low protein binding); 0.2 µm pore size	Pall, USA
Syringe-driven filters MILLEX®-HV (Durapore® membrane, low protein binding); 0.45 µm pore size	Millipore, USA
Syringes; 5 ml, 60 ml	Becton Dickinson, USA
Tissue culture dishes; 15 cm	TPP, Switzerland
Tissue culture flasks; 25 cm², 75 cm², 150 cm²	TPP, Switzerland
Tissue culture plates; 6 wells, 12 wells, 96 wells (8.960 cm²/well, 3.596 cm²/well, 0.335 cm²/well)	TPP, Switzerland
Ultra-low attachment dishes; 60 × 15 mm	Corning, USA
Whatman™ filter paper	GE Healthcare, UK

2.12 Software

Table 2-16   List of software.
In alphabetical order.

Software	Company / Institute
AxioVision Rel. 4.8	Zeiss, Germany
CellQuest™Pro Version 4.0.2	BD Biosciences, USA
Clustal Omega Version 1.2.1	EMBL – European Bioinformatics Institute, UK free online tool at: http://www.ebi.ac.uk/Tools/msa/clustalo Sievers et al., 2011
Compute pI/Mw	Swiss Institute of Bioinformatics (SIB), Switzerland free online tool at: http://web.expasy.org/compute_pi Gasteiger et al., 2005
Cyflogic Version 1.2.1	© Perttu Terho / CyFlo Ltd, Finland freeware to download at: http://www.cyflogic.com
GenomeStudio™ V2011.1	Illumina, USA
IrvanView	© Irfan Skiljan freeware to download at: http://www.irfanview.com
MS Office® (Excel, Word, PowerPoint)	Microsoft, USA
Multiexperiment Viewer (MeV) Version 4.8.1	© MeV Development Team / TM4, USA freeware to download at: http://www.tm4.org Saeed et al., 2006
OligoAnalyzer 3.1	Integrated DNA Technologies, USA free online tool at: http://eu.idtdna.com/analyzer/applications/oligoanalyzer
Photoshop®	Adobe, USA
Primer-BLAST	National Center for Biotechnology Information (NCBI), USA free online tool at: http://www.ncbi.nlm.nih.gov/tools/primer-blast Ye et al., 2012
SDS 2.2.1	Applied Biosystems, USA
VENNY	© Juan Carlos Oliveros / BioinfoGP / CNB-CSIC, Spain free online tool at: http://bioinfogp.cnb.csic.es/tools/Venny

2.13 Online databases

Data, information and knowledge used for this PhD work were up-to-date at the time this work was performed.

Table 2-17   List of online databases.
In alphabetical order.

Database	Organization / Website URL / Reference
Database for Annotation, Visualization and Integrated Discovery (**DAVID**) v6.7	LIB & DAVID Bioinformatics, USA http://david.abcc.ncifcrf.gov Huang et al., 2009a; Huang et al., 2009b
Gene Ontology (**GO**) database	The International Gene Ontology Consortium http://www.geneontology.org Ashburner et al., 2000
Kyoto Encyclopedia of Genes and Genomes (**KEGG**) pathway database	Kanehisa Laboratories / Kyoto University, Japan http://www.genome.jp/kegg Kanehisa and Goto, 2000
Protein ANalysis THrough Evolutionary Relationships (**PANTHER**) pathway database	© Paul Thomas / University of Southern California, USA http://www.pantherdb.org Mi and Thomas, 2009
PubMed scientific literature database	National Center for Biotechnology Information (NCBI), U.S. National Library of Medicine, USA http://www.ncbi.nlm.nih.gov/pubmed Roberts, 2001
REACTOME pathway database	The International REACTOME Team http://www.reactome.org Croft et al., 2011
Reference Sequence (**RefSeq**) collection database	National Center for Biotechnology Information (NCBI), USA http://www.ncbi.nlm.nih.gov/refseq Pruitt et al., 2005
Universal Protein (**UniProt**) resource database	The International UniProt Consortium http://www.uniprot.org UniProt Consortium, 2011

3 Methods

3.1 Basic *in vitro* cell culture of eukaryotic cells

Work with cells (Chapter 2.9) was undertaken under aseptic conditions inside laminar flow clean benches using cell culture grade reagents and sterilized consumables. All cells were incubated in a tissue culture incubator at 37 °C in a humidified 5 % CO_2 / 95 % air atmosphere. Feeding was performed using pre-warmed cell culture media (Chapter 2.8). The culture conditions which are required for the growth of human pluripotent stem cells are fundamentally different and more challenging compared to those of somatic cells; hence, these conditions are described separately in the following two subchapters.

3.1.1 Cell culture of somatic cell lines

3.1.1.1 Growth conditions

Somatic cell lines (Table 2-12) were grown adherent on conventional tissue culture plastic surfaces. HEK-293T cells and mouse embryonic fibroblasts (MEFs) were cultured in conventional DMEM medium (Table 2-10) containing 10 % fetal bovine serum (FBS). Chorionic villi cells (CV cells) were cultured in Chang medium (Table 2-10) containing 15 % embryonic stem cell-qualified FBS. This special medium formulation was developed for the primary culture of cell and tissue samples isolated for the purpose of prenatal diagnosis, e.g. amniotic fluid cells (De Coppi et al., 2007; Wolfrum et al., 2010). The medium was routinely replaced by an adequate volume of fresh medium every 2–3 days, depending on the color of the pH indicator phenol red present in all media.

3.1.1.2 Trypsinization and passaging

Cells were routinely passaged by conventional trypsinization at an average splitting ratio of 1:4. Passaging was performed every few days (depending on the cell line and passage number), once a confluency of 80–90 % was attained. For passaging, the medium was aspirated and the cells were quickly washed by rinsing with DPBS to remove traces of remaining medium. Thereafter, 0.05 % trypsin-EDTA was added on the cells till the plastic surface was completely covered and the cells were incubated at 37 °C for 3–5 min. During the incubation, the tissue culture dishes or flasks were agitated from time to time to detach the cells and inspected under a microscope. Once the cells were completely dissociated, the trypsin solution was diluted 1:5–1:10 by adding normal cell culture medium containing FBS to stop trypsin activity. The cell suspension was transferred into a 15 ml or 50 ml conical tube and centrifuged at 500 × g for 5 min. After centrifugation, the supernatant was decanted and the remaining cell pellet was resuspended in fresh medium. Upon mixing by vortexing, the cells were seeded into new tissue culture dishes or flasks.

3.1.1.3   Counting and adjustment of cell concentration

In case it was required to seed or freeze a defined number of cells, the amount present in the suspension was determined using a Neubauer chamber. In some cases, e.g. after thawing of cryopreserved cells, trypan blue was applied as a vital stain to mark death cells. The cell concentration (cells/ml) was calculated by extrapolation based on the individual pre-dilution factor. Adjustment of cell concentration was performed by either increasing the volume of medium or centrifugation followed by resuspension of the cell pellet in less volume.

3.1.1.4   Cryopreservation and thawing

For cryopreservation, cells were trypsinized and centrifuged as described for passaging (Chapter 3.1.1.2). The cell pellet was resuspended in freeze medium (Table 2-10) containing 10 % dimethyl sulphoxide (DMSO) as a cryoprotectant. Aliquots of 0.5 ml or 1 ml were transferred into cryo freezing tubes, which were immediately put in a cryo freezing container filled with isopropanol. The container was directly placed in a freezer at −80 °C to let the cells slowly cool down at a rate of −1 °C/min. The cryopreserved cells were transferred within 3 days at the latest into a liquid nitrogen tank (−196 °C) for long-term storage. For thawing, the tubes were placed in a 37 °C water bath. As soon as the ice inside the tubes had disappeared, the cells were diluted 1:10 in normal cell culture medium to decrease the cytotoxic effect of DMSO. The cell suspensions were centrifuged at 500 × g for 5 min to sediment the cells, which were then resuspended in fresh medium for seeding.

3.1.2   Cell culture of human pluripotent stem cells

3.1.2.1   Growth on feeder layers of mitotically inactivated mouse embryonic fibroblasts (MEFs)

For general maintenance and expansion, hESCs and hiPSCs (Table 2-12) were grown adherent on a feeder layer of mitotically inactivated mouse embryonic fibroblasts (MEFs) on Matrigel-coated 6-well tissue culture plates (Chapter 3.1.2.5 to 3.1.2.7) in hESC medium (Table 2-10) supplemented with 8 ng/ml recombinant human Basic Fibroblast Growth Factor (bFGF). This culture system is well-established for the long-term culture of human pluripotent stem cells (reviewed by McDevitt and Palecek, 2008). bFGF supports the self-renewal of hESCs (Levenstein et al., 2006; Greber et al., 2007a). MEFs, also commonly referred to as "feeder cells" or "feeders" when mitotically inactivated, are known to secrete important biomolecules whose presence in the medium is needed to maintain human pluripotent stem cells in an undifferentiated state. Activin A can be seen as the key factor (Jozefczuk et al., 2012), but also components such as heparan sulfate proteoglycans which stabilize bFGF in the medium and mediate its binding to the surface of hESCs are supportive (Levenstein et al., 2008). The hESC medium was replaced daily or every other day (at weekends) by fresh medium. The volume of medium was gradually adapted depending on the confluency of the hESC/hiPSC colonies and color of the pH indicator phenol red. It ranged from 2 ml per 6-well the day after

passaging up to 6 ml the day before passaging. Due to the thermal instability of bFGF, only the required volume of hESC medium was pre-warmed in a water bath.

3.1.2.2 Feeder-free growth using MEF-conditioned medium (MEF-CM)

For isolation of protein/DNA/RNA samples, human pluripotent stem cells were grown in the absence of feeder layers, so as to avoid the presence of contaminating MEFs at cell lysis. Feeder-free growth was performed on Matrigel-coated tissue culture plates (Chapter 3.1.2.5) using MEF-conditioned medium (MEF-CM) (Table 2-10) in order to compensate for the missing feeder cells. MEF-CM corresponds to hESC medium which had been pre-conditioned with the supportive factors secreted by MEFs via previous incubation on mitotically inactivated MEFs (Chapter 3.1.2.8). MEF-CM was regularly replaced as described for the feeder-dependent growth conditions (Chapter 3.1.2.1).

3.1.2.3 Removal of differentiated cells and passaging

A critical aspect for the successful expansion and experimental application of pluripotent stem cells is their maintenance in an undifferentiated state. Since a small variable proportion of cells undergoes spontaneous differentiation during *in vitro* culture, these cells need to be regularly removed from the whole population. For removal of differentiated cells and passaging of undifferentiated hESCs/hiPSCs, an exclusive mechanical method was applied. Mechanical dissociation of hESC colonies, in comparison to dissociation involving proteolytic enzymes, has been suggested to decrease the risk of acquiring chromosomal abnormalities during long-term culture (McDevitt and Palecek, 2008). All mechanical manipulations described in the following were performed manually under the control of a stereo microscope Leica MZ9.5 placed inside a HERAguard® HPH 9 laminar flow clean bench.

Passaging of human pluripotent stem cells grown on feeder layers was routinely done at a splitting ratio of 1:3 every 7–10 days, once a confluency of > 80 % was reached. At first, the whole plastic surface of each 6-well was uniformly scratched in a grid-like pattern using a 19 gauge hypodermic needle. The distance between the scratches was chosen to obtain square colony fragments of nearly uniform size (approx. 200–400 cells per square). During this process, areas of differentiated cells which stuck only weakly to the Matrigel were detached. Remaining areas of differentiated cells were removed one by one using a P200 filter pipette tip. Differentiated areas of colonies were distinguished from the undifferentiated areas by means of their non-homogeneous look and variance in contrast (more transparent than whitish). The detached cell clumps floating in the cell culture medium were removed from the wells by aspiration. The remaining adherent colony fragments were detached using a cell spatula and finally collected in one 6-well using a P1000 filter pipette tip. Since hESC/hiPSC colony fragments in suspension are very fragile and do break easily, pipetting was performed gently. Cell debris and MEFs were removed by discarding the medium supernatant of cell suspension as soon as the colony fragments had sedimented to the bottom of the well (repeated three times by refilling the well with hESC medium). Oversized fragments were separated by turning the plate a few times, which made these fragments accumulate at the border of the well. The uniform-sized colony fragments

which had accumulated in the center of the well were transferred into a 50 ml conical tube. The suspension was diluted using the appropriate kind of fresh medium at the required volume. Finally, the suspension was gently mixed by only inverting the tube, and the colony fragments were seeded evenly distributed into new plates in a volume of 2 ml medium per 6-well.

3.1.2.4   Cryopreservation and thawing

Cryopreservation and thawing of human pluripotent stem cells were performed as described for somatic cell lines (Chapter 3.1.1.4), with following differences: Instead of trypsinization to single cells, colony fragments of hESCs/hiPSCs were obtained by mechanical dissociation as described for passaging (Chapter 3.1.2.3), sedimented by centrifugation and resuspended in freeze hESC medium (Table 2-10). Typically, the content of ½ to 1 nearly confluent 6-well was cryopreserved in a volume of 0.5–1 ml per cryo freezing tube. Thawed cells, upon removal of DMSO, were seeded onto a feeder layer of mitotically inactivated MEFs. Usually, the content of ½ to 1 tube was seeded per 6-well. Thawed hESCs/hiPSCs require up to 14 days for their recovery until they can be passaged, and many cells don't survive the process of cryopreservation. Extensive cell death of feeder cells can occur towards the end of this period. This sometimes required a reseeding of feeder cells or switch from hESC medium to MEF-CM.

3.1.2.5   Coating of tissue culture plates with Matrigel

hESCs/hiPSCs do not attach on conventional tissue culture plastic surfaces. This requires coating of the plates to mimic the extracellular matrices which are underlying many cells in their natural *in vivo* environments (Xu et al., 2001a). Matrigel™ (registered trademark of Becton Dickinson, USA) is a solubilized basement membrane preparation extracted from the Engelbreth-Holm-Swarm mouse sarcoma, a tumor rich in ECM proteins such as laminins, collagen type-IV and heparan sulfate proteoglycans (Kleinman et al., 1982). For coating of plates, the needed quantity of 0.5 ml (or 1 ml) 30X Matrigel stock concentrate aliquots was thawed at room temperature and immediately diluted 1:30 using 14.5 ml (or 29 ml) of 4 °C cold KnockOut™ DMEM per aliquot to obtain a 1X concentration. 1.5 ml of the mixture were added per single well of a 6-well plate (8.960 cm²) or 600 µl per single well of a 12-well plate (3.596 cm²). The plates were sealed with Parafilm® and immediately stored at 4 °C for at least 2–3 days to enable a slow and complete polymerization to a homogeneous structure. Stored plates were used within two weeks. For usage, the Parafilm was removed and the plates were pre-warmed at 37 °C in the tissue culture incubator for at least 15 minutes. Finally, the liquid was removed and the suspensions of feeder cells or hESCs/hiPSCs were promptly seeded into the wells to avoid a dehydration of the ECM layer.

Preparation of 30X Matrigel stock concentrate: Matrigel (~ 10 mg/ml in 10 ml volume) was kept frozen at −20 °C. For preparation of a 30X stock concentrate, it was slowly thawed on ice at 4 °C overnight to avoid gel clumping. On the next day, the Matrigel was diluted 1:2 by adding 10 ml of 4 °C cold KnockOut™ DMEM and mixed well. The mixture was aliquoted

into pre-cooled 15 ml conical tubes on ice (0.5 ml or 1 ml per tube). Aliquots were frozen and stored at −20 °C.

3.1.2.6   Mitotic inactivation of MEFs

MEFs were mitotically inactivated to serve as feeder cells or for preparation of MEF-CM. Only low-passage (passage 2−3) MEFs were used, since their age significantly affects the efficiency of how these cells produce the hESC/hiPSC-supportive factors. MEFs were expanded in 15 cm tissue culture dishes at a splitting ratio of 1:4 as described for somatic cell lines (Chapter 3.1.1). Due to their origin (Table 2-12), the "quality" of MEFs can greatly vary. Proliferation rate and morphology of MEFs served as important criteria to determine the ideal moment for stopping expansion and starting inactivation. Generally, "good" MEFs are fast proliferating and should not yet possess a flattened cell shape. Mitotic inactivation of cells was achieved using mitomycin C, a cytotoxic antibiotic isolated from the bacterium *Streptomyces caespitosus*. It acts as a potent cross-linker of DNA and leads to cell cycle arrest, which makes it an important antitumor drug (Tomasz, 1995). 2 mg mitomycin C powder were freshly resuspended in 2 ml DPBS, 0.2 μm sterile-filtered and further diluted in 200 ml DMEM medium to obtain a 10 μg/ml working concentration (protected from light). The cell culture medium was removed from the dishes containing the MEFs to be inactivated and replaced by the mitomycin C-containing medium (using 16 ml per dish). After incubation for 2 h at 37 °C, the medium was removed and the cells were washed three times by rinsing the dishes with DPBS to completely remove mitomycin C. Finally, mitotically inactivated MEFs were cryopreserved (Chapter 3.1.1.4) in small working aliquots ($1-5 \times 10^6$ cells per tube) or immediately used as needed.

3.1.2.7   Preparation of MEF feeder layers

Approximately 0.2×10^6 mitotically inactivated MEFs were seeded in a volume of 2 ml hESC medium per Matrigel-coated 6-well. Cryopreserved feeder cells were freshly thawed (Chapter 3.1.1.4) and counted using trypan blue as a vital stain (Chapter 3.1.1.3). The feeder layer was prepared not earlier than 1 day and not later than 8 hours before the planned seeding of the hESCs/hiPSCs. The medium was aspirated from the wells just before seeding of the resuspended colony fragments onto the adherent growing feeder layer.

3.1.2.8   Preparation of MEF-CM

At first, the plastic surface of 150 cm² tissue culture flasks was coated with gelatin to facilitate attachment of MEFs. 20 ml of 0.2 % (w/v) gelatin solution (from bovine skin, type B; dissolved in DPBS and sterilized by autoclaving) were added per flask and incubated at room temperature for 1−2 h. Thereafter, the liquid was removed and mitotically inactivated MEFs were seeded at a density of 8.4×10^6 living cells per flask (56,000 cells/cm²) in 20 ml DMEM medium. The following day, the medium was removed and the cells were washed twice by rinsing with DPBS to remove traces of remaining FBS. Then, 75 ml of hESC medium, which was supplemented with only 4 ng/ml instead of 8 ng/ml recombinant human bFGF (= unconditioned medium, UM), were added per flask (0.5 ml/cm²). 24 h later, the

conditioned medium (CM) was collected from the flasks and replaced by 75 ml of fresh UM per flask. This procedure was repeated for the next 6 days. The daily collected CM was stored at −20 °C. After 1 week, all collected CM batches were pooled together, 0.2 µm sterile-filtered and supplemented again with 4 ng/ml bFGF to obtain a final concentration of 8 ng/ml. This concentration is equal to that of hESC medium. The supplementation with 4 ng/ml bFGF already prior to the conditioning step is needed to boost the MEFs to release the hESC/hiPSC-supportive factors, as discovered by our laboratory (Greber et al., 2007a). The resulting MEF-CM was aliquoted into 50 ml conical tubes which were stored at −80 °C for up to 3 months.

After the first year of this PhD project, the isolation, expansion, inactivation and cryopreservation of MEFs, and the preparation of MEF-CM, were performed by our technical assistant Elisabeth Socha.

3.2   Generation of human induced pluripotent stem cells (hiPSCs)

All work with viruses was carried out in a BSL-2 laboratory with adequate safety precautions taken.

3.2.1   Production of retroviral vectors encoding human OCT4, SOX2, KLF4 and c-MYC

3.2.1.1   Transient transfection of HEK-293T cells with plasmids for retroviral vector production

VSV-G-pseudotyped Moloney-based retroviruses were produced in HEK-293T cells serving as host cells (Table 2-12), similar as described before (Huangfu et al., 2008b). For this purpose, HEK-293T cells were transiently transfected with plasmids (Table 2-5) by the conventional chemical-based calcium phosphate precipitation method. 24 h before transfections, low-passage (passage 7) HEK-293T cells were seeded into 15 cm tissue culture dishes (9×10^6 cells in 20 ml DMEM medium per dish) (Chapter 3.1.1). Two dishes were prepared for each of the four different transgene-carrying retroviruses to produce (OCT4, SOX2, KLF4, c-MYC). Two additional dishes were prepared to serve as positive and negative controls in order to confirm the success of transfections. 3 h before transfections, the DMEM medium was replaced by 22 ml Iscove's medium (Table 2-10). Individual plasmid DNA mixtures were prepared by adding 9 µg of envelope plasmid, 20 µg of packaging plasmid and 32 µg of individual transfer vector plasmid into ddH2O (adjusted to 1125 µl volume). The transfer vector plasmid was either encoding one of the four reprogramming factors or the reporter gene Enhanced Green Fluorescent Protein (eGFP (Cormack et al., 1996); used for the transfection positive control dish). One plasmid DNA mixture was prepared per dish to be transfected. Thereafter, 125 µl of 2.5 M CaCl₂ solution (0.2 µm sterile-filtered) were added into each mixture. The calcium phosphate precipitate with bound DNA was formed by a dropwise addition (1−2 drops per second) of 1250 µl of 2X HBS buffer (0.2 µm sterile-filtered) to the 1250 µl of DNA/CaCl₂ mixture while vortexing at full speed. The precipitate was added to the

HEK-293T cells by spreading it on the entire surface of the Iscove's medium. After 14 h incubation, the Iscove's medium was replaced by 16 ml DMEM medium per dish. After 36 h incubation in DMEM medium, the cells of the transfection positive control dish and the negative control dish (left untransfected) were fixed with paraformaldehyde fixing buffer and analyzed by flow cytometry (Chapter 3.7.4) in order to determine the percentage of GFP-expressing cells.

3.2.1.2 Isolation and enrichment of virus particles

After 36 h incubation in DMEM medium, the media supernatants containing the produced virions were collected. Media of the two dishes containing the same type of transgene-carrying retrovirus were pooled together and cleaned from cell debris using low protein binding 0.45 μm syringe-driven filters. The filtrates were transferred into polyallomer 25×89 mm centrifuge tubes and centrifuged at $72,100 \times g$ for 2 h at 4 °C in vacuum using a Beckman L7 ultracentrifuge with swinging-bucket rotor type SW-28. The supernatants were discarded and each remaining virus pellet was resuspended in 400 μl pure KnockOut™ DMEM. Small working aliquots of 10 μl were stored at −80 °C.

3.2.2 Reprogramming of primary human chorionic villi (CV) cells by retroviral transduction

Primary human chorionic villi (CV) cells (Table 2-12) were reprogrammed by classical retroviral transduction of the four Yamanaka-factors OCT4, SOX2, KLF4 and c-MYC (Takahashi et al., 2007), similar as previously described for this cell type (Ye et al., 2009). Cryopreserved CV cells were thawed and expanded in Chang medium (Chapter 3.1.1). Passage 5 cells were seeded into 6-well plates at a density of 1×10^5 cells in 2 ml Chang medium per well. The resulting low confluency of approximately 25 % ensured that the cells were kept in a proliferative state during infection. The next day, the medium was replaced by 2 ml of fresh Chang medium per well and cells were transduced. Transduction was done by adding 40 μl of a 1:1:1:1 cocktail of 10 μl aliquots containing similar titers of the four retroviral vectors into each well. Infection rate was supported by supplementation of the medium with 4 μg/ml of the cationic polymer hexadimethrine bromide (Polybrene®) (Davis et al., 2004) and by centrifugation of the tissue culture plates (sealed with Parafilm) at $2000 \times g$ for 99 minutes. After 24 h incubation, the viral medium was removed and the retroviral transduction was repeated once more.

3.2.3 Cell culture conditions post-transduction

24 hours after beginning of the second transduction cycle, the viral medium was removed and the adherent cells were washed three times with DPBS. This time point was defined as day 0 post-transduction. After subsequent culture in Chang medium for 24 h, the CV cells were trypsinized (Chapter 3.1.1.2) at day 1 post-transduction and splitted at a ratio of 1:3 on MEF feeder layers (Chapter 3.1.2.7) growing in 6-well plates coated with Matrigel (Chapter 3.1.2.5). Alternatively, some wells were used to determine the transduction efficiencies by

immunocytochemical staining (Chapter 3.7.5) for OCT4, SOX2, KLF4 and c-MYC. At day 3 post-transduction, the Chang medium was switched to hESC medium (Table 2-10). The hESC medium was supplemented with 1 mM of the small molecule and known histone deacetylase inhibitor valproic acid (VPA). VPA has been shown to enhance reprogramming efficiency, which suggests that chromatin remodeling is a rate-limiting step in this process (Huangfu et al., 2008a; Huangfu et al., 2008b). The hESC medium with VPA was replaced daily by fresh medium. Upon onset of significant feeder cell death around day 15, the hESC medium was switched to MEF-CM (Chapter 3.1.2.8). Supplementation with VPA was stopped at day 18 post-transduction.

3.2.4 Picking and expansion of CV cell-derived hiPSC clones

At day 31 post-transduction, hiPSC-like colonies which had emerged and increased in diameter were manually picked. This work was conducted under the control of a stereo microscope placed inside a tissue culture hood to ensure aseptic conditions. Selected colonies were mechanically fragmented using a 19 gauge hypodermic needle. The dislodged cell clumps of each individual colony were transferred into one well of a tissue culture plate using a P20 filter pipette tip. Subsequent separate culture and expansion of the independent clonal hiPSC lines were conducted as described for human pluripotent stem cells (Chapter 3.1.2).

3.3 *In vitro* and *in vivo* differentiation assays of hiPSCs

3.3.1 Embryoid body formation assay

For *in vitro* differentiation, iPS1 and iPS2 colonies were grown feeder-free using MEF-CM (Chapter 3.1.2) and detached using a cell spatula. The detached colonies were subsequently cultured in ultra-low attachment dishes in DMEM medium (Table 2-10) containing 10 % FBS. Due to the special hydrophilic and neutrally charged dish surface, passive adsorption of biomolecules was greatly reduced, which forced the cells to stay in suspension. The presence of FBS in the medium, which was replaced every 2–3 days, induced their spontaneous differentiation and formation of embryoid bodies (EBs). After 7 days, the floating EBs were transferred into separate wells of 12-well plates, which had been coated with gelatin (0.8 ml/well; as described in Chapter 3.1.2.8), allowing their attachment. After subsequent culture in DMEM medium for additional 3 days and 14 days, the adherent growing random differentiated cells were fixed with paraformaldehyde fixing buffer and analyzed by immunocytochemistry (Chapter 3.7.5) for expression of lineage markers.

3.3.2 Teratoma formation assay

3.3.2.1 Teratoma induction in immunodeficient mice

For *in vivo* differentiation, iPS1 and iPS2 colonies were grown on MEF feeder layers (Chapter 3.1.2) and dissociated into single cells by trypsinization, similar as described before

(Chapter 3.1.1.2). After repeated washing/centrifugation steps with DPBS (3x), cell pellets consisting of approximately $1-2 \times 10^6$ cells were resuspended in 50 µl DPBS and instantly mixed at a ratio of 1:2 with Matrigel. The 100 µl mixtures were at once subcutaneously injected into the right latus of the abdomen of immunodeficient NOD.Cg-Prkdc^{scid} Il2rg^{tm1Wjl} / Szj mice, commonly known as NOD scid gamma (NSG) mice. One sample (cell line) was injected per mouse to induce the formation of a teratoma. On day 43 post-transplantation, once the developed teratomas had reached a critical volume in relation to the average body weight of the mice (1 cm³ versus approx. 22 g), the mice were sacrificed. An autopsy was performed at which the teratomas were dissected. The work involving animals was conducted by qualified staff of the Experimental Pharmacology & Oncology (EPO) GmbH (Robert-Rössle-Straße 10, 13125 Berlin, Germany; http://www.epo-berlin.com).

3.3.2.2 Histology

The dissected teratomas were conserved in formalin and subsequently processed according to standard protocols for paraffin embedding. Paraffin-embedded tissues were sectioned by microtome and stained with hematoxylin and eosin (H&E) (Fischer et al., 2008; Chan, 2014). Histological analysis was conducted by the veterinary pathologist Dr. Wolfram Haider (Institut für Tierpathologie, Schönhauser Straße 62, 13127 Berlin, Germany; http://www.tierpathologie-berlin.de).

3.4 BMP treatments of human pluripotent stem cells

For BMP studies, the two hESC lines H1 and H9 (passage 40–55) and two hiPSC lines iPS1 and iPS2 (passage 25–40) were used (Table 2-12). All experiments were carried out using the established chemically-defined medium N2B27 (w/o vitamin A, w/o bFGF, w/o Activin A; Table 2-10 (Liu et al., 2006a; Yao et al., 2006)), as described before for BMP4 signaling studies concerning hESCs (Sudheer et al., 2012). This aimed at avoiding the disadvantages of undefined culture systems containing xenogeneic contaminants such as feeder cells and serum. For instance, MEFs are subjected to biological batch-to-batch variations and known to secrete Activin A, several BMP antagonists and bFGF (Greber et al., 2007a; Wang et al., 2005). All those factors could obscure the effect of BMPs.

hESCs/hiPSCs were grown to at least 80 % confluency on MEF feeder layers (Chapter 3.1.2). After removal of differentiated cells and MEFs, colony fragments of relatively uniform size (approx. 200–400 cells) were prepared as described (Chapter 3.1.2.3). Fragments were seeded into Matrigel-coated 6-well plates (Chapter 3.1.2.5) under feeder-free conditions in a volume of 2 ml MEF-CM (Chapter 3.1.2.8) per well. For each experimental series, aliquots of equal volumes of gently mixed cell suspension were seeded, in order to guarantee alike colony numbers per well. The seeding was performed at a low density to ensure enough space between the colonies for their future expansion and differentiation. After incubation overnight, the MEF-CM was substituted by 2 ml chemically-defined N2B27 medium per well, upon gently rinsing the wells twice with DPBS. After adaptation of the cells to the N2B27 medium for 6 h in the incubator, appropriate doses (in 20 µl volume) of BMPs and controls

(Table 2-8) were added into the wells as indicated and the plates were gently mixed. Thawed aliquots of recombinant human proteins were never frozen again but stored at 4 °C for maximum 48 hours under sterile conditions. For long-term BMP stimulation experiments, media and supplements were replaced every 24 h by fresh media and supplements at a volume of 2 ml per 6-well. At the indicated time points, the media supernatants of the wells were collected for ELISA (Chapter 3.7.7) and the cells were washed twice with DPBS. Washed cells were either fixed with paraformaldehyde fixing buffer for immunocytochemistry (Chapter 3.7.5) or lysed for protein and RNA isolation (Chapter 3.7.6.1 and 3.8.1.1). Fixed cells were stored in DPBS at 4 °C and media supernatants and whole cell lysates were stored at −80 °C until further analysis.

3.5   Photo documentation of cell morphology

The morphology of cells was inspected by means of an inverted phase-contrast microscope Olympus CK2 or a stereo microscope Leica MZ9.5 and photographed using the digital camera Canon PowerShot A650 IS. Scale bars in the images were constructed based on the grid of a Neubauer chamber serving as a reference for calibration. The grid was photographed under identical conditions with regard to optical magnification of the microscope and digital zoom mode of the camera.

3.6   DNA work and cytogenetics

3.6.1   Amplification of plasmids in *E.coli* bacteria and purification of plasmid DNA

Plasmids (Table 2-5) were amplified in *Escherichia coli* (*E.coli*) bacteria serving as host cells. Transformation of plasmid DNA into bacterial cells was conducted by heat shock transformation. Chemically competent *E.coli* bacteria (Table 2-13) were stored at −80 °C and thawed on ice. In order to provide a sterile atmosphere to prevent contamination with airbone germs, all work which did not involve the usage of selective antibiotics was done directly next to a gas flame. 1 µg of each individual plasmid DNA was added into 100 µl of *E.coli* cell suspension and briefly mixed by vortexing. After being kept on ice for 10 min, the cell/DNA suspensions were immediately heated at 42 °C for 1 min and then instantly cooled down on ice for 5 min. Afterwards, 300 µl of LB medium (Table 2-11; w/o antibiotic) were added into each suspension. The suspensions were incubated at 37 °C for 30 min while shaking at 180 rpm to enable bacteria building up resistance to antibiotics. Afterwards, the bacteria suspensions were evenly spread on LB agar plates (Table 2-11) supplemented with ampicillin. The plates were incubated upside down at 37 °C overnight. The next day, a single colony of each plate was picked using a sterile pipette tip and transferred into a 2 liter Erlenmeyer flask containing 300 ml of LB medium supplemented with ampicillin. The cultures were incubated at 37 °C while shaking at 180 rpm overnight. After 12−16 h, when the cultures had reached an OD_{600} of ~ 4, bacteria were harvested by centrifugation for

20 min at 4 °C at 4000 × g. Amplified plasmids were isolated and purified by Maxiprep using the NucleoBond® Xtra Maxi EF Kit according to the manual of the kit. Retrieved plasmid DNA was reconstituted in 300 μl of endotoxin-free H2O provided by the kit and stored at −20 °C. Integrity of plasmids was assessed by agarose gel electrophoresis of 1 μg DNA aliquots (Chapter 3.6.6).

3.6.2 Diagnostic restriction enzyme digestion

Diagnostic restriction enzyme digestion of OCT4, SOX2, KLF4 and c-MYC plasmids was performed using appropriate restriction enzymes (Table 2-5). The buffer system for the reactions was chosen following the manufacturer's recommendations in order to ensure optimal enzyme activity. 25 μl digestion reactions were prepared as stated below (restriction enzyme added last):

Component, per reaction:	Volume	Final concentration (amount)
ddH2O	ad 25 μl	
BSA (10 mg/ml)	0.25 μl	100 ng/μl (2.5 μg)
Plasmid DNA (1 μg/μl)	5.00 μl	200 ng/μl (5 μg)
NEBuffer 3 (10X)	2.50 μl	1X
*Not*I (10,000 U/ml)	1.00 μl	0.4 U/μl (10 U; 2 U per μg DNA substrate)
or		
NEBuffer 4 (10X)	2.50 μl	1X
*Xho*I (20,000 U/ml)	0.50 μl	0.4 U/μl (10 U; 2 U per μg DNA substrate)

The reaction tubes were incubated at 37 °C for 2 h, followed by heat inactivation of the enzyme at 65 °C for 20 min. 5 μl of each reaction mixture (= 1 μg of digested plasmid DNA) were subsequently analyzed by agarose gel electrophoresis (Chapter 3.6.6).

3.6.3 Isolation of genomic DNA

Genomic DNA of feeder-free human pluripotent stem cells and chorionic villi cells was isolated using the PureLink® Genomic DNA Mini Kit according to the manufacturer's guidelines. An enzymatic digestion of RNA by RNase A and proteins by Proteinase K was included. Purified DNA was eluted using 50 μl of the elution buffer provided by the kit and stored at −20 °C.

3.6.4 Determination of quantity and quality of DNA

Plasmid and genomic DNA concentration and purity were assessed using the spectrophotometer NanoDrop® 2000. All samples (1 μl aliquots) were blanked against the liquid which had been used for reconstitution or elution of DNA. Absorbance measurements were made at 230, 260 and 280 nm wavelength. A_{260}/A_{280} and A_{260}/A_{230} ratios of ~ 1.8 were generally accepted as "pure" DNA.

3.6.5 Polymerase chain reaction (PCR)

Target regions of genomic DNA were amplified by polymerase chain reaction (PCR) (Saiki et al., 1988). 30 µl PCR reactions were prepared as stated below, with items pipetted in the same order:

Component, per reaction:	Volume	Final concentration (amount)
H2O, ultrapure	ad 30 µl	
Phusion® HF buffer (5X)	6.00 µl	1X
dNTP mix (25 mM each)	0.24 µl	200 µM
Forward/reverse primer mix (5 µM each)	3.00 µl	0.5 µM
DMSO	0.90 µl	3 % (v/v)
Phusion® DNA polymerase (2 U/µl)	0.30 µl	0.02 U/µl (0.6 U)
DNA template (50 ng/µl)	2.00 µl	3.33 ng/µl (100 ng)

The PCR tube strips were placed into the thermal cycler DNA Engine Dyad® and the following PCR program was applied:

Step	Temperature	Time	Cycles
Initial denaturation	96 °C	1 min	1x
1. Denaturation 2. Annealing 3. Extension	96 °C 56 °C 72 °C	30 s 30 s 30 s	35x
Final extension	72 °C	5 min	1x
Hold	4 °C	∞	1x

3.6.6 Agarose gel electrophoresis

Agarose gel electrophoresis was employed for separation of nucleic acids. The gel matrix was prepared by dissolving agarose powder in the selected buffer. The mixture was heated in a microwave until the agarose was completely melted, leading to a clear solution without visible smears. Then, 5 µl of 1 % ethidium bromide (EtBr) solution were added per 100 ml. The mixture was briefly shaken and immediately poured into the chamber of a horizontal electrophoresis system with a comb attached to generate the pockets for sample loading. After the gel had polymerized, the chamber was filled with buffer and the comb was removed. The DNA samples were mixed at a ratio of 6:1 with 6X blue DNA/RNA sample loading buffer and loaded into the pockets. Alternatively, selected markers were loaded: HyperLadder™ V (leading to a DNA ladder consisting of 12 fragment lengths ranging from 25−500 bp) or Perfect Plus™ 1 kb DNA ladder (leading to a DNA ladder consisting of 13 fragment lengths ranging from 250−10,000 bp). Finally, voltage was applied for varying periods of time and the EtBr-stained DNA bands were visualized under UV light and photographed using the AlphaImager™ gel imaging system.

Depending on the DNA samples, different gel/buffer systems and running parameters were chosen, so as to achieve the desired band resolution:

- For purified plasmids and digested plasmids: 1.5 % standard agarose gel of 20.8 cm length, 1X TAE buffer, 1 μg plasmid DNA or 500 ng marker load (Perfect Plus 1 kb DNA ladder), 3.5 h running time at constant 70 V (3.4 V/cm field strength).
- For PCR products of DNA fingerprinting analysis and real-time qPCRs: 3.5 % standard agarose gel of 20.8 cm length, 1X TAE buffer, 5 μl PCR reaction products or 576 ng marker load (HyperLadder V), 60 min running time at constant 40 V (1.9 V/cm field strength).
- For PCR products of sex determination analysis: 3.5 % low range ultra agarose gel of 7.2 cm length, 1X SB buffer (low conductivity), 3 μl PCR reaction products or 480 ng and 960 ng marker load (HyperLadder V), 40 min running time at constant 100 V (13.9 V/cm field strength).

3.6.7 DNA fingerprinting analysis and sex determination

Genomic regions containing STRs and X-/Y-chromosomal loci were amplified by PCR (Chapter 3.6.5) using established primer sets from forensic science (Table 2-6). The resulting PCR products were subsequently analyzed by agarose gel electrophoresis (Chapter 3.6.6).

3.6.8 Chromosome analysis

Cytogenetic GTG-banding chromosome analysis (Bickmore, 2001; Moore and Best, 2001) of feeder-free iPS1 and iPS2 cells was conducted by the human geneticist Prof. Dr. Gundula Thiel (Praxis für Humangenetik, Friedrichstraße 147, 10117 Berlin, Germany; http://www.humangenetik-berlin.de). Of each sample, 18 metaphases were counted and 10 karyograms were analyzed.

3.7 Protein analyses (expression, phosphorylation and enzyme activity)

3.7.1 Alkaline phosphatase staining

Alkaline phosphatase staining was performed using the Alkaline Phosphatase Detection Kit following the recommended protocol.

3.7.2 β-Galactosidase staining

β-Galactosidase staining was performed using the Senescence β-Galactosidase Staining Kit following the recommended protocol.

3.7.3 Telomerase activity assay

Telomerase activity in individual cell lines was measured using the TRAPEZE® RT Telomerase Detection Kit (Uehara et al., 1999) according to the manufacturer's recommendations. The assay is based on fluorometric detection of telomerase activity in whole cell extracts using energy transfer-labeled Amplifluor® primers. These primers only emit a fluorescence signal if they are incorporated into a double-stranded PCR product (Nazarenko et al., 1997).

In short: Telomerase substrate oligonucleotides, Amplifluor primers, dNTPs and DNA polymerase were added to the cell extracts (closed-tube format). In the first step, the telomerase enzyme present in the cell extracts was given time and optimum temperature to add telomeric repeats on the 3'-ends of substrate oligonucleotides. Afterwards, the extended oligonucleotides were amplified via real-time qPCR reactions (similar as described in Chapter 3.8.1.5) by means of the DNA polymerase in combination with Amplifluor primers and dNTPs. The detected fluorescence emission (C_t value; C_t = threshold cycle) for the individual samples was directly proportional to the amount of PCR products generated by the polymerase enzyme. The C_t values were then converted into copy numbers (= amount of substrate oligonucleotides extended by the telomerase) on the basis of a standard curve. The standard curve was created by means of C_t values of real-time qPCR reactions containing a 1:10 serial dilution of control templates of known quantity (0.004–40 amoles). 300 ng of total proteins from CV cells, undifferentiated feeder-free human pluripotent stem cells and telomerase positive control cells provided by the kit were used for the reactions (all samples with and without preliminary heat treatment). The protein concentrations were quantified as described (Chapter 3.7.6.2) and adjusted to 150 ng/µl with CHAPS lysis buffer provided by the kit. Alternatively, equivalent volumes (2 µl) of CHAPS lysis buffer and RNAse-free H2O were used instead of protein extracts. The reactions were operated in technical triplicates in a 96-well optical reaction plate using the 7900HT Fast Real-Time PCR System and recommended Titanium™ Taq DNA polymerase. The following parameters had been optimized: Heat treatments of cell extracts serving as negative controls were carried out at 95 °C instead of 85 °C in order to ensure a complete destruction of the telomerase enzyme; the last 45 °C step of the PCR program was extended from 10 s to 30 s.

3.7.4 Flow cytometry

3.7.4.1 Cell sample preparation

Flow cytometry (Fulwyler, 1965; Hulett et al., 1969) was applied for measurement of GFP expression in HEK-293T cells to determine the transfection efficiency of plasmids for retroviral vector production (Chapter 3.2.1.1). Transfected and non-transfected cells were trypsinized and transferred as single cell suspensions into 15 ml conical tubes. The cells were spun down at 2000 × g for 5 min, resuspended in DPBS and spun down again. After this washing step, the cell pellets were fixed with paraformaldehyde fixing buffer for 15 min at room temperature, while vortexing every few minutes. This fixing step ensured the inactivation of any hazardous viral particles which had been produced in the transfection positive control cells. After two additional washing steps with DPBS, the cell pellets were resuspended in DPBS and transferred into BD Falcon™ round-bottom tubes.

3.7.4.2   Data acquisition and analysis

For flow cytometric analysis, cell suspensions in round-bottom tubes were further diluted in FACSFlow™ buffer. The flow cytometer FACSCalibur™ and software CellQuest™ Pro Version 4.0.2 (Table 2-16) were used for data acquisition. A total of 10,000 events were counted for each sample. The raw data were processed using the software Cyflogic Version 1.2.1 (Table 2-16). Calculation of green fluorescent cells was restricted to the main cell population based on light scatter properties.

3.7.5   Immunocytochemistry

3.7.5.1   Immunofluorescence staining of cells

Adherent growing cells were briefly washed twice by rinsing the wells with 1X PBS buffer and then fixed with paraformaldehyde fixing buffer for 15 min at room temperature. Pipetting was performed slowly to avoid detachment of cells. After removal of PFA, the wells were rinsed twice with PBS. Unless stated otherwise, all subsequent steps were performed with the tissue culture plates being gently shaked. The cells were permeabilized and blocked for 1 h with blocking buffer at room temperature. Thereafter, primary antibodies (Table 2-3) were diluted at 1:100–1:300 in blocking buffer and either incubated for 2 h at room temperature or overnight at 4 °C, followed by 3x 10 min washing with PBS. Then, appropriate fluorescence-labeled secondary antibodies (Table 2-4) were diluted at 1:300 in blocking buffer and applied under the same conditions (plates stored out of light). After 3x 10 min washing with PBS, the nuclei were counterstained with DAPI staining solution for 3 min at room temperature. After removal of DAPI, the wells were rinsed twice with PBS and then filled with PBS. The fluorescence-stained cell samples were either immediately analyzed or stored at 4 °C in the dark (without shaking).

3.7.5.2   Fluorescence microscopy

Fluorescence microscopy and imaging was carried out using the fluorescence microscope Zeiss Axiovert 200M with camera AxioCam MRm. Images were saved as Zeiss Vision Image file (*.zvi). Image processing was performed using the software AxioVision Rel. 4.8 (Table 2-16).

3.7.6   Western immunoblotting

3.7.6.1   Protein isolation

Adherent growing cells in 6-well plates were washed twice with DPBS and then lysed on ice in 200 µl pre-cooled RIPA lysis buffer (including protease and phosphatase inhibitors) per well using a cell scraper. The lysates were transferred into 0.5 ml reaction tubes and subjected to Bioruptor® ultrasonic treatment for homogenization and release of nuclear proteins. The ultrasonication program included repeated cycles of 30 s on (highest level) / 30 s off, for a total period of 10 min, while rotating the tubes in 4 °C pre-cooled water. Afterwards, cellular debris was removed by means of centrifugation (10,000 rpm at 4 °C for

10 min). The protein supernatants were transferred into new tubes, briefly vortexed and stored at −80 °C.

3.7.6.2   Protein quantification

Protein concentration in cell lysates was measured by the colorimetric bicinchoninic acid (BCA) method (Smith et al., 1985) using the Pierce® BCA Protein Assay Kit as per protocol. The reactions were carried out in technical duplicates in a clear 96-well tissue culture plate. 10 µl of samples (lysate aliquots, pure lysis buffer as a background reference, and BSA protein standards) were applied in a total reaction volume of 210 µl. Absorbance at 562 nm wavelength was measured using the microplate spectrophotometer SpectraMax® 250. Samples, whose protein concentration exceeded the capacity of the assay's reaction or the linear range of the Lambert-Beer law, were pre-diluted with lysis buffer. The averaged A_{562} values were background-subtracted and converted into protein concentrations based on the BSA standard curve and pre-dilution factor.

3.7.6.3   Sodium dodecyl sulfate - polyacrylamide gel electrophoresis (SDS-PAGE)

SDS-PAGE according to the discontinuous Laemmli method (Laemmli, 1970) was employed for separation of proteins.

Gel preparation: Polyacrylamide gels of 1.5 mm thickness were prepared in advance using the equipment of the Mini-PROTEAN® vertical electrophoresis 2-gel system. A 10 % resolving gel was prepared by mixing (in this order): 4.1 ml ddH2O, 2.5 ml 1.5 M Tris-Cl buffer (pH 8.8), 100 µl 10 % (w/v) SDS, 3.3 ml acrylamide/bis-acrylamide (30 % / 0.8 %; 37.5:1), 50 µl 10 % (w/v) APS and 5 µl TEMED. Immediately after initiation of the free radical polymerization, the mixture was poured into the assembled casting chamber, until the filling height was 1.5 cm below the bottom of the future comb wells. The mixture was covered with 1 ml isopropanol to ensure formation of an even surface and to avoid dehydration of the gel. Once the mixture had solidified, a 5 % stacking gel was prepared by mixing (in this order): 2.8 ml ddH2O, 1.2 ml 0.5 M Tris-Cl buffer (pH 6.8), 50 µl 10 % (w/v) SDS, 0.8 ml acrylamide/bis-acrylamide (30 % / 0.8 %; 37.5:1), 50 µl 10 % (w/v) APS and 10 µl TEMED. Immediately after initiation of the reaction, the isopropanol was completely discarded, the mixture was poured onto the resolving gel, and a 15-well-comb was attached on top.

Protein sample preparation: 8–20 µg of total proteins (but uniform amount for all samples) were adjusted to 19 µl volume by RIPA lysis buffer on ice. Then, 11 µl of 3X blue protein sample loading buffer were added. Upon mixing, the 30 µl samples were heated at 95 °C for 5 min to denature proteins, and instantly chilled on ice.

Gel electrophoresis: To guarantee identical conditions, all protein samples of a given experimental series were electrophoresed simultaneously in the same gel chamber. The solidified gels were placed into the cell of the electrophoresis system and the anode and cathode chambers were filled with 1X SDS-PAGE running buffer. Upon removal of the combs, the 30 µl protein samples were loaded into the wells. Alternatively, 3 µl of the marker PageRuler™ were loaded, which led to a protein ladder with colored reference bands that covered 10 molecular weights ranging from 10–170 kDa. The gels were initially

electrophoresed at constant 80 V. Once the dye front had passed the interface between stacking and resolving gel, the voltage was increased to 150 V. Once an adequate resolution of the reference bands had been achieved, the electrophoresis was stopped. The resolving gels containing the separated proteins were further processed by western blot.

3.7.6.4 Western blot

Western blots were conducted using the Mini Trans-Blot® electroblotting system according to the wet sandwich method. The proteins were blotted onto nitrocellulose membranes with 0.45 µm pore size. To guarantee identical conditions, gels containing all samples of a given experimental series for a given antigen to detect were simultaneously blotted onto the same membrane. The cassettes were assembled in 1X blotting buffer as follows (direction: anode(+) side → cathode(−) side): One fiber pad, one Whatman™ filter paper, one entire gel or two truncated gels, one membrane, one filter paper, one fiber pad. Up to two cassettes were inserted into the electrode module of the cell, which was filled with 1X blotting buffer. Protein transfer was executed at a constant current of 400 mA for 150 min while the whole system was cooled on ice. Preliminary stainings of test gels with Coomassie Brilliant Blue had determined these parameters as ideal. The membranes with immobilized proteins were further processed by immunodetection.

3.7.6.5 Immunodetection

Reversible Ponceau S staining: At first, uniform protein loading and transfer was confirmed by reversible Ponceau S staining (Romero-Calvo et al., 2010). Each membrane was soaked in Ponceau S staining solution for 30 s at room temperature and then briefly rinsed with ddH2O to visualize the pattern of protein bands. The staining was removed by washing the membrane 1x 3 min in ddH2O while gently shaking, followed by washing the membrane 1x 3 min in TBS-T buffer.

Antibody labeling: All steps were carried out while gently shaking. Nitrocellulose membranes were blocked in blocking buffer for 1 h at room temperature. Primary antibodies (Table 2-3) were, according to the manufacturers' instructions, diluted either at 1:1000 or 1:2000 (GAPDH 1:20,000) in TBS-T buffer containing either 5 % (w/v) skim milk powder or 5 % (w/v) BSA, and applied at 4 °C overnight. Afterwards, membranes were washed 3x 5 min in TBS-T buffer. Then, appropriate horseradish peroxidase (HRP)-conjugated secondary antibodies (Table 2-4) were diluted at 1:5000 in TBS-T buffer containing 5 % (w/v) skim milk powder and applied at room temperature for 1 h. Upon removal of secondary antibodies, the membranes were washed 3x 10 min in TBS-T buffer.

Chemiluminescence detection: HRP enzyme activity was determined using the Amersham™ ECL™ Prime Western Blotting Detection Reagent Kit according to the manufacturer's instructions. Great care was taken to ensure a consistent treatment of the whole membrane surface. Chemiluminescence signals were detected on Lumi-Film chemiluminescent detection films placed inside a film cassette. The films were developed using the X-ray film developing machine CURIX 60. The exposure times ranged from 0.5 s up to 10 min. In case of very strong signals (e.g. for GAPDH), up to three films stacking on top of

each other were used. For each membrane, the positions of the reference bands were marked on the film. To ensure quantitative results, membranes were never stripped.

3.7.7 Enzyme-linked immunosorbent assay (ELISA)

Human Chorionic Gonadotropin (hCG) hormone present in cell culture media supernatants was quantified using the Human Chorionic Gonadotropin ELISA Kit, which is based on a direct solid phase sandwich ELISA method (Cole, 1997). The assay (96-well format) was conducted according to the manual of the kit using a P200 12-channel pipette. Prior to use, the −80 °C-stored media samples were completely thawed and homogenized by vortexing. Absorbance reads were made at 450 nm wavelength using the microplate spectrophotometer SpectraMax® 250. The concentrations were calculated by means of a calibration curve which was obtained by applying the serial dilution of hCG standards of known concentration provided by the kit. Since equal numbers of colony fragments of human pluripotent stem cells were initially seeded per well, no normalization for either number of cells or DNA content was necessary.

3.8 Gene expression analyses

3.8.1 Gene expression analysis by real-time quantitative polymerase chain reaction (real-time qPCR)

Real-time qPCRs (Kubista et al., 2006) were employed for expression analysis of selected single genes.

3.8.1.1 Isolation of total RNA

Total RNA of cells was isolated using the RNeasy® Mini Kit following the procedure of the kit's manual. Adherent growing cells in 6-well plates were washed twice with DPBS and then lysed on ice in 350 µl pre-cooled RLT lysis buffer (provided by the kit and supplemented 1:100 with β-mercaptoethanol) per well using a cell scraper. On-column digestion of DNA was done by enzymatic DNase I digestion according to the manual of the kit. Purified RNA was eluted by 40 µl RNase-free water into RNase-free 1.5 ml reaction tubes. The eluates were gently vortexed and stored at −80 °C. All subsequent work with RNA was performed using RNaseZap® spray and RNase-free consumables to avoid RNase contamination.

3.8.1.2 Determination of quantity and quality of RNA

Concentration and purity of RNA were determined using the spectrophotometer NanoDrop® 2000 as described (Chapter 3.6.4). A_{260}/A_{280} and A_{260}/A_{230} ratios of ~ 2.0 were generally accepted as "pure" RNA. Since the integrity of RNA is a very critical requirement for obtaining meaningful gene expression data (Fleige and Pfaffl, 2006), RNA integrity was confirmed by 2 % standard agarose gel electrophoresis (Chapter 3.6.6) of 1 µl aliquots using 1X TAE

buffer. Non-degraded total RNA showed two sharp bands without smear, comprising 28S rRNA (5070 nt length) and 18S rRNA (1869 nt length), at an intensity ratio of ~ 2:1.

3.8.1.3   Reverse transcription of RNA to cDNA

Reverse transcription from quality-checked total RNA for generation of cDNA was carried out with random hexamer primers. The reactions were conducted using the thermal cycler DNA Engine Dyad® and PCR tube strips. 25 µl reverse transcription reactions were prepared on ice in a 2-step protocol as stated below:

In the first tube, RNA and primers were combined:

Component, per reaction:	Volume or amount	Final concentration
RNase-free H2O	ad 10 µl	
RNA template	0.5–2 µg (but uniform amount for all samples)	20–80 ng/µl
Random hexamer primers	1 µg	40 ng/µl

RNA/primer mixes were heated to 75 °C for 5 min and then immediately chilled on ice to prevent RNAs from folding secondary structures. In the meantime, a reverse transcription mix was prepared as master mix for all single reactions (enzyme added last):

Component, per reaction:	Volume	Final concentration (amount)
RNase-free H2O	ad 15 µl	
M-MLV reaction buffer (5X)	5.00 µl	1X
dNTP mix (25 mM each)	0.50 µl	500 µM
M-MLV reverse transcriptase (200 U/µl)	0.25 µl	2 U/µl (50 U)

Then, 15 µl of the master mix were added into each 10 µl RNA/primer mix on ice. The 25 µl reactions were first kept at room temperature for 10 min to allow an early primer extension by the enzyme and thus to circumvent a preterm dissociation of hexamers from RNA. Then, the temperature was increased to 42 °C and the tube strips were incubated for 45 min, followed by heat inactivation of the enzyme at 95 °C for 5 min. The cDNA samples were briefly vortexed and finally stored at −20 °C.

3.8.1.4   Design and validation of primers for real-time qPCR

Design of primers: Specific primers for mRNA targets (Table 2-7) were designed using the software Primer-BLAST (Table 2-16). This program uses Primer3 to design PCR primers and then uses BLAST and global alignment algorithm to screen primers against user-selected databases in order to avoid primer pairs (all combinations, including forward-reverse, forward-forward and reverse-reverse pairs) that can cause non-specific amplifications. The default settings of the program were used, with the following parameters modified:

As PCR template, the database "RefSeq mRNA" for the organism *Homo sapiens* was chosen, which contains mRNA only from NCBI's Reference Sequence collection database (Table 2-17). Preference was set for annealing on exon junctions or spanning of introns. Primers were not allowed to bind on regions known to contain single-nucleotide

polymorphisms (SNPs). The maximum PCR product (amplicon) size was reduced to 250 bp. Primers were designed to detect all distinct transcripts in case a gene was known to lead to alternatively spliced mRNA variants. All primers were *in silico* evaluated to possess thermodynamic properties which do not significantly facilitate the formation of secondary structures. These include hairpin structures within a primer, self-dimers between two same-sense primers and heterodimers between forward/reverse primer of a given primer pair. This analysis was done using the software OligoAnalyzer 3.1 (Table 2-16) based on the default settings of the program. For hairpins, an estimated ∆G value (G = Gibbs free energy) of not less than −3 kcal/mol, and for self- and heterodimers of not less than −6 kcal/mol, was tolerated.

Validation of primers: The suitability of all primer pairs (Table 2-7) for a common annealing temperature of 60 °C was confirmed in practice by using a heterogeneous cDNA mixture of random cell types for real-time qPCR test reactions (Chapter 3.8.1.5 and 3.8.1.6). Specificity of primer pairs was certified by means of a single dissociation peak (melting curve) obtained for the reactions. Analysis of the corresponding reaction products by agarose gel electrophoresis (Chapter 3.6.6) must have led to a single band of expected amplicon size (Table 2-7). Applicability of primer pairs for relative quantification of gene expression over a wide range was certified by means of C_t values obtained for reactions containing a 1:10 dilution series of cDNA (undiluted, 1:10, 1:100, 1:1000). The C_t values must have differed ~ 3.3 among the dilutions, in agreement with an assumed exponential amplification of PCR products. It was also ensured that no substantial falsification of the results by primer-related side products, which are typically favored at low mRNA target concentrations, occurred. For this reason, primer pairs should not have led to C_t values < 37 when the reactions were carried out using an equal volume of ultrapure water instead of cDNA.

3.8.1.5 Real-time qPCR

Real-time qPCR reactions were carried out in 384-well optical reaction plates. The 8 µl reactions were set up on ice as stated below:

Component, per reaction:	Volume	Final concentration (amount)
H2O, ultrapure	ad 8 µl	
SYBR® Green PCR master mix (2X)	3.00 µl	0.75X
Forward/reverse primer mix (5 µM each)	1.00 µl	0.625 µM
cDNA template (1:5–1:20 diluted with ultrapure H2O; but uniform dilution for all samples)	2.00 µl	≙ 0.25–4 ng/µl (2–32 ng) of reverse-transcribed RNA

The reactions were initially prepared based on master mixes (one per individual primer pair) without cDNA template. 6 µl aliquots were added per well using the electronic repetitive pipette PIPETMAN M (P200M) with Diamond D200 pipette tips. Then, 2 µl individual cDNA template were added to each single well using the pipette PIPETMAN Classic™ (P2) with filter tips. The reactions were operated in technical triplicates with additional no-template-controls for all individual primer pairs (cDNA substituted by 2 µl ultrapure water). To

guarantee identical conditions, all samples of a given experimental series (cell line, time point) were processed on the same plate in respect of a given target gene. The plate was sealed with optical adhesive film and centrifuged at 2000 × g for 2 min. Afterwards, the following program parameters were applied using the 7900HT Fast Real-Time PCR System with fluorescence detector set for SYBR® Green:

Stage	Temperature	Time	Cycles
Initial	50 °C 95 °C	2 min 10 min	1x
1. Melt 2. Anneal & extend	95 °C 60 °C	15 s 1 min	40x
Dissociation curve	95 °C 60 °C 95 °C	15 s 15 s 15 s	1x
Hold	4 °C	∞	1x

3.8.1.6 Data analysis

Dissociation curves and C_t values (C_t = threshold cycle) of acquired data were generated using the software SDS 2.2.1 (Table 2-16). C_t values were exported to Excel and the analysis of relative gene expression was performed according to the comparative threshold cycle method ($\Delta\Delta C_t$) (Schmittgen and Livak, 2008). *GAPDH* was chosen as an appropriate endogenous internal standard (Murphy and Polak, 2002). For each individual cell sample (treatment, time point), the ΔC_t value for a given gene was calculated by subtracting the average C_t value of *GAPDH* from the average C_t value of the gene:

$$\Delta C_{t,\, gene} = C_{t,\, gene} - C_{t,\, GAPDH}$$

The ΔC_t value was then normalized against the ΔC_t value of the solvent/carrier-treated reference cells of the corresponding time point, leading to a $\Delta\Delta C_t$ value for the gene:

$$\Delta\Delta C_{t,\, gene} = \Delta C_{t,\, treated\ cells} - \Delta C_{t,\, reference\ cells}$$

The $\Delta\Delta C_t$ value was converted into a fold change value under the assumption of PCR product doubling for each PCR cycle:

$$\text{Fold change} = 2^{-\Delta\Delta Ct}$$

This value indicates the fold change of gene expression relative to the reference cell sample. The ratios were transformed into $\log_2$ values and displayed together with their standard deviation (STDEV) in bar charts created in Excel.

3.8.2 Gene expression analysis by microarray

Microarrays (Schena et al., 1995) were employed for whole-genome (global) gene expression analysis, since this technique allows the monitoring of thousands of genes in parallel.

3.8.2.1   cRNA synthesis, BeadChip hybridization and scanning

For analysis of the transcriptional signature of the two generated hiPSC lines iPS1 and iPS2 (Chapter 4.1), the total RNA of undifferentiated human pluripotent stem cells (H1, H9, iPS1, iPS2) growing feeder-free on Matrigel in MEF-CM (Chapter 3.1.2.2) and the total RNA of parental CV cells growing in Chang medium (Chapter 3.1.1.1) were used. For analysis of BMP-treated H1 hESCs (Chapter 4.2), the total RNA of H1 cells growing feeder-free on Matrigel in N2B27 medium (Chapter 3.4) was used. Isolation and assessment of total RNA were performed as aforementioned (Chapter 3.8.1.1 and 3.8.1.2).

cRNA synthesis: 400 ng of quality-checked total RNA served as input for preparation of biotinylated cRNA using the Illumina® TotalPrep™ RNA Amplification Kit. The kit is based on the RNA amplification protocol developed in the laboratory of James Eberwine (Van Gelder et al., 1990). Briefly, total RNA was primed with an oligo(dT) primer bearing a T7 RNA polymerase promoter (TTTT-P_{T7}). mRNA was reverse transcribed using ArrayScript™ reverse transcriptase to generate first- and second-strand full length cDNA. Then, RNA molecules were degraded and cDNA was purified to serve as template for T7 RNA polymerase. *In vitro* transcription of cDNA was carried out using MEGAscript™ T7 RNA polymerase along with biotin-UTP to generate hundreds to thousands of biotin-labeled antisense cRNA copies of each mRNA in a sample.

BeadChip hybridization and scanning: The cRNA was purified and directly hybridized onto Illumina® BeadChips (whole-genome gene expression arrays). The BeadChips consist of bead-linked single-stranded DNA oligonucleotides (50-mer gene-specific probes) which are held in microwells on the surface of the chip. Each bead type contains hundreds of thousands of copies of a covalently attached 50-mer probe. Data quality and reproducibility are supported by the high level of bead redundancy: Several copies of a bead type exist on every array on the BeadChip. In addition, distinct 50-mer probes can be present for an individual gene (one probe type per bead type), whereat the probes represent distinct sequence-specific regions of the gene's transcript. 29-mer address sequences present on each bead are used to map the array, identifying the location of each bead. For analysis of hiPSCs, one HumanRef-8_v3_BeadChip (8-sample format) was used and samples were hybridized in one biological and one technical replicate. For analysis of BMP-treated cells, two HumanHT-12_v4_BeadChips (12-sample format) were used and samples were hybridized in two biological and one technical replicates. Hybridized samples were washed, blocked and stained with Streptavidin-Cy3 using reagents and following protocols supplied by Illumina. BeadChips were scanned to obtain array images which contain fluorescence intensities for all spotted beads (data points).

cRNA synthesis, BeadChip hybridization and scanning were performed by the ATLAS Biolabs GmbH (Friedrichstraße 147, 10117 Berlin, Germany; http://www.atlas-biolabs.com).

3.8.2.2   Raw data processing

All subsequent data analyses were carried out using the software GenomeStudio™ V2011.1 (Table 2-16), unless stated otherwise.

Raw data were processed using the content descriptor / annotation file "HumanRef-8_V3_0_R3_11282963_A.bgx" (for HumanRef-8_v3_BeadChip) or "HumanHT-12_V4_0_R2_15002873_B.bgx" (for HumanHT-12_v4_BeadChips). The "Direct Hyb" (direct hybridization) mode was selected. Raw data were normalized using the "Rank Invariant" algorithm with background subtraction (Schmid et al., 2010) and were then filtered for significant expression on the basis of signal intensities of negative control beads that have no corresponding target in the sample, as described by Kuhn et al. (Kuhn et al., 2004). Data of two biological replicates were grouped together as one sample.

3.8.2.3   Basic expression analysis

For one-replicate-samples, the detected signal intensity (arbitrary units) of each gene was calculated together with the corresponding standard error (SE) of the gene's bead replicates. For grouped biological duplicate samples, the average (AVG) detected signal intensity of each gene was calculated together with the corresponding standard deviation (STDEV) of both arrays. For each individual gene a "Detection P-value" (P_{Det}) was calculated by the program. The P-value (P) is a measure for the likelihood that the data has occurred by chance, assuming the null hypothesis is true. Its scale ranges from 0 to 1. A P_{Det} of 0 (1) indicates a 100 % (0 %) probability that a gene is expressed and the null hypothesis to be rejected. A gene was considered as being significantly expressed in a given cell sample, if its P_{Det} was < 0.01. All data were exported to Excel.

3.8.2.4   Pearson's correlation coefficient and hierarchical cluster analysis

Pearson's correlation coefficient analysis (r^2 values) was done among paired combinations of individual samples. Genes were filtered to be only included in this analysis if their P_{Det} was < 0.01 for both samples to be compared. Dendograms of hierarchical cluster analysis, based on Pearson's correlation coefficients, were prepared choosing "Metric Correlation" for the samples.

3.8.2.5   Differential expression analysis

Differential expression analysis of BMP samples was performed choosing the error model "Illumina Custom" (Kuhn et al., 2004) and application of multiple testing corrections using the Benjamini & Hochberg "False Discovery Rate" (FDR) algorithm (Benjamini and Hochberg, 1995). The resulting "Differential P-value" (P_{Diff}), which was calculated by the program for each individual gene, indicates the probability that a gene is differentially expressed between a sample of interest and a reference sample. The BMP-treated cell samples were compared against the solvent/carrier-treated cell sample of the corresponding time point (= reference sample). Then, all data were exported to Excel and all AVG signal intensity values of < 10 were defined as 10. This arbitrary cut-off value should eliminate negative gene expression signals which might have occurred as result of the background subtraction during raw data processing. The fold change values (ratios) of gene expression were calculated by dividing the AVG signal intensity of a given sample by the AVG signal intensity of the reference sample. This calculation was done for each individual gene and sample (ligand, time point).

A gene was considered as being significantly differentially expressed between BMP sample and reference sample, if the following three criteria were fulfilled: 1.) The gene was significantly expressed in at least one of both samples ($P_{Det} < 0.01$ for BMP and/or reference sample). 2.) Its P_{Diff} was < 0.05. 3.) Its fold change value was > 1.5 or < 0.66 (= set threshold values for upregulated and downregulated gene expression, respectively).

Error analysis: To display the ratios of significantly differentially expressed genes in bar charts, the error bars were calculated as follows:

$$\frac{dX}{X} = \sqrt{\left(\frac{dA}{A}\right)^2 + \left(\frac{dB}{B}\right)^2}$$

X = ratio of AVG signal intensities (BMP-treated versus reference sample)

dX = STDEV of X

A = AVG signal intensity (BMP sample)

dA = STDEV of A

B = AVG signal intensity (reference sample)

dB = STDEV of B

Heatmaps: Heatmaps for color-coded visualization of signal intensities and gene expression ratios (independent of P-values and thresholds) were created using the software Multiexperiment Viewer (MeV) Version 4.8.1 (Table 2-16).

Venn diagrams: Venn diagrams displaying total numbers of unique and common significantly differentially expressed genes among BMP samples were created using the software VENNY (Table 2-16), which compares lists with Venn diagrams.

3.9 Bioinformatics

3.9.1 *In silico* predictions based on large gene lists

In-depth analyses of microarray-based gene lists were performed using the Database for Annotation, Visualization and Integrated Discovery (DAVID) v6.7 (Table 2-17). DAVID provides a comprehensive set of functional annotation tools for investigators to understand the biological meaning behind large gene lists (Huang et al., 2009a; Huang et al., 2009b). Gene lists with official gene symbols were run as queries against the background of *Homo sapiens*. Unless stated otherwise, all studies were executed based on the default parameter settings of DAVID. Data outputs were exported to Excel.

3.9.1.1 Tissue correlation analysis

Tissue correlation analysis was performed using the UP_TISSUE tool implemented in DAVID for significantly upregulated and downregulated genes, respectively. For individual BMP samples (ligand versus HCl/BSA reference sample of the same time point), the following criteria were applied: Only major tissues and anatomical compartments which were

identified as enriched (versus the whole genome) by the UniProt database (Table 2-17) for at least one gene list by at least 2 distinct genes with a correlation P-value of < 0.05 were accepted. Heatmaps for color-coded visualization of correlation P-values were prepared using the software MeV Version 4.8.1 (Table 2-16). For shared genes between day 5 samples (BMP5 ∩ BMP10 ∩ BMP13 versus reference), the analysis was done as described for the cellular component analysis.

3.9.1.2   Global pathway analysis

Global pathway analysis for individual BMP samples was done as described for the tissue correlation analysis using the PATHWAYS tool implemented in DAVID. The KEGG, PANTHER and REACTOME pathway databases (Table 2-17) were chosen as references.

3.9.1.3   Cellular component analysis

Gene Ontology (GO)-term analysis regarding cellular components (CCs) was performed using the GOTERM_CC tool implemented in DAVID, which uses the GO database (Table 2-17) as a reference. The analysis was performed for commonly upregulated and for commonly downregulated genes (BMP5 ∩ BMP10 ∩ BMP13 versus reference) of day 5 samples. The lists of genes to input were obtained using the software VENNY (Table 2-16). CC outputs were only considered, if they represented in at least one case (up- or downregulated genes) ≥ 1 % of the input genes. All correlation P-values were accepted, because this analysis was not focused on the enrichment of CCs in relation to the whole genome.

3.9.2   Alignment of protein sequences

Multiple sequence alignment of protein sequences in FASTA format was done using Clustal Omega Version 1.2.1 (Table 2-16) based on the default settings of the program.

4 Results

This results chapter is divided into two parts. The first part (Chapter 4.1) shows the results of the creation of human induced pluripotent stem cells (hiPSCs), which served – beside human embryonic stem cells (hESCs) – as a model system for studying BMPs. The second part (Chapter 4.2) comprises the main part and topic of this PhD project and shows the results of the BMP signaling and differentiation studies on human pluripotent stem cells.

4.1 Generation and verification of the human induced pluripotent stem cell lines iPS1 and iPS2 to be used for the BMP studies

4.1.1 Generation of hiPSCs from primary human chorionic villi (CV) cells

Primary human chorionic villi (CV) cells were reprogrammed by classical retroviral transduction of the four Yamanaka-factors OCT4, SOX2, KLF4 and c-MYC (Takahashi et al., 2007). For this purpose, retroviral vectors had to be prepared. Plasmids used for retrovirus production were initially amplified in *Escherichia coli* (*E.coli*) bacteria. The integrity of the purified plasmids was confirmed by agarose gel electrophoresis (Figure 4-1A). In addition, the identity of the four plasmids encoding the reprogramming factors was confirmed by diagnostic restriction enzyme digestion, followed by separation of the resulting DNA fragments by agarose gel electrophoresis (Figure 4-1B).
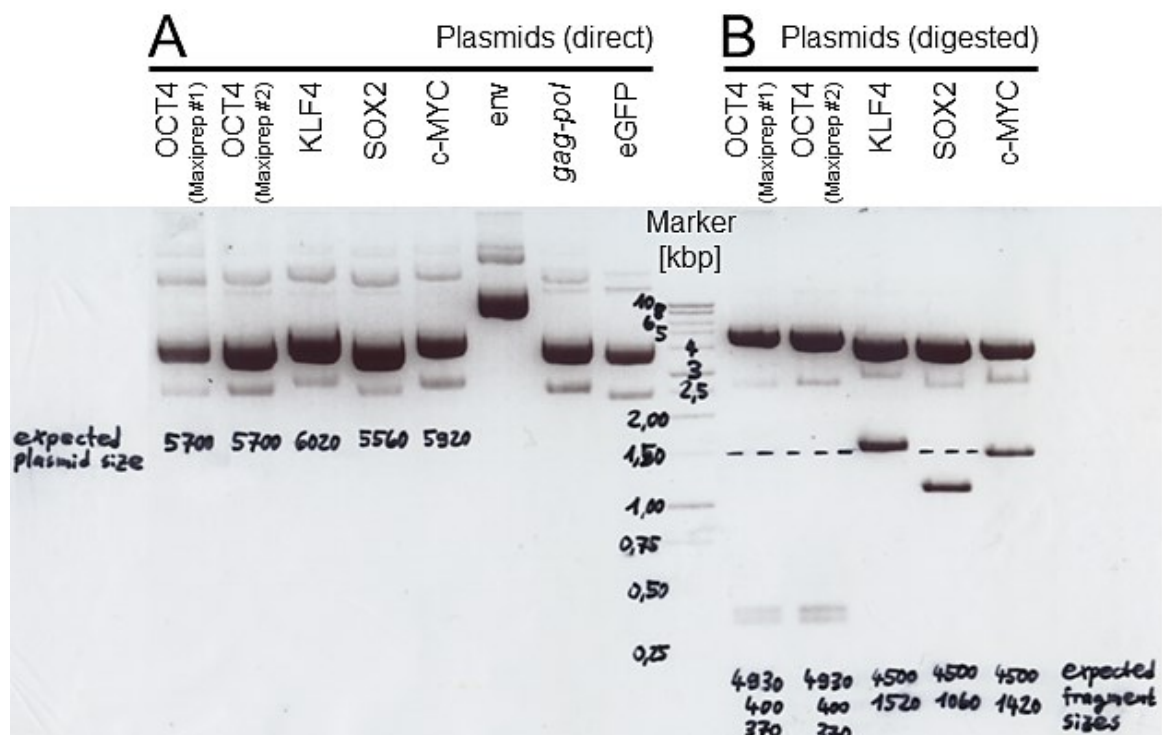
Figure 4-1   Confirmation of integrity and identity of the plasmids used for retroviral vector production.
(A) Plasmids were amplified in *E.coli* bacteria and isolated by Maxiprep. Aliquots containing 1 µg DNA of each purified plasmid were analyzed by agarose gel electrophoresis. The main bands indicate that the plasmid DNA

was predominantly present in its supercoiled, covalently closed circular form, which possesses a faster electrophoretic mobility than linear and relaxed open-circle conformations. **(B)** Aliquots of purified plasmids encoding the transgenes *OCT4*, *SOX4*, *KLF4* and *c-MYC* were subjected to diagnostic restriction enzyme digestion and analyzed by agarose gel electrophoresis. The positions of the obtained bands are in agreement with the expected fragment lengths according to the individual plasmid maps (Table 2-5).

Transgene-carrying retroviruses were produced in HEK-293T host cells by co-transfection of envelope plasmid, packaging plasmid and individual transfer vector plasmid (OCT4, SOX2, KLF4 or c-MYC). The success of transfections was confirmed by means of a negative and a positive control. As positive control, the cells were co-transfected using a transfer vector plasmid that encodes Enhanced Green Fluorescent Protein (eGFP) as reporter gene. At 36 h post-transfection, a transfection efficiency of about 51 % GFP$^+$ cells was determined by flow cytometry (Figure 4-2).

36 hours post-transfection
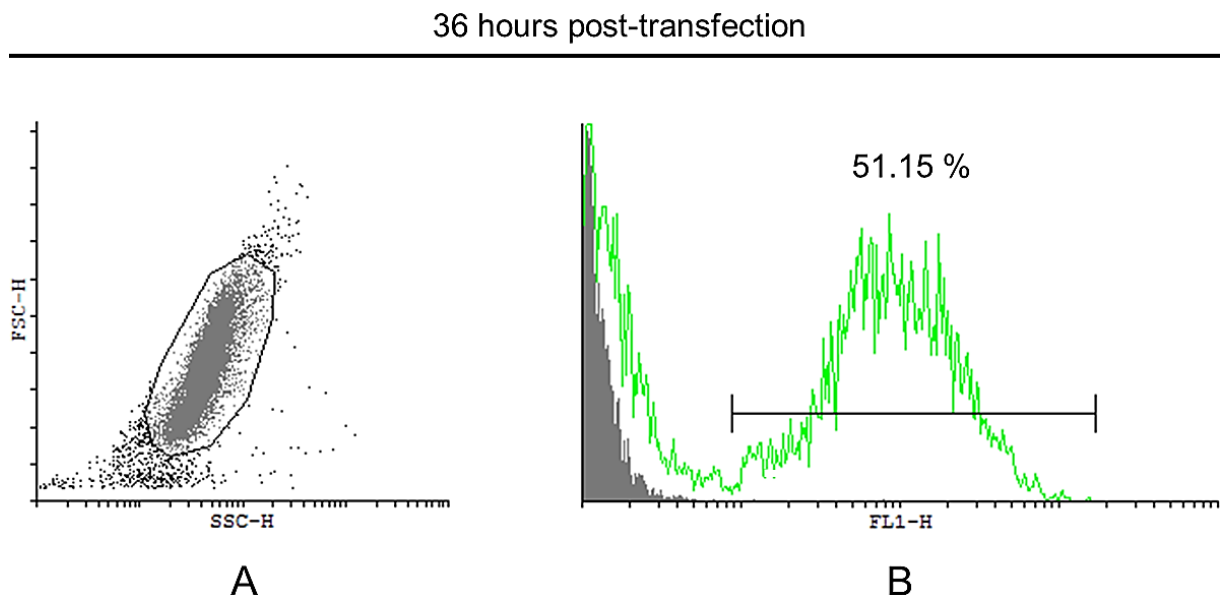
Figure 4-2   Determination of transfection efficiency of transfer vector plasmids into HEK-293T host cells used for retrovirus production.
36 h post-transfection, cells were fixed with PFA and analyzed by flow cytometry. **(A)** Dot plot based on light scatter properties of untreated HEK-293T cells (negative control). FSC = forward scatter, SSC = side scatter. The bordered area represents the selected main cell population which was considered for further analysis in (B) for both samples. A total of 10,000 events were counted. **(B)** Histogram: Cell count versus detected green fluorescence intensity (FL1; $\log_{10}$). Overlay of untreated HEK-293T cells serving as reference for autofluorescence background (grey) and cells co-transfected with GFP transfer vector plasmid (green). Counts of both samples were normalized to fit in scale (maxima represent 67 counts (grey) and 37 counts (green)). About 51 % of transfected cells were GFP$^+$.

A 1:1:1:1 cocktail of produced OCT4, SOX2, KLF4 and c-MYC retroviruses was used for transduction of CV cells. The transduction efficiency was determined for each of the four reprogramming factors at 72 h post-infection. Immunocytochemistry was applied, since this method not only allows quantitative conclusions regarding protein expression, but also provides information about the subcellular localization of proteins. 70 % of cell nuclei were stained as OCT4$^+$, 72 % as SOX2$^+$, 75 % as KLF4$^+$ and 46 % as c-MYC$^+$ (Figure 4-3).

72 hours post-transduction
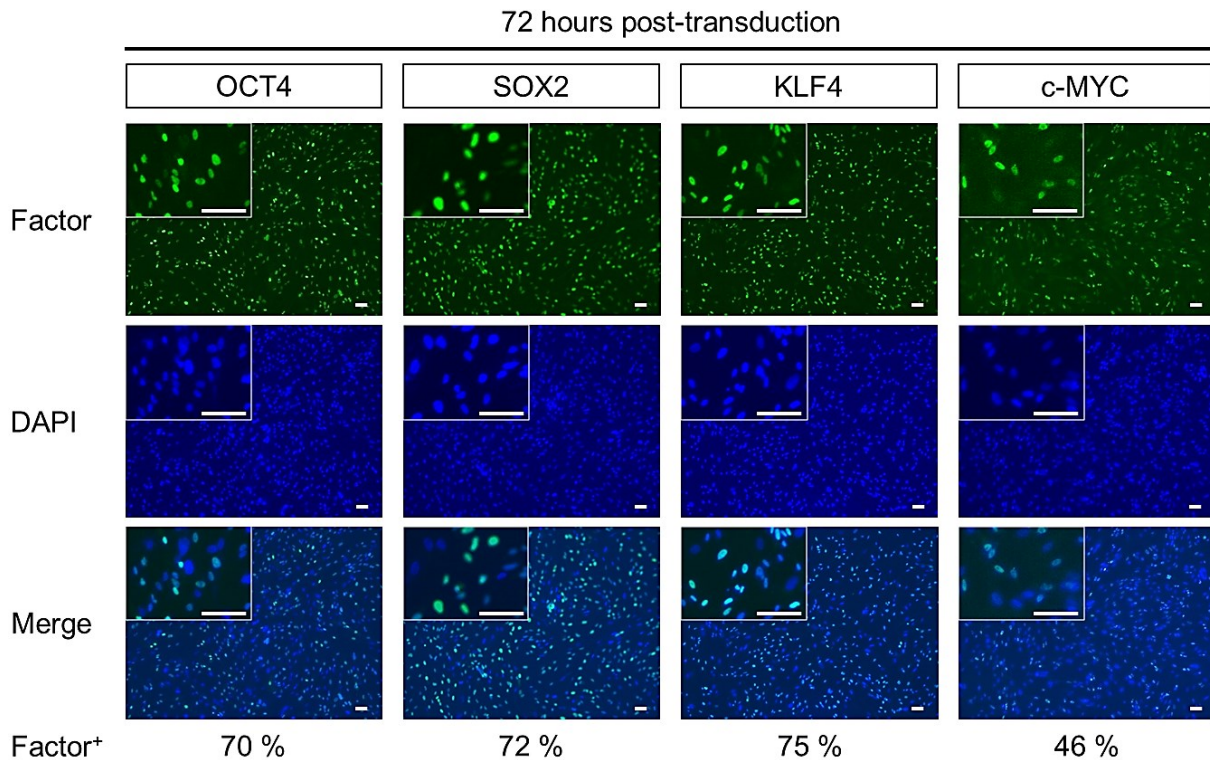
Figure 4-3   Determination of transduction efficiency of CV cells infected with retroviral vectors carrying the transgenes OCT4, SOX2, KLF4 and c-MYC.
72 h post-infection, cells were fixed with PFA and stained by immunocytochemistry using specific antibodies directed against these factors. Nuclei were counterstained with DAPI. Stained cells were visualized by fluorescence microscopy (green channel, blue channel and overlay). At least 2 × 100 cells, which were localized in different areas, were counted to calculate the percentage of transduced (factor⁺) cells. The higher magnified image sections confirm the nuclear location of the four transcription factors. The presence of nuclei which were only positive for DAPI excludes the possibility of an endogenous expression of these factors by CV cells or a non-specificity of the used fluorescence-labeled secondary antibodies. Scale bars represent 100 µm.

The transduced CV cells were subsequently grown under culture conditions for human pluripotent stem cells on feeder layers of mitotically inactivated mouse embryonic fibroblasts (MEFs). First morphological changes of CV cells were observed at day 12 post-transduction. At some places, tiny granulated cell aggregates appeared between the CV cells and MEFs (Figure 4-4A). This indicated the onset of mesenchymal-to-epithelial transition, the reverse process of EMT during gastrulation (Chapter 1.1.1.2). In the following weeks, those structures grew and transformed into cell colonies which were looking like typical hiPSC colonies, as described before (Takahashi et al., 2007): Similar to hESCs (Thomson et al., 1998), undifferentiated hiPSCs possess a small round shape due to their high nucleus-to-cytoplasm ratio, and grow densely packed in colonies with clearly defined borders. At day 31 post-transduction, individual colonies (Figure 4-4B) were manually picked for separate expansion of the distinct clonal cell lines.

On average, 19 colonies developed per 6-well. Based on an initial input of 1×10^5 CV cells per well, and after adjustment for one splitting step of 1:3, this yields a reprogramming efficiency of 0.057 %.
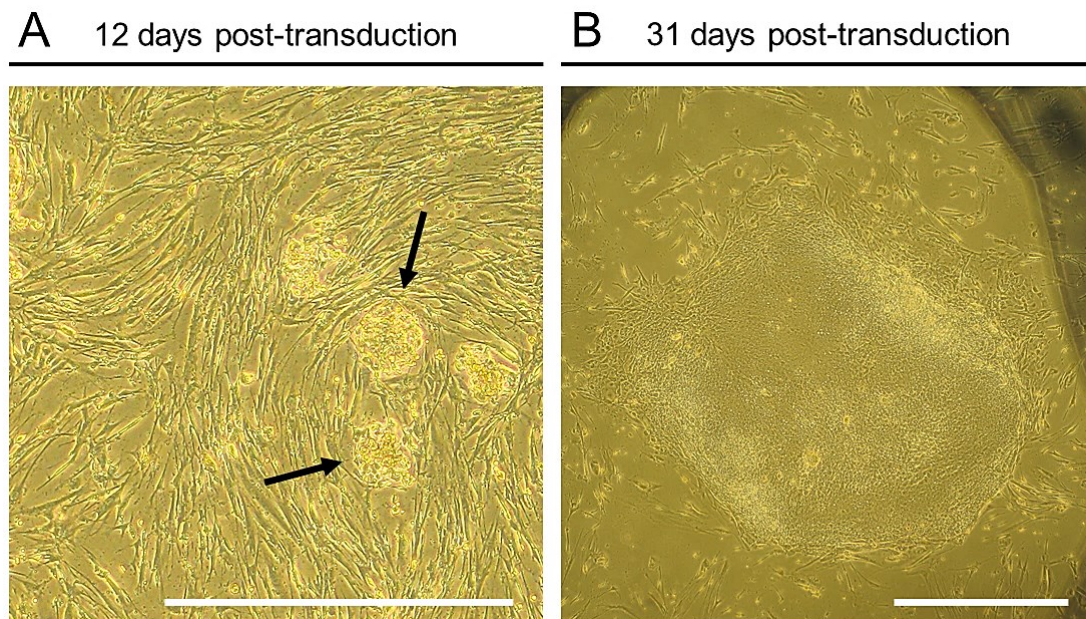
Figure 4-4   Morphological transformation of transduced CV cells during their reprogramming to hiPSCs.
(A) Arrows indicate emerged small, tightly packed cell clusters located between somatic cells at day 12 post-transduction. **(B)** Typical hiPSC-like colony at day 31 post-transduction. Scale bars represent 1 mm.

4.1.2 Verification of the two clonal lines iPS1 and iPS2 as being hiPSCs

Two of the separately expanded clonal cell lines, which were named iPS1 and iPS2, were entirely and successfully characterized as being hiPSCs according to the standard protocols (Takahashi et al., 2007; Ohnuki et al., 2009).

4.1.2.1 Expression of pluripotency markers on the level of proteins, glycolipids and sulfated carbohydrates

At first, the expression of typical pluripotency markers that are known to be associated with the undifferentiated state of hESCs was confirmed.

hESCs can be characterized by a high expression level of Tissue-nonspecific Alkaline Phosphatase (AP) on their cell membranes (Thomson et al., 1998; International Stem Cell Initiative, 2007). This hydrolase enzyme is responsible for removing phosphate groups from many types of substrates and works most efficient in alkaline environments. Staining of iPS1 and iPS2 colonies for AP enzyme activity confirmed both cell lines as AP$^+$ (Figure 4-5A).

Immunocytochemical staining of PFA-fixed iPS1 and iPS2 colonies (Figure 4-5B) showed that both cell lines were positive for the proteins OCT4, SOX2, NANOG and LIN28. The transcription factors OCT4, SOX2 and NANOG belong to the core gene regulatory network required to maintain the pluripotent phenotype of hESCs (Boyer et al., 2005). NANOG, which was not part of the reprogramming factors, is a downstream target of OCT4 and SOX2 due to the presence of OCT4/SOX2 binding sites in the promoter region of its gene (Rodda et al., 2005). LIN28 is a cytoplasmic mRNA-binding protein involved in regulating self-renewal of hESCs and proposed to enhance the translation of OCT4 mRNA (Qiu et al., 2010). Moreover, iPS1 and iPS2 cells were stained positive for the glycolipid antigens SSEA-3 and SSEA-4 (stage-specific

embryonic <u>a</u>ntigens) and the keratan sulfate antigens TRA-1-60 and TRA-1-81 (<u>Tra</u>falgar antigens), known to be expressed on the surface of hESCs (Thomson et al., 1998).
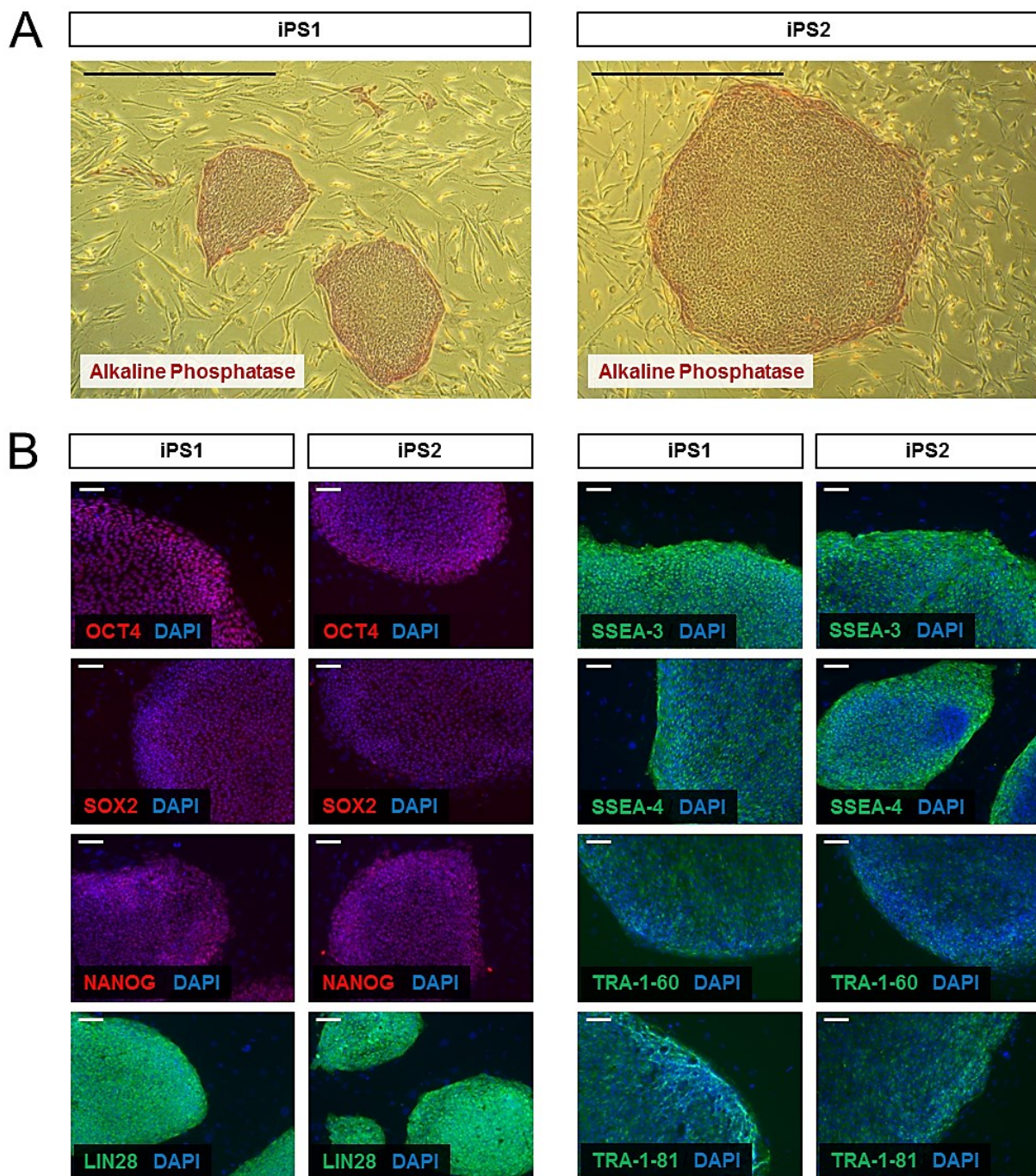
Figure 4-5   Expression of pluripotency markers on the level of proteins, glycolipids and sulfated carbohydrates by iPS1 and iPS2 cells.
(A) Alkaline Phosphatase (AP) activity (ruby red color) of iPS1 and iPS2 colonies which are growing between feeder cells (AP-negative). Scale bars represent 1 mm. **(B)** Immunocytochemical staining of PFA-fixed iPS1 and iPS2 colonies for several hESC markers as indicated (fluorescence microscopy). Nuclei were counterstained with DAPI. Transcription factors are labeled with red fluorescent dye, leading to a violet overlay color. Cytoplasm- or cell membrane-located antigens are labeled with green fluorescent dye. Scale bars represent 100 μm. (Figure modified from Lichtner et al., 2013.)

4.1.2.2   Expression of pluripotency markers on the level of mRNA

The expression of previous five proteins was further inspected on mRNA level by means of microarray analysis for the two clonal cell lines iPS1 and iPS2, the parental CV cells from which they were derived, and the two independent hESC lines H1 (male) and H9 (female) (Figure 4-6). mRNA of Tissue-nonspecific AP (*ALPL* gene) was significantly expressed in iPS1, iPS2, H1 and H9 cells ($P_{Det} = 0$), and also in original CV cells ($P_{Det} = 0.003$), but in the latter at least 57.6-fold weaker. The genes *OCT4*, *SOX2*, *NANOG* and *LIN28* were significantly expressed in iPS1, iPS2, H1 and H9 cells ($P_{Det} = 0$), but not in CV cells ($P_{Det} \geq 0.556$). The expression levels of these genes in iPS1 and iPS2 cells were in the range of hESCs.
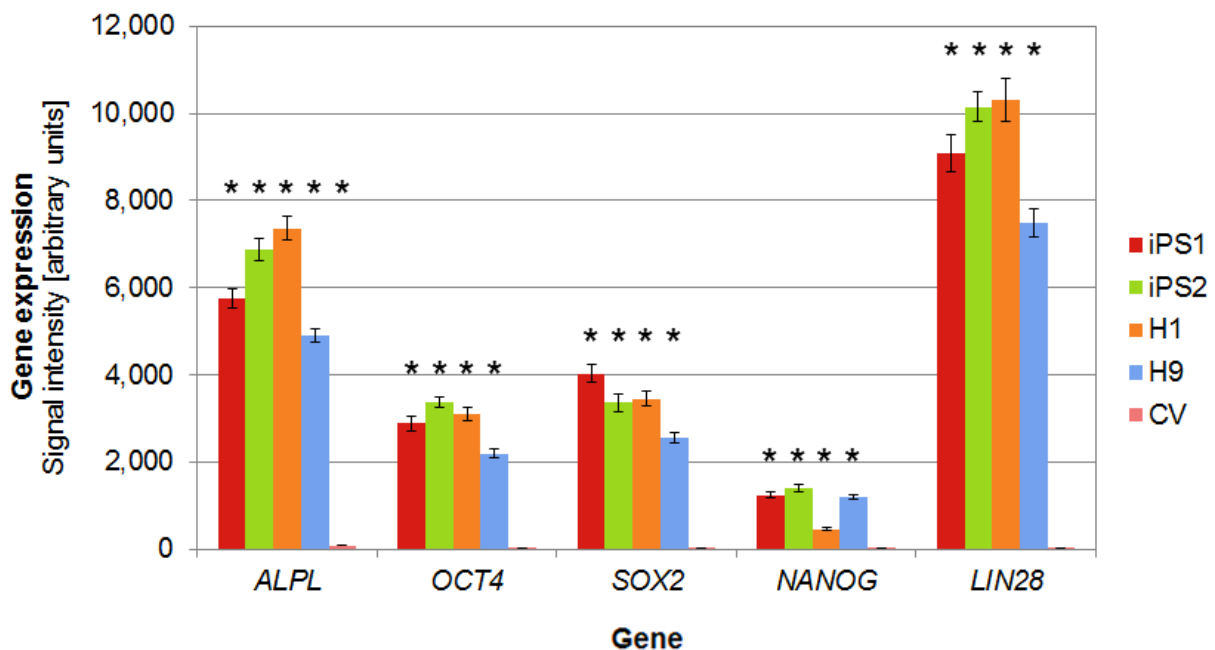
Figure 4-6   Gene expression levels of pluripotency markers in iPS1 and iPS2 cells, H1 and H9 hESCs and CV cells prior to their reprogramming.
Levels of gene expression in parental CV cells, CV cell-derived hiPSCs (clonal lines iPS1 and iPS2) and hESCs (lines H1 and H9) were determined by microarray analysis of cRNA samples. *: $P_{Det} < 0.01$. Error bars indicate SE of the bead replicates.

4.1.2.3   Reactivation of telomerase activity and bypassing of cellular senescence

Reactivation of telomerase activity:

A key feature of hESCs, germline cells and many cancer cells is their potential immortality due to a high telomerase activity – in contrast to normal human somatic tissues where this enzyme is repressed (Thomson et al., 1998; Kim et al., 1994). The telomerase is a ribonucleoprotein and functions as reverse transcriptase by *de novo* addition of repetitive DNA sequences on the 3'-end of DNA strands of the telomeres (Greider and Blackburn, 1989). Telomeres are the end regions of the linear chromosomes of eukaryotes. They are continually shortened with each cell division due to the incapability of the DNA polymerase to synthesize the outside 5'-end of the lagging strand. In humans, telomeres consist of thousands of non-coding tandem repeats of the six bases 5'-TTAGGG (Blackburn, 1991). The telomere length is a critical factor which

influences the life span of cells. Once a critical chromosome length is reached, genomic instability (Lundblad, 2000), cellular senescence and programmed cell death occur (Urquidi et al., 2000; Mondello and Scovassi, 2004).

Hence, the telomerase activity in whole cell extracts of iPS1/iPS2 cells, parental CV cells and H1/H9 hESCs was measured. The method applied directly quantifies the number of synthetic substrate oligonucleotides that had been added to the cell extracts and were subsequently extended by the present enzyme with telomeric repeats on their 3'-ends. The results clearly confirmed a reactivation of telomerase activity in iPS1/iPS2 cells upon reprogramming of CV cells (Figure 4-7): The quantified copy numbers of extended oligonucleotides measured for iPS1 and iPS2 cells were similar to the levels measured for H1 and H9 cells serving as references (log_{10} 7.05 and 7.28 versus 7.74 and 6.86). In contrast, the measured activity in CV cell extracts did not exceed the background levels of the negative control samples (log_{10} range 4.62–4.82).
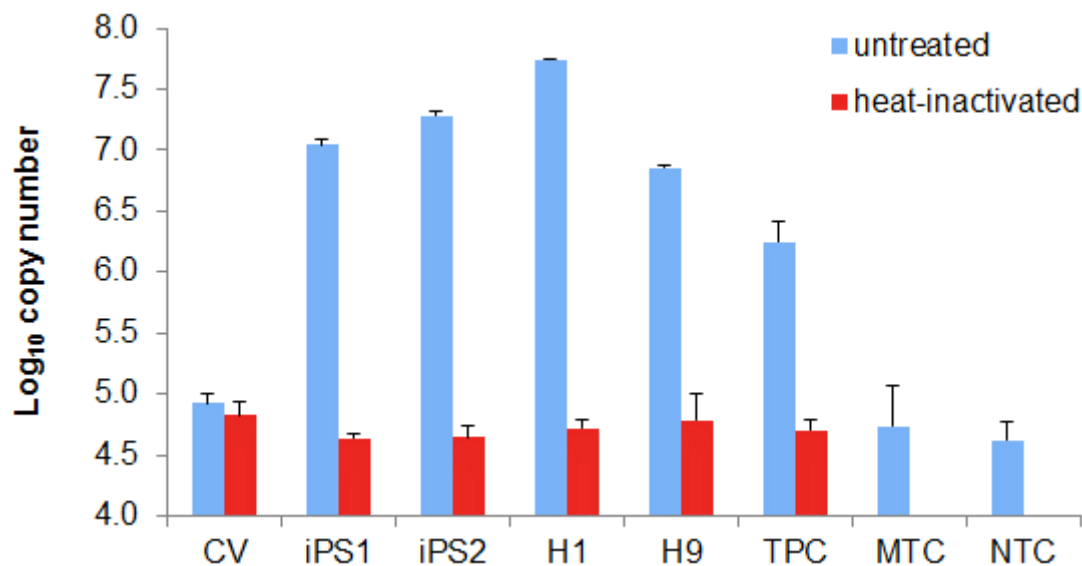
Figure 4-7   Reactivation of telomerase activity in iPS1 and iPS2 cells.
The telomerase activity was low in CV cells. Upon reprogramming, the enzyme activity was reactivated. References for high telomerase activity: hESC lines H1 and H9 and the telomerase-positive cell extract (TPC) provided by the kit. Negative controls: Minus-telomerase control (MTC, only CHAPS lysis buffer), no-template control (NTC, only RNase-free H2O) and heat-treated cell extracts. Average values, error bars indicate STDEV (technical triplicates). (Figure modified from Lichtner et al., 2013.)

Bypassing of cellular senescence:

In agreement with the non-detection of telomerase activity in CV cells, thawed passage 5 CV cells acquired typical signs of cellular senescence after additional 5−7 weeks in culture. These included a big and flat "fried egg" cell shape, accompanied by a strong decrease in their proliferation rate (Sherwood et al., 1988) (Figure 4-8A-B). In addition, the cells were stained positive for the senescence marker β-Galactosidase (Figure 4-8C). This pH-dependent lysosomal enzyme catalyzes the hydrolysis of beta-galactosides into monosaccharides and is known to be overexpressed and accumulated in senescent cells (Dimri et al., 1995; Lee et al., 2006).

Extensive cell death of senescent cells occurred after around 12–13 weeks (Figure 4-8D). The observed phenomenon can be explained by the "Hayflick limit" (Hayflick, 1965), which is the maximum number of times a normal somatic cell population can divide in *in vitro* culture, until the cells remain in a post-mitotic state. This ultimate destination will be reached, even if the cell culture medium contains serum to stimulate mitosis, and no contact inhibition exists. In contrast, iPS1 and iPS2 cells were able to bypass cellular senescence and did not show any signs of aging after 10 months of non-stop maintenance in culture (Figure 4-8E).
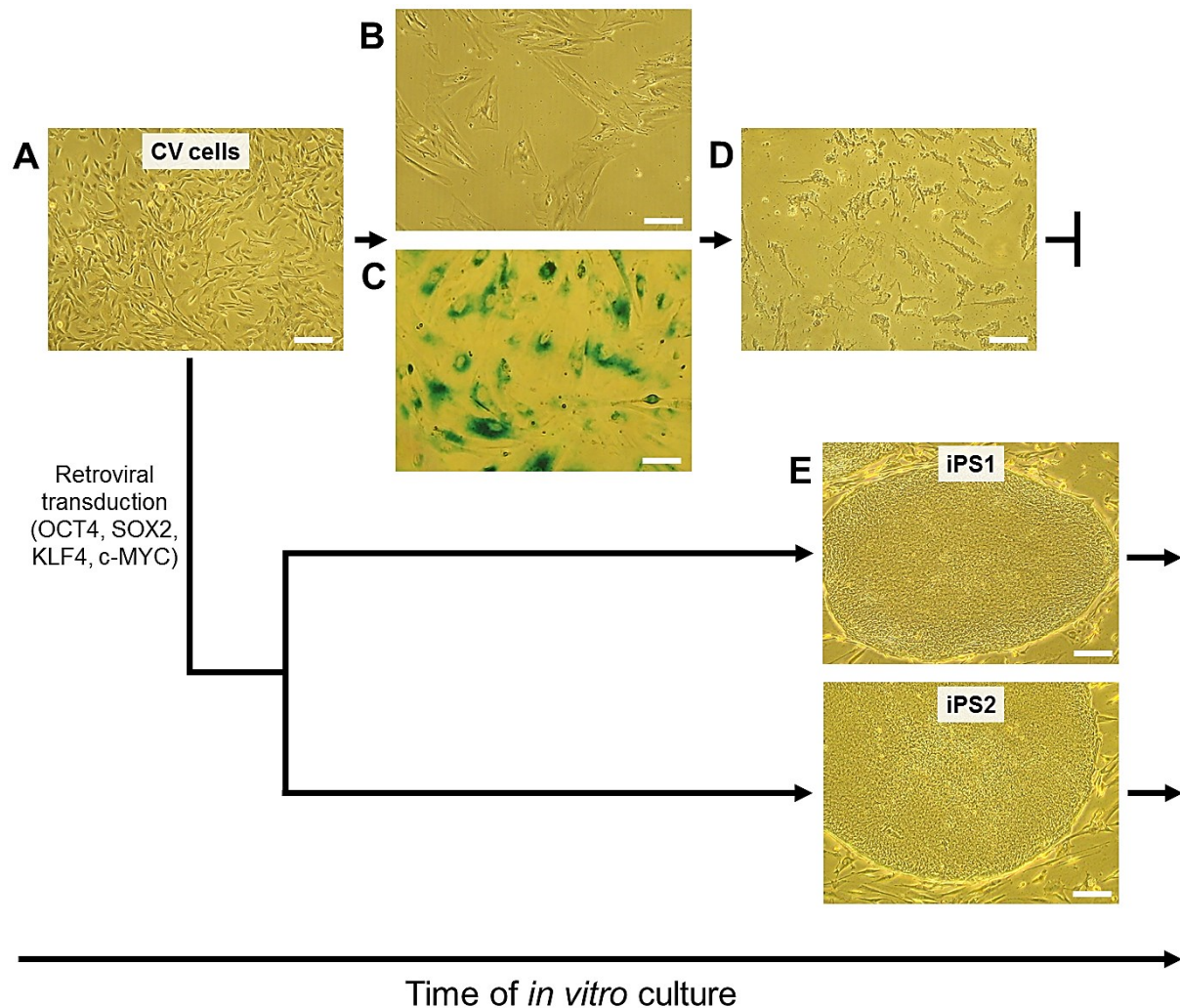
Figure 4-8   Bypassing of cellular senescence by iPS1 and iPS2 cells.
(A) Fast proliferating, low-passage primary human CV cells were either reprogrammed to hiPSCs or left untreated. Cells were maintained non-stop in culture, regularly fed and routinely passaged when confluent. **(B)** Senescent CV cells with large flattened morphology and decreased proliferation rate. **(C)** Senescent CV cells stained positive for β-Galactosidase (turquoise color). **(D)** Decay of senescent CV cells after 3 months. **(E)** Typical colonies of CV cell-derived iPS1/iPS2 hiPSCs after 10 months. Scale bars represent 200 μm.

4.1.2.4   Pluripotency under *in vitro* conditions

The differentiation capacity of iPS1 and iPS2 cells was assessed under *in vitro* conditions by applying the "embryoid body formation assay" (Itskovitz-Eldor et al., 2000). Colonies of undifferentiated cells were at first forced to spontaneously differentiate in suspension,

69

leading to the formation of three-dimensional structures called embryoid bodies (EBs) (Figure 4-9A). Afterwards, the EBs were allowed to attach and to further spontaneously differentiate (Figure 4-9B). Finally, the adherent outgrowth of random differentiated cells was evaluated by immunocytochemistry using specific antibodies directed against selected lineage markers, in order to find out whether they represented all three germ layers (ectoderm, mesoderm and endoderm; Chapter 1.1.1.2). Two time points of differentiation were evaluated: 7 days in suspension + 3 days and 14 days adherent growth. This is because some lineage markers are known to be expressed exclusively throughout early development, while others are known to be expressed only in more advanced differentiated cells.

SOX17, FOXA2 and Alpha-Fetoprotein (AFP) were chosen as endoderm markers. The transcription factors SOX17 and FOXA2 are expressed in definitive endoderm cell populations (King et al., 2008). AFP is a marker of extraembryonic endoderm (= primitive endoderm) cell populations (Hyslop et al., 2005) and hepatic (progenitor) cells, which belong to definitive endoderm (Jozefczuk et al., 2011) and can become binucleated and tetraploid as they mature (Gentric et al., 2012). The transcription factor Brachyury (also known as Protein T) is specific for cells belonging to the primitive streak (= mesendoderm) (Herrmann et al., 1990; Rivera-Pérez and Magnuson, 2005). Alpha-Smooth Muscle Actin (α-SMA) was chosen as a mesoderm marker and labels the thin actin filaments of smooth muscle cells, myofibroblasts and myoepithelial cells (Perrin and Ervasti, 2010). Ectoderm cell fate was determined by staining for PAX6, Nestin and Tubulin Beta-3 Chain (βIII-Tubulin). The transcription factor PAX6 is expressed in neural progenitor cells (Ericson et al., 1997). The intermediate filament protein Nestin is expressed in neural and glial cells in the developing human central nervous system (Messam et al., 2000). βIII-Tubulin is a constituent of the cylindrical bundles of microtubules of neurites. Neurites are projections that extend from the cell body of immature neurons and can become axons or dendrites (da Silva and Dotti, 2002).

Fluorescence microscopy revealed positive subpopulations within random differentiated iPS1 and iPS2 cells for each of the tested marker proteins (Figure 4-9C). Thus, both clonal cell lines were rated as being pluripotent under *in vitro* conditions.
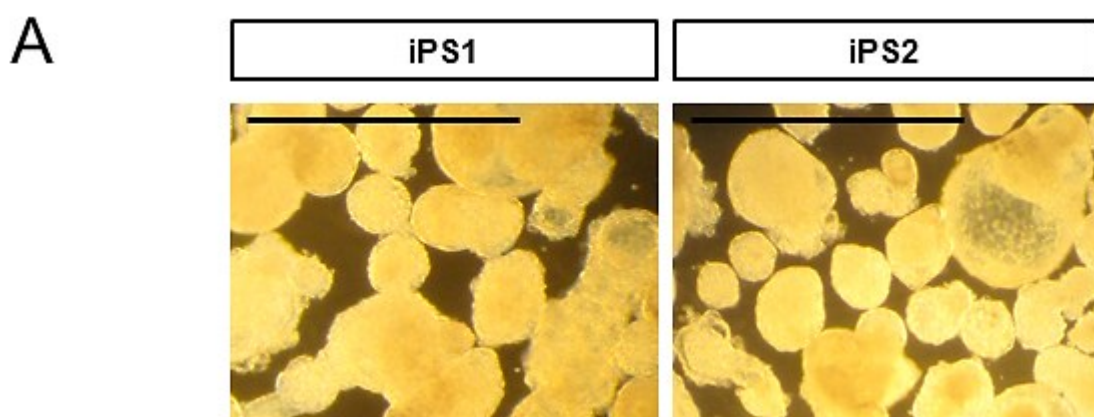
(continued from previous page)
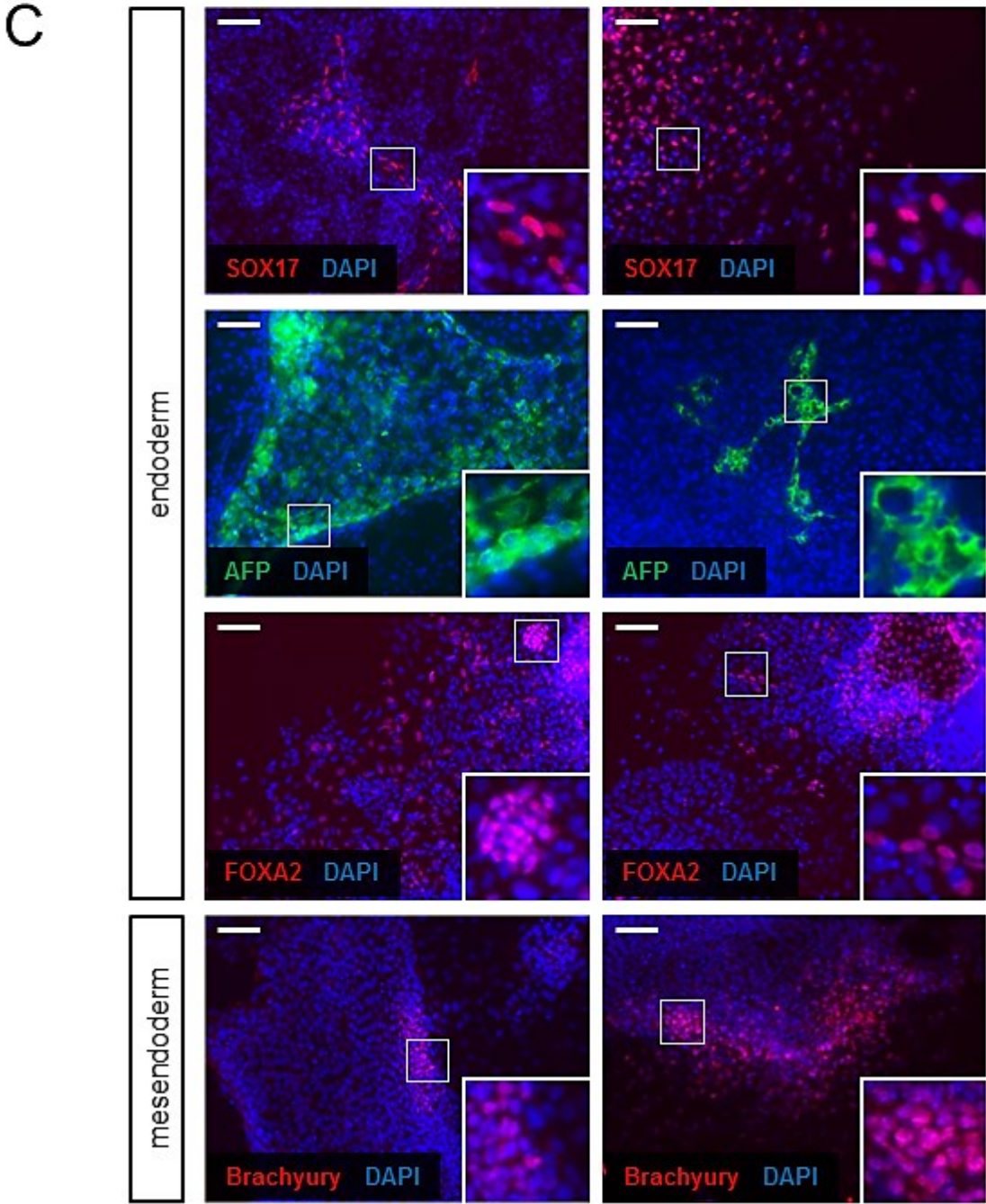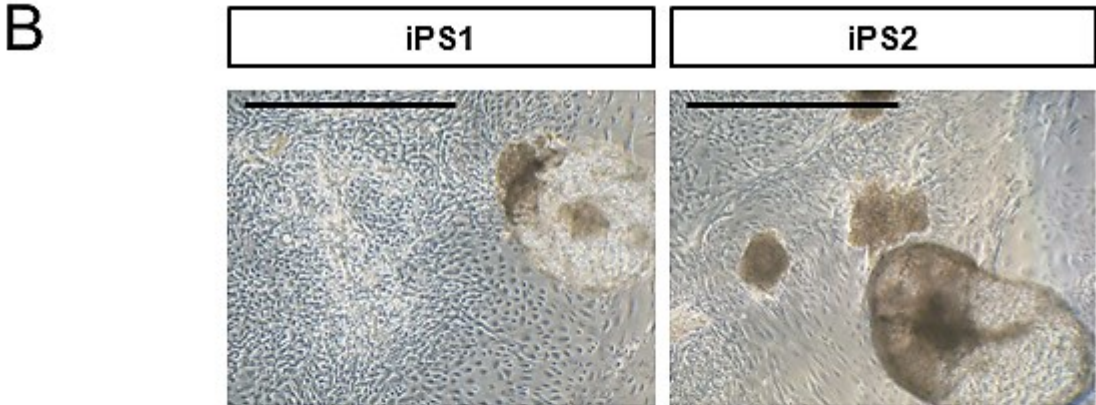
(continued from previous page)

Figure 4-9   Embryoid body formation assay of iPS1 and iPS2 cells.
(A) Embryoid bodies (EBs) after 7 days in suspension (immediately before plating on gelatin). **(B)** Randomly differentiated EB cells after 14 days adherent growth on gelatin. **(C)** Fluorescence microscopy photos of immunocytochemical-stained PFA-fixed cells for lineage markers representing endoderm, mesendoderm, mesoderm and ectoderm as indicated. Nuclei were counterstained with DAPI. Transcription factors are labeled with red fluorescence dye, leading to a violet color in combination with DAPI. Scale bars represent 1 mm (black) and 100 µm (white). (Figure modified from Lichtner et al., 2013.)

4.1.2.5   Pluripotency under *in vivo* conditions

In the next step, the pluripotency of both cell lines was confirmed under *in vivo* conditions by applying the "teratoma formation assay" (Gropp et al., 2012). Undifferentiated iPS1 and iPS2 cells were injected into mice with depleted immune system to prevent a rejection of the xenografts. The injected cells continued to grow and led to the formation of an encapsulated tumor referred to as teratoma, which consisted of randomly differentiated cells. Induced tumors could be felt starting from day 26 post-transplantation and grew exponentially from that day on. After 43 days, both teratomas had reached a critical size of > 1 cm³ in relation to the average body weight of the mice (approx. 22 g) (Figure 4-10A). The mice were sacrificed for dissection of teratomas (Figure 4-10B). Histological analysis of tissue sections revealed that both teratomas contained complex tissue structures, e.g. tubular structures and cartilage islands, which represented all three germ layers (Figure 4-10C).
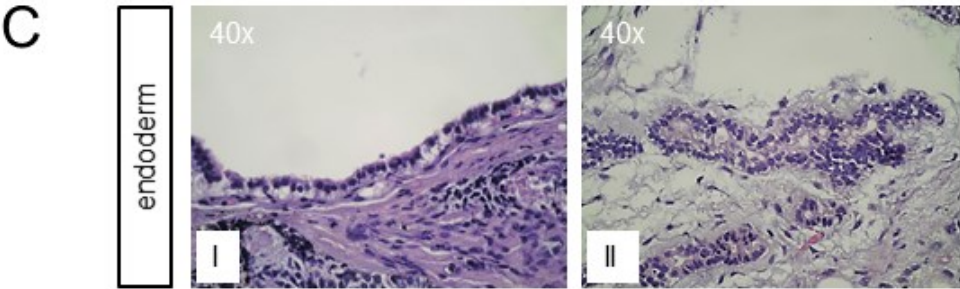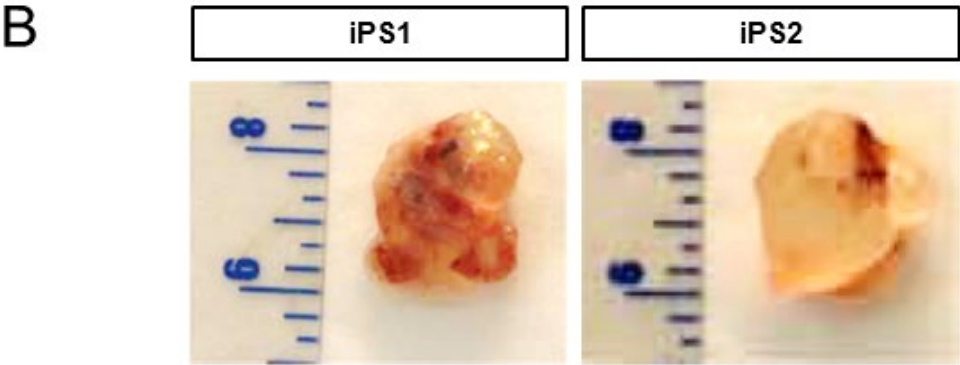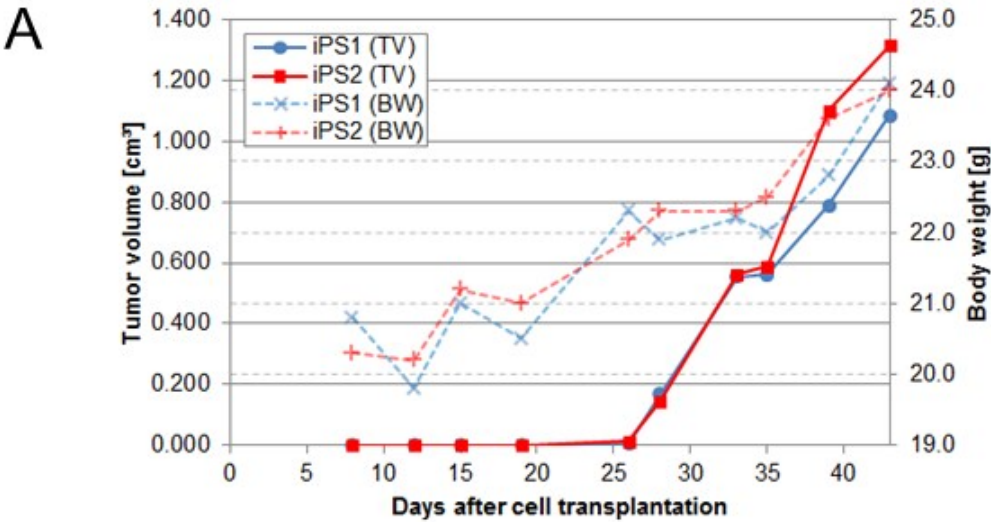
(continued on next page)

(continued from previous page)
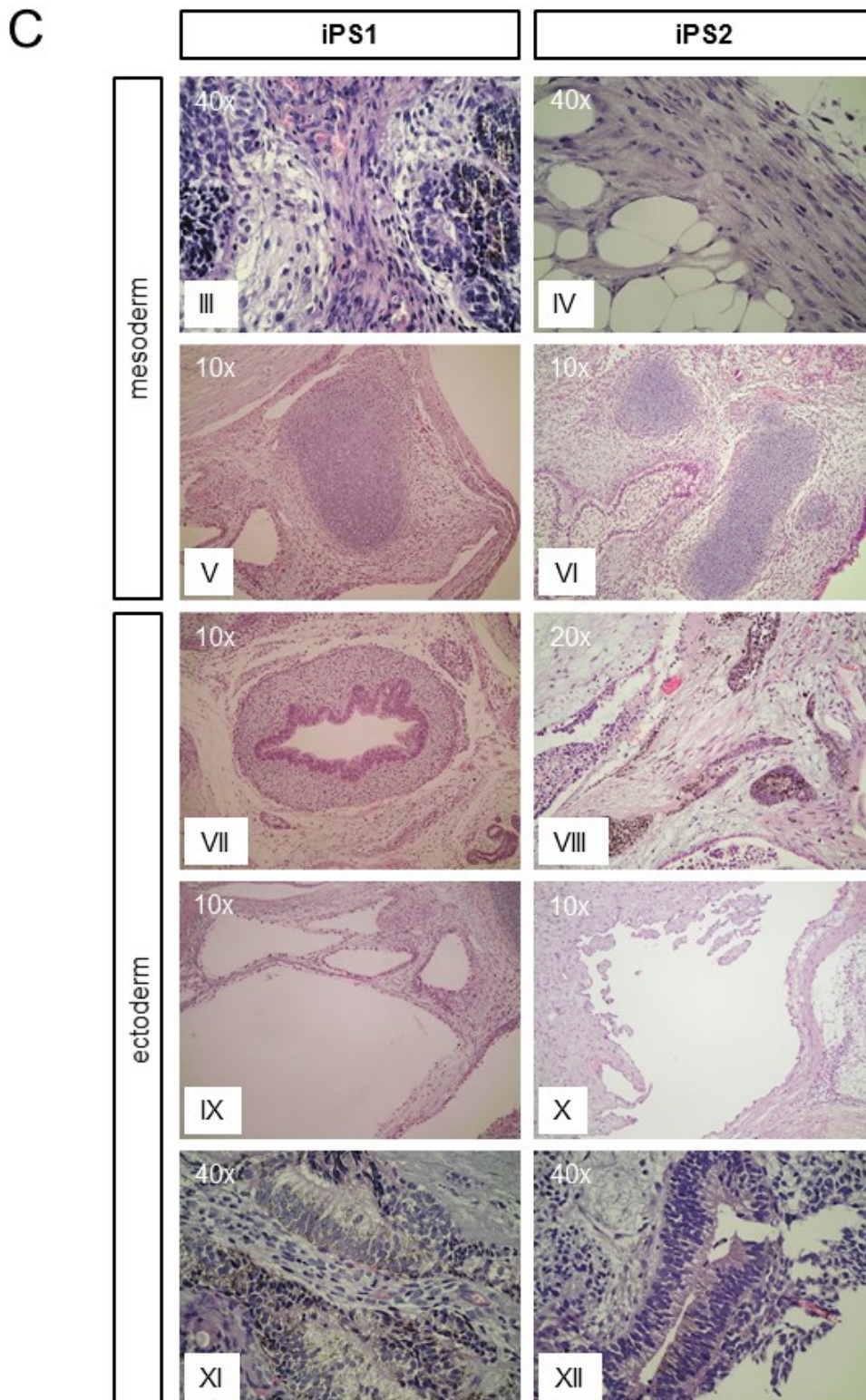
Figure 4-10   Teratoma formation assay of iPS1 and iPS2 cells.
(A) Rate of tumor growth in mice. Tumor volume (TV; solid line) and body weight (BW; dashed line) as indicated. **(B)** Photos of dissected teratomas (metric scale ruler). **(C)** Histological analysis of paraffin-embedded H&E-stained tissue sections representing structures of all three germ layers as indicated. I: Respiratory epithelium; II: Tubular structure, gland-like; III: Collagenous connective tissue; IV: Adipose and collagenous connective tissue; V: Cartilage and connective tissue; VI: Cartilage islands; VII: Lumen with high prismatic epithelium; VIII: Epithelium with melanin; IX: Cysts with cuboidal epithelium; X: Cyst with endothelial lining; XI and XII: Pigmented neuroepithelial structures. (Figure modified from Lichtner et al., 2013.)

74

4.1.2.6 Karyotype

Retroviral-based reprogramming can lead to genomic instability, since each hiPSC genome can contain multiple copies of each reprogramming factor (Shao et al., 2009), and the proviral integration site selection can occur randomly (Daniel and Smith, 2008; Nowrouzi et al., 2011). It is known that in particular hiPSC lines derived from aged donors frequently harbor chromosomal aberrations such as aneuploidy and translocations, which were *de novo* acquired during reprogramming (Prigione et al., 2011a). In order to verify that iPS1 and iPS2 cells possess a normal karyotype, a standard cytogenetic GTG-banding chromosome analysis was performed. The karyograms showed a normal human female karyotype (46,XX). No abnormalities in chromosome number or structural rearrangements were observed under optical microscope at the given resolution (Figure 4-11).
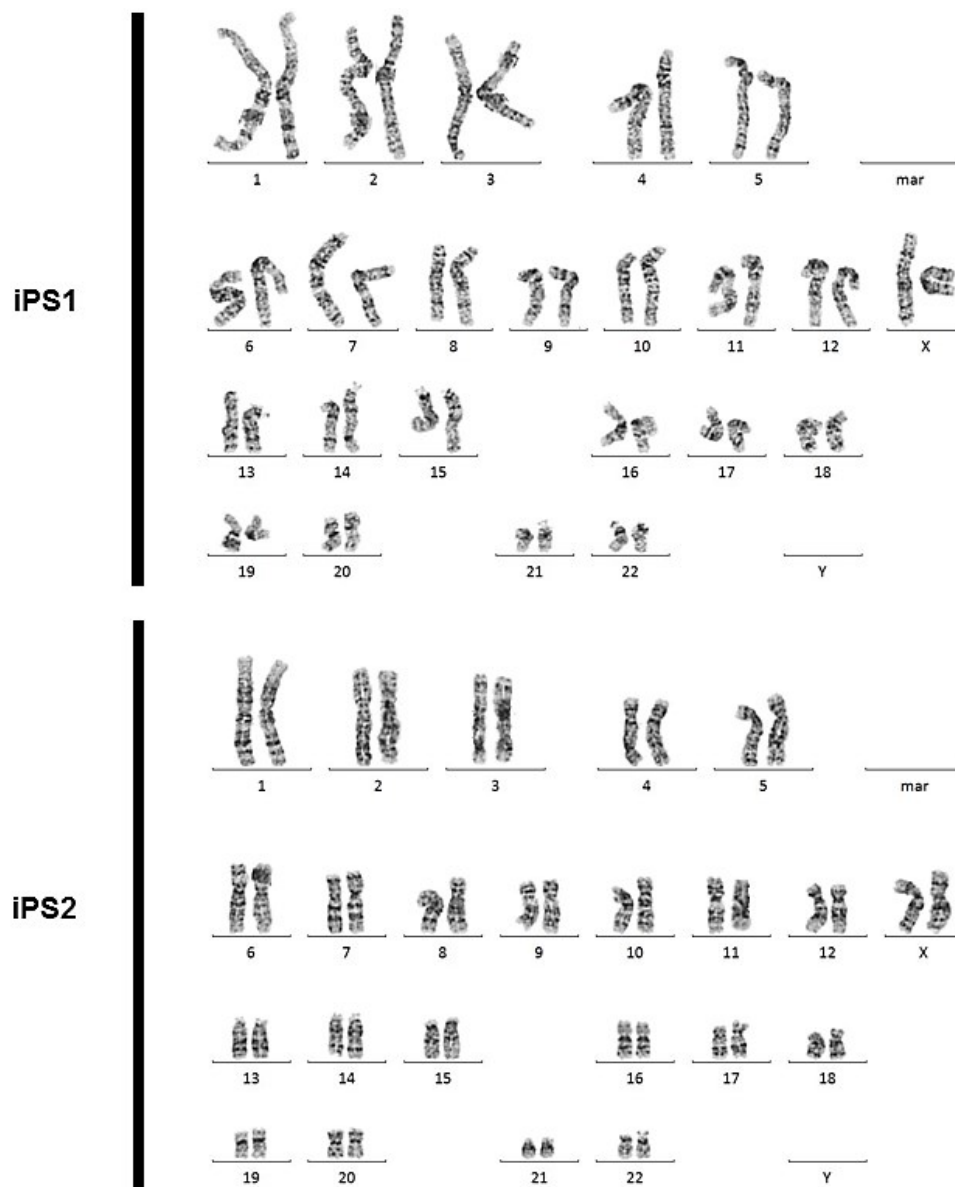
Figure 4-11   Karyograms of iPS1 and iPS2 cells.
GTG-banding chromosome analysis of metaphase cells revealed a normal female karyotype (46,XX) for both retroviral-derived hiPSC lines. (Figure modified from Lichtner et al., 2013.)

75

4.1.2.7 DNA profile

The genetic origin of iPS1 and iPS2 cells was confirmed by means of DNA fingerprinting analysis. Genomic DNA of individual cell lines was isolated and short tandem repeat (STR) loci were analyzed. STRs are satellite DNA sequences which consist of tandem repeats of usually 2−6 bp short units, whereat the copy number often varies between individuals. Four distinct STR loci were analyzed by PCR using established primer pairs that are flanking these genomic regions (Park et al., 2008). The resulting amplicons were separated by agarose gel electrophoresis dependent on their length. A comparison of the obtained band patterns confirmed that both hiPSC lines iPS1 and iPS2 were genetic clones of the CV cells (Figure 4-12A).
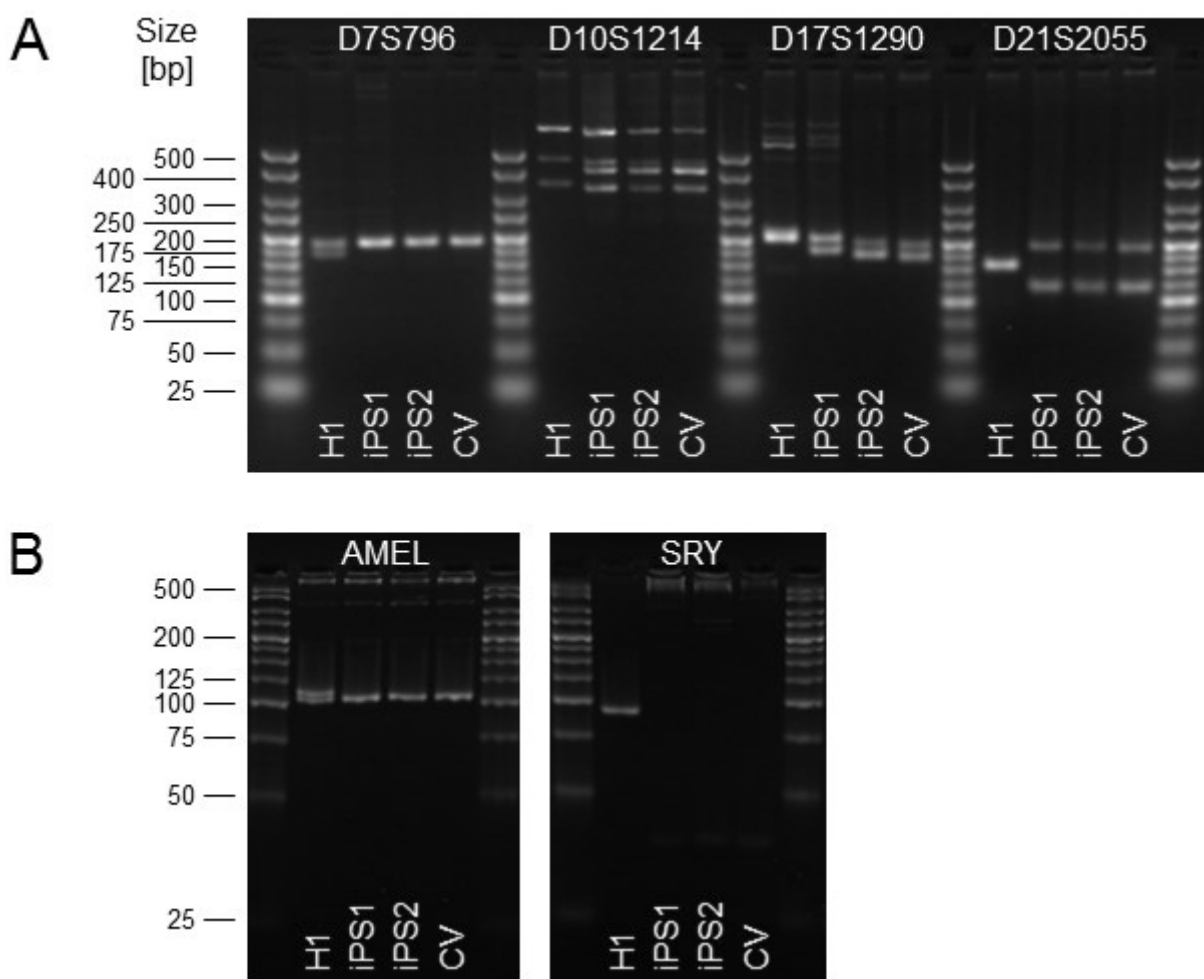
Figure 4-12   DNA fingerprinting analysis and sexing of iPS1 and iPS2 cells.
(**A**) Analysis of four STR loci as indicated confirmed the CV cells as origin of the derived hiPSC lines iPS1 and iPS2. In contrast, other independent cell lines such as hESC line H1 showed DNA profiles distinguishable from CV/iPS1/iPS2 cells. (**B**) Analysis of an X-Y homologous gene region (*AMEL*) and Y-associated gene region (*SRY*) confirmed the CV/iPS1/iPS2 cells as female (no PCR product for *SRY*; only one band for *AMEL* at 106 bp, representing the X chromosome). Positive control for male gender: hESC line H1, which was derived from a male embryo (one 93 bp PCR product for *SRY*; two bands for *AMEL* at 106 and 112 bp). (Figure modified from Lichtner et al., 2013.)

Two additional loci were analyzed for sexing: 1.) A segment of the X-Y homologous gene of Amelogenin, which is involved in the development of tooth enamel and located on the X and Y chromosomes, leading to 106 bp (*AMELX*) and 112 bp (*AMELY*) long PCR products, respectively (Mannucci et al., 1994). 2.) A segment of the *SRY* gene, which encodes a transcription factor involved in testis development and is only located on the male Y chromosome, leading to a 93 bp long PCR product. The SRY test should exclude the possibility of an incorrect typing of male as female in consequence of a known deletion polymorphism which can occur in *AMELY* (Santos et al., 1998). The results confirmed the female gender of CV, iPS1 and iPS2 cells (Figure 4-12B).

4.1.2.8 Transcriptional signature

Finally, the global gene expression in iPS1/iPS2 cells, CV cells and H1/H9 hESCs was compared by means of microarray analysis of cRNA samples. Hierarchical clustering of transcriptomes between the samples (Figure 4-13A) based on Pearson's correlation coefficients (Figure 4-13B) revealed that both hiPSC lines cluster together with hESCs and apart from the CV cells from which they were derived (r^2 at best 0.9555 for hiPSCs compared with hESCs versus 0.6133 compared with CV cells). This demonstrates that in the course of reprogramming, iPS1 and iPS2 cells underwent a change in overall gene expression from an originally somatic transcriptome profile (CV cells) back to a pluripotent transcriptome profile (hESCs). Furthermore, iPS1 and iPS2 cluster closer to H9 than to H1, probably due to the fact that H1 is of male origin and H9 of female origin.
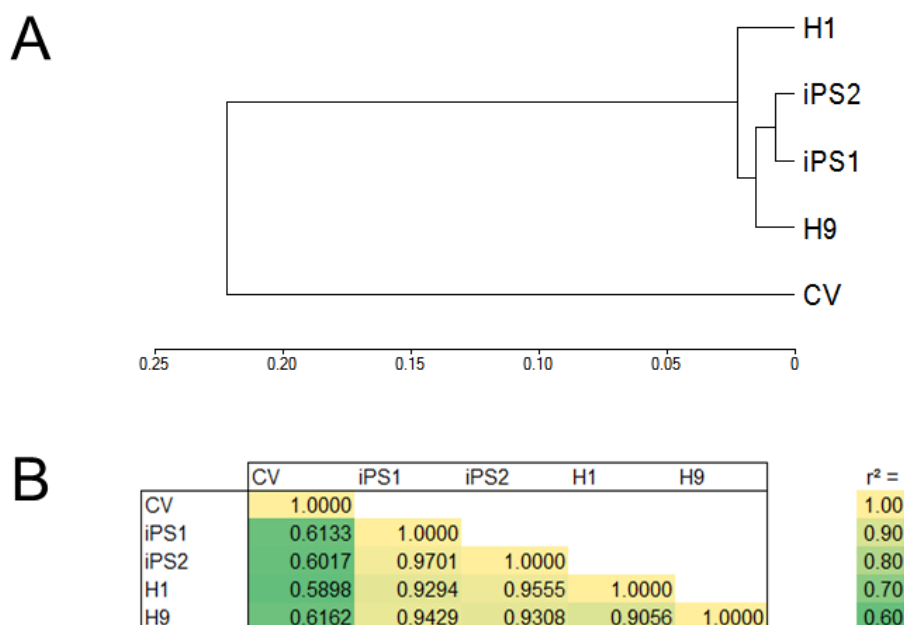
Figure 4-13   Microarray-based hierarchical cluster analysis of transcriptomes between iPS1 and iPS2 hiPSCs, their parental CV cells and H1 and H9 hESCs.
(A) Dendrogram based on Pearson's correlation coefficients. **(B)** Tabulated Pearson's correlation coefficients between samples. Conditional formatting: yellow = high correlation, green = low correlation. (Figure modified from Lichtner et al., 2013.)

4.2 BMP signaling and differentiation studies on human pluripotent stem cells

4.2.1 Morphological changes of hESCs/hiPSCs induced by treatment with distinct BMPs

At first it was investigated whether BMP5, BMP10 and BMP13 influence the self-renewal and undifferentiated state of hESCs and hiPSCs.

As positive controls for BMP-induced differentiation of these cells, BMP6 and BMP7 were chosen. Both ligands belong to the same subgroup like BMP5, the so-called "BMP7 subgroup" (Figure 1-3), and have already been tested on hESCs, but not hiPSCs under chemically-defined conditions (Chapter 1.4.1). All ligands were purchased as recombinant human proteins (homodimers of mature ligands; Table 2-8). Feeder-free colonies of undifferentiated human embryonic stem cells (line H1) growing adherent on Matrigel in chemically-defined N2B27 medium (w/o vitamin A, w/o bFGF, w/o Activin A) were treated with BMPs for 5 days. The medium and BMPs were replaced every 24 h. An initial dose of 100 ng/ml was chosen for all ligands. This is in the range of the concentrations used in other published hESC-related BMP studies and corresponds to 3.21–4.10 nM of homodimeric BMP5, BMP6, BMP7, BMP10 and BMP13. As reference for comparison with BMP-stimulated cells, H1 hESCs were instead incubated with an equivalent volume of solvent which was used for reconstitution of the lyophilized proteins (20 µl of 4 mM HCl + 0.1 % BSA carrier protein, hereinafter also referred to as "HCl/BSA"). Culture in N2B27 medium only should ensure that the solvent had no effect on the cells per se. Culture in N2B27 medium supplemented with 20 ng/ml bFGF served as an additional control to indicate the extent of any spontaneous differentiation which might have occurred in the reference samples due to the absence of exogenous bFGF in the cell culture medium.

Treatment of H1 hESCs with BMP5, BMP6, BMP7, BMP10 (all at 100 ng/ml) or BMP13 (at high concentration of 1 µg/ml, not significant at 100 ng/ml) induced differentiation of these cells. The differentiation was apparent due to changes in cell morphology: Cells located at the border of hESC colonies enlarged, flattened and expanded into the surrounding Matrigel-coated space, but they still remained connected in cell-cell contact. All colonies of a given ligand-treated sample were affected simultaneously from differentiation and retained their nearly symmetric shape. This excludes spontaneous random differentiation as potential cause. Similar morphological observations have been described before for hESCs which were treated with BMP4 under culture conditions lacking bFGF supplementation (Das et al., 2007; Amita et al., 2013). However, the time points of induced differentiation and its progression towards the colony centers were highly ligand-dependent. The onset of differentiation was at first observed at 24 h with BMP10. At 48 h, significant differences in differentiation kinetics became obvious, with BMP10 clearly being the most and BMP13 the least potent ligand. The activity of BMP5 was similar to its both subgroup members BMP6 and BMP7 (Figure 4-14).
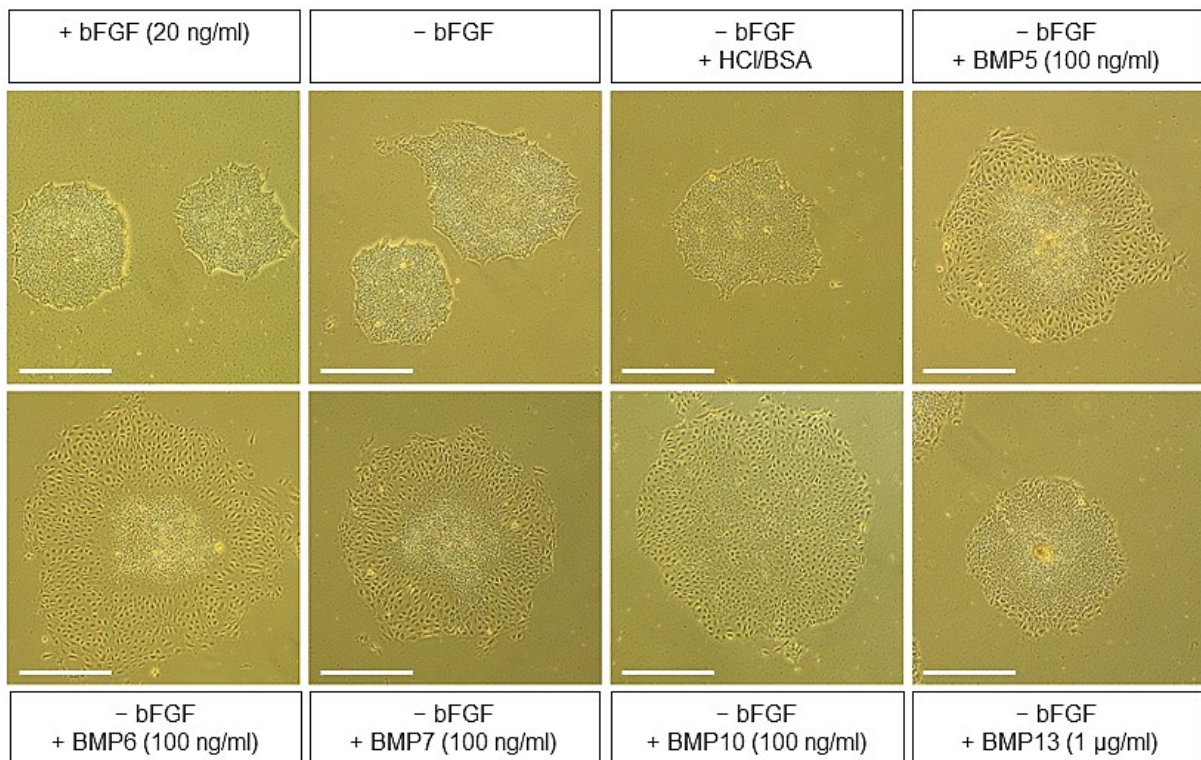
Figure 4-14   Morphological changes of hESCs (line H1) in response to 48 hours treatment with BMP5/6/7, BMP10 and BMP13.
Feeder-free hESC colonies were treated with recombinant human BMP5, BMP6, BMP7, BMP10, BMP13 or equivalent volume of 20 µl solvent/carrier protein (= undifferentiated reference cells) as indicated in N2B27 medium on Matrigel. Media and supplements were replaced every 24 h. Phase-contrast images of representative colonies at 48 h of treatment (ligands and controls). Scale bars represent 0.5 mm. (Figure modified from Lichtner et al., 2013.)

At day 5, the morphology of H1 hESCs treated with members of the BMP7 subgroup and BMP13 were similar: An aggregate of densely packed cells remained in the center of most colonies. In contrast, cells within BMP10-treated colonies mainly lacked central aggregates (Figure 4-15A). Instead, they featured randomly distributed flat structures that were several times larger than the surrounding differentiated cells. Within these structures, no shape of individual (mononuclear) cells could be observed (Figure 4-15B). This suggests that these structures were fused cells, which is characteristic of multinucleated syncytiotrophoblasts. Formation of syncytiotrophoblasts, among other trophoblast cell types, is known to be induced upon treatment of hESCs with BMP4 in the absence of exogenous bFGF (Sudheer et al., 2012; Amita et al., 2013). H1 hESCs of the HCl/BSA reference sample remained predominantly undifferentiated. This was indicated by the enduring presence of small cells with high nucleus-to-cytoplasm ratio that were growing tightly packed in colonies. These homogeneous monolayer colonies had increased in diameter due to ongoing proliferation (Figure 4-15B). Differentiation of cells only occurred at few sporadic locations, which is characteristic of spontaneous differentiation leading to random cell types. No differences in the degree of spontaneous differentiation, i.e. in the ratio of colonies affected from differentiation and in the extent of differentiation within individual colonies, could be visually observed among the non-BMP-treated controls (Figure 4-15A). This indicates that
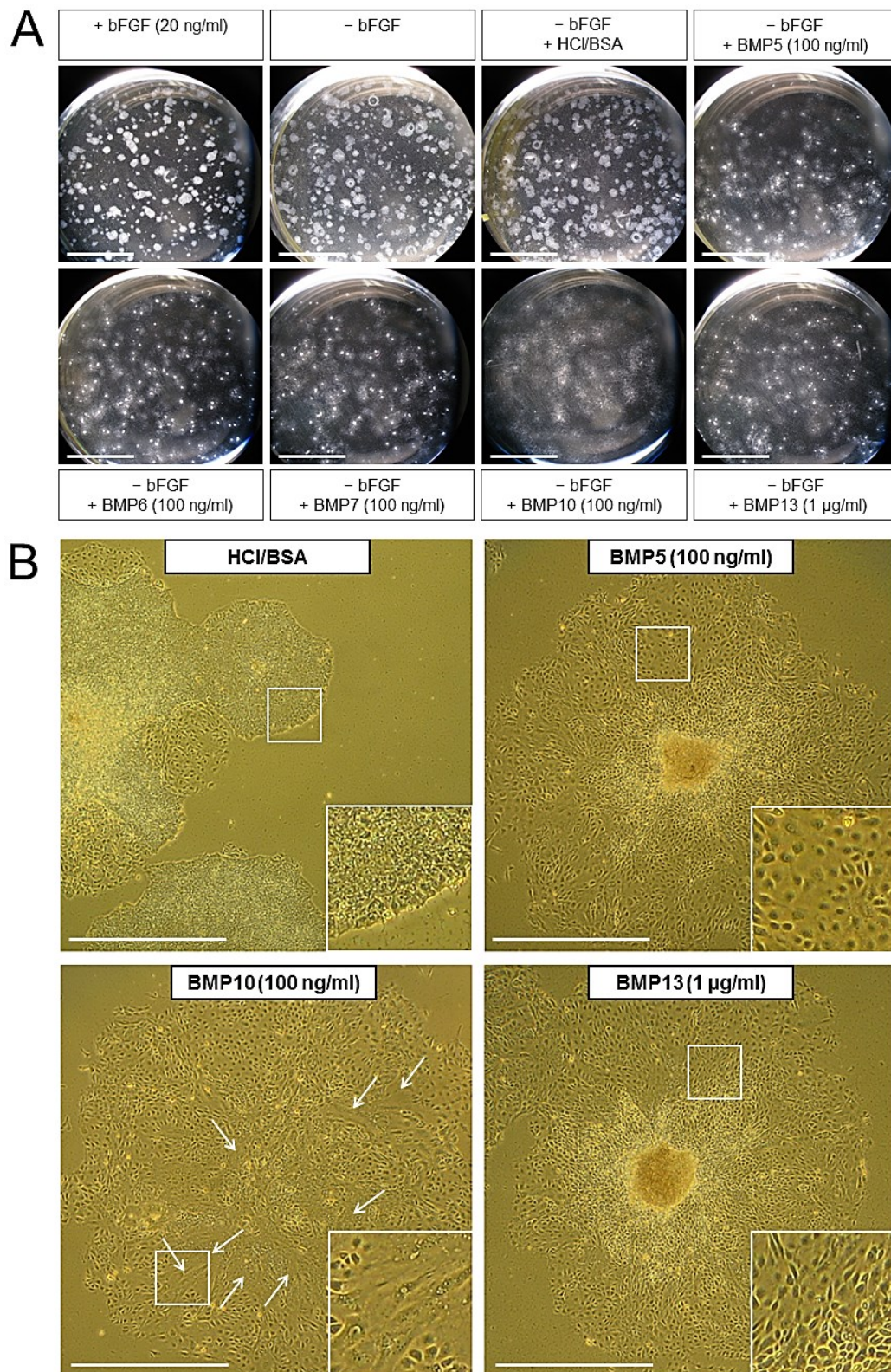
Figure 4-15   Morphology of differentiated hESCs (line H1) after 5 days treatment with BMP5/6/7, BMP10 and BMP13.
(A) Overview of individual samples in 6-well plates at day 5. Cells were treated as described in Figure 4-14. Areas of differentiated cells can be identified on the basis of their high translucency. In contrast, undifferentiated cells appear more white. Note the little white spots which remained in the center of most colonies of all BMP samples except BMP10. Scale bars represent 1 cm (6-well diameter: 34.5 mm). **(B)** Close-up view of representative colonies (novel tested ligands and HCl/BSA reference). White frames mark the magnified areas, white arrows indicate structures looking like fused cells. Scale bars represent 1 mm. (Figure modified from Lichtner et al., 2013.)

neither the solvent nor the absence of exogenous bFGF had an effect on the undifferentiated state. The latter observation is in agreement with a previous study demonstrating that hESCs can be maintained in N2B27 medium lacking bFGF for up to 4 passages (Liu et al., 2006a).

The BMP treatments were repeated for the human embryonic stem cell line H9 and the two generated (Chapter 4.1) human induced pluripotent stem cell lines iPS1 and iPS2. The results were similar regarding the appearance of induced morphological differentiation and the observed hierarchy of ligand potency. However, in contrast to both hESC lines, the two hiPSC lines showed an increased tendency to spontaneous differentiation when cultured in N2B27 medium without BMP treatment. This phenomenon appeared after approximately 3−4 days, regardless whether bFGF was supplemented or not.

4.2.2 Determination of cell lineage identity of differentiated hESCs/hiPSCs obtained by treatment with distinct BMPs

Next, the cell lineage identity of the differentiated cells obtained by treatment of H1 hESCs with the novel tested ligands was determined. Three time points were analyzed: 18 h, 3 d and 5 d (early response, intermediate and late differentiation). Microarray-based transcriptome analysis was employed to compare cells treated with either BMP5, BMP10 or BMP13 with the HCl/BSA-treated cells serving as reference for the undifferentiated state. The fold changes in gene expression of markers representing the undifferentiated state of hESCs and of differentiation markers representing all major cell lineages (Chapter 1.1.1) were investigated. These included:

- Definitive endoderm, mesoderm and ectoderm as the three somatic germ layers which constitute the embryo;
- primitive streak as an interim state (= mesendoderm) of early differentiated ICM cells at the initiation of gastrulation, whose further differentiation capacity is restricted to mesoderm and endoderm;
- extraembryonic endoderm (alias primitive endoderm) and trophoblast as extraembryonic lineages; and
- germline-related cells leading to gametes.

Extraembryonic mesoderm and extraembryonic ectoderm were excluded from this analysis, because to this day there are no markers identified which are specific to characterize these lineages. Several genes were monitored for each lineage. This took into account that many lineage markers are not pan-markers and are therefore only representative for subpopulations of cells within a given major cell lineage. Such examples are the cluster of differentiation antigen CD34, which is expressed on hematopoietic stem cells of mesoderm (Furness and McNagny, 2006), and the transcription factor PDX1, which is expressed in pancreatic progenitor cells of definitive endoderm (Hui and Perfetti, 2002). Thus, the absence of upregulation of individual markers does not necessarily mean the absence of the whole major cell lineage in the sample, but rather the absence of particular lineage-associated cell types. In addition,

some of the absent cell types could require more than 5 days – the time frame investigated in this study – for their *in vitro* formation. Moreover, not all established and commonly used lineage markers are exclusively restricted to derivatives of a certain major cell lineage. Some can also be related to specific cell types of additional lineages, which makes these markers incompetent to clearly distinguish between the concerned lineages. For instance, the transcription factors OCT4, SOX2 and NANOG are pan-markers of pluripotent stem cells (Boyer et al., 2005), but SOX2 is also expressed by distinct subtypes of neural progenitor cells (ectoderm) (Hutton and Pevny, 2011), and OCT4 and NANOG by primordial germ cells (germline) (Gaskell et al., 2004; Clark et al., 2004b). The transcription factor HAND1 is a marker of trophoblast lineage, but also expressed in the heart (mesoderm) (Knöfler et al., 1998; Riley et al., 1998). The plasma protein AFP is a marker of extraembryonic endoderm (Hyslop et al., 2005) and hepatocytes (definitive endoderm) (Jozefczuk et al., 2011). β-hCG (encoded by *CGB*), as constituent of the glycoprotein hormone hCG, marks trophoblast lineage, but is also made by multiple primary non-trophoblastic malignancies (Cole, 2010). Therefore, a combination of various markers is indispensable when the identity of uncharacterized cells needs to be accurately determined.

Figure 4-16 shows the fold changes in expression of numerous marker genes representing all major cell lineages. It reveals that H1 hESCs responded to all BMPs in a similar manner – namely, they predominantly differentiated to trophoblast lineage, but also showed a marginal co-differentiation to mesendoderm.

The exit of H1 hESCs from their undifferentiated state was confirmed by the strong downregulation of all pluripotency-associated markers, consistent with the morphological changes (Chapter 4.2.1). Typical hESC-related genes such as *OCT4*, *SOX2*, *NANOG*, *ZSCAN10*, *ZIC3*, *DNMT3B*, *PRDM14*, *TDGF1* and *DPPA2* were among the top of downregulated genes identified in this microarray analysis (Table A-2 in Appendix).

The emergence of trophoblast lineage was marked by the early (18 h, 3 d) activation of transcription factors characteristic of placenta development *in vivo* and *ex vivo*. These include *MSX2* (Quinn et al., 2000), *CDX2* (Niwa et al., 2005; Strumpf et al., 2005), *HAND1* (Riley et al., 1998; Knöfler et al., 1998; Knöfler et al., 2002), *GATA2* and *GATA3* (Ma et al., 1997), *TFAP2A* (Cheng et al., 2004; Handwerger, 2010), *DLX3* (Peng and Payne, 2002; Gupta et al., 2012) and *DLX5* (Kato et al., 2008), *ELF4* (Aryee et al., 1998) and *GCM1* (Baczyk et al., 2004). During the course of proceeding differentiation of hESCs, which was indicated by the reduction in expression of pluripotency markers at 3 d and 5 d, numerous genes known to be expressed in placenta tissue *in vivo* were upregulated. Among these were genes encoding

– structural proteins such as basement membrane-associated collagens (*COL4A1* (Colorado et al., 2000), *COL4A2* (Brazel et al., 1988)) and cytoskeletal-associated keratins (*KRT7*, *KRT8*, *KRT18* (Mühlhauser et al., 1995));
– calcium-binding proteins (*S100P*, *S100A3*, *S100A11* (Becker et al., 1992; Assou et al., 2012; Lafond and Simoneau, 2006));
– transporters (*SLC39A2* (Peters et al., 2007), *SLC13A4* (Girard et al., 1999), *SLC22A11* (Cha et al., 2000), *SLC40A1* (Donovan et al., 2000));
– secreted hormones or growth factors (*CGA*, *CGB* (Muyan and Boime, 1997), *CRH* (Thomson, 2013), *INSL4* (Laurent et al., 1998), *IGF2* (Hamilton et al., 1998), *PGF* (Vrachnis et al., 2013)); and the
– long non-coding RNA H19 (*H19* (Jinno et al., 1995)).
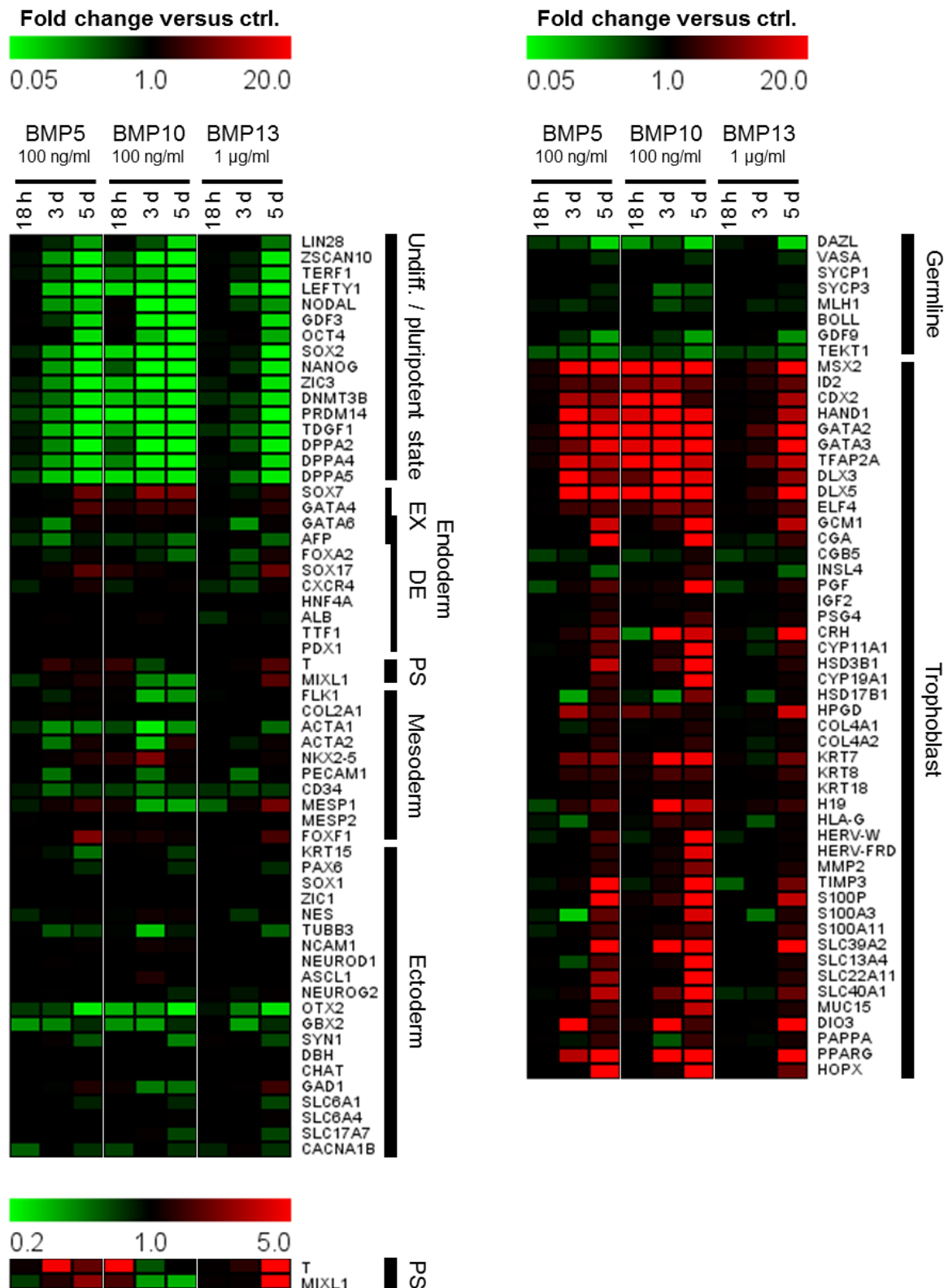
Figure 4-16   Cell lineage identity of H1 hESCs after treatment with BMP5, BMP10 and BMP13 for 18 h, 3 d and 5 d. (Microarray)

Cells were treated as described in Figure 4-14. Gene expression levels of pluripotency and differentiation markers as indicated were determined by microarray analysis of cRNA samples. The heatmap visualizes the fold changes in gene expression (ligand versus HCl/BSA reference cells of the same time point), calculated as ratios of average signal intensities (grouped biological duplicates). Red = UP↑, green = DOWN↓. Abbreviations: DE = definitive, EX = extraembryonic, PS = primitive streak. The intensity raw data on which the ratios are based on are visualized in Figure A-1 (in Appendix) for all genes and samples. (Figure modified from Lichtner et al., 2013.)

Many of these placenta-associated genes have also been reported to be associated with the emergence of trophoblast cells from hESCs treated with BMP4 *in vitro* (Xu et al., 2002; Marchand et al., 2011; Ezashi et al., 2012; Sudheer et al., 2012). In accordance with the observed morphological changes of cells (Chapter 4.2.1), BMP10 induced the fastest and BMP13 (at 10 times higher dose) the slowest kinetics in terms of upregulation of trophoblast markers and corresponding downregulation of pluripotency markers. In addition, the degree of upregulation and downregulation of these markers was most significant for BMP10 and least significant for BMP13. At 18 h, when BMP10-treated H1 hESCs still looked morphologically undifferentiated, the expression of more than half of the assessed pluripotency markers was already reduced in these cells to 0.50-fold or less compared to their basal expression levels.

The co-differentiation of H1 hESCs to mesendoderm was indicated by upregulation of the transcription factors and primitive streak markers *T* (encoding Brachyury) (Herrmann et al., 1990; Rivera-Pérez and Magnuson, 2005) and *MIXL1* (Pearce and Evans, 1999; Robb et al., 2000). It is remarkable that the time frame of mesendoderm formation differed among the ligands: In the case of BMP10, induction of *T* and *MIXL1* was detected exclusively at the early 18 h time point (5.0-fold and 2.2-fold). At 3 d, expression of both genes was already lower relative to the HCl/BSA-treated reference cells. This indicates that after a short initial promotion of mesendoderm differentiation concurrently with trophoblast differentiation, the triggered differentiation by BMP10 in the remaining undifferentiated hESCs had a tendency away from mesendoderm and exclusively favored trophoblast lineage. This is in contrast to the weaker ligands BMP5 and BMP13. Here, induction of *T* and *MIXL1* was delayed (first detection at day 3), but persisted until day 5 (up to 7.5-fold). However, in the case of all BMPs, the degree of induction of *T* and *MIXL1* was in general much lower compared to trophoblast-associated transcription factors, whose upregulation often exceeded 20.0-fold. Moreover, only a small number of the monitored markers representing mesoderm and endoderm were subsequently upregulated, and if so, then rather on a weak level compared to placenta-associated markers: *Inter alia SOX7* and *GATA4* for extraembryonic endoderm (Hyslop et al., 2005; Brown et al., 2010) (maximum 11.2-fold), *SOX17* and *CXCR4* for definitive endoderm (D'Amour et al., 2005; King et al., 2008) (maximum 8.7-fold), and *MESP1* (Chan et al., 2013) and *FOXF1* (Mahlapuu et al. 2001) for mesoderm (maximum 10.5-fold). The gene expression levels of the majority of mesoderm and endoderm markers remained unchanged or were even downregulated. In contrast, trophoblast-associated markers were among the top of upregulated genes identified in this microarray analysis (Table A-1 in Appendix). A significant development of primitive streak/mesendoderm cell population would have led to a stronger upregulation of *T* and *MIXL1*, closely followed by a strong upregulation of a widely diversified portfolio of derivatives belonging to mesoderm and endoderm.

No evidences for ectoderm differentiation or the existence of cells belonging to the germline were found:

Ectoderm was examined by means of *KRT15*, a marker of skin epidermis (Waseem et al., 1999) and hair follicle stem cells (Al-Refu et al., 2009) as structures of the surface ectoderm, and numerous early and late markers of the neuroectoderm. The early markers include genes which are involved in neural stem cell self-renewal and early neurogenesis (*PAX6, NEUROG2*,

ASCL1 (Sansom et al., 2009)) as well as markers of immature neurons (*NES* (Messam et al., 2000), *TUBB3* (da Silva and Dotti, 2002)). Among the assessed late markers were those of synaptic neurons, such as genes encoding enzymes involved in neurotransmitter biosynthesis (*DBH* (Rush and Geffen, 1980), *CHAT* (Oda, 1999), *GAD1* (Jin et al., 2003)), voltage-dependent calcium channels involved in the release of neurotransmitters (*CACNA1B* (Williams et al., 1992)), and transporters involved in the uptake of neurotransmitters (*SLC6A1/GAT1* (Deken et al., 2000), *SLC6A4/SERT* (Fuller, 1994), *SLC17A7/VGLUT1* (Takamori et al., 2000)).

Germ cell lineage was examined by means of markers representing all stages of gamete development: *DAZL* for primordial germ cells and *VASA* for gonocytes and gonia (= pre-meiotic stages); *SYCP1*, *SYCP3*, *MLH1*, *BOLL* for undifferentiated spermatocytes/oocytes, *TEKT1* for sperm and *GDF9* for mature oocytes (= post-meiotic stages) (Clark et al., 2004a).

The microarray data of Figure 4-16 were confirmed by real-time qPCR for all samples at 18 h, 3 d and 5 d using specific primers for 27 selected marker genes covering all major lineages (Figure 4-17). In addition, it was confirmed that the differentiation outcome induced by BMP6 and BMP7 in H1 hESCs with respect to the obtained cell lineage identity was equivalent to the novel tested BMPs. The potency of BMP6 and BMP7 was similar to BMP5, indicated by comparable levels of upregulation of trophoblast markers and downregulation of pluripotency markers at a given time point. As expected from the morphological observations (Figure 4-14; Figure 4-15), both additional non-BMP-treated controls (N2B27 medium +/− bFGF) showed no significant differences in overall marker gene expression relative to the HCl/BSA-treated reference cells.

The differentiation experiments were repeated under the same conditions using the hESC line H9 and the two clonal hiPSC lines iPS1 and iPS2. cDNA of reverse-transcribed total RNA of day 5 samples was subjected to real-time qPCR analyses for the same set of 27 markers. Due to the increased tendency of hiPSCs to spontaneous differentiation in N2B27 medium, day 3 samples instead of day 5 samples served as a reference for undifferentiated iPS1 and iPS2 cells (= non-BMP-treated controls). As observed for H1 hESCs, all three independent human pluripotent stem cell lines differentiated to trophoblast lineage upon treatment with distinct BMPs (Figure 4-18). The differences in potency among individual ligands were clearly reproducible for all tested cell lines (BMP10 > BMP5 ≈ BMP6 ≈ BMP7 >> BMP13). This was assessed based on the degree of downregulation of pluripotency-associated genes (*OCT4*, *NANOG*) and the degree of upregulation of late trophoblast markers (*HERV-W*, *HERV-FRD*, *CGA*, *CGB*). However, co-differentiation towards primitive streak/mesendoderm was less obvious compared to hESC line H1 (Figure 4-17).
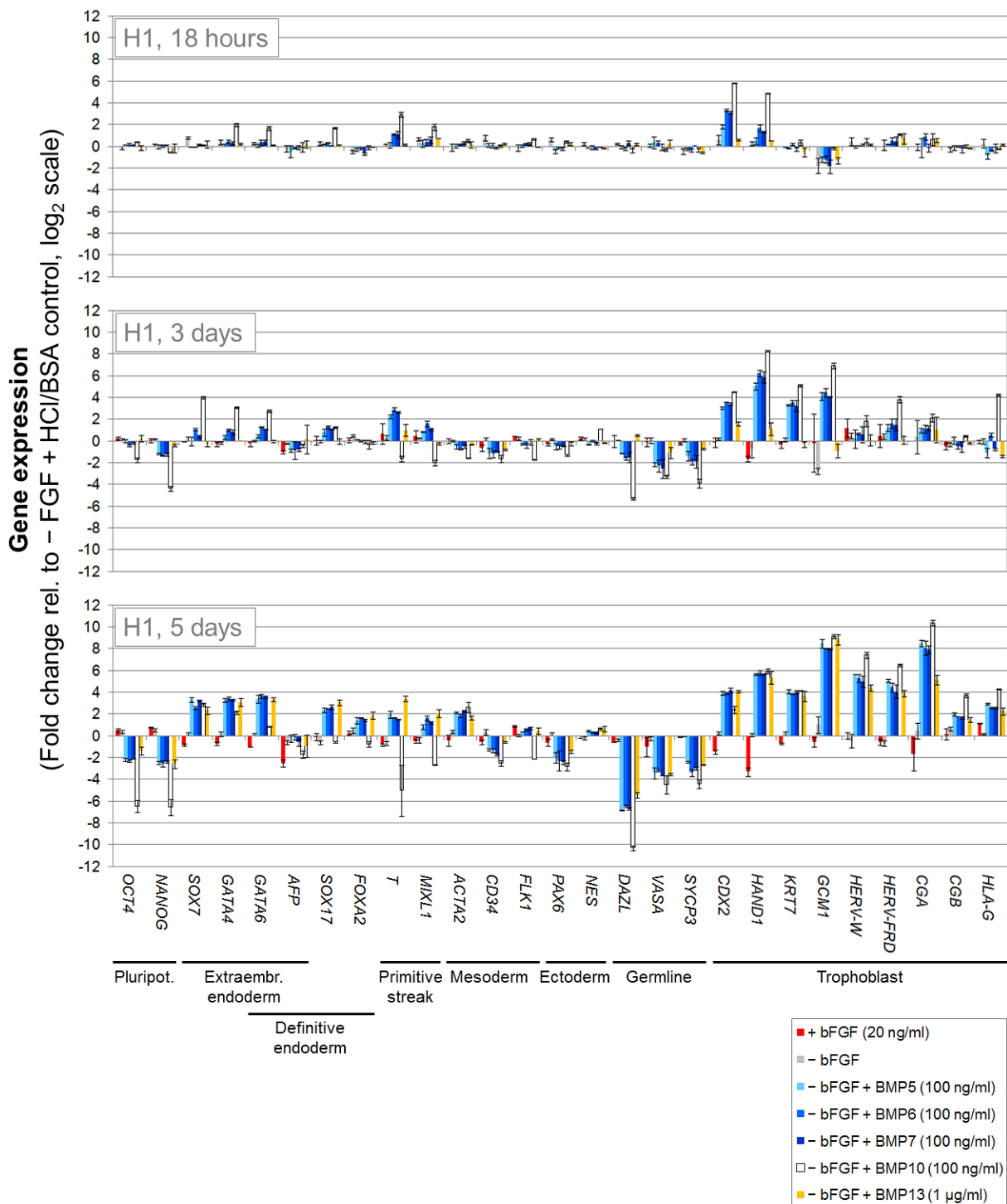
Figure 4-17   Cell lineage identity of H1 hESCs after treatment with BMP5/6/7, BMP10 and BMP13 for 18 h, 3 d and 5 d. (Real-time qPCR)
Confirmation of the microarray data (Figure 4-16) for 27 selected markers covering all major cell lineages as indicated. Fold changes in gene expression of markers were determined by real-time qPCR of cDNA samples according to the comparative threshold cycle method ΔΔC$_t$ (relative to the HCl/BSA-treated reference cells of the corresponding time point). Values were normalized against the housekeeping gene *GAPDH*. Error bars indicate STDEV (biological duplicates, technical triplicates). (Figure modified from Lichtner et al., 2013.)
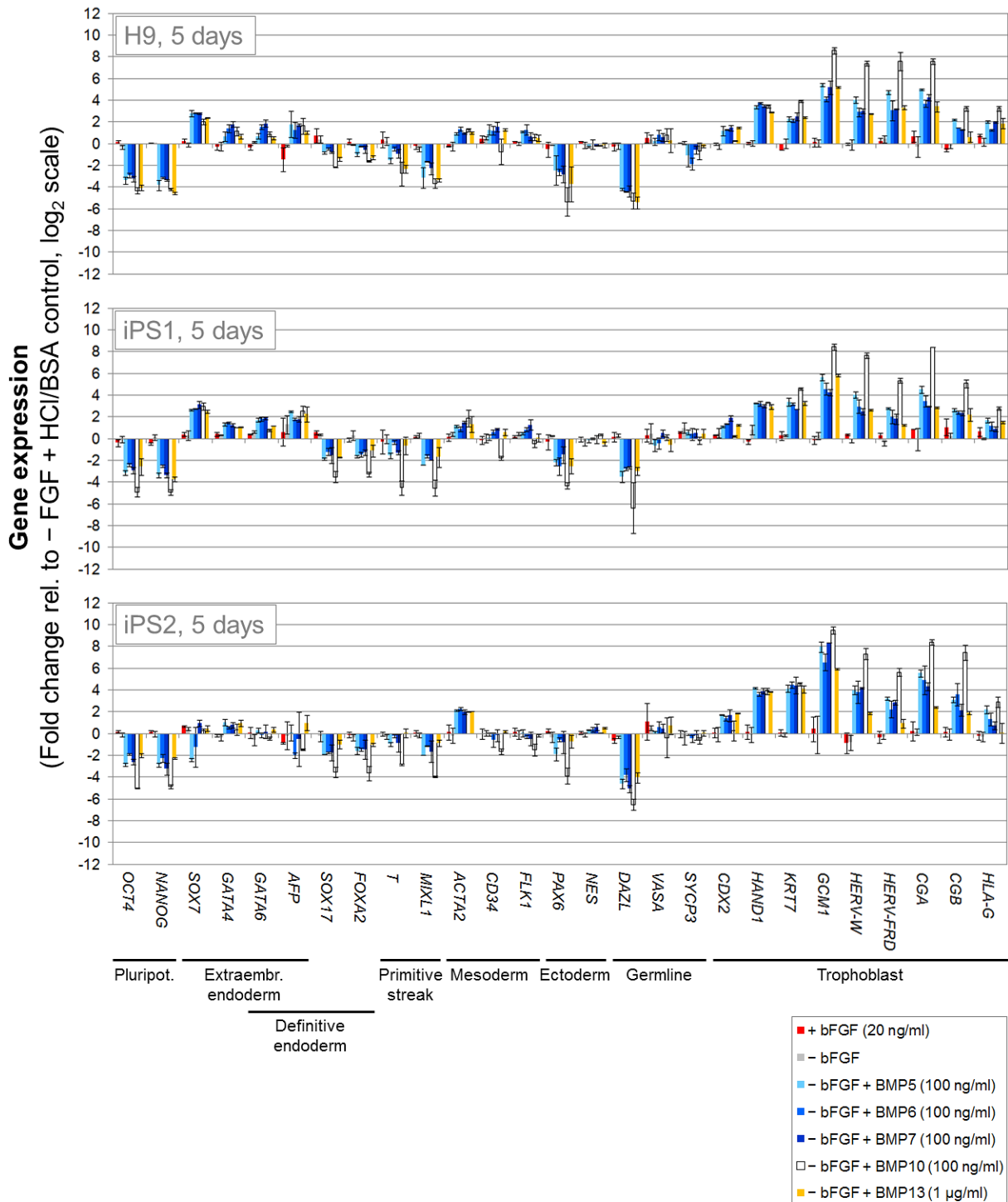
Figure 4-18   Cell lineage identity of H9 hESCs and iPS1/iPS2 hiPSCs after treatment with BMP5/6/7, BMP10 and BMP13 for 5 d. (Real-time qPCR)

Cells were treated in N2B27 medium on Matrigel as indicated. Media and supplements were replaced every 24 h. Fold changes in gene expression of pluripotency and differentiation markers covering all major cell lineages as indicated were determined by real-time qPCR of cDNA samples ($\Delta\Delta C_t$ method). Data were normalized against the HCl/BSA-treated reference cells of day 5 (H9) or day 3 (iPS1 and iPS2) and *GAPDH* as endogenous internal standard. Error bars indicate STDEV (biological duplicates, technical triplicates). (Figure modified from Lichtner et al., 2013.)

4.2.3   Global gene expression profiling of BMP-induced differentiated hESCs

4.2.3.1   Transcriptional signature

The global gene expression in BMP5-, BMP10-, BMP13- and HCl/BSA-treated H1 hESCs was compared by means of microarray analysis of cRNA samples. The used bead chips target more than 47,000 probes, which provide genome-wide transcriptional coverage of well-characterized genes, gene candidates and splice variants derived from NCBI's RefSeq collection database (Chapter 2.13; Release 38, 7 November 2009). All genes which were detected as significantly expressed in the samples were processed for hierarchical clustering of transcriptomes between the samples.

The results revealed that the BMP10-treated cells cluster further apart from the reference hESCs than any of the other BMP-treated cells at all time points investigated (18 h, 3 d, 5 d) (Figure 4-19A). At 18 h, the BMP10 sample already forms an independent branch apart from the main cluster consisting of the BMP5, BMP13 and reference sample. At day 5, all BMP samples cluster together, indicating that the differentiated cells had acquired a similar transcriptome; unlike the undifferentiated reference cells which now form an independent branch. In the course of progressing differentiation (day 3 samples), BMP5 showed a faster kinetics in shifting towards the BMP10 branch than BMP13. Further evidence for this can be seen from the corresponding Pearson's correlation coefficients (Figure 4-19B-C). The similar nature of the differentiated cells with respect to their transcriptional signature is in agreement with a common differentiation fate, which was determined as being predominantly trophoblast lineage (Chapter 4.2.2). The chronology of acquisition of the cells' similar transcriptomes reflects the observed strong variations in biological activity among the ligands (Chapter 4.2.1 and 4.2.2).
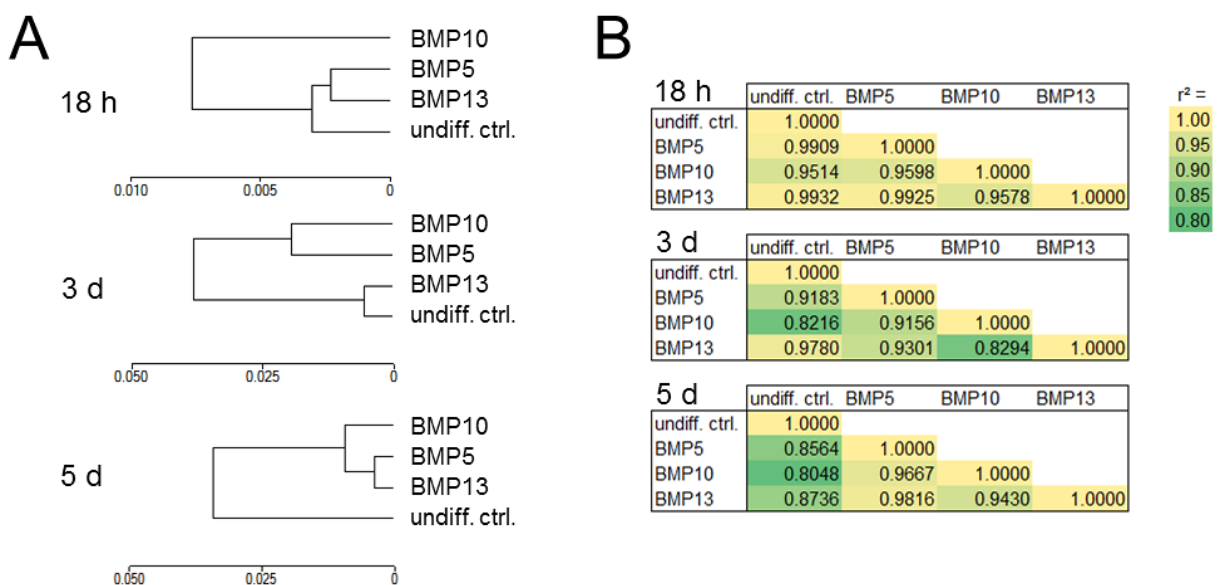
(continued from previous page)
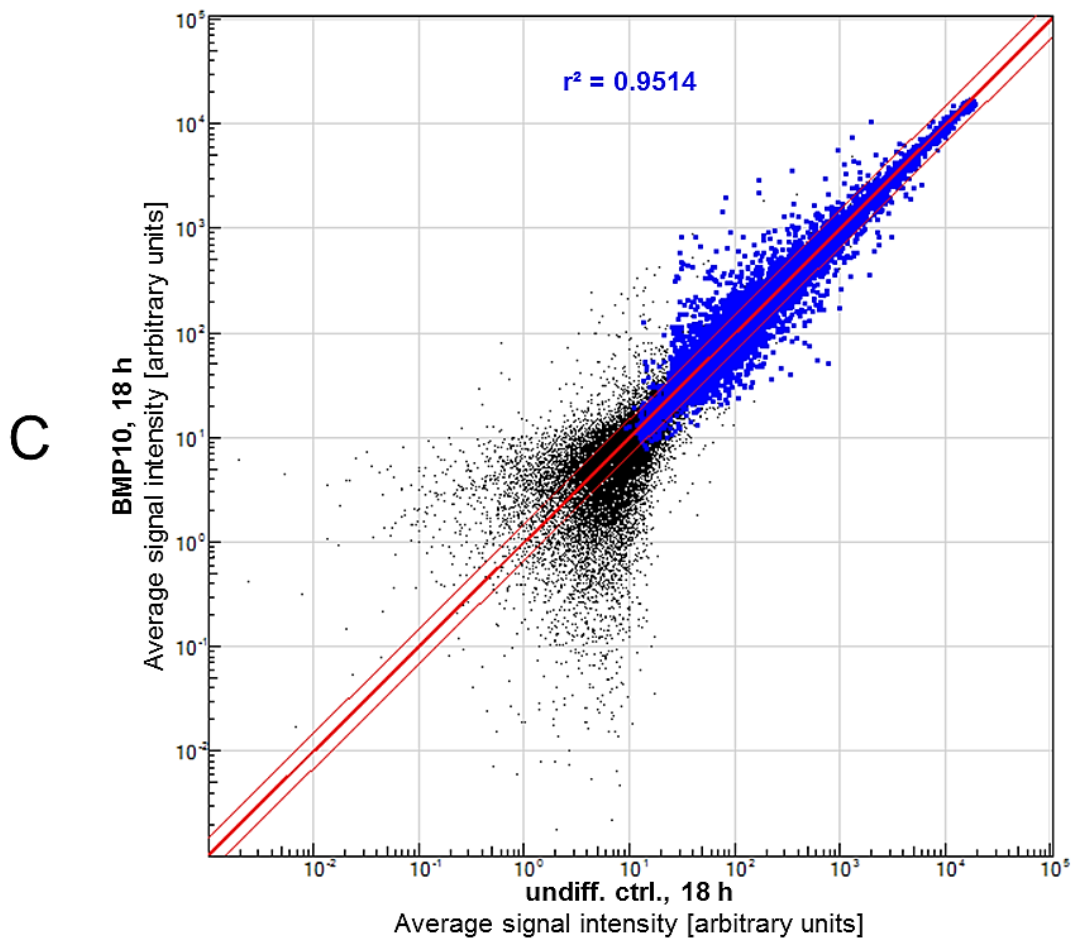
Figure 4-19   Transcriptional signature of H1 hESCs after treatment with BMP5, BMP10, BMP13 or HCl/BSA (= reference) for 18 h, 3 d and 5 d.
(A) Dendograms displaying microarray-based hierarchical cluster analysis of transcriptomes (samples of Figure 4-16; grouped biological duplicates). **(B)** Tabulated Pearson's correlation coefficients between samples. Conditional formatting: yellow = high correlation, green = low correlation. **(C)** Exemplary dot plot showing the pairing of two samples (BMP10 versus HCl/BSA control at 18 h) for determination of their Pearson's correlation coefficient. Each dot represents one gene transcript which was probed on the array. All genes which were significantly expressed ($P_{Det} < 0.01$) in both samples were considered for the analysis (blue dots). Logarithmic scales represent the detected average (AVG) signal intensity of each gene for both samples. Dots above the upper red line represent genes which were upregulated > 1.5-fold in the BMP10 sample relative to the reference sample (≙ downregulated < 0.66-fold in the reference sample relative to the BMP10 sample). The opposite applies for dots below the lower red line. The middle line indicates equal AVG signal intensities among samples (≙ unchanged gene expression; $r^2 = 1$). (Figure modified from Lichtner et al., 2013.)

4.2.3.2   Statistics of differentially expressed genes

In this step, all significantly expressed genes were filtered for genes which were significantly differentially expressed in ligand-treated H1 hESCs relative to the HCl/BSA-treated reference cells of the same time point. The filtered genes were statistically analyzed regarding the following three criteria to gain general information about whole-genome temporal gene expression changes of the differentiating hESCs:

1.) Count of significantly differentially expressed genes in BMP samples
    (bar chart and table in Figure 4-20).

2.) Fold change distribution of significantly differentially expressed genes (scatter diagrams in Figure 4-21).

3.) Count of overlapping and unique significantly differentially expressed genes between BMP samples (Venn diagrams in Figure 4-22).

At all three time points (18 h, 3 d, 5 d), treatment with BMP10 led to the strongest influence with respect to the numbers of up- and downregulated genes (Figure 4-20), as well as the corresponding ratio ranges (Figure 4-21), followed by the ligands BMP5 and BMP13. This is most evident at 18 h, when BMP10 treatment already led to an upregulation of 889 genes (up to 28.3-fold) and downregulation of 497 genes (up to 0.07-fold) compared to their basal expression levels in non-BMP-treated hESCs. In contrast, treatment with BMP5 led to an upregulation of only 21 genes (up to 2.9-fold) and downregulation of 10 genes (up to 0.50-fold); treatment with BMP13 at 10 times higher dose to an upregulation of 7 genes (up to 1.8-fold) and no significant downregulation of any gene. Towards the end of the differentiation period (day 3–5), the quantity and proportion of differentially expressed genes which were affected in common by BMP5, BMP10 and BMP13 continually increased (Figure 4-22). This is in conformance with the shift of BMP branches in the dendograms (Figure 4-19A). At day 5, 1198 genes were significantly up- and 1408 genes were significantly downregulated in common (BMP5 ∩ BMP10 ∩ BMP13). In fact, many of the genes which were identified as members of the top 100 lists of differentially expressed genes in BMP10-treated cells at 18 h, such as pluripotency-associated proteins (down) and trophoblast-associated transcription factors (up) (Chapter 4.2.2), can be found in the corresponding top 100 lists of BMP5- and BMP13-treated cells at 3 d and/or 5 d (see Table A-1 and Table A-2 in Appendix).

These statistics of differentially expressed genes once more underline that the main difference between individual BMP samples is the kinetics of induced differentiation rather than the fate of induced differentiation.

A

B

Time	Ligand	Diff. expressed genes versus undiff. ctrl.		
		UP	DOWN	total
18 h	BMP5	21	10	31
	BMP10	889	497	1386
	BMP13	7	0	7
3 d	BMP5	1243	1568	2811
	BMP10	2048	2670	4718
	BMP13	202	156	358
5 d	BMP5	1977	1994	3971
	BMP10	2330	2680	5010
	BMP13	1565	1651	3216
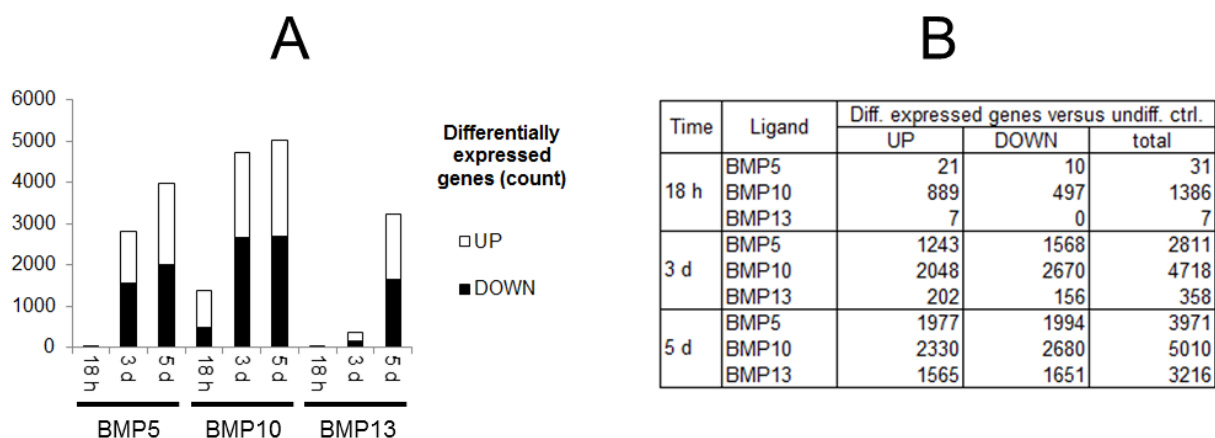
Figure 4-20   Count of significantly differentially expressed genes in differentiating BMP5-, BMP10- and BMP13-treated versus reference H1 hESCs at 18 h, 3 d and 5 d.
Significantly up- and downregulated genes in BMP-treated versus HCl/BSA-treated cells of the same time point (microarray samples of Figure 4-16; grouped biological duplicates). Criteria: > 1.5-fold up or < 0.66-fold down, $P_{Diff} < 0.05$, $P_{Det} < 0.01$ for at least one of both samples (ligand and/or reference). **(A)** Bar chart. **(B)** Tabulated numbers. (Figure modified from Lichtner et al., 2013.)
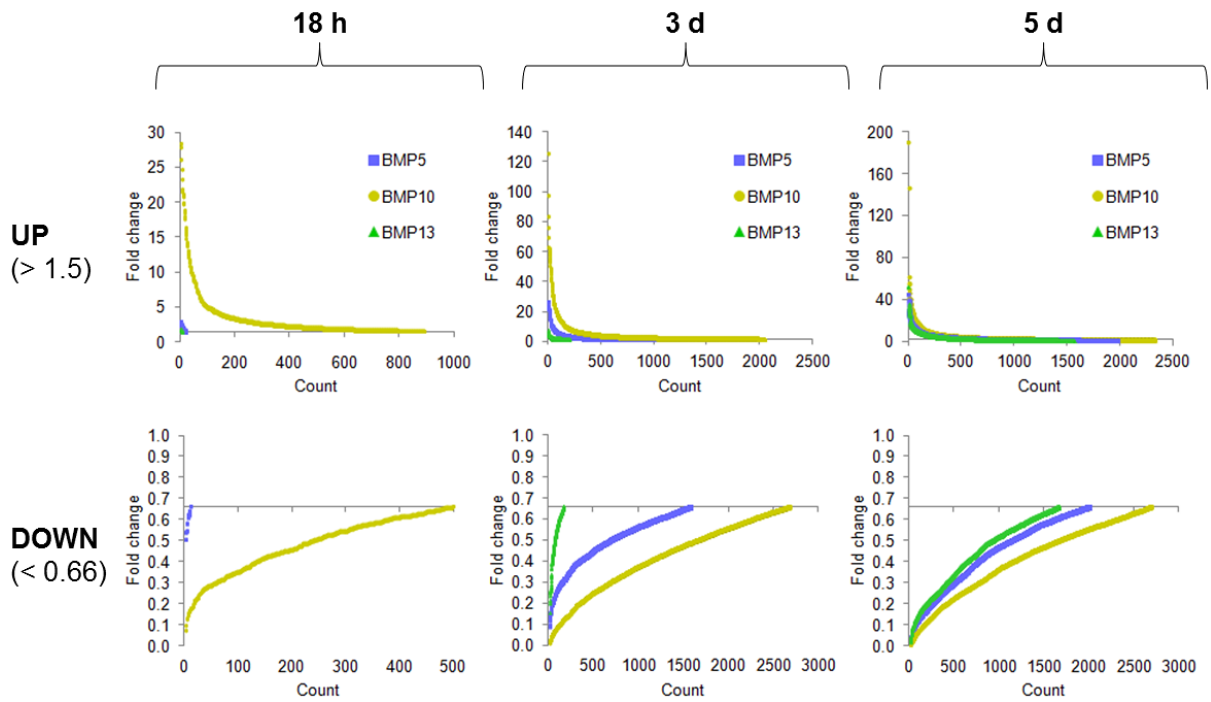
Figure 4-21   Fold change distribution of significantly differentially expressed genes in differentiating BMP5-, BMP10- and BMP13-treated versus reference H1 hESCs at 18 h, 3 d and 5 d.
Further processing of the microarray data of Figure 4-20. The top 100 up- and downregulated genes of all ligands and time points are listed in Table A-1 and Table A-2 (in Appendix).
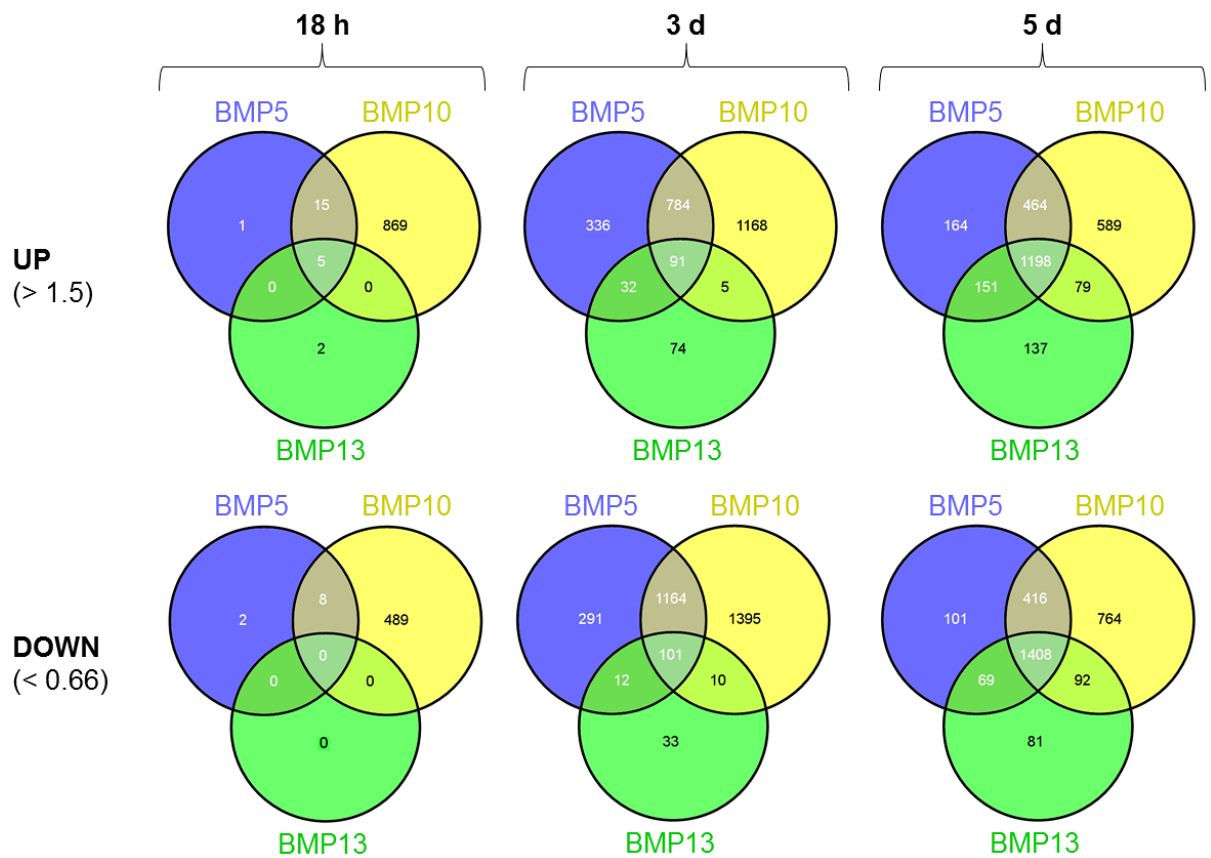
Figure 4-22   Count of unique and common significantly differentially expressed genes between BMP5/BMP10/BMP13 samples versus the HCl/BSA reference samples at 18 h, 3 d and 5 d of treatment of H1 hESCs.
Further processing of the microarray data of Figure 4-20. (Figure modified from Lichtner et al., 2013.)

4.2.4 Tissue correlation analysis of differentiated hESCs after exposure to individual BMP family members for increasing periods of time

The determination of trophoblast lineage as leading differentiation fate for BMP-treated hESCs and hiPSCs was based on the gene expression levels of selected lineage markers (Chapter 4.2.2). These markers (113 in total) only represented a small minority of all differentially expressed genes (as little as 2.3 % in case of BMP10, 5 d). It was therefore highly recommended to verify the identity of the obtained cells by means of an additional independent bioinformatics approach that is capable of considering all differentially expressed genes. For this purpose, an *in silico*-based tissue correlation analysis was performed, which permits the input of large gene lists containing thousands of genes. These gene lists are then allocated to major tissues and anatomical compartments. The allocations are based on the information stored in the UniProt resource database (Chapter 2.13) about each individual gene regarding the tissues in which it has been found to be expressed. Lists of genes that were identified as significantly differentially expressed in H1 hESCs treated with either BMP5, BMP10 or BMP13 relative to the undifferentiated control cells of the same time point were run as queries. The outputs and corresponding P-values are summarized in Figure 4-23.

Exclusively placenta was identified with the clearly lowest P-values for the lists of upregulated genes:

– At 18 h: 1.20×10^{-5} (BMP10), no identification for BMP5 and BMP13
– At 3 d: 4.96×10^{-21} (BMP10), 5.06×10^{-13} (BMP5), 6.56×10^{-3} (BMP13)
– At 5 d: 6.99×10^{-44} (BMP10), 1.07×10^{-29} (BMP5), 6.66×10^{-29} (BMP13)

This means that placenta-associated genes were clearly most overrepresented in the BMP samples. In contrast, the analogous analysis for the lists of downregulated genes yielded no clear identification of a single major tissue or anatomical compartment. Instead, the hits were spread across several terms, with epithelium, eye and teratocarcinoma being on top. Teratocarcinoma was to be expected, because hECCs, which reside as stem cells inside of these germ cell tumors, are the malignant counterparts of hESCs (Andrews, 1988). They express typical hESC-associated genes (Sperger et al., 2003; Liu et al., 2006b; Josephson et al., 2007) and underly similar gene regulatory networks (Greber et al., 2007b; Jung et al., 2010). Epithelium might have been identified because hESCs resemble epithelial cells (Baum et al., 2008).
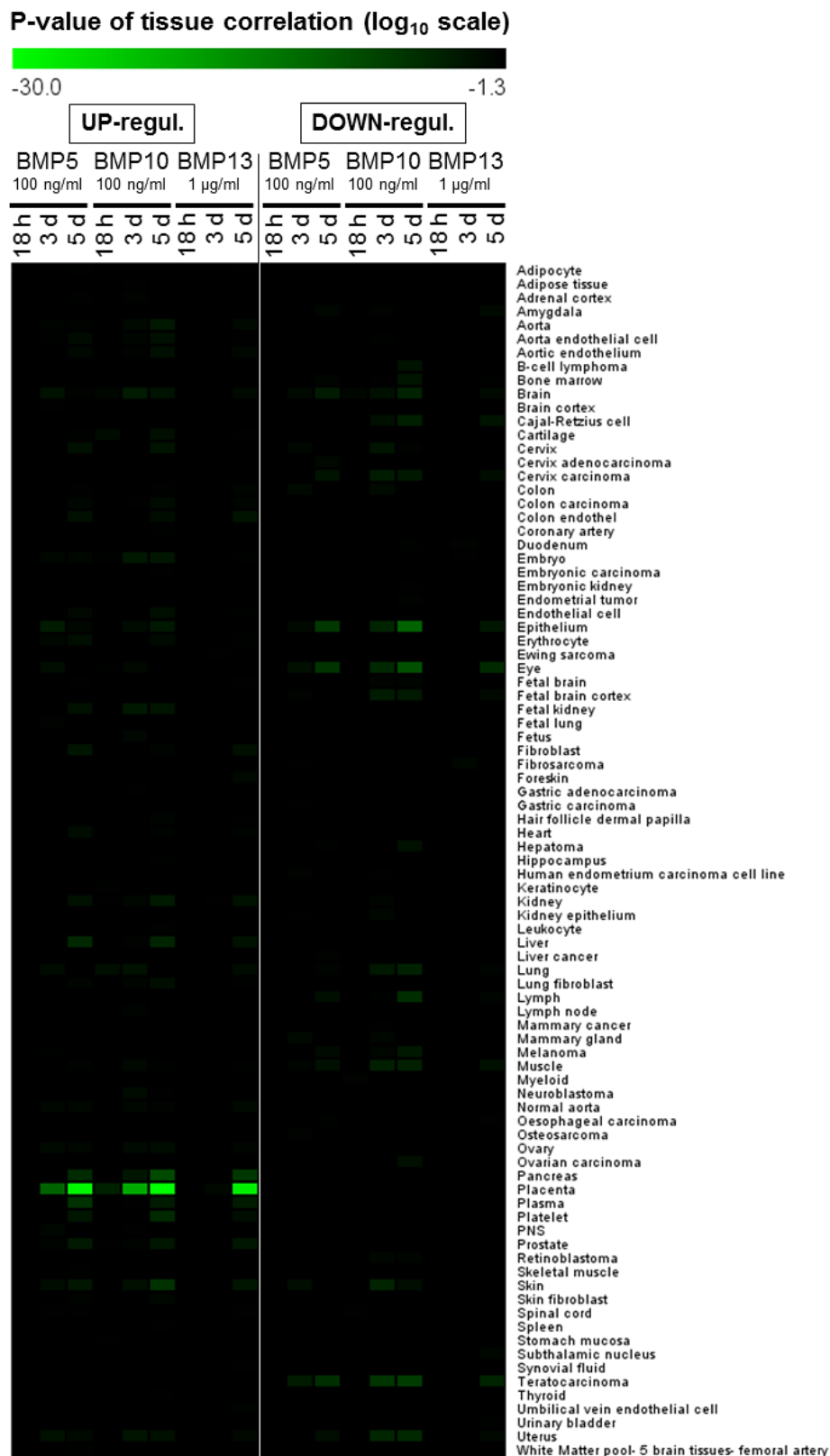
Figure 4-23   Tissue correlation of hESC-derived (line H1) differentiated cells obtained by treatment with BMP5, BMP10 and BMP13 at 18 h, 3 d and 5 d.

The microarray data of the samples of Figure 4-16 were further processed by bioinformatics analysis. Lists of significantly up- and downregulated genes (ligand versus reference cells of the same time point; numbers shown in Figure 4-20) were used as input for computer-based allocations to major tissues and anatomical compartments by means of the UniProt database. Accepted outputs (threshold: $P < 0.05$) are listed in alphabetical order and the corresponding correlation P-values are color-coded visualized for all samples (ligand, time point). $0.05 \triangleq -1.3$ in $\log_{10}$ scale. (Figure modified from Lichtner et al., 2013.)

Next, a tissue correlation analysis was performed for the significantly differentially expressed genes that were shared by the differentiated H1 hESCs (BMP5/BMP10/BMP13 versus HCl/BSA) of the latest time point (day 5). The goal was to reveal common overall tissue-related properties acquired by the cells upon treatment with any of the three ligands. As this analysis was not focused on the enrichment of tissue-associated gene groups versus the whole genome, all P-values were accepted for the outputs. The pie charts in Figure 4-24 display the identified major tissues and anatomical compartments together with the percentage of genes that were found to be associated with them. The following tissues were identified as top 5 outputs:

For the upregulated genes (BMP5 ∩ BMP10 ∩ BMP13; count: 1198):

1. Brain (44.1 %, 485 genes)
2. Placenta (30.9 %, 340 genes)
3. Testis (18.2 %, 200 genes)
4. Epithelium (15.5 %, 170 genes)
5. Lung (15.1 %, 166 genes)

For the downregulated genes (BMP5 ∩ BMP10 ∩ BMP13; count: 1408):

1. Brain (43.1 %, 536 genes)
2. Testis (20.5 %, 255 genes)
3. Placenta (16.1 %, 200 genes)
4. Epithelium (15.8 %, 197 genes)
5. Lung (15.0 %, 186 genes)

It is obvious that the top 5 outputs for both gene lists comprise the same terms, with brain as the leading tissue. However, the placenta-associated gene group was almost twice as high for the upregulated genes compared to the downregulated genes (30.9 % versus 16.1 % of all genes). In contrast, the gene groups which were associated with brain, testis, epithelium and lung were in comparable ranges for both lists. For instance, brain (lung) represented 44.1 % (15.1 %) of upregulated genes and 43.1 % (15.0 %) of downregulated genes, i.e. these matches seem to "neutralize" each other. Since many genes, unless they are specific lineage markers, are known to be expressed by a broad range of tissues, such neutralizing tissue allocations most likely occurred by chance and can therefore be regarded as meaningless for cellular phenotyping. This assumption is supported by the fact that the shared downregulated genes in day 5 differentiated cells, which led to a variety of identified tissues (Figure 4-24), represent those genes which were upregulated in HCl/BSA-treated reference H1 hESCs relative to the ligand-treated cells, and have therefore to be significantly expressed in these cells ($P_{Det} < 0.01$). The undifferentiated phenotype of the reference cells was confirmed by means of morphology (Figure 4-15) and high expression levels of pluripotency markers (Figure 4-16). Remarkable, none of the other allocated tissues appeared as outstanding as did placenta for the upregulated genes compared to the downregulated genes in day 5 differentiated cells (Figure 4-24).
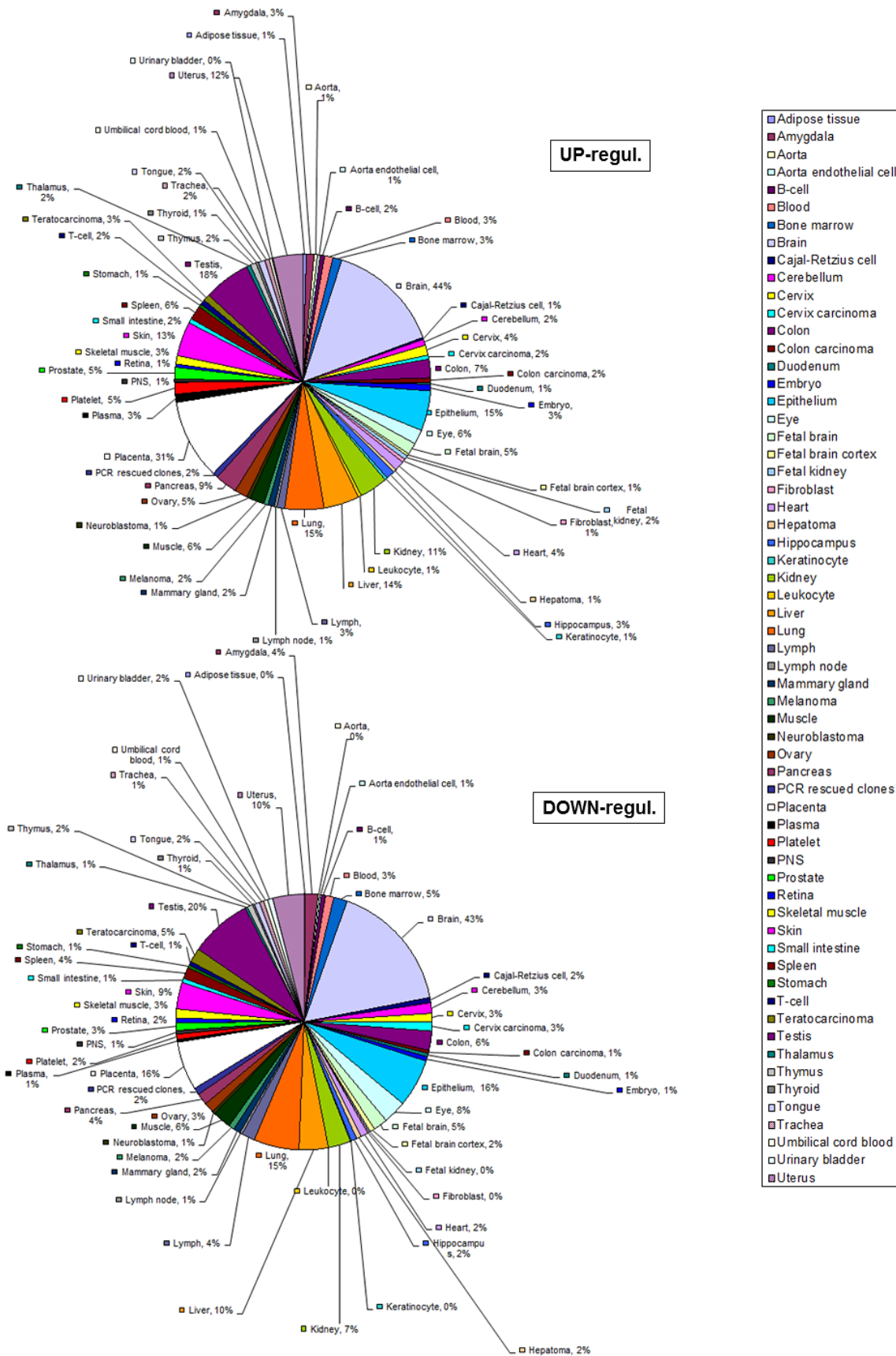
Figure 4-24   Tissue   correlation   of   overlapping   (BMP5 ∩ BMP10 ∩ BMP13)   significantly   up-   and downregulated genes in hESC-derived (line H1) differentiated cells obtained by 5 days treatment with ligands relative to undifferentiated cells.

The microarray data of the samples of Figure 4-16 were further processed by bioinformatics analysis. Shared significantly upregulated genes (1198) and shared significantly downregulated genes (1408) between BMP

samples (BMP5 ∩ BMP10 ∩ BMP13) versus the HCl/BSA reference samples (Venn diagrams of Figure 4-22) were allocated to major tissues and anatomical compartments by means of the UniProt database. The identified terms (threshold: representation of at least 1 % of input genes for one list) are displayed clockwise in alphabetical order together with the percentage of genes that were found to be associated with them. The percentages of pie sectors may exceed 100 % in total, because a single gene can be expressed in more than one tissue.

Taken together, all *in silico* prediction approaches indicate that the differentiated cells represented a placenta-like phenotype. The predictions were based on the global gene expression of individual BMP samples (ligand, time point) as well as on the global gene expression that all BMP samples of day 5 had in common. Because placenta is the tissue to which cells of the trophoblast lineage are dedicated to develop *in vivo* (Chapter 1.1.2), these results strongly support the assumed trophoblast identity of the hESC-derived cells.

4.2.5 Investigation of trophoblast subtype identity of BMP-driven hESC-derived trophoblast cells

All previous analyses revealed trophoblast cells / placenta-like tissue as outcome of BMP-induced differentiation in human pluripotent stem cells under the chosen experimental conditions. The relevance of other major cell lineages could be excluded (Chapter 4.2.2 and 4.2.4). Consequently, further investigations concentrated on this particular lineage. During pregnancy, the villous cytotrophoblast cells of the human placenta are progenitor cells that further specialize by either fusing to form multinucleated syncytiotrophoblast cells or by developing to an invasive phenotype of extravillous cytotrophoblast cells (Chapter 1.1.2.2). In order to determine the subtype identity of the trophoblast cells obtained by the three novel tested ligands, the emphasis was placed on trophoblast markers that are known to be restricted to one of both terminal differentiation pathways. The knowledge of function, chronology and subcellular location of these markers is important to understand the purpose of the subsequent studies and drawn conclusions; hence, they are briefly described in the following two paragraphs (human gene names are written in italicized capital letters as per the international conventions).

1.) Monitored markers involved in specialization of villous cytotrophoblast cells to **multinucleated syncytiotrophoblast cells** (**SCTs**):

Villous cytotrophoblasts differentiating to SCTs express the transcription factor Glial Cell Missing Homolog 1 (*GCM1*) (Baczyk et al., 2004). GCM1 activates expression of the HERV envelope glycoproteins Syncytin-1 (*HERV-W*) (Yu et al., 2002) and Syncytin-2 (*HERV-FRD*) (Liang et al., 2010), which are responsible for the morphological transformation due to their membrane-fusogenic activities (Oren-Suissa and Podbilewicz, 2007; Sapir et al., 2008). Multinucleated SCTs are known to secrete several peptide and steroid hormones to regulate pregnancy, such as the pregnancy hormone Human Chorionic Gonadotropin (hCG) (Malassiné and Cronier, 2002). hCG is a heterodimer that consists of two peptide subunits, α-hCG (*CGA*) and β-hCG (encoded by 6 *CGB* genes and pseudogenes, but predominantly transcribed from *CGB5*). Among those, the β-subunit is unique to hCG, whereas the α-subunit is also a common constituent of other glycoprotein

hormones (Liu and Roberts, 1996). Expression of the α-subunit already starts in villous cytotrophoblasts prior to cell fusion, however the β-subunit is only co-expressed in SCTs. Therefore, formation of dimeric hCG exclusively occurs in SCTs (Hoshina et al., 1982; Muyan and Boime, 1997). Enzymes involved in the biosynthesis of steroid hormones by SCTs are 'P450 Cholesterol Side Chain Cleavage Enzyme' (*CYP11A1*) and '3beta-Hydroxysteroid Dehydrogenase Isoform Type I' (*HSD3B1*) for progesterone (Malassiné and Cronier, 2002; Peng et al., 2004), and 'Cytochrome P450 Aromatase, Family 19, Subfamily A, Polypeptide 1' (*CYP19A1*) and '17β-Hydroxysteroid Dehydrogenase Isozyme Type I' (*HSD17B1*) for estrogens (Cross et al., 2002; Fournet-Dulguerov et al., 1987). The transporter Ferroportin-1 (*SLC40A1*) is a transmembrane protein expressed by SCTs and involved in iron exchange between maternal and fetal blood circulation (Donovan et al., 2000).

2.) Monitored markers involved in specialization of villous cytotrophoblast cells to **invasive extravillous cytotrophoblast cells** (**EVTs**):

Characteristic of EVTs is the secretion of several protease systems, consisting of ECM-degrading proteases and their corresponding inhibitors, which mediate the cells' autoregulated invasive properties. The protease systems include Matrix Metalloproteinases (MMPs) and their inhibitors, Tissue Inhibitor of Metalloproteinase (TIMPs). MMP2 (*MMP2*) and MMP9 (*MMP9*) are known as the key MMP enzymes (Staun-Ram and Shalev, 2005), but also other MMPs, including MMP10 (*MMP10*), have been associated with trophoblast invasion (Pang and Xing, 2003; Williams et al., 2011). Among the expressed TIMPs are TIMP1 (*TIMP1*), TIMP2 (*TIMP2*) and TIMP3 (*TIMP3*) (Huppertz et al., 1998; Higuchi et al., 1995; Bass et al., 1997). Two other involved protease systems are Urokinase-type Plasminogen Activator (*PLAU*) and its inhibitor Plasminogen Activator Inhibitor (*PAI1*) (Chou et al., 2002; Knöfler, 2010), and Cathepsin L1 (*CTSL1*) (Varanou et al., 2006; Knöfler, 2010) and its inhibitor Cystatin C (*CST3*) (Song et al., 2010a). Invading EVTs express high levels of Human Leukocyte Antigen G (*HLA-G*) on their cell membrane, which provides maternal immune tolerance of the fetal semi-allograft (Ellis et al., 1990; McMaster et al., 1995). Expression of HLA-G mRNA already occurs in not yet invasive cytotrophoblast cells, but its translation is delayed by post-transcriptional regulation (Copeman et al., 2000). EVTs express the maternally imprinted gene *IGF2*, which encodes Insulin-like Growth Factor-II, to support fetal growth (Han et al., 1996; Hamilton et al., 1998; Constância et al., 2002). Their cell surface is positive for the cluster of differentiation antigen CD9 (*CD9*) (Hirano et al., 1999a; Hirano et al., 1999b).

4.2.5.1   Classification based on gene expression

Figure 4-25 shows the fold changes in gene expression of aforementioned SCT/EVT-related markers between BMP5-, BMP10- and BMP13-induced day 5 trophoblast cells and undifferentiated H1 hESCs. Most of the markers were significantly upregulated to varying degrees, at least upon BMP10 treatment. This means that the hESC-derived trophoblast cells were able to enter both terminal differentiation pathways, and accordingly passed through a precursor state which resembles an *in vitro* counterpart of placental villous cytotrophoblast cells. Further evidence for this can be seen from Figure 4-17, which reveals that the timing of induction of genes involved in SCT differentiation reflected the chronology known from *in vivo* placentation (*GCM1* → *HERV* fusogenes → *CGA* → *CGB*). It is worth noting that the

expression patterns of individual SCT/EVT markers of day 5 trophoblast cells were comparable among the BMP samples and only differed in the level of upregulation (BMP10 > BMP5 > BMP13) (Figure 4-25). This implies that none of the distinct ligands promoted the emerged trophoblast cells to mature more to either SCTs or EVTs compared to the other ligands. It is only the kinetics of differentiation that varied. BMP10 was the most potent, as judged by expression of *CGA* (190.0-fold), *HSD3B1* (61.9-fold) and *SLC40A1* (41.6-fold) as top 3 upregulated markers representing SCT differentiation, and *TIMP3* (36.5-fold), *CDH5* (13.2-fold) and *MMP2* (10.4-fold) as top 3 upregulated markers representing EVT differentiation.
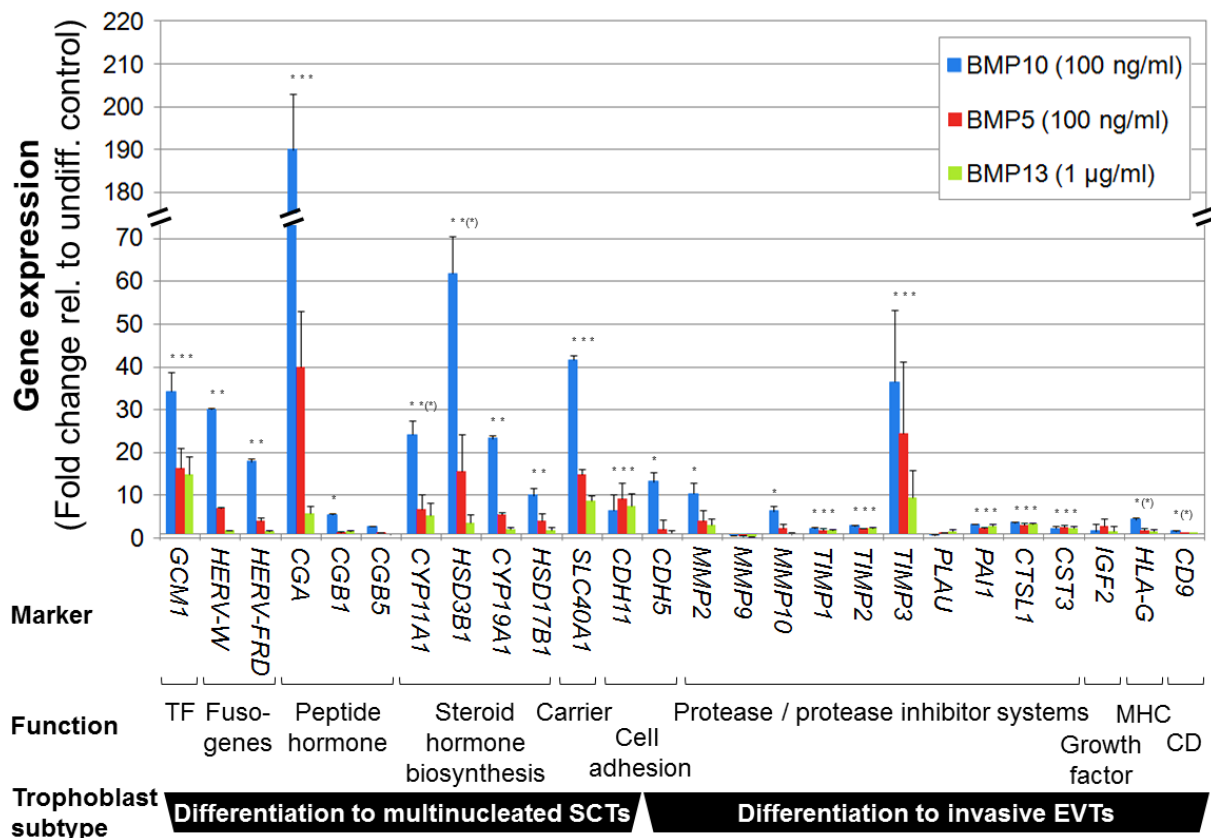
Figure 4-25   Microarray-based determination of cellular subtype identity of day 5 trophoblast cells generated by treatment of H1 hESCs with BMP5, BMP10 and BMP13.
Terminal maturation to either multinucleated syncytiotrophoblasts (SCTs) or invasive extravillous cytotrophoblasts (EVTs) was investigated for the day 5 samples of Figure 4-16 by monitoring the gene expression levels of cell fate-specific markers. Shown are the fold changes (BMP versus HCl/BSA reference cells), calculated as ratios of average signal intensities (microarray data). Horizontal axis = 1-fold (unchanged). *: $P_{Diff} < 1 \times 10^{-4}$, (*): $P_{Diff} < 0.05$. Error bars indicate array STDEV (grouped biological duplicates). Abbreviations: CD = cluster of differentiation, MHC = major histocompatibility complex, TF = transcription factor. (Figure modified from Lichtner et al., 2013.)

4.2.5.2   Classification based on protein expression

As next step, the trophoblast subtype identity was investigated on protein level for selected key markers. Immunocytochemistry was the method of choice, because it provides insights into the actual distribution of antigens within whole cell populations and on

subcellular level. This valuable "*in situ*" information would get lost in case of downstream procedures such as trypsinization to single cells or cell lysis to be applied for flow cytometry or western immunoblotting. H1 hESCs were treated as before with BMP5, BMP10 (both 100 ng/ml), BMP13 (1 µg/ml) or equivalent volume of solvent/carrier protein (HCl/BSA) as reference in N2B27 medium lacking bFGF on Matrigel. Media and supplements were replaced every 24 h. After 5 days, cells were fixed with PFA, stained using specific antibodies and visualized by fluorescence microscopy (Figure 4-26).

The undifferentiated state of the vast majority of HCl/BSA-treated reference cells was confirmed by nuclear co-expression of the pluripotency-associated TFs OCT4 and NANOG (Figure 4-26A).

Staining of the BMP-treated cells for the pan-trophoblast marker Cytokeratin-7 (KRT7) revealed that nearly all visible cells across the colonies were KRT7$^+$, confirming their trophoblast identity (Figure 4-26B). KRT7 was chosen as marker, since it has been proven to be more specific for all subpopulations of trophoblast cells than other keratin filament types such as Cytokeratin-8 and -18, which are also expressed in placental mesenchymal cells (Haigh et al., 1999; Blaschitz et al., 2000). Co-staining for the cell adhesion protein E-Cadherin (Epithelial-Cadherin) revealed that the majority of KRT7$^+$ cells was also positive for this epithelial cell marker (Figure 4-26B). Villous cytotrophoblast cells are – like hESCs – of epithelial phenotype (Floridon et al., 2000). This could imply that most of the trophoblast cells have not yet terminally differentiated. It is known that villous cytotrophoblast cells during cell fusion to multinucleated SCTs downregulate E-Cadherin and upregulate Cadherin-11 expression (Getsios and MacCalman, 2003) (*CDH11* gene in Figure 4-25), and that villous cytotrophoblast cells maturing to invasive EVTs downregulate E-Cadherin and upregulate VE-Cadherin (Vascular Endothelial-Cadherin) expression (Zhou et al., 1997) (*CDH5* gene in Figure 4-25).

The presence of SCTs in BMP-treated samples was identified by staining for the β-subunit of the pregnancy hormone Human Chorionic Gonadotropin (hCG) (Figure 4-26C), the subunit specific for hCG. β-hCG$^+$ areas were randomly distributed throughout differentiated colonies. It is obvious that more cell fusion events took place in BMP10-treated cells compared to those treated with BMP5 or BMP13. This is in agreement with the morphological observations (Figure 4-15) and gene expression analysis (*CGA* gene (encoding the α-subunit), *CGB* genes (encoding the β-subunit); Figure 4-25). The identity of β-hCG$^+$ structures was further confirmed to be SCTs by co-staining for E-Cadherin to verify their polynuclear nature (Figure 4-26D). β-hCG$^+$ areas that contained several nuclei were lacking E-Cadherin$^+$ cell membranes, unlike the surrounding β-hCG$^-$ mononuclear cells. Co-staining for the cell fusion-mediating membrane protein Syncytin-1 (*HERV-W* gene in Figure 4-25) revealed that this protein was co-localized with β-hCG and also expressed by subpopulations of β-hCG$^-$ cells (Figure 4-26E). Multinucleated SCTs are known for their continued expression of Syncytin-1 (Pötgens et al., 2004). The Syncytin-1$^+$/β-hCG$^-$ cells were either localized at the outer border of β-hCG$^+$ areas or at independent places. This indicates that these cells were just about to be incorporated into an existing syncytium or to aggregate and fuse to form new syncytia.
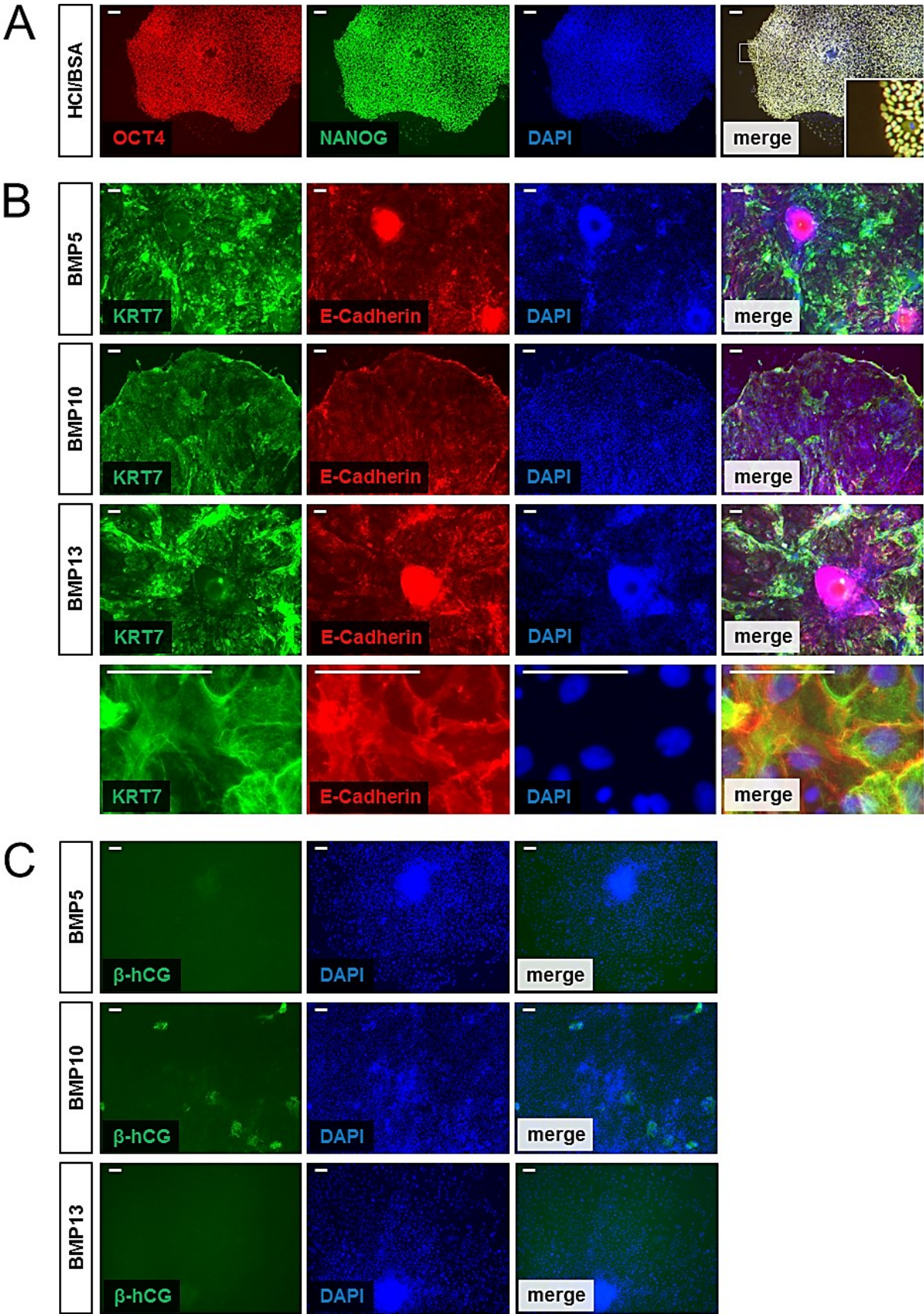
(continued from previous page)
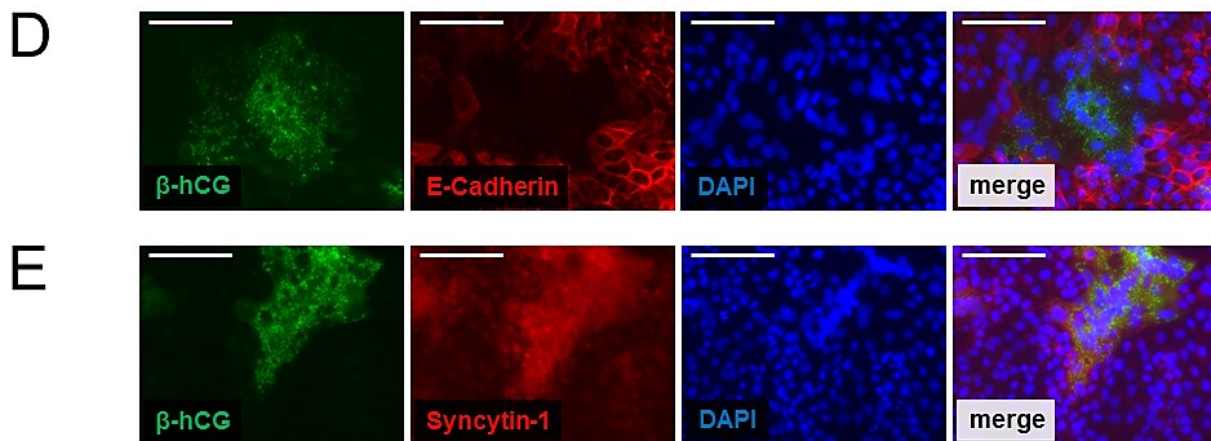
Figure 4-26   Immunocytochemical-based phenotyping of trophoblast cells generated by treatment of H1 hESCs with BMP5, BMP10 and BMP13 for 5 days.
Feeder-free hESC colonies were treated with recombinant human BMP5 (100 ng/ml), BMP10 (100 ng/ml), BMP13 (1 µg/ml) or 20 µl HCl/BSA equivalent (= undifferentiated reference cells) as indicated in N2B27 medium w/o bFGF on Matrigel. Media and supplements were replaced every 24 h. PFA-fixed cells were analyzed by immunocytochemistry. Nuclei were counterstained with DAPI. Shown are fluorescence microscopy photos of representative colonies. Scale bars represent 100 µm. **(A)** Confirmation of the undifferentiated state of HCl/BSA-treated reference hESCs (OCT4$^+$/NANOG$^+$ nuclei). **(B)** Identification of BMP-driven differentiated cells as trophoblast cells (KRT7$^+$) and confirmation of their epithelial character (E-Cadherin$^+$). **(C)** Identification of syncytiotrophoblasts (SCTs) within differentiated colonies (β-hCG$^+$). **(D)** Validation of β-hCG$^+$ SCTs as polynuclear by co-staining for E-Cadherin to confirm lack of cell membranes inside areas containing several nuclei. **(E)** Proof of membrane-fusogenic activities by Syncytin-1 (expression co-localized with β-hCG and at β-hCG$^-$ areas). (Figure modified from Lichtner et al., 2013.)

The presence of dimeric hCG secreted by endocrine active SCTs was confirmed by ELISA-based quantification of media supernatants. This method was considered as being accurate, since the BMP treatments were conducted in equal volumes, and the media and supplements were replaced every 24 h. Analysis for BMP-treated H1 hESCs was done using collected aliquots from samples of the same experimental series which were analyzed earlier by microarray and real-time qPCR (Chapter 4.2.2). Figure 4-27A shows the measured hCG concentrations of all samples (ligand, time point). In concordance with the upregulation of the genes that encode the α- and β-subunit of dimeric hCG (*CGA* and *CGB,* Figure 4-17), the hormone was not detectable in media supernatants before day 5 of differentiation. The highest concentration was measured for the day 5 sample of BMP10 (18.9 ± 1.3 mIU/ml).

The ELISA assay was repeated with day 5 media supernatants of the BMP-treated H9 hESCs and iPS1/iPS2 hiPSCs, whose cell lineage identities – including expression levels of *CGA*/*CGB* – were determined by real-time qPCR in Figure 4-18. Dimeric hCG was detectable in the medium of all three independent human pluripotent stem cell lines (Figure 4-27B). The results were similar to H1 hESCs in respect of the observed patterns of ligand potency.
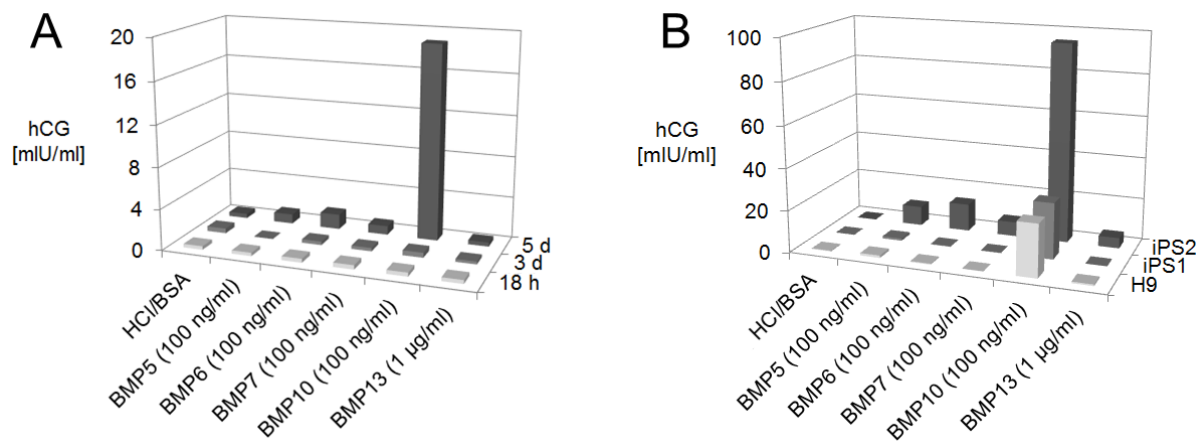
Figure 4-27   Secretion of Human Chorionic Gonadotropin (hCG) by endocrine active syncytiotrophoblasts obtained by treatment of hESCs (H1/H9) and hiPSCs (iPS1/iPS2) with BMP5/6/7, BMP10 and BMP13.
Shown are the average concentrations which accumulated within 24 h prior to the mentioned time point as determined by ELISA (biological duplicates). IU = international unit (a standard defined by the World Health Organization). **(A)** Media supernatants of H1 cell samples at 18 h, 3 d and 5 d (samples of Figure 4-17). **(B)** Media supernatants of H9, iPS1 and iPS2 cell samples at day 5 (samples of Figure 4-18). (Figure modified from Lichtner et al., 2013.)

4.2.5.3   Classification based on cell morphology

The results raised the question of how the distribution of cellular phenotypes would have been if the generated trophoblast cells had time beyond 5 days for their terminal differentiation. To answer that question, a follow-up experiment was performed. H1 hESCs were treated under the same experimental conditions over an extended period of 10 days. Since the BMPs only differed in the kinetics, but not in the outcome of induced differentiation, this experiment was conducted with BMP10 as the most efficient ligand.

Between day 5–8, an increase in the formation of multinucleated SCTs with respect to quantity (number of cell fusion events) and size (diameter of syncytia structures) was observed. However, beginning around day 9, a massive onset of decay of syncytia structures, along with missing formation of new syncytia and missing incorporation of mononuclear cells into existing syncytia, was observed. Furthermore, as of day 8–9, it was observed that a fraction of the mononuclear cells located at the periphery of differentiated colonies lost cell-cell contact and migrated away as independent single cells (Figure 4-28).

The phenomenon of syncytia decay could be explained due to the experimental conditions (N2B27 medium perhaps not suited for the *in vitro* culture of SCTs) or the limited life span of SCTs *in vivo* (i.e. representing an *in vitro* counterpart of *in vivo* syncytia apoptosis and shedding (Chapter 1.1.2.2), similar as described (Gupta et al., 2004)). The phenomenon of detachment of mononuclear cells from the border of colonies does very likely resemble invasive EVTs *in vivo*, which are detaching from the distal sites of cell columns of anchoring villi to invade the maternal decidua (Knöfler, 2010) (Chapter 1.1.2.2). The invasive feature of HLA-G-positive and MMP-secreting EVTs, gained via embryoid body- or BMP4-based approaches from hESCs, has been demonstrated before by *in vitro* cell migration and invasion assays (Udayashankar et al., 2011; Amita et al., 2013).
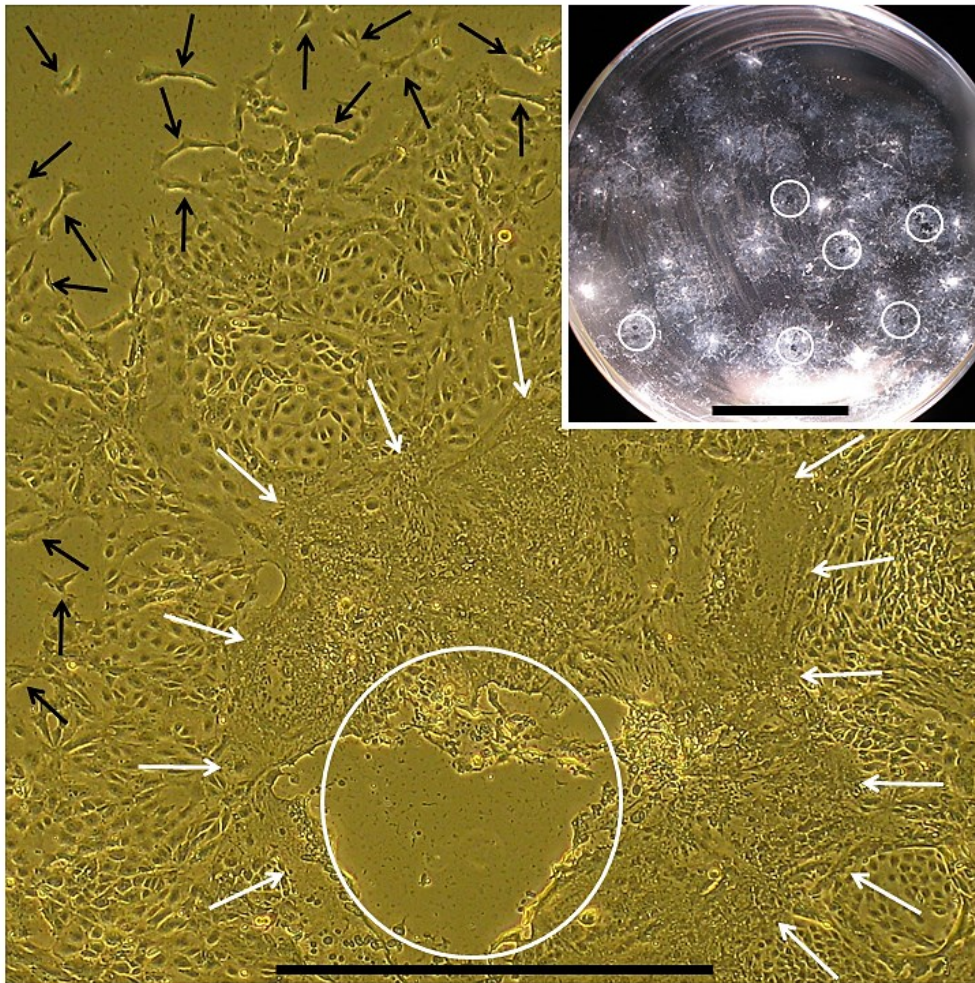
Figure 4-28   Morphology of trophoblast cells derived from H1 hESCs after prolonged treatment with BMP10 for 10 days.
Feeder-free hESC colonies were treated in N2B27 medium w/o bFGF on Matrigel with 100 ng/ml of ligand (replaced every 24 h). Phase-contrast images of representative colonies (overview of 6-well and close-up view). White arrows mark the periphery of a large polynuclear syncytium. White circles mark decayed areas within syncytia structures. Black arrows indicate detached single cells migrating away from the periphery of a differentiated colony. Black scale bars represent 1 mm (close-up picture) and 1 cm (overview picture). (Figure modified from Lichtner et al., 2013.)

4.2.6 Global overview of pathways involved in BMP-induced trophoblast differentiation of hESCs

The next part of this work is focused on the pathways which were affected during the course of BMP-driven trophoblast differentiation of human pluripotent stem cells. A bioinformatics approach was applied to investigate which pathways were up- and downregulated in H1 hESCs treated with either BMP5, BMP10 or BMP13 at 18 h, 3 d and 5 d. The queries were run against the KEGG, PANTHER and REACTOME databases (Chapter 2.13). Pathways which were identified by *in silico* prediction as being enriched are listed in Table 4-1 together with the count of pathway-related genes and corresponding P-values. The analysis was performed separately for all significantly upregulated and downregulated genes.

4.2.6.1   Overrepresented pathways

Table 4-1A provides a global overview of all pathways that were found to be enriched for the upregulated genes in BMP-induced trophoblast cells (relative to the reference cells).

The outputs could be grouped into four categories:

1.) Signaling
2.) Cell adhesion / ECM interaction
3.) Metabolism
4.) Other pathways

The majority of identified pathways was related to signaling. As expected, canonical BMP signaling and TGF-β superfamily signaling, which includes BMP signaling (Chapter 1.3), were clearly identified as overrepresented for samples of all three BMPs. Key signal transduction pathways that are known to promote the migration and invasion of EVTs *in vivo* and *ex vivo* were identified as enriched at 3 d and/or 5 d in trophoblast cells generated by BMP5, BMP10 and BMP13. These include focal adhesion-, cadherin-, integrin-, MAPK-, Rho GTPase- and Wnt signaling (reviewed by Knöfler, 2010; Zhou et al., 1997). The identified pathways related to p53-, PDGF-, PPAR-, MAPK- and Wnt signaling have been reported to be active in trophoblast cells, including multinucleated SCTs, derived from hESCs by treatment with BMP4 *in vitro* (Sudheer et al., 2012; Marchand et al., 2011). GnRH signaling, which was identified at day 5 for BMP10, is known to regulate the expression of hCG (Lee et al., 2010) and pro-angiogenic chemokines (Cavanagh et al., 2009) at the maternal-fetal interface during human placentation.

Cell adhesion / ECM interaction-related terms (integrin cell surface interactions, ECM-receptor interaction, focal adhesion) belonged to the most significantly overrepresented pathways and were affected in common (BMP5 ∩ BMP10 ∩ BMP13) at the later stages of trophoblast differentiation (3 d, 5 d). This might be explained by the fact that villous cytotrophoblast cells differentiating to either SCTs or EVTs undergo a change in their expression patterns of cell adhesion proteins on their cell membranes (SCT differentiation: Getsios and MacCalman, 2003; Aplin et al., 2009; EVT differentiation: Zhou et al., 1997; Harris et al., 2009). These include, among others, cadherins as compounds of adherens junctions (mainly involved in cell-cell adhesion (Yonemura, 2011)) and integrins as compounds of focal adhesions (mainly involved in cell-ECM adhesion (van der Flier and Sonnenberg, 2001; Wehrle-Haller, 2012)). The switch of adhesion molecule phenotype is known to be most dramatic and flexible for cells differentiating along the invasive pathway (Chapter 1.1.2.2), and necessary for proper development and function of EVTs during human placentation. Besides their roles in cell attachment via coupling of individual extracellular ligands to the cells' cytoskeleton, cadherins and integrins also function as receptors that mediate signals from the outside to the inside of cells (Juliano, 2002). The multiplicity of adhesive interactions between trophoblast cells and their surrounding environment, e.g. the maternal decidua during pregnancy, results in distinct signals that are intracellular transmitted. All these signals exert influence on trophoblast cell behavior, e.g. by regulating the expression levels of specific types of ECM-degrading proteases to be secreted by invasive EVTs (Xu et al., 2001b).

Metabolism-related pathways which were most significantly enriched in trophoblast cells are steroid hormone biosynthesis (characteristic of SCTs; Chapter 4.2.5) and metabolism of lipids and lipoproteins.

4.2.6.2 Underrepresented pathways

Table 4-1B provides a global overview of all pathways that were found to be enriched for the downregulated genes in BMP-induced trophoblast cells (relative to the reference cells).

The outputs could be grouped into four categories:

1.) Metabolism
2.) Cell cycle / DNA maintenance
3.) Signaling
4.) Other pathways

Most of the identified pathways were common among BMP5/BMP10/BMP13 samples and related to metabolism or cell cycle / DNA maintenance. The latter include processes such as mitosis, DNA replication, telomere maintenance and several types of DNA repair mechanisms. These pathways were not yet affected in undifferentiated hESCs after 18 h BMP stimulation, but only in trophoblast cells after 3 d and/or 5 d treatment. This is consistent with the known high proliferation rate of hESCs (Thomson et al., 1998), which also have a high telomerase activity (Chapter 4.1.2.3) and enhanced repair capacities of multiple forms of DNA damage (Maynard et al., 2008) in order to maintain their genomic integrity. In contrast, the proliferation rate of villous cytotrophoblast cells is decreased, and SCTs and EVTs are known to be mitotically inactive (Baczyk et al., 2009).

Underrepresented metabolism-related pathways mainly concerned amino acids and nucleic acids, including *de novo* purine and pyrimidine biosynthesis. Compared to hESCs this suggests a consequently lower demand of trophoblast cells for components for the biosynthesis of nucleic acids and proteins. Interestingly, glycolysis as the prevalent form of energy production by hESCs (Prigione et al., 2011b) was not among the terms.

Table 4-1   Over- and underrepresented pathways during BMP5-, BMP10- and BMP13-driven trophoblast differentiation of H1 hESCs at 18 h, 3 d and 5 d.
The microarray data of the samples of Figure 4-16 were further processed by bioinformatics analysis. Lists of significantly up- and downregulated genes (ligand versus reference cells of the same time point; numbers shown in Figure 4-20) were used as input for computer-based identifications of enriched pathways by means of the three reference databases KEGG (KEG), PANTHER (PAN) and REACTOME (REA). The identified pathways were classified into categories. Shown are the numbers of associated genes and corresponding correlation P-values (threshold: P < 0.05) for all samples (ligand, time point). **(A)** Overrepresented pathways. **(B)** Underrepresented pathways. Conditional formatting: light blue for P < 0.05, mid blue for P < 0.01, dark blue for P < 0.001. (Table modified from Lichtner et al., 2013.)

A

Overrepresented pathways

Database	Term number	Pathway	18h BMP5 Count	Pvalue	18h BMP10 Count	Pvalue	18h BMP13 Count	Pvalue	3d BMP5 Count	Pvalue	3d BMP10 Count	Pvalue	3d BMP13 Count	Pvalue	5d BMP5 Count	Pvalue	5d BMP10 Count	Pvalue	5d BMP13 Count	Pvalue
Category: Signaling																			
KEG	hsa04920	Adipocytokine signaling	-	-	-	-	-	-	-	-	-	-	-	-	-	-	15	1.9 E-2	-	-
PAN	P00002	Alpha adrenergic receptor signaling	-	-	-	-	-	-	-	-	-	-	-	-	5	3.4 E-2	-	-	-	-
KEG	hsa04662	B cell receptor signaling	-	-	-	-	-	-	-	-	-	-	-	-	-	-	15	4.6 E-2	-	-
REA	REACT_12034	BMP signaling	-	-	7	5.2 E-5	-	-	7	6.5 E-4	9	3.4 E-4	3	1.5 E-2	10	1.2 E-4	8	8.9 E-3	6	2.0 E-2
PAN	P04380	Cortocotropin releasing factor receptor signaling	-	-	-	-	-	-	-	-	-	-	-	-	9	2.9 E-2	-	-	-	-
KEG	hsa05120	Epithelial cell signaling in Helicobacter pylori infection	-	-	-	-	-	-	-	-	-	-	-	-	-	-	14	4.5 E-2	-	-
KEG	hsa04912	GnRH signaling	-	-	-	-	-	-	-	-	-	-	-	-	-	-	19	3.0 E-2	-	-
KEG	hsa04340	Hedgehog signaling	-	-	-	-	-	-	6	3.7 E-4	-	-	-	-	12	2.6 E-2	-	-	10	4.5 E-2
REA	REACT_6900	Immune system signaling	-	-	-	-	-	-	-	-	-	-	-	-	37	3.4 E-2	-	-	-	-
KEG	hsa04010	MAPK signaling	-	-	7	4.5 E-2	-	-	-	-	-	-	-	-	-	-	49	9.9 E-4	32	4.3 E-2
KEG	hsa04722	Neurotrophin signaling	-	-	-	-	-	-	-	-	-	-	-	-	-	-	24	1.4 E-2	-	-
PAN	P00045	Notch signaling	-	-	7	4.0 E-2	-	-	-	-	-	-	-	-	-	-	-	-	-	-
KEG	hsa04115	p53 signaling	-	-	8	1.3 E-2	-	-	9	4.4 E-2	-	-	-	-	13	4.5 E-2	14	4.5 E-2	12	2.7 E-2
PAN	P00059	p53 signaling	-	-	-	-	-	-	-	-	-	-	-	-	-	-	13	2.8 E-2	-	-
KEG	hsa05200	Pathways in cancer	-	-	21	1.9 E-2	-	-	31	9.0 E-3	44	2.6 E-2	-	-	57	8.1 E-5	66	5.1 E-6	44	2.3 E-3
PAN	P00047	PDGF signaling	-	-	-	-	-	-	-	-	-	-	-	-	-	-	33	4.6 E-2	-	-
REA	REACT_16888	PDGF signaling	-	-	8	3.4 E-3	-	-	9	1.2 E-2	13	5.6 E-3	-	-	20	2.8 E-6	25	1.5 E-8	15	1.0 E-4
KEG	hsa03320	PPAR signaling	-	-	-	-	-	-	-	-	13	3.4 E-2	-	-	15	9.9 E-3	-	-	13	1.2 E-2
PAN	P04393	Ras signaling	-	-	-	-	-	-	-	-	-	-	-	-	-	-	20	2.3 E-2	-	-
REA	REACT_11044	Rho GTPases signaling	-	-	-	-	-	-	14	6.6 E-3	21	2.4 E-3	-	-	23	1.8 E-3	27	5.4 E-4	19	2.1 E-3
KEG	hsa04350	TGF-beta signaling	4	3.8 E-4	14	1.6 E-5	-	-	13	4.4 E-3	17	9.3 E-3	7	2.3 E-4	21	4.4 E-4	19	9.4 E-3	15	1.4 E-2
PAN	P00052	TGF-beta signaling	-	-	18	1.6 E-3	-	-	-	-	-	-	7	1.8 E-2	-	-	-	-	-	-
REA	REACT_6844	TGF-beta signaling	-	-	3	4.0 E-3	-	-	-	-	-	-	-	-	-	-	4	1.8 E-2	-	-
PAN	P04394	Thyrotropin-releasing hormone receptor signaling	-	-	-	-	-	-	-	-	-	-	-	-	13	4.5 E-2	-	-	-	-
KEG	hsa04310	Wnt signaling	-	-	6	1.6 E-2	-	-	18	6.7 E-3	24	2.1 E-2	-	-	11	3.6 E-2	-	-	21	3.0 E-2
PAN	P00057	Wnt signaling	-	-	-	-	-	-	32	1.2 E-2	46	3.5 E-2	-	-	-	-	-	-	-	-
PAN	P00012	Cadherin signaling	-	-	-	-	-	-	19	7.6 E-3	28	5.5 E-3	-	-	-	-	-	-	-	-
PAN	P00034	Integrin signalling	-	-	20	1.4 E-2	-	-	22	2.8 E-2	34	1.7 E-2	-	-	44	3.5 E-4	57	2.0 E-7	36	2.0 E-3
Category: Cell adhesion / ECM interaction																			
REA	REACT_13552	Integrin cell surface interactions	-	-	-	-	-	-	-	-	-	-	-	-	24	5.8 E-7	24	8.8 E-6	19	8.2 E-6
KEG	hsa04520	Adherens junction	-	-	-	-	-	-	11	1.4 E-2	14	3.5 E-2	-	-	-	-	16	2.8 E-2	-	-
KEG	hsa04512	ECM-receptor interaction	-	-	8	3.6 E-2	-	-	-	-	17	6.6 E-3	-	-	31	3.3 E-10	29	8.9 E-8	23	1.1 E-6
KEG	hsa04510	Focal adhesion	-	-	-	-	-	-	19	4.6 E-2	37	2.1 E-4	-	-	54	4.1 E-11	61	6.7 E-13	41	1.8 E-7
Category: Metabolism																			
KEG	hsa00150	Androgen and estrogen metabolism	-	-	-	-	-	-	-	-	-	-	-	-	6	8.3 E-3	-	-	-	-
REA	REACT_13433	Biological oxidations	-	-	-	-	-	-	-	-	18	1.4 E-2	-	-	19	2.0 E-2	10	3.3 E-2	16	1.5 E-2
KEG	hsa00480	Glutathione metabolism	-	-	-	-	-	-	-	-	-	-	-	-	11	3.0 E-2	-	-	10	2.3 E-2
KEG	hsa00563	GPI-anchor biosynthesis	-	-	-	-	-	-	-	-	-	-	-	-	-	-	8	2.0 E-2	-	-
REA	REACT_15314	Hormone biosynthesis	-	-	-	-	-	-	-	-	-	-	-	-	6	1.5 E-2	6	4.8 E-2	-	-
REA	REACT_602	Metabolism of lipids and lipoproteins	-	-	-	-	-	-	-	-	22	1.1 E-2	-	-	24	1.1 E-2	27	9.9 E-3	20	8.3 E-3
KEG	hsa00980	Metabolism of xenobiotics by cytochrome P450	-	-	-	-	-	-	-	-	7	2.0 E-2	-	-	-	-	-	-	-	-
KEG	hsa00511	Other glycan degradation	-	-	-	-	-	-	-	-	-	-	-	-	6	1.9 E-2	-	-	-	-
KEG	hsa00040	Pentose and glucuronate interconversions	-	-	-	-	-	-	-	-	4	2.5 E-2	-	-	-	-	-	-	-	-
KEG	hsa00140	Steroid hormone biosynthesis	-	-	-	-	-	-	-	-	6	2.3 E-2	-	-	7	4.7 E-3	7	9.4 E-3	6	1.0 E-2
Category: Other																			
PAN	P00004	Alzheimer disease-presenilin pathway	-	-	6	3.8 E-2	-	-	18	2.8 E-3	26	2.0 E-3	-	-	-	-	-	-	-	-
PAN	P00005	Angiogenesis	-	-	-	-	-	-	8	1.9 E-2	17	1.7 E-2	-	-	-	-	42	1.3 E-2	-	-
KEG	hsa05412	Arrhythmogenic right ventricular cardiomyopathy	-	-	-	-	-	-	-	-	-	-	-	-	16	1.0 E-2	18	5.1 E-5	13	2.5 E-2
REA	REACT_18266	Axon guidance	-	-	6	8.3 E-3	-	-	14	3.8 E-2	21	2.5 E-2	-	-	22	2.3 E-2	27	3.0 E-3	18	4.4 E-2
KEG	hsa04360	Axon guidance	-	-	-	-	-	-	9	2.3 E-3	11	6.0 E-3	-	-	15	9.3 E-5	15	4.9 E-4	11	1.8 E-3
PAN	P00007	Axon guidance mediated by semaphorins	-	-	-	-	-	-	8	3.0 E-2	-	-	-	-	-	-	-	-	-	-
KEG	hsa04060	Cytokine-cytokine receptor interaction	-	-	-	-	-	-	-	-	-	-	-	-	19	3.9 E-3	20	3.7 E-2	-	-
KEG	hsa04144	Endocytosis	-	-	-	-	-	-	19	2.1 E-2	-	-	-	-	-	-	32	1.9 E-2	-	-
KEG	hsa04666	Fc gamma R-mediated phagocytosis	-	-	-	-	-	-	-	-	-	-	-	-	-	-	19	2.3 E-2	-	-
REA	REACT_604	Hemostasis	-	-	-	-	-	-	-	-	-	-	-	-	40	1.8 E-4	50	2.6 E-6	29	3.5 E-3
KEG	hsa05410	Hypertrophic cardiomyopathy	-	-	-	-	-	-	-	-	-	-	-	-	-	-	18	1.6 E-2	-	-
KEG	hsa04142	Lysosome	-	-	-	-	-	-	-	-	24	7.9 E-4	-	-	28	4.2 E-5	36	5.0 E-8	25	3.4 E-5
KEG	hsa04916	Melanogenesis	-	-	-	-	-	-	15	1.7 E-3	17	3.0 E-2	-	-	-	-	20	1.7 E-2	-	-
REA	REACT_11123	Membrane Trafficking	-	-	-	-	-	-	-	-	9	1.8 E-2	-	-	13	2.3 E-4	18	3.8 E-7	10	1.8 E-3
KEG	hsa04810	Regulation of actin cytoskeleton	-	-	-	-	-	-	-	-	-	-	-	-	32	3.4 E-2	42	7.0 E-4	-	-
KEG	hsa04130	SNARE interactions in vesicular transport	-	-	-	-	-	-	-	-	-	-	-	-	11	4.2 E-3	11	9.2 E-3	9	1.3 E-2
KEG	hsa05110	Vibrio cholerae infection	-	-	-	-	-	-	-	-	-	-	-	-	-	-	13	2.4 E-2	-	-

B

Underrepresented pathways

Database	Term number	Pathway	18h BMP5 Count/Pvalue	18h BMP10 Count/Pvalue	18h BMP13 Count/Pvalue	3d BMP5 Count/Pvalue	3d BMP10 Count/Pvalue	3d BMP13 Count/Pvalue	5d BMP5 Count/Pvalue	5d BMP10 Count/Pvalue	5d BMP13 Count/Pvalue
Category: Metabolism											
KEG	hsa00250	Alanine, aspartate and glutamate metabolism	-	-	-	-	12 / 8.8 E-04	-	9 / 3.4 E-03	-	7 / 2.1 E-02
KEG	hsa00970	Aminoacyl-tRNA biosynthesis	-	-	-	9 / 6.2 E-03	17 / 1.6 E-05	-	9 / 1.9 E-02	14 / 4.8 E-04	9 / 7.9 E-03
KEG	hsa00330	Arginine and proline metabolism	-	5 / 4.5 E-02	-	10 / 9.6 E-03	16 / 1.6 E-03	-	12 / 4.1 E-03	13 / 1.6 E-02	11 / 4.0 E-03
KEG	hsa00410	beta-Alanine metabolism	-	-	-	-	7 / 4.9 E-02	-	-	-	-
KEG	hsa00532	Chondroitin sulfate biosynthesis	-	-	-	-	8 / 1.5 E-02	-	-	-	-
KEG	hsa00270	Cysteine and methionine metabolism	-	-	-	7 / 2.7 E-02	13 / 5.4 E-04	-	12 / 6.6 E-05	13 / 2.6 E-04	9 / 2.3 E-03
PAN	P02738	De novo purine biosynthesis	-	-	-	-	11 / 6.6 E-03	-	8 / 1.4 E-02	10 / 6.1 E-03	8 / 8.6 E-03
PAN	P02740	De novo pyrimidine ribonucleotides biosynthesis	-	-	-	-	-	-	-	7 / 8.6 E-03	5 / 3.8 E-02
KEG	hsa00310	Lysine degradation	-	-	-	-	12 / 1.7 E-02	-	-	11 / 2.6 E-02	-
REA	REACT_1698	Metablism of nucleotides	-	-	-	-	19 / 9.3 E-03	-	-	16 / 4.7 E-02	11 / 4.8 E-02
REA	REACT_13	Metabolism of amino acids	-	-	-	21 / 5.5 E-03	43 / 6.6 E-06	-	27 / 1.5 E-03	-	26 / 1.9 E-04
REA	REACT_474	Metabolism of carbohydrates	-	6 / 3.6 E-02	-	-	-	-	-	-	-
REA	REACT_11052	Metabolism of non-coding RNA	-	-	-	-	-	-	8 / 1.9 E-03	14 / 2.3 E-07	-
KEG	hsa00910	Nitrogen metabolism	-	-	-	-	-	-	6 / 4.0 E-02	-	-
KEG	hsa00230	Purine metabolism	-	-	-	-	39 / 1.8 E-05	-	24 / 4.4 E-03	35 / 1.1 E-04	22 / 3.0 E-03
KEG	hsa00240	Pyrimidine metabolism	-	-	-	15 / 5.3 E-03	28 / 2.4 E-05	-	16 / 1.3 E-02	24 / 3.8 E-04	17 / 1.1 E-03
KEG	hsa03018	RNA degradation	-	-	-	-	15 / 9.1 E-03	-	12 / 7.2 E-03	22 / 5.8 E-07	-
KEG	hsa00450	Selenoamino acid metabolism	-	-	-	-	9 / 1.2 E-02	-	8 / 4.7 E-03	10 / 1.8 E-03	6 / 3.6 E-02
KEG	hsa00290	Valine, leucine and isoleucine biosynthesis	-	-	-	-	5 / 3.9 E-02	-	-	-	-
KEG	hsa00280	Valine, leucine and isoleucine degradation	-	-	-	-	12 / 1.7 E-02	-	-	-	-
PAN	P02787	Vitamin B6 metabolism	-	-	-	3 / 4.2 E-02	-	-	-	-	-
Category: Cell cycle / DNA maintenance											
KEG	hsa03410	Base excision repair	-	-	-	-	-	-	9 / 7.5 E-03	-	7 / 3.7 E-02
KEG	hsa04110	Cell cycle	-	-	-	-	30 / 6.1 E-04	-	26 / 3.4 E-05	34 / 2.9 E-06	22 / 2.0 E-04
REA	REACT_1538	Cell Cycle Checkpoints	-	-	-	-	29 / 4.2 E-04	-	25 / 2.1 E-05	31 / 2.0 E-05	19 / 8.9 E-04
REA	REACT_152	Cell Cycle, Mitotic	-	-	-	-	71 / 5.1 E-07	-	50 / 7.9 E-06	71 / 3.8 E-08	44 / 6.7 E-06
REA	REACT_216	DNA Repair	-	-	-	-	23 / 1.1 E-02	-	18 / 6.2 E-03	21 / 2.2 E-02	14 / 3.0 E-02
KEG	hsa03030	DNA replication	-	-	-	-	14 / 2.5 E-04	-	14 / 3.6 E-06	17 / 6.8 E-07	14 / 5.9 E-07
PAN	P00017	DNA replication	-	-	-	-	-	-	-	-	7 / 6.3 E-03
REA	REACT_383	DNA Replication	-	-	-	-	28 / 7.6 E-05	-	27 / 9.0 E-08	28 / 2.5 E-05	25 / 3.9 E-08
KEG	hsa03430	Mismatch repair	-	-	-	-	-	-	6 / 4.0 E-02	8 / 1.3 E-02	6 / 2.2 E-02
KEG	hsa03420	Nucleotide excision repair	-	-	-	-	-	-	-	-	8 / 3.6 E-02
KEG	hsa04114	Oocyte meiosis	-	-	-	-	-	-	-	20 / 4.7 E-02	-
REA	REACT_7970	Telomere Maintenance	-	-	-	-	-	-	-	15 / 6.6 E-03	15 / 2.6 E-05
Category: Signaling											
PAN	P05911	Angiotensin II sign. through G proteins and β-arrestin	-	5 / 4.0 E-02	-	-	-	-	-	-	-
PAN	P00027	G-protein Gq alpha and Go alpha mediated signaling	-	9 / 3.1 E-02	-	-	-	-	-	-	-
PAN	P04385	Histamine H1 receptor mediated signaling	-	-	-	-	-	-	8 / 4.8 E-02	-	8 / 3.1 E-02
PAN	P00045	Notch signaling	-	-	-	-	12 / 4.9 E-02	2 / -	-	-	-
KEG	hsa04115	p53 signaling	-	-	-	-	17 / 8.5 E-03	2 / -	-	-	-
KEG	hsa05200	Pathways in cancer	-	-	-	-	-	7 / 3.7 E-02	-	-	-
KEG	hsa04350	TGF-beta signaling	-	-	-	-	-	6 / 4.8 E-04	-	-	-
PAN	P00052	TGF-beta signaling	-	-	-	-	-	6 / 9.2 E-03	-	-	-
KEG	hsa04310	Wnt signaling	-	13 / 4.0 E-04	-	-	-	-	-	-	-
Category: Other											
REA	REACT_71	Gene Expression	-	-	-	-	-	-	43 / 1.6 E-02	78 / 5.8 E-08	-
PAN	P00022	General transcription by RNA polymerase I	-	-	-	-	7 / 4.4 E-02	-	-	-	-
REA	REACT_604	Hemostasis	-	-	-	-	-	5 / 3.8 E-02	-	-	-
REA	REACT_6185	HIV Infection	-	-	-	-	38 / 4.3 E-03	-	29 / 2.1 E-03	43 / 3.4 E-05	24 / 5.8 E-03
REA	REACT_6167	Influenza Infection	-	-	-	-	-	-	-	31 / 8.5 E-03	-
REA	REACT_1675	mRNA Processing	-	-	-	-	-	-	-	9 / 3.7 E-02	-
PAN	P00049	Parkinson disease	-	-	-	-	-	-	-	18 / 3.9 E-02	-
REA	REACT_769	Pausing and recovery of elongation	-	-	-	-	-	-	14 / 7.8 E-04	-	-
REA	REACT_125	Processing of Capped Intron-Containing Pre-mRNA	-	-	-	-	-	-	21 / 1.0 E-03	42 / 8.3 E-12	-
KEG	hsa03020	RNA polymerase	-	-	-	7 / 1.1 E-02	12 / 3.2 E-04	-	7 / 2.7 E-02	10 / 3.2 E-03	-
KEG	hsa03040	Spliceosome	-	-	-	-	-	-	20 / 8.9 E-03	42 / 2.0 E-10	-
REA	REACT_1788	Transcription	-	-	-	-	30 / 2.6 E-03	-	24 / 7.3 E-04	37 / 1.5 E-06	16 / 4.7 E-02

Summarized, this overall view of biochemical pathways, which was obtained by an unprejudiced bioinformatics approach, provides an in-depth insight into molecular processes involved in trophoblast development from hESCs. BMP5, BMP10 and BMP13 samples displayed a high level of conformity with respect to the kind and chronological order of affected pathways within the investigated time frame (18 h – 5 d). Therefore, this analysis provides evidence for collective rather than for different mechanisms of action between the individual ligands in inducing trophoblast lineage from human pluripotent stem cells *in vitro*.

4.2.7 Cellular components affected by BMP-induced morphological differentiation of hESCs to trophoblast cells

Human pluripotent stem cells undergo a dramatic change in cell morphology and structural rearrangements during their trophoblast differentiation (Chapter 4.2.1; Figure 4-26; Figure 4-28). This prompted to investigate the weighting of the different cellular components (CCs) between undifferentiated H1 hESCs and the trophoblast cells derived thereof. CCs comprise any kind of subcellular organelles, structures and macromolecular complexes. For this purpose, a bioinformatics Gene Ontology (GO) analysis was performed for all shared (BMP5 ∩ BMP10 ∩ BMP13 versus reference) significantly upregulated and for all shared significantly downregulated genes of day 5 trophoblast cells. The queries were run against the GO database (Chapter 2.13) for *in silico* predictions of CCs via the known subcellular locations of the genes' proteins. The identified GO-CC terms were grouped into categories and are shown in Figure 4-29. Several individual CCs and whole categories of grouped CCs were revealed as being strongly over- or underrepresented in day 5 trophoblast cells compared to undifferentiated hESCs.

CCs enriched in trophoblast cells:

- Extracellular space (including collagens belonging to the ECM)
- Cell adhesion / ECM interaction
- Plasma membrane (including lipid rafts)
- Other membranous organelles/vesicles (foremost vacuoles, lysosomes and cytoplasmic vesicle membranes)
- Intermediate filament cytoskeleton (foremost keratins as structural components)

CCs enriched in undifferentiated hESCs:

- Nucleus (including nucleoli and chromosomes)
- Ribosomes
- Mitochondrial matrix

The results for hESCs are in agreement with their high nucleus-to-cytoplasm ratio (Chapter 4.2.1) and identified nucleus-associated pathways (e.g. for maintenance of genomic integrity; Chapter 4.2.6.2). The abundance of ribosomes in hESCs could indicate a high activity in protein biosynthesis, as already indicated by overrepresented metabolism-related pathways concerning amino acids and the biosynthesis of aminoacyl-tRNA (Chapter 4.2.6.2). Structural rearrangements involving keratins as part of the intermediate filament

cytoskeleton were confirmed by immunocytochemistry for trophoblast cells (Chapter 4.2.5.2). Enrichment of membrane-related CCs for trophoblast cells is in agreement with their overrepresented pathway "metabolism of lipids and lipoproteins" (Chapter 4.2.6.1). CCs related to cell adhesion and the extracellular space reflect the importance of cell-cell / cell-ECM interactions and secretion of proteins (e.g. hormones for extracellular signaling, proteases) for trophoblast cells (Chapter 4.2.6.1).
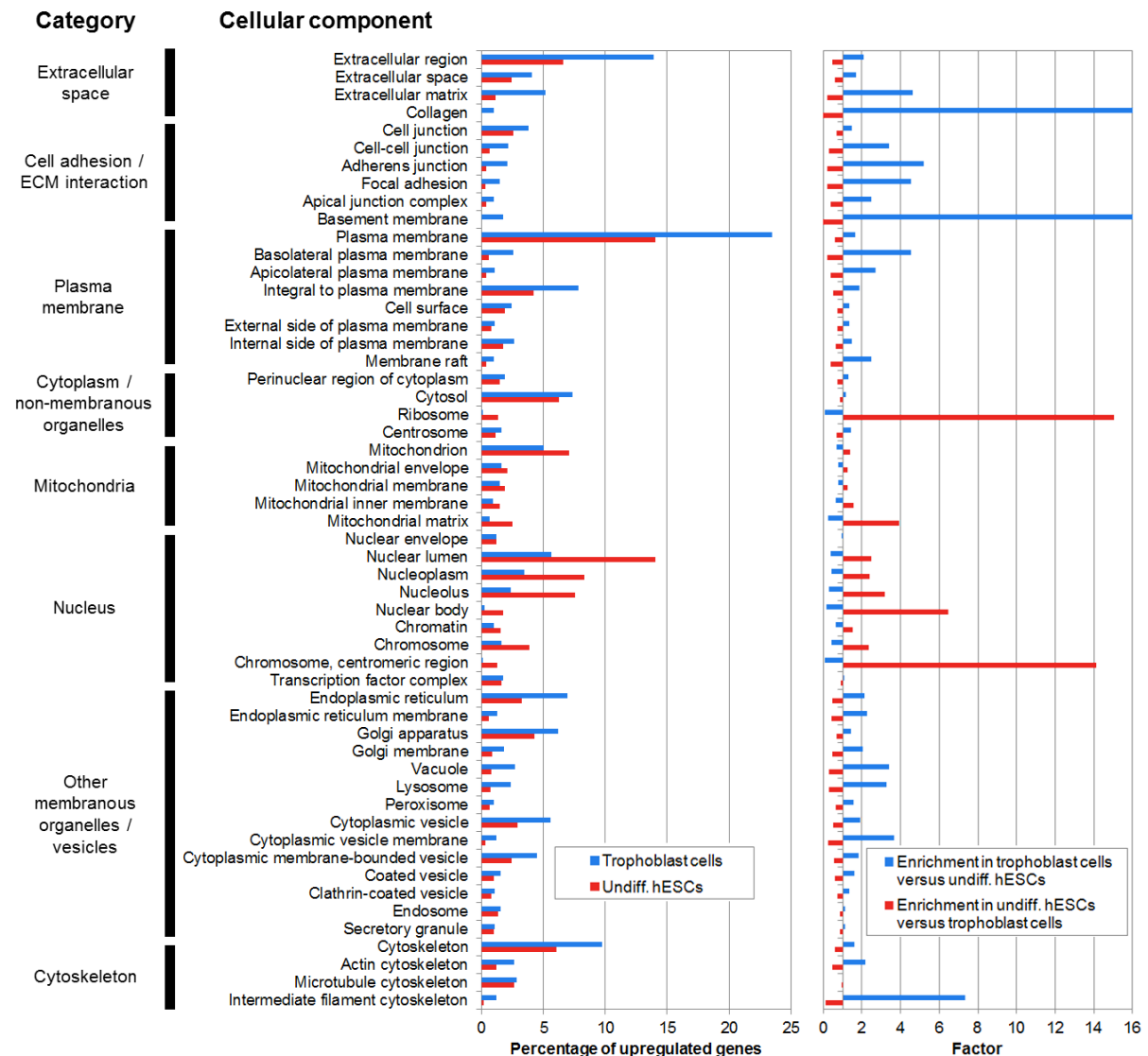
Figure 4-29   Over- and underrepresented cellular components in hESC-derived (line H1) day 5 trophoblast cells relative to undifferentiated hESCs.
The microarray data of the samples of Figure 4-16 were further processed by bioinformatics analysis. Overlapping significantly upregulated genes (1198) and overlapping significantly downregulated genes (1408) of BMP samples (BMP5 ∩ BMP10 ∩ BMP13) versus the HCl/BSA reference samples (Venn diagrams of Figure 4-22) were allocated to cellular components (CCs) by Gene Ontology (GO)-term analysis. The identified GO-CC terms (threshold: representation of at least 1 % of input genes for one list) were classified into categories. Upregulated genes represent those expressed in trophoblast cells and downregulated genes represent those expressed in undifferentiated hESCs. Factor of CC enrichment in trophoblast cells versus undifferentiated hESCs was calculated as the ratio between the percentage of upregulated genes in trophoblast cells and the percentage of upregulated genes in hESCs that were found to be CC-associated (and vice versa). Vertical axis = 1-fold (unchanged). (Figure modified from Lichtner et al., 2013.)

109

4.2.8   Expression of BMP-related TGF-β superfamily type-I and type-II receptor subtypes by hESCs/hiPSCs

The availability of individual TGF-β superfamily type-I and -II receptors on the cell surface greatly restricts the possible modes of receptor oligomerization and binding options for extracellular BMP agonists (Sieber et al., 2009). The following four type-I and three type-II receptor subtypes are known to be involved in canonical BMP signaling (Chapter 1.3.3):

Type-I:

  – BMPR1A/ALK3
    (Bone Morphogenetic Protein Receptor Type-1A / Activin Receptor-like Kinase 3)
  – BMPR1B/ALK6
    (Bone Morphogenetic Protein Receptor Type-1B / Activin Receptor-like Kinase 6)
  – ACVRL1/ALK1
    (Activin Receptor-like Kinase 1)
  – ACVR1/ALK2
    (Activin Receptor Type-1 / Activin Receptor-like Kinase 2)

Type-II:

  – BMPR2
    (Bone Morphogenetic Protein Receptor Type-2)
  – ACVR2A
    (Activin Receptor Type-2A)
  – ACVR2B
    (Activin Receptor Type-2B)

Therefore, the gene expression levels of these receptors were determined for all four human pluripotent stem cell lines that served as model system for the BMP studies, and for the chorionic villi (CV) cells as parental cells of the hiPSCs (Figure 4-30).

Genes of all receptors except *BMPR1B/ALK6* and *ACVRL1/ALK1* were detected as significantly expressed ($P_{Det} < 0.05$ or < 0.01), with *ACVR1/ALK2* being most abundantly expressed ($P_{Det} = 0$). Under the assumption that the expression on mRNA level also reflects the actual expression on protein level, these results are in compliance with the knowledge of the "general occurrence" of BMP-related receptor subtypes with respect to dissimilar cell types: The type-I receptors BMPR1A/ALK3 and ACVR1/ALK2 and all type-II receptors are widely expressed by many cell types; in contrast, expression of the type-I receptor BMPR1B/ALK6 is more restricted, and expression of the type-I receptor ACVRL1/ALK1 is limited to specific cell types such as endothelial cells (Miyazono et al., 2010).

Both hESC lines (H1, H9) and hiPSC lines (iPS1, iPS2) shared a very similar pattern of BMP receptor expression in their undifferentiated state, as opposed to CV cells from which the two clonal hiPSC lines were derived. CV cells possessed a clearly distinct expression pattern for *ACVR1/ALK2* and *BMPR2*, which were expressed 2.6–4.0-fold and 5.2–12.6-fold higher in CV cells compared to human pluripotent stem cells. These differences provide evidence that

in the course of cellular reprogramming hiPSCs acquire a receptor profile similar to that of hESCs and distinct from their somatic cells of origin.
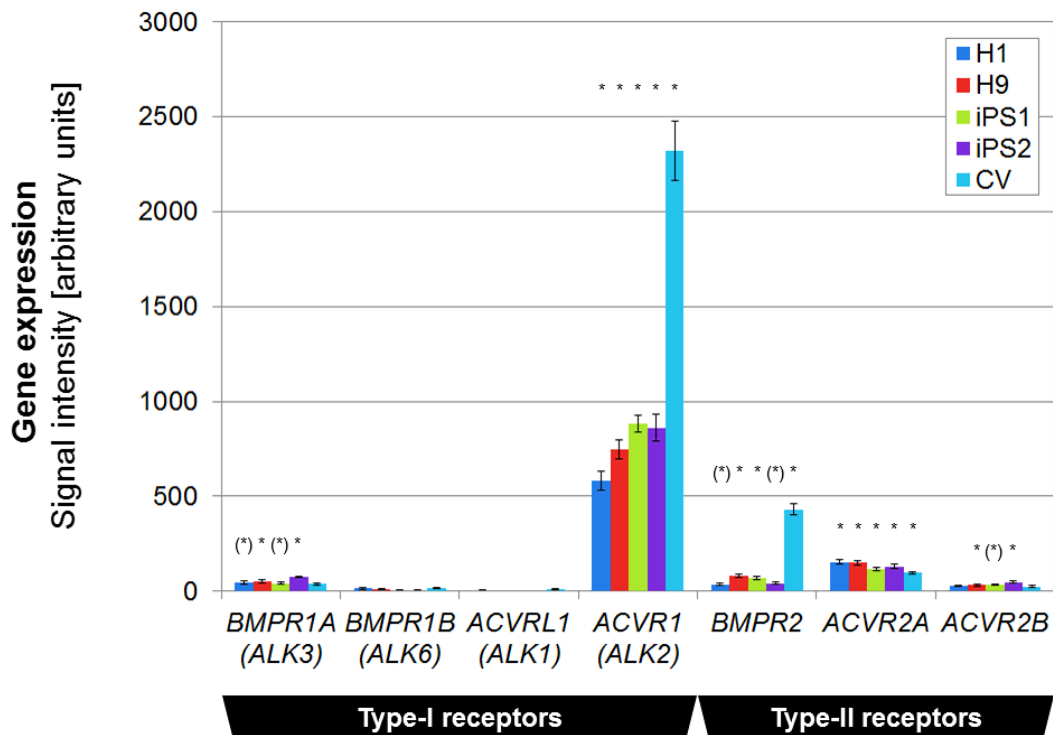
Figure 4-30   Gene expression levels of BMP-related TGF-β superfamily type-I and type-II receptor subtypes in hESCs (lines H1 and H9), hiPSCs (lines iPS1 and iPS2) and CV cells prior to their reprogramming to hiPSCs. Levels of gene expression were determined by microarray analysis of cRNA samples. The data were obtained from the microarray analysis which was performed for the verification of the generated hiPSC lines in the first part of this results chapter (4.1.2.8). Gene symbols are given with alternative names in parentheses. *: $P_{Det} < 0.01$, (*): $P_{Det} < 0.05$. Error bars indicate SE of the bead replicates. (Figure modified from Lichtner et al., 2013.)

4.2.9   Activation of signal transduction pathways downstream of BMP receptors in hESCs/hiPSCs by different BMPs

4.2.9.1   Canonical BMP signaling during BMP-induced trophoblast differentiation of hESCs

Canonical BMP signaling occurs through activation of the intracellular signal transducers SMAD1, SMAD5 and SMAD8 downstream of activated BMP receptors (Chapter 1.3.3). The status of canonical BMP signaling during the course of differentiation of H1 hESCs to trophoblast lineage was analyzed depending on the type of ligand applied.

Western immunoblotting of total protein lysates of BMP-treated and HCl/BSA-treated control cells was performed to measure the expression levels of phosphorylated (= activated) SMAD1/5 and total protein forms of SMAD1 at 18 h, 3 d and 5 d (Figure 4-31). Equal protein loading and transfer was confirmed by reversible Ponceau S staining and detection of the housekeeping enzyme GAPDH serving as internal standard. The progress of differentiation was monitored by detection of expression levels of the pluripotency markers OCT4 and NANOG and the pan-trophoblast marker Cytokeratin-7 (KRT7).

As expected, all ligands activated canonical BMP signaling in the cells. BMP10 led to higher intensity ratios of phospho-SMAD1/5 versus total-SMAD1 than any of the other assayed BMPs at all time points. BMP13 was the least potent ligand, most evident at 18 h. The kinetics of induced differentiation (OCT4↓, NANOG↓, KRT7↑) correlated with the strength of SMAD1/5 activation and therefore with the strength of induced canonical BMP signaling. The level of total SMAD1 protein species continually decreased as differentiation proceeded. This supposes that trophoblast cells contain less amounts of this signal transducer compared to undifferentiated hESCs.
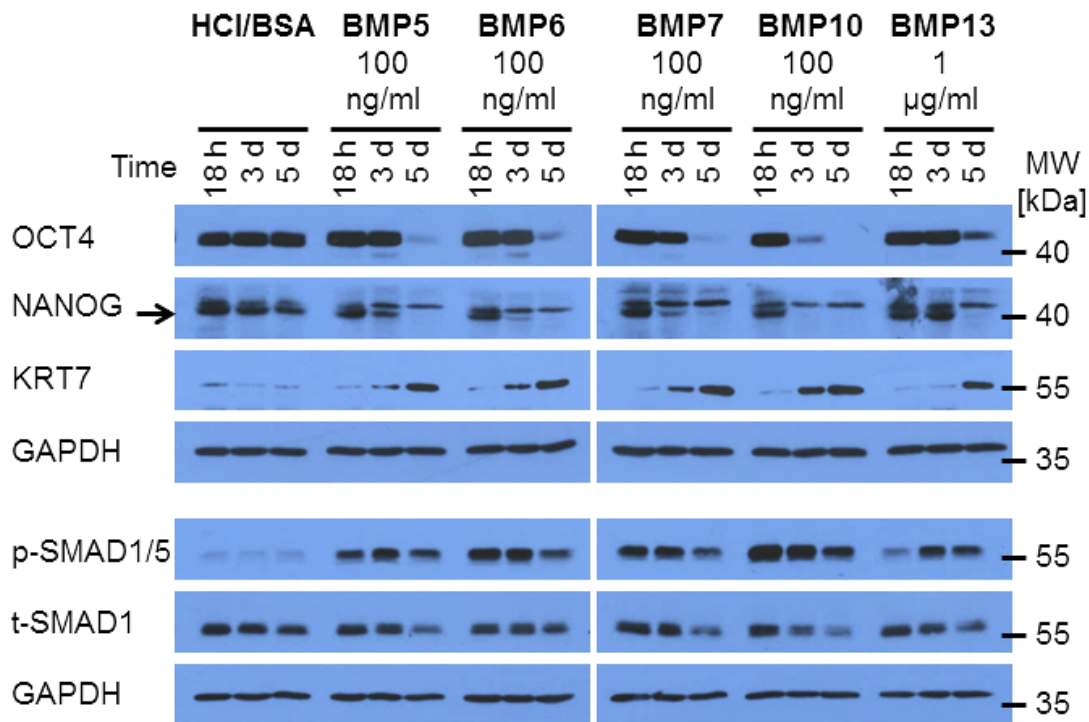
Figure 4-31   Activation levels of canonical BMP signaling (acting via SMAD1/5/8) during trophoblast differentiation of H1 hESCs induced by BMP5/6/7, BMP10 and BMP13 at 18 h, 3 d and 5 d.
Feeder-free hESC colonies were treated in N2B27 medium w/o bFGF on Matrigel with ligands or equivalent volume of 20 µl solvent/carrier protein (= undifferentiated reference cells) as indicated. Media and supplements were replaced every 24 h. Total protein lysates were separated by SDS-PAGE and analyzed by western immunoblotting for expression levels of phosphorylated (p-) (= activated) SMAD1/5 and total (t-) protein species of SMAD1, OCT4 and NANOG (hESC markers), KRT7 (pan-trophoblast marker) and GAPDH (loading control). (Figure modified from Lichtner et al., 2013.)

4.2.9.2   SMAD-dependent versus SMAD-independent signaling upon stimulation of hESCs and hiPSCs with BMPs

It is known that BMP signaling can also be transduced via SMAD-independent pathways. These include members of different MAPK pathways (ERK1/2, p38 and SAPK/JNK) and signaling via Akt (Chapter 1.3.4). Crucial for the initiation of SMAD- versus non-SMAD signaling is the mode of receptor oligomerization of BMP receptor complexes (Sieber et al., 2009), which is influenced by various factors. For example, the oligomerization pattern is very flexible and susceptible to modulation by the bound ligand (Gilboa et al., 2000). BMP5, BMP10 and

BMP13 represent ligands of different subgroups and are known to have differing receptor affinities (Miyazono et al., 2010). Consequently, it was investigated which of the SMAD-independent pathways are activated upon stimulation of hESCs with these ligands.

In order to do this, a kinetic study was conducted with emphasis placed on the early time period following BMP stimulation. H1 hESCs growing on Matrigel were simultaneously treated as before with BMP5, its both subgroup members BMP6 and BMP7, BMP10 (all 100 ng/ml), BMP13 (1 µg/ml) or equivalent volume of solvent/carrier protein (= reference) in N2B27 medium lacking bFGF for 10, 30, 60 and 240 min. Before the ligands and controls were added directly into the medium of the wells, the cells were allowed to adapt to the N2B27 medium for 6 h in the incubator, following the replacement of the old medium from the 6-well plates by fresh pre-warmed (37 °C) N2B27 medium. This adaptation step considered that Akt signaling is also known to be affected by nutrient metabolism (Manning and Cantley, 2007). The use of ideally pre-warmed medium considered that MAPK cascades are also known to be activated by stress, including hypothermia (Roberts et al., 2002). Total protein lysates were analyzed by western immunoblotting using specific antibodies directed against phosphorylated (= activated) and total protein forms of SMAD1/5, ERK1/2, p38, SAPK/JNK and Akt (Figure 4-32). Importantly, the reference samples were analyzed for all individual time points. This should expose any potential non-BMP-related secondary effects on the assayed signaling pathways, which might have occurred during the investigated time frame for whatever reason, and would lead to wrong conclusions regarding BMP-related effects. The undifferentiated state of hESCs for all individual samples was confirmed by detection of consistent high OCT4 expression levels.

Measurement of SMAD1/5 phosphorylation confirmed that all five ligands activated canonical BMP signaling in a time-dependent manner. The activation was detectable after 10 min at the earliest and then increased towards individual saturation levels. BMP10 was clearly the strongest and BMP13 the weakest ligand in inducing canonical BMP signaling. The potency of BMP5 lay in between and was of similar strength compared to its two subgroup members. In accordance with the increase in band intensity of phospho-SMAD1/5, an additional band for total-SMAD1 appeared, which was shifted slightly upwards due to the decreased electrophoretic mobility of phosphorylated protein species. Among all investigated SMAD-independent pathways, only signal transduction via MAPK p38 could be observed upon BMP stimulation. This was most evident for the ligand BMP10 and the late time points (60 min, 240 min). In the case of the other BMPs it remains speculative whether the levels of phospho-p38 exceeded the basal levels of the HCl/BSA reference samples at the corresponding time points. In either case, activation of p38 remained very weak in contrast to SMAD1/5 activation. Differences in the levels of p38 activation were also less apparent among individual BMPs compared to SMAD1/5.
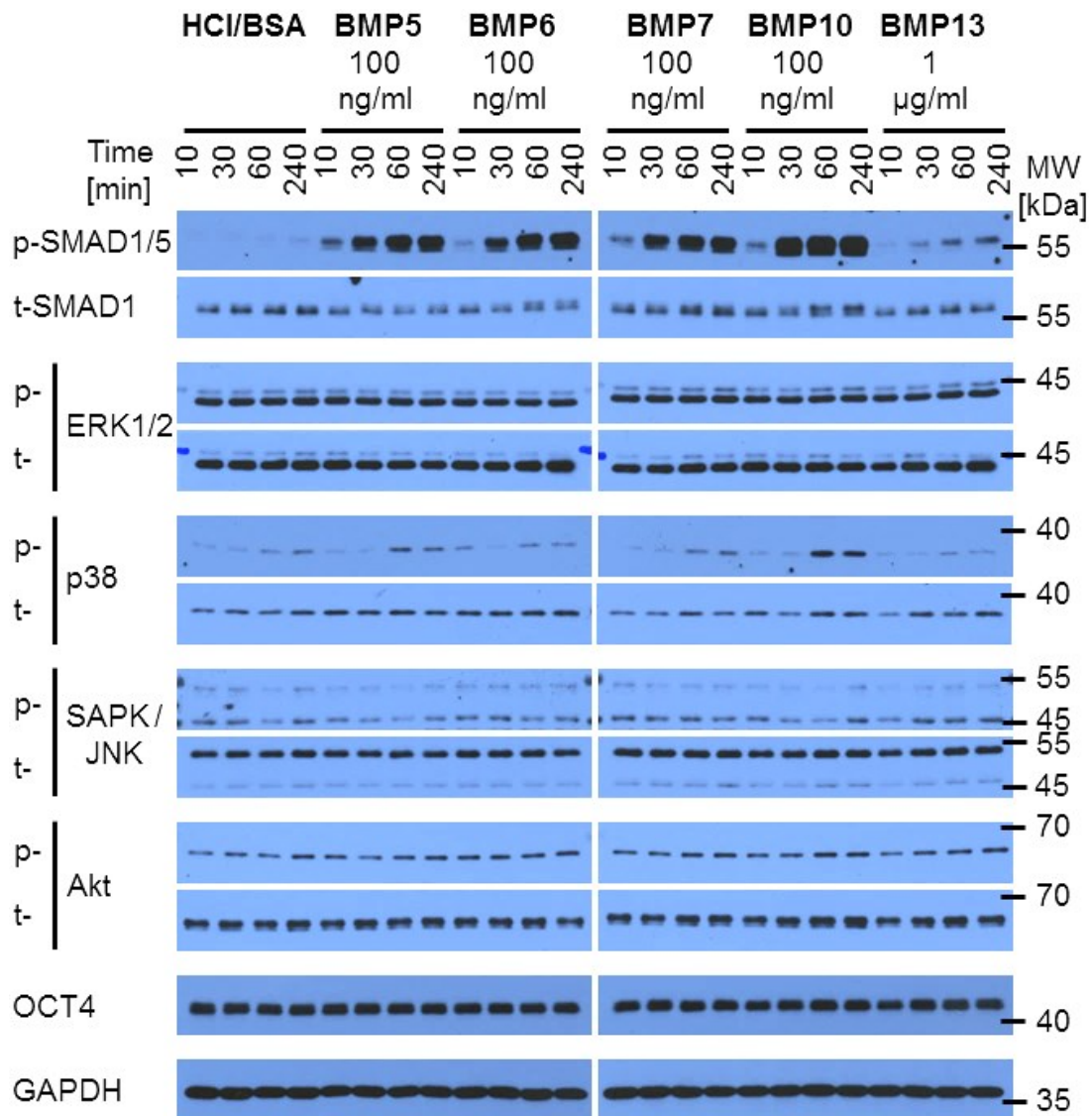
Figure 4-32   Activation states of SMAD-dependent versus SMAD-independent signal transduction pathways downstream of BMP receptors upon stimulation of H1 hESCs with BMP5/6/7, BMP10 and BMP13 for 10, 30, 60 and 240 min.
Feeder-free hESC colonies were treated in N2B27 medium w/o bFGF on Matrigel with ligands or equivalent volume of 20 µl solvent/carrier protein (= reference) as indicated. Total protein lysates were separated by SDS-PAGE and analyzed by western immunoblotting for expression levels of phosphorylated (p-) (= activated) and total (t-) protein species of key players of known signaling pathways as indicated, OCT4 (hESC marker) and GAPDH (loading control). (Figure modified from Lichtner et al., 2013.)

The experiment was repeated for the earliest (10 min) and the latest (240 min) time point using the hESC line H9 and hiPSC lines iPS1 and iPS2 (Figure 4-33). The results were very similar to those obtained for hESC line H1 (Figure 4-32).
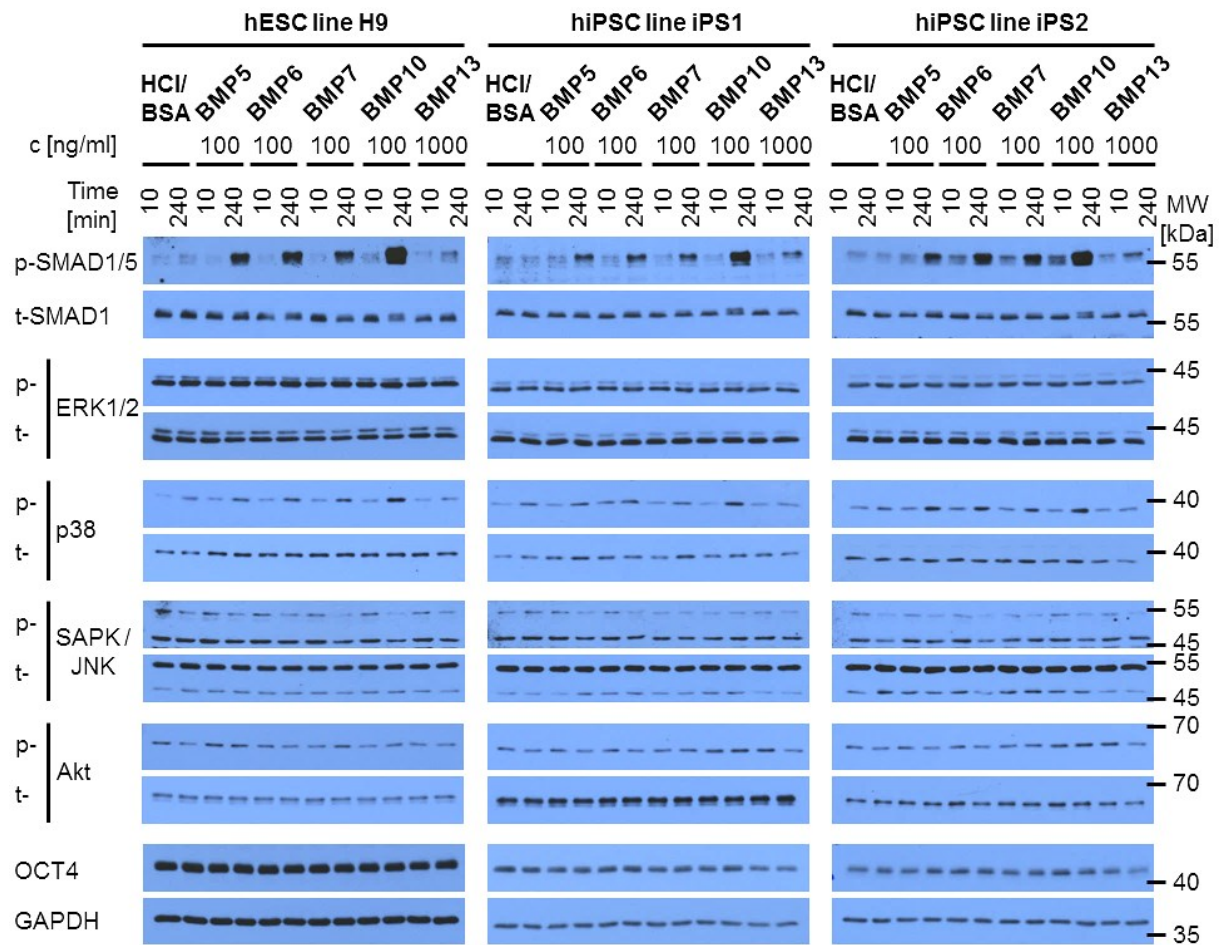
Figure 4-33   Activation states of SMAD-dependent versus SMAD-independent signal transduction pathways downstream of BMP receptors upon stimulation of H9 hESCs and iPS1/iPS2 hiPSCs with BMP5/6/7, BMP10 and BMP13 for 10 min and 240 min.
Feeder-free cells were treated with BMPs and controls as indicated. Treatments and analyses of total protein lysates were performed as described in Figure 4-32. (Figure modified from Lichtner et al., 2013.)

In summary, BMP10 is a more powerful inducer of SMAD-dependent and SMAD-independent (via MAPK p38) signaling than members of the BMP7 subgroup (BMP5, BMP6, BMP7) at equal and BMP13 at 10 times higher concentration. No evidence for signal transduction via ERK1/2, SAPK/JNK or Akt was found for any of the assayed BMPs under the chosen experimental conditions. As activation of SMAD1/5 signaling clearly reflected the strengths of the individual ligands in inducing trophoblast differentiation in hESCs (line H1, Figure 4-17; line H9, Figure 4-18) and hiPSCs (lines iPS1 and iPS2, Figure 4-18), canonical BMP signaling is the predominant trigger for inducing trophoblast differentiation in human pluripotent stem cells. The possibility of a synergistic interaction between the SMAD and the p38 pathway remains to be investigated.

4.2.10 Activation of gene regulatory networks downstream of BMP receptors in hESCs by different BMPs

After all kinds of known signal transduction pathways downstream of BMP receptors had been investigated for the different BMP family members in hESCs and hiPSCs, their induced transcriptional responses were examined. The activation of genes encoding transcription factors associated with trophoblast development, and the downregulation of pluripotency-associated genes, were already unveiled before (Chapter 4.2.2).

4.2.10.1 TGF-β superfamily signaling network

Next, the attention was focused on the TGF-β superfamily signaling network in detail by monitoring genes from which it is known that they can be involved in TGF-β superfamily signaling in various cell types at various biological processes. Key players of the BMP/GDF branch (acting, with few exceptions, via SMAD1/5/8) and of the Activin/Nodal branch (acting via SMAD2/3), which is known to compete with the BMP/GDF branch for binding to their shared Co-SMAD SMAD4 (Chapter 1.3.3), were monitored. The key players covered all hierarchies of the TGF-β superfamily signaling network, including direct inducible target genes, ligands, receptors, SMADs, negative and positive modulators.

Figure 4-34 shows the fold changes in gene expression between BMP-treated (BMP5, BMP10 or BMP13) and HCl/BSA-treated control H1 hESCs. The time points analyzed (18 h, 3 d, 5 d) ranged from early responses in undifferentiated hESCs to advanced trophoblast differentiation. The progression of differentiation was tracked based on expression levels of the pluripotency markers *OCT4* and *NANOG* and the pan-trophoblast marker *KRT7*. The attention was focused on time points representing the undifferentiated state (*OCT4$^+$*, *NANOG$^+$, KRT7$^-$*).

This analysis revealed mainly similarities in induced transcriptional responses among the three novel tested ligands:

The common features included the systematic activation of the direct inducible BMP target genes *ID1−4*, *MSX1−2*, *GATA2−3* (Hollnagel et al., 1999; Miyazono et al., 2005), *DLX3* (Park and Morasso, 2002) and *DLX5* (Miyama et al., 1999). The degree of induction was ligand-dependent (BMP10 > BMP5 > BMP13) and most significant for *DLX5* (up to 63.3-fold), *GATA2* (up to 50.7-fold) and *MSX2* (up to 48.9-fold).

Furthermore, the expression of typical members of the "BMP4 synexpression gene group" (*BMP4*, *BMPR2*, *SMAD6*, *SMAD7*, *BAMBI*) was induced to varying degrees (> 1.5-fold, P_{Diff} < 0.01). A BMP4 morphogen gradient is essential for dorsal-ventral body axis patterning in early embryogenesis of diverse animal species such as *Drosophila* and *Xenopus*. This evolutionarily conserved gradient is proven to be self-regulated and its mechanism includes the coordinated induction of a set of certain genes by BMP4 (Karaulanov et al., 2004; Paulsen et al., 2011). The BMP4 synexpression gene group includes genes of ligands and receptors to support BMP signaling (*inter alia* BMP4, BMP Receptor Type-2) as well as of feedback inhibitors (*inter alia* inhibitory-SMADs SMAD6 and SMAD7, decoy-receptor BAMBI). Thus, this study provides evidence that this feedback loop is also systematically activated in hESCs upon treatment

with agonists of different BMP subgroups *in vitro*. Remarkable, besides their common activation of the BMP4 gene, none of the applied BMPs induced expression of its own gene.

On the contrary, the genes encoding the ligands Activin A and Nodal (*INHBA* and *NODAL*) were downregulated upon stimulation of hESCs with all BMPs. This is in agreement with the knowledge that this branch of TGF-β superfamily signaling needs to be active in hESCs in order to maintain their undifferentiated state. hESCs are known for autocrine Activin/Nodal signaling. Upon differentiation, SMAD2/3 signaling decreases, and SMAD1/5/8 signaling increases (Besser, 2004; James et al., 2005; Greber et al., 2008). Similarly, the genes encoding GDF3 (*GDF3*; a ligand which acts via SMAD2/3 instead of the BMP/GDF branch-typical signal transducers SMAD1/5/8) and Left-right Determination Factor 1 (*LEFTY1*; a secreted inhibitor of Nodal, which is involved in left-right asymmetry determination during embryogenesis), two known pluripotency-associated markers (Besser, 2004; Levine and Brivanlou, 2006), were strongly downregulated upon BMP treatments.

However, distinct BMPs also showed subtle differences in transcriptional changes. These differences mainly concerned BMP10 when compared with BMP5/BMP13:

The transcription factors and known responsive target genes of the Notch signaling pathway, HEY1 and HES1, have recently been identified as immediate target genes of BMPs in various cellular systems such as endothelial cells (by BMP9 and BMP10 (Ricard et al., 2012)), renal proximal tubule epithelial cells (by BMP2 and BMP7 (Larman et al., 2012)) and mesenchymal stem cells (by BMP9 (Sharff et al., 2009)). In this study with respect to human pluripotent stem cells, BMP10 induced a strong and constant upregulation of *HEY1* at all three time points (20.5- to 21.9-fold, $P_{Diff} \leq 1.93 \times 10^{-23}$), and a peaked upregulation of *HES1* at 18 h (7.2-fold, $P_{Diff} = 4.22 \times 10^{-36}$). These findings suggest *HEY1* and *HES1* as potential early target genes in undifferentiated hESCs that are preferentially activated by BMP10 rather than by BMP5 or BMP13. It is worth mentioning in this context that canonical BMP signaling and Notch signaling are known to interact – either synergistic or non-cooperative – on various biological processes, with HES1 and HEY1 being cross-talk factors (Miyazono et al., 2005; Guo and Wang, 2009).

BMP10, in contrast to BMP5/BMP13, also induced an early, strong (16.3-fold at 18 h, $P_{Diff} = 7.60 \times 10^{-12}$) and persisting expression of the gene *SMAD8*, encoding the BMP/GDF branch-specific R-SMAD SMAD8.

In addition, starting at 18 h in hESCs, BMP10 induced an elevated gene expression of the secreted BMP antagonists Noggin (*NOG*) (12.6-fold, $P_{Diff} = 4.22 \times 10^{-36}$) and 'Protein Related to DAN and Cerberus' (*PRDC*), also known as Gremlin-2 (9.9-fold, $P_{Diff} = 4.22 \times 10^{-36}$); and starting at 3 d in trophoblast cells, expression of Chordin (*CHRD*) (10.4-fold, $P_{Diff} = 2.12 \times 10^{-36}$). In contrast, induction of these inhibitors remained either absent or was much later and weaker in the case of BMP5 at equal and BMP13 at 10 times higher applied ligand concentration. Secreted BMP antagonists are known for their important functions in early embryonic development by enabling the formation of BMP morphogen gradients needed for body axis formation and organ patterning (Kishigami and Mishina, 2005; Yanagita, 2005; Gazzerro and Canalis, 2006; Umulis et al., 2009). However, their expression, in particular that of Noggin (reviewed by Krause et al., 2011), is also known to be activated in several cell types as a physiological response to BMP stimulation *in vivo* and *in vitro*. This negative feedback mechanism aims at
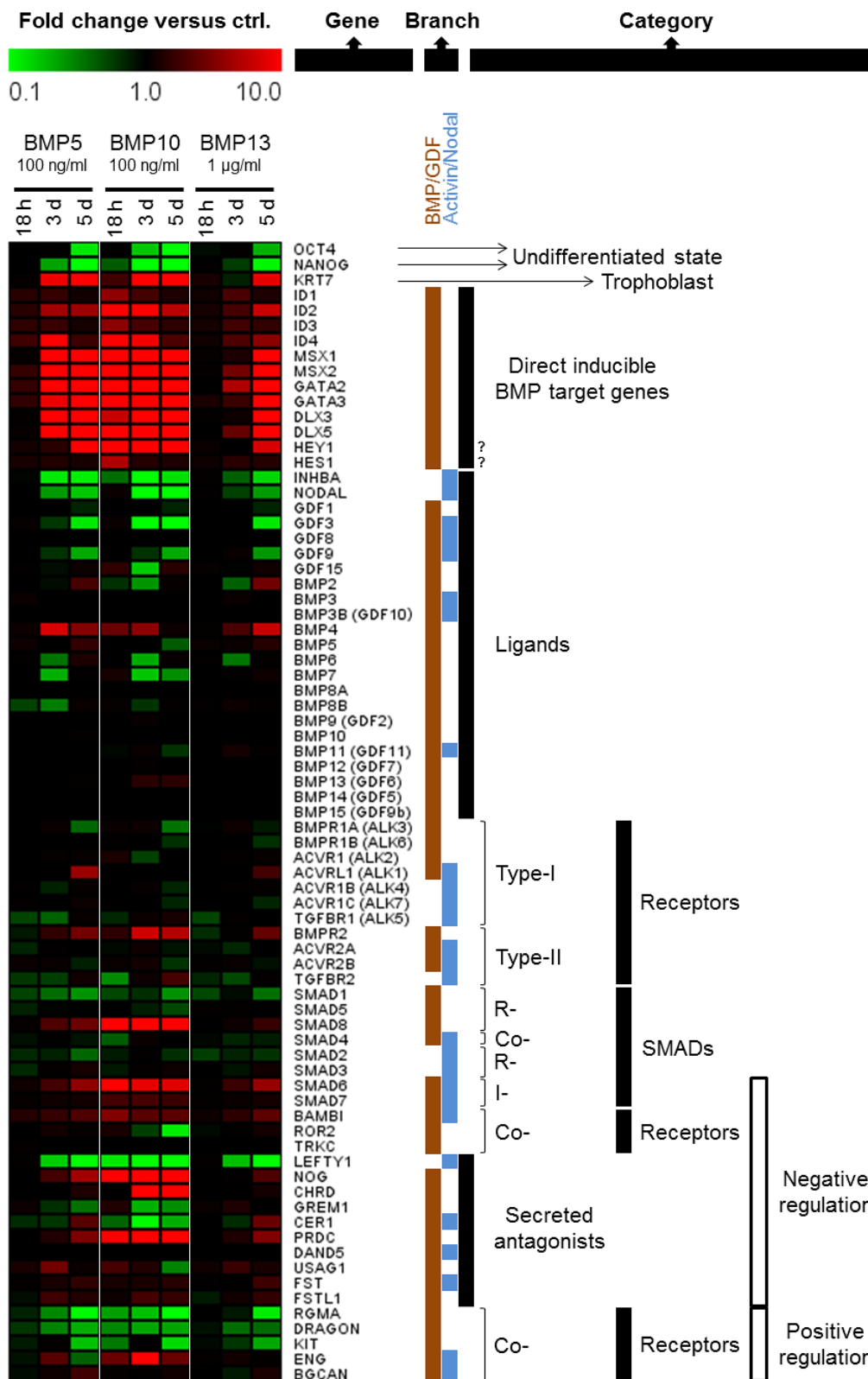
Figure 4-34   Induced transcriptional responses related to the TGF-β superfamily signaling network in H1 hESCs upon stimulation with BMP5, BMP10 and BMP13.

Expression levels of genes covering all hierarchies of the TGF-β superfamily signaling network as indicated (microarray data of the samples of Figure 4-16). The heatmap visualizes the fold changes in gene expression (ligand versus HCl/BSA reference cells of the same time point), calculated as ratios of average signal intensities (grouped biological duplicates). Red = UP↑, green = DOWN↓. Brown and blue bars indicate the branch to which the gene products belong to or act on (e.g. by agonizing, antagonizing or mediating signals). Gene symbols are given with alternative names in parentheses. The intensity raw data on which the ratios are based on are visualized in Figure A-2 (in Appendix) for all genes and samples. (Figure modified from Lichtner et al., 2013.)

attenuating BMP signaling (Gazzerro et al., 1998; Nifuji and Noda, 1999; Seemann et al., 2009). Thus, rather than being BMP10-specific targets, these genes were most likely induced due to the strength of BMP10 in inducing canonical BMP signaling.

Figure 4-35 shows the BMP-activated expression of Noggin in undifferentiated hESCs and trophoblast cells in detail.
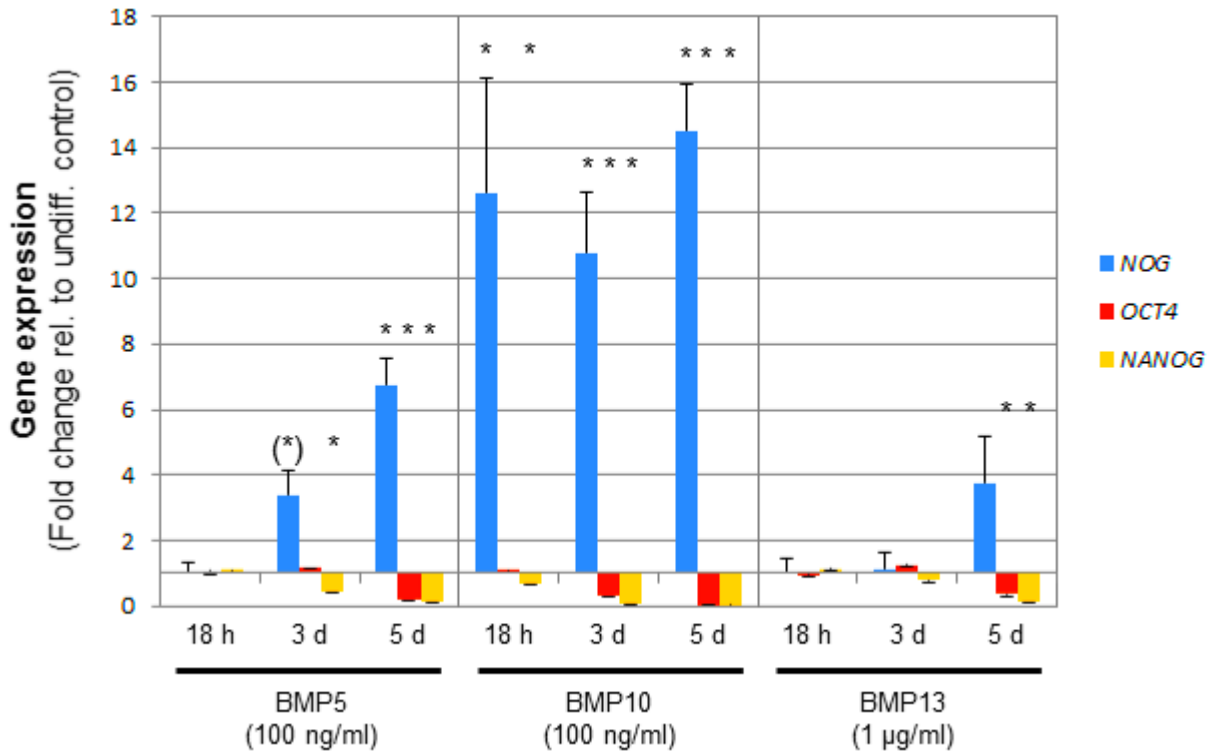
Figure 4-35   Gene activation of the BMP antagonist Noggin in H1 hESCs upon stimulation with BMP5, BMP10 and BMP13.
Expression levels of the Noggin gene (*NOG*). Shown are the fold changes (BMP versus HCl/BSA reference cells), calculated as ratios of average signal intensities (microarray data of the samples of Figure 4-16). The onset of hESC differentiation is indicated by the downregulation of the pluripotency markers *OCT4* and *NANOG*. Horizontal axis = 1-fold (unchanged). *: $P_{Diff} \leq 7.97 \times 10^{-6}$, (*): $P_{Diff} < 0.05$. Error bars indicate array STDEV (grouped biological duplicates).

4.2.10.2 Autocrine Basic Fibroblast Growth Factor (bFGF) signaling

hESCs are known for autocrine Basic Fibroblast Growth Factor (bFGF) signaling, which is crucial for their undifferentiated state (Dvorak et al., 2005; Greber et al., 2007b; Eiselleova et al., 2009). bFGF, acting via its receptors, is known to modulate TGF-β superfamily signaling in hESCs to support hESC self-renewal by supporting SMAD2/3 signaling and antagonizing competing SMAD1/5/8 signaling (Greber et al., 2007a). This prompted to investigate the state of bFGF expression of BMP-treated hESCs.

The results (Figure 4-36) revealed a vice versa relationship between the endogenous expression of the bFGF gene (*FGF2*) and canonical (via SMAD1/5/8) BMP signaling: Upon stimulation with either BMP5, BMP10 or BMP13, expression of *FGF2* in H1 hESCs decreased. The reduction was reciprocal to the strength of induced canonical BMP signaling (Figure

4-31): At 18 h, BMP10-treated – yet undifferentiated cells – already exhibited a reduction in bFGF mRNA down to factor 0.55 of the basal expression level in HCl/BSA-treated reference cells. In cells treated with the weaker ligands BMP5 and BMP13, the onset of significant downregulation of *FGF2* expression was delayed to the later time points (3 d, 5 d). In day 5 trophoblast cells, *FGF2* expression was downregulated to 0.03-fold (BMP10), 0.08-fold (BMP5) and 0.13-fold (BMP13) relative to undifferentiated hESCs. This is in agreement with the findings that endogenous bFGF expression decreases during hESC differentiation, and that knockdown of bFGF induces differentiation of hESC (Eiselleova et al., 2009).
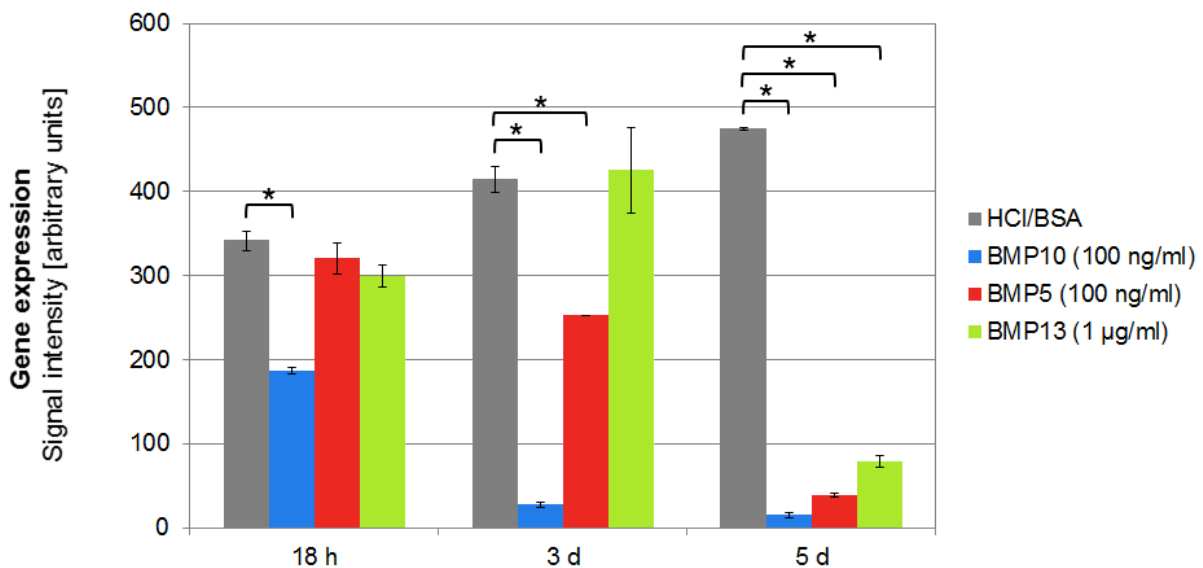
Figure 4-36   Gene repression of Basic Fibroblast Growth Factor (bFGF) in H1 hESCs upon stimulation with BMP5, BMP10 and BMP13.
Expression levels of the bFGF gene (*FGF2*) in ligand- and HCl/BSA-treated cells (= reference). Shown are the average signal intensities (microarray data of the samples of Figure 4-16). *FGF2* was significantly expressed in all samples ($P_{Det} \leq 0.004$). *: $P_{Diff} \leq 1.06 \times 10^{-9}$ (other: $P_{Diff} > 0.05$). Error bars indicate array STDEV (grouped biological duplicates).

4.2.11 Dose-response relationship of BMP10 and comparison of its potency on hESCs with BMP4

Finally, it was verified that the effect of BMP10-induced signaling on hESCs is dose-dependent. In addition, the performance of BMP10 was compared with that of the "standard ligand" BMP4. For this purpose, H1 hESCs were treated with 1:5 dilutions (100, 20 and 4 ng/ml) of either recombinant human protein under the same experimental conditions as before. Based on the previous results, two different criteria were assessed:

1.) Levels of SMAD1/5 phosphorylation as indication for the strength of activated canonical BMP signaling in undifferentiated hESCs after 60 minutes stimulation.

2.) Concentrations of hCG in media supernatants as indication for the degree of terminal trophoblast differentiation of hESCs towards syncytiotrophoblasts after 7 days treatment. In view of the previous results (Chapter 4.2.5), this time point was found to be more eligible in revealing differences in differentiation kinetics between BMP

samples compared to day 5 (low degree of syncytia formation) and day 10 (massive cell death of syncytia).

The results clearly confirmed a dose-response relationship of BMP10 in inducing canonical BMP signaling (Figure 4-37A) and trophoblast differentiation (Figure 4-37B) in hESCs. A dose of 20 ng/ml BMP10, corresponding to 0.82 nM of homodimeric protein, was already sufficient for gaining a high degree of endocrine active SCTs (average hCG concentrations: 2665.0 mIU/ml (for 100 ng/ml), 1931.3 mIU/ml (for 20 ng/ml), 12.5 mIU/ml (for 4 ng/ml) and 0.6 mIU/ml (for HCl/BSA)). Furthermore, the results indicated that BMP10 is more effective than BMP4 on human pluripotent stem cells (20 ng/ml ≙ 0.76 nM of homodimeric BMP4).
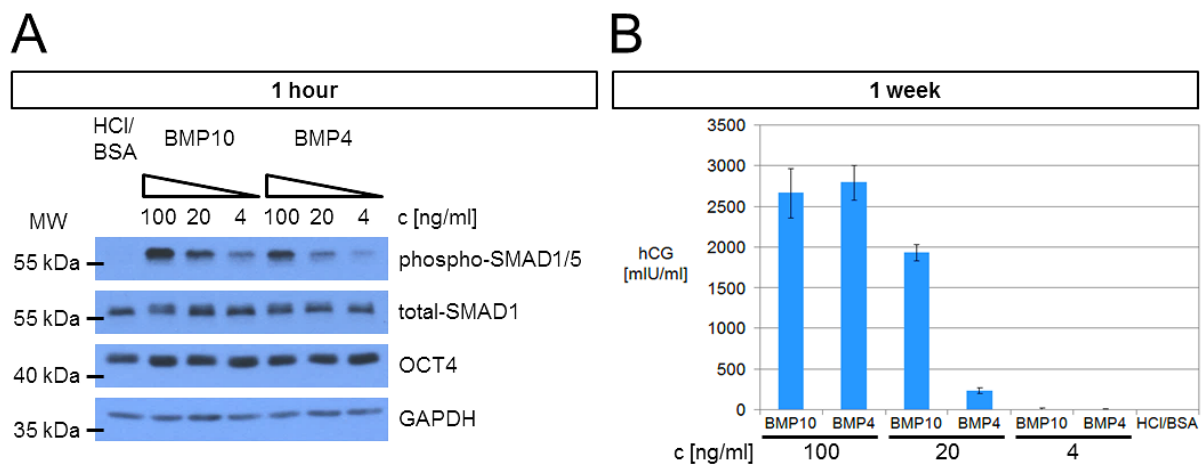
Figure 4-37   Dose-response relationship of BMP10 and comparison of its potency on H1 hESCs with BMP4.
(A) Activation levels of canonical BMP signaling: Feeder-free hESC colonies were treated in N2B27 medium w/o bFGF on Matrigel with decreasing concentrations of ligands or equivalent volume of 20 µl solvent/carrier protein (= reference) as indicated for 1 hour. Total protein lysates were separated by SDS-PAGE and analyzed by western immunoblotting for expression levels of phosphorylated (= activated) SMAD1/5 and total protein species of SMAD1, OCT4 (hESC marker) and GAPDH (loading control). **(B)** Degrees of syncytiotrophoblast formation: Cells were treated under conditions of (A) for 1 week. Media and supplements were replaced every 24 h. Concentrations of hCG which accumulated within 24 h prior to day 7 in the media were determined by ELISA. Average values, error bars indicate STDEV (biological triplicates, technical duplicates). IU = international unit (a standard defined by the World Health Organization). (Figure modified from Lichtner et al., 2013.)

5   Discussion

5.1   Cell lineage differentiation fate of human pluripotent stem cells obtained by treatment with distinct BMPs

5.1.1   Trophoblast lineage derivatives as the major outcome

In the present PhD project an in-depth investigation of the effects that distinct members of the BMP family exert on human pluripotent stem cells was carried out. It was demonstrated in a representative, reproducible and comparative approach under chemically-defined conditions, that BMP5, BMP10 and BMP13 induce differentiation towards trophoblast lineage in the absence of exogenous Basic Fibroblast Growth Factor (bFGF) and presence of autocrine Activin/Nodal signaling and autocrine bFGF signaling. These results are in agreement with model studies using the "standard ligand" BMP4 (reviewed by Ezashi et al., 2012). In 2011, a controversial debate arose concerning the true identity of BMP4-triggered differentiated human embryonic stem cells (Greber, 2011; Roberts et al., 2014), after a study had claimed that the cells would rather represent an (extra-)embryonic mesoderm phenotype than trophoblast (Bernardo et al., 2011). In agreement with recent studies, which confirmed BMP4-induced trophoblast differentiation in hESCs (Amita et al., 2013; Li et al., 2013; Sudheer et al., 2012) and hiPSCs (Chen et al., 2013b), this work further confirms that the same findings are also valid for other independent BMP subgroup members, which had been untested with respect to both hESCs and hiPSCs:

Cells treated with BMP5, BMP10 or BMP13 for 5 days developed predominantly to a Cytokeratin-7$^+$ epithelium (E-Cadherin$^+$) (Figure 4-26B), which is characteristic of villous cytotrophoblast cells (Haigh et al., 1999; Blaschitz et al., 2000; Floridon et al., 2000; Getsios and MacCalman, 2003; Zhou et al., 1997). This conversion involved a transient upregulation of the transcription factor *CDX2* (BMP10, 18 h – 3 d; Figure 4-16), in conformance with recent findings using BMP4 (Amita et al., 2013; Sudheer et al., 2012; Marchand et al., 2011). This cell population further underwent terminal maturation to either multinucleated syncytiotrophoblasts (SCTs) or invasive extravillous cytotrophoblasts (EVTs). SCT differentiation was detected by means of morphological syncytia formation (Figure 4-15; Figure 4-26C–E; Figure 4-28), secretion of the pregnancy hormone Human Chorionic Gonadotropin (hCG) (Figure 4-27; Figure 4-37B) and upregulation of markers including genes which encode for enzymes involved in biosynthesis of steroid hormones (*CYP11A1* and *HSD3B1* for progesterone, *CYP19A1* and *HSD17B1* for estrogens) (Figure 4-25). EVT differentiation was detected by means of *HLA-G* expression and other markers required for acquisition of invasive properties, including several protease / protease inhibitor systems (Figure 4-25). Furthermore, critical pathways (including signaling, metabolism and other categories) known to be involved in the development of either SCTs or EVTs were identified as overrepresented in BMP5/BMP10/BMP13-treated differentiated hESCs (Table 4-1A), whilst pathways known to be predominantly activated in undifferentiated hESCs were identified as underrepresented (Table 4-1B). The ability to specialize to both cellular fates is known to be unique to villous cytotrophoblast precursor

cells during placentation *in vivo* (Bischof and Irminger-Finger, 2005), and was confirmed by others for BMP4-driven, hESC-derived (Amita et al., 2013; Das et al., 2007; Sudheer et al., 2012; Marchand et al., 2011) and hiPSC-derived (Chen et al., 2013b) trophoblast cells. Finally, completely unbiased bioinformatics analyses illustrated that the obtained differentiated hESCs acquired overall similar (Figure 4-19; Figure 4-22) and placenta-like (Figure 4-23; Figure 4-24) global gene expression profiles after exposure to different members of the BMP family for increasing periods of time.

Altogether, previous studies and this research project provide strong evidence for a true BMP4-driven trophoblast identity of the differentiated cells, and do not support the claim of mesoderm-like identity. Several cellular components were found as strongly enriched in the obtained trophoblast cells compared to undifferentiated hESCs (Figure 4-29). This highlights the impact of these subcellular organelles, structures and macromolecular complexes for BMP-driven morphological differentiation of hESCs and the structural reorganization of trophoblast cells. Remarkably, the strength of inducing trophoblast differentiation varied immensely among the tested ligands. BMP10 was by far the most potent ligand, followed by BMP5 with a potency similar to its both subgroup members BMP6 and BMP7, and finally BMP13 as the weakest ligand (Figure 4-17; Figure 4-18; Figure 4-31). The potency of BMP10 was also higher than that of BMP4 (Figure 4-37).

5.1.2 Mesendoderm (primitive streak) formation as possible "side effect" of autocrine bFGF signaling

The observed marginal co-differentiation to mesendoderm (primitive streak) for H1 hESCs (Figure 4-16; Figure 4-17) was most likely the result of autocrine bFGF signaling present during the BMP treatments, as bFGF is known to be endogenously expressed and released by hESCs (Dvorak et al., 2005). A study by the Thomson Lab (Yu et al., 2011) revealed that the presence of bFGF switches the fate of BMP4-induced hESC differentiation from trophoblast to mesendoderm via prolonging NANOG expression through the MEK-ERK pathway. The chemically-defined N2B27 medium used for the BMP experiments in this PhD work was not supplemented with exogenous bFGF, nor was this signaling pathway inhibited; however, the cells were cultured on plastic surfaces coated with a thin layer of growth factor reduced Matrigel™ basement membrane matrix. Matrigel is known to contain trace amounts of bFGF molecules (Vukicevic et al., 1992), but according to the manufacturer's certificate of analysis in a concentration of less than 0.1 pg/ml. This negligible concentration refutes Matrigel as potential cause for the co-differentiation to mesendoderm and supports the assumption of autocrine bFGF signaling as being the trigger. Further evidence for this can be seen from the endogenous expression levels of bFGF mRNA, which were highest in undifferentiated H1 hESCs (Figure 4-36). Interestingly, no increase in the level of activated MAPK ERK1/2 was observed upon stimulation of H1, H9, iPS1 and iPS2 cells with any of the ligands (Figure 4-32; Figure 4-33). This indicates that mesendoderm formation via this pathway/mechanism was so marginal that it was below the sensitivity of the assay compared to the basal levels of phospho-ERK1/2 protein species. On the other hand, Valera et al. (Valera et al., 2010) observed a strong activation of ERK1/2 upon stimulation of H9 hESCs with recombinant human BMP2,

BMP2/6 heterodimers and BMP6 (BMP6 was also tested in this work). However, their experimental system included mTeSR1™ medium, which contains a high concentration of bFGF (100 ng/ml), and the induced differentiation led to a high degree of mesoderm and endoderm derivatives.

Thus, the results of this work and those of Valera et al. are in agreement with and supporting the findings of the Thomson Lab regarding the bFGF-mediated switch of BMP4-induced hESC differentiation from trophoblast towards mesendoderm via the MEK-ERK pathway:

| hESCs + **recombinant BMP4** | **(+) bFGF** → mesendoderm → mesoderm & endoderm derivatives |
| | **(–) bFGF** → trophoblast lineage |
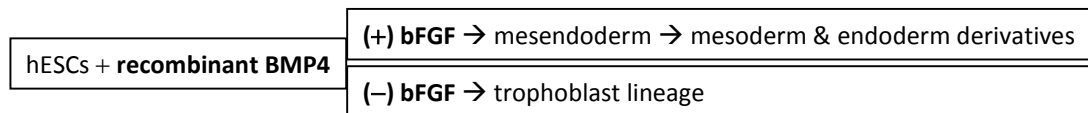
Moreover, this research project has revealed that BMPs with higher potency more easily "override" the "side effect" of mesendoderm fate as a result of autocrine bFGF signaling compared to BMPs with lower potency: The time window of primitive streak formation observed for BMP10 (only at 18 h) was shorter compared to BMP5 and BMP13 (3 d – 5 d) (Figure 4-16; Figure 4-17). In accordance with this observation, the level of endogenous bFGF mRNA expression in H1 hESCs (Figure 4-36) negatively correlated with the strength of induced canonical BMP signaling by the distinct ligands in these cells (Figure 4-31).

The extent of autocrine bFGF signaling is most likely dependent on the individual cell line, seeding density and diameter of colonies: Differences in the expression levels of certain genes have been reported to exist between individual hESC lines (International Stem Cell Initiative, 2007), which could also concern genes contributing to bFGF signaling. The colony size could exert influence on signaling due to "quorum sensing", a phenomenon well known from the world of single-celled microorganisms, e.g. bacterial biofilms (Waters and Bassler, 2005; Hall-Stoodley et al., 2004; Karatan and Watnick, 2009). Support for the latter hypothesis can also be drawn from the detected levels of bFGF mRNA in HCl/BSA-treated H1 hESCs, which served as a reference for the undifferentiated state. The basal expression levels sustained and gradually increased over time (18 h → 3 d → 5 d; Figure 4-36), in conformance with an increasing diameter of the colonies as a result of ongoing self-renewal of the cells (scale bars in Figure 4-14 / 48 h versus Figure 4-15 / 5 d). All these factors would explain the observed differences in the extent of primitive streak formation between the independent experimental series involving H1, H9, iPS1 and iPS2 cells (Figure 4-17; Figure 4-18).

The onset of co-differentiation to mesendoderm could be prevented by blocking bFGF/MEK-ERK signaling using specific inhibitors of the respective FGF receptors. Our laboratory demonstrated in this regard that inhibition of bFGF signaling alone, or in combination with either Activin/Nodal inhibition or BMP4 stimulation, is sufficient to support differentiation of hESCs towards SCTs. This indicates that bFGF inhibition is a key in directing BMP4-induced differentiation of hESCs towards SCTs (Sudheer et al., 2012). The accelerating effect of inhibition of bFGF and Activin/Nodal signaling on BMP4-driven trophoblast differentiation of hESCs has recently been confirmed (Amita et al., 2013), and it had

been shown before that the presence of bFGF slows BMP4-driven trophoblast differentiation of hESCs (Das et al., 2007).

5.1.3 Absence of ectoderm-related cells

All four BMP-driven differentiated human pluripotent stem cell lines were lacking derivatives of the ectoderm lineage (Figure 4-16; Figure 4-17; Figure 4-18). This is in compliance with the knowledge that BMP signaling in hESCs prevents neural ectoderm formation, and conversely, inhibition of BMP signaling induces their differentiation to neural precursor cells (Pera et al., 2004; Itsykson et al., 2005). The mechanism of neural induction through BMP antagonism can be regarded as being adopted by hESCs *in vitro* from the native *in vivo* system, since the same also occurs during early vertebrate embryogenesis (Gaulden and Reiter, 2008). The results of the present study provide evidence that BMP signaling in general – even if mediated by ligands that are differing in their tissue locations and physiological roles *in vivo* – follows this universal rule of not supporting ectoderm formation, both for hESCs and hiPSCs.

5.1.4 Absence of cells belonging to the germline

Previous studies demonstrated that treatment of hESCs and hiPSCs in the presence of fetal bovine serum (FBS) with either BMP4 alone or in combination with BMP7 and BMP8b, but not BMP7 or BMP8b alone, increased their differentiation to primordial germ cells (PGCs) (Kee et al., 2006; Panula et al., 2011; Geens et al., 2011). This indicates that BMP4 was required for the initial induction and BMP7 and BMP8b for the additional support of PGCs (Kee et al., 2006). PGC formation occurred within 3 days to 1 week, independent of whether the cells were cultured in suspension (embryoid body approach) or grown adherent. The PGCs were able to further develop to meiotic and post-meiotic haploid germ cells (Panula et al., 2011).

In the present work, germ cell-specific genes were examined in respect of BMPs and human pluripotent stem cells under chemically-defined conditions. No indications for formation of early PGCs or of germ cells of any later developmental stage were found for any sample (Figure 4-16; Figure 4-17; Figure 4-18). There are two possible explanations for the absence of cells belonging to the germline under the chosen experimental conditions: Firstly, the ligands BMP4, BMP7 and BMP8b, which were used in above cited studies, are known to be required for development of murine PGCs *in vivo* (Kee et al., 2006). It is therefore uncertain whether BMP5, BMP10 and/or BMP13 could functionally substitute any of these ligands in the murine and/or human model system *in vitro*. Secondly, the very low yield of roughly 5 % PGCs in these studies is suspicious and implies that PGC formation has not directly occurred from pluripotent stem cells. It was most likely a "secondary effect" of BMPs which acted on other sorts of progenitor cells that had coincidentally developed due to the presence of 20 % (v/v) FBS in the medium. FBS is not well-defined and contains plenty of unknown growth factors and other interfering biochemical ingredients at varying concentrations. Hence, additional studies using the same sets of BMPs under both experimental conditions would help to confirm or withdraw any of both assumptions.

5.2   hiPSCs in comparison to hESCs with respect to their response to BMP treatments

Due to their genesis and background, human induced pluripotent stem cells can be regarded as a kind of "artificial" cells, in contrast to human embryonic stem cells as their "natural counterparts" (Chapter 1.2). Therefore, another main objective of this PhD project was to investigate how comparable hiPSCs are to hESCs in their characteristics with respect to treatments with individual BMPs.

For this purpose, hiPSCs were generated by reprogramming of primary human chorionic villi (CV) cells via classical retroviral transduction (Chapter 4.1.1). Since randomly located proviral integration sites and/or spontaneous reactivation of transcriptionally silenced transgenes can alter the "normal" behavior of a given cell, two independent hiPSC lines served as model systems. The two clonal cell lines iPS1 and iPS2, which were used for these studies, had been fully and successfully characterized to be hiPSCs (Chapter 4.1.2).

As observed for the two hESC lines H1 (male) and H9 (female), both clonal hiPSC lines iPS1 and iPS2 (female) exhibited an overall similar behavior when being exposed to different BMP family members under the same experimental conditions:

– Like H1 and H9 hESCs, iPS1 and iPS2 hiPSCs differentiated predominantly to trophoblast lineage after long-term treatment with BMPs for 5 days (Figure 4-17; Figure 4-18).

– Short-term stimulation with BMPs for 10–240 min revealed conserved properties in terms of the kinds of activated SMAD-dependent (via SMAD1/5/8) and SMAD-independent (via MAPK p38) signal transduction pathways downstream of BMP receptors among hESCs and hiPSCs (Figure 4-32; Figure 4-33).

– Furthermore, both hiPSC lines and hESC lines demonstrated conserved properties in terms of ligand potency (BMP10 > BMP5 ≈ BMP6 ≈ BMP7 >> BMP13), as assessed by the strength of activation of signal transduction pathways (Figure 4-32; Figure 4-33) and kinetics of induced trophoblast differentiation (Figure 4-17; Figure 4-18; Figure 4-27).

This research project has revealed that in the course of cellular reprogramming, hiPSCs undergo a switch in their expression profile of BMP-related TGF-β superfamily type-I and type-II receptor subtypes away from their parental cells of origin, and acquire a profile similar to that of hESCs (Figure 4-30). The comparable receptor expression between hiPSCs and hESCs may explain all abovementioned common signaling and differentiation properties. This is due to the fact that these receptors are the key for the extracellular binding of ligands and the intracellular transmission of downstream signals, which decide how external stimuli are processed and interpreted by a given cell (Chapter 1.3.3 and 1.3.4).

However, unlike hESCs, both hiPSC lines showed an increased tendency to spontaneous differentiation when cultured in chemically-defined N2B27 medium lacking BMPs (Chapter 4.2.1). This phenomenon could be explained due to the "epigenetic memory" of hiPSCs: After reprogramming, hiPSCs still harbor residual DNA methylation signatures which are

characteristic of their somatic tissue of origin and favor their differentiation back to lineages related to the cell type from which they were derived (Kim et al., 2010). In the case of CV cells, this would be ICM-derived extraembryonic mesoderm / villous mesenchymal core (Chapter 1.1.2.1). Remarkably, the differentiation to alternative cell fates (here: trophoblast lineage in the presence of BMPs) was not restricted for iPS1/iPS2 cells. Another explanation for spontaneous differentiation could be the fact that individual human pluripotent stem cell lines can tolerate feeder cell-free propagation in defined culture systems differently well (International Stem Cell Initiative Consortium, 2010).

5.3 Variations in the biological activity of distinct BMPs with respect to human pluripotent stem cells

The simultaneously tested ligands displayed large differences in their effectiveness to induce canonical (SMAD1/5/8-dependent) BMP signaling in human pluripotent stem cells (Figure 4-31; Figure 4-32; Figure 4-33; Figure 4-37A). This led to corresponding large differences in the kinetics of induced differentiation among individual BMP samples (Figure 4-14; Figure 4-17; Figure 4-18; Figure 4-31; Figure 4-37B). The following order of ligand potency was determined:

> **Hierarchy:**
>
> BMP10 > BMP7 subgroup (BMP5 ≈ BMP6 ≈ BMP7) >> BMP13
> BMP10 > BMP4

This raises the question regarding the molecular reason behind the tremendous variations in the ligands' biological activities. A plausible explanation is that these variations are the consequence of receptor complexity existing for BMP signaling (Chapter 1.3.4).

At least four TGF-β superfamily type-I receptors (BMPR1A/ALK3, BMPR1B/ALK6, ACVRL1/ALK1, ACVR1/ALK2) and three type-II receptors (BMPR2, ACVR2A, ACVR2B) are known to be involved in mediating canonical BMP signaling. Each receptor subtype itself has multiple receptor subtypes and ligands as potential binding partners, and the individual BMPs are known to have differing receptor preferences (Miyazono et al., 2010). For example, BMP13 has demonstrated a preferential affinity for BMPR1B/ALK6 and BMPR2 in the rat osteoprogenitor cell line ROB-C26. Complexes of BMP13 with BMPR1A/ALK3 and BMPR2 were barely detectable and transduced weaker signals (Williams et al., 2008). BMP13 has in general a higher affinity for type-I receptors compared to type-II receptors, and therefore initially binds type-I receptors followed by binding to type-II receptors (Nickel et al., 2009). Interestingly, no binding to the type-I receptor ACVR1/ALK2 could be detected in surface plasmon resonance studies using immobilized receptor extracellular domain fusion proteins (Berasi et al., 2011). The microarray analysis of the present work revealed that genes of all receptor subtypes, excluding *BMPR1B/ALK6* and *ACVRL1/ALK1*, were significantly expressed in hESCs and hiPSCs, with the type-I receptor *ACVR1/ALK2* being most abundantly expressed (Figure 4-30). These features would explain the extremely low performance of BMP13 with regard to

human pluripotent stem cells, despite its application at 10 times higher concentration compared to the other tested agonists. On the other hand, BMP10 was described as functional activator of the endothelial cell-specific type-I receptor ACVRL1/ALK1 *in vitro* (David et al., 2007), which means that this ligand must have effected its strong signals in hESCs and hiPSCs via other type-I receptor subtypes than ALK1.

The homo- and hetero-oligomerization pattern of the BMP receptors is very flexible and susceptible to modulation by bound ligands (Gilboa et al., 2000). Even if distinct BMPs are able to bind the same set of receptor subtypes, already slight differences in binding affinity can favor other receptor combinations to be assembled and thus alter downstream signal transduction (Nickel et al., 2009). For instance, in murine multipotent C2C12 cells, BMP4 induced phosphorylation and nuclear translocation of all three R-SMADs. However, despite being highly homologous (phylogenetic tree in Figure 1-3), only SMAD1 and SMAD5, but not SMAD8, were efficiently recruited and activated by BMP6- and BMP7-assembled receptor complexes (Aoki et al., 2001).

It is important to note that BMP signaling can additionally be regulated by co-receptors and other unknown factors from various protein families as well as microRNAs (Sieber et al., 2009). Further studies are needed to clarify the oligomerization pattern of type-I/-II receptors and binding preferences of individual BMPs on the surface of hESCs. Biochemical methods such as cross-linking and co-immunoprecipitation, and biophysical methods such as surface plasmon resonance and immunofluorescence co-patching, could be helpful.

5.4 Collective molecular events leading to BMP-mediated trophoblast differentiation in human pluripotent stem cells

The overall experimental results of this comprehensive study indicate that the outcome of differentiation of hESCs and hiPSCs induced by distinct Bone Morphogenetic Proteins and related Growth Differentiation Factors is in general identical and independent of the ligand type and subgroup, provided that the ligands

1.) are applied under the same experimental conditions with regard to the differentiation medium and its supplements; and
2.) induce activation of canonical BMP signaling via the intracellular signal transducers SMAD1/5/8.

The second criterion would exclude the few exceptional ligands which are known to signal via SMAD2/3, namely BMP3 (Bonner et al., 2011), BMP3b (alias GDF10) (Matsumoto et al., 2012), BMP11 (alias GDF11) (Hannan et al., 2009), GDF3 (Levine and Brivanlou, 2006), GDF8 (Hannan et al., 2009) and GDF9 (Mazerbourg et al., 2004). Indeed, GDF3, BMP11 and GDF8 have been reported to support the undifferentiated growth of hESCs (Levine and Brivanlou, 2006; Hannan et al., 2009).

Additionally, the findings of previous studies support in conjunction with the results of this PhD project the claim of a "collective" identical cell fate for all SMAD1/5/8-acting BMPs/GDFs with respect to human pluripotent stem cells, provided equal treatment conditions: In the initial hESC-related BMP study of Xu et al. (Xu et al., 2002), BMP2, BMP7 and

GDF5 (alias BMP14) were described to induce "similar morphological changes" of hESCs as observed for BMP4. The BMP4-driven cell fate was identified by the authors as trophoblast lineage. However, no precise phenotyping of the differentiated cells obtained by the other three ligands has been performed, except the superficial assessment of their optical appearance. Regarding hiPSCs, our group demonstrated that BMP4 and its subgroup member BMP2 induce trophoblast differentiation in amniotic fluid cell-derived hiPSCs (Wolfrum et al., 2010). Both ligands were applied under culture conditions lacking exogenous bFGF and including inhibition of autocrine Activin/Nodal signaling. However, the possible coexistence of cells belonging to other lineages than trophoblast has not been assayed in this study.

The responsible molecular mechanism of action which backs up the drawn conclusions can be seen from the same sets of genes, whose expression in hESCs were systematically affected in common by BMP5, BMP10 and BMP13. The onset of up- or downregulation of these genes occurred early upon stimulation with BMPs – albeit to varying degrees, depending on the ligands' strengths in inducing SMAD1/5/8 signaling.

Upregulated gene sets included direct inducible target genes of canonical BMP signaling (Figure 4-34) and of factors with transcription regulatory activity known to be involved in early trophoblast differentiation (Figure 4-16). Some of the latter factors are also known to be direct inducible BMP target genes as well, due to the presence of BMP-responsive elements (BREs) / SMAD-binding elements within their promoter regions, e.g. *ID2*, *MSX2*, *GATA2*, *GATA3*, *DLX3* and *DLX5* (references for being BMP-responsive genes: Hollnagel et al., 1999; Miyazono et al., 2005; Park and Morasso, 2002; Miyama et al., 1999; references for functions in trophoblast development: Janatpour et al., 2000; Quinn et al., 2000; Ma et al., 1997; Peng and Payne, 2002; Kato et al., 2008).

In contrast, several genes involved in the maintenance of the undifferentiated and pluripotent state were repressed upon treatment with distinct BMPs, most rapidly by BMP10. Their downregulation cooperatively promoted exit from hESC self-renewal. These included key players of the competing Activin/Nodal branch of TGF-β superfamily signaling, acting via SMAD2/3 (Chapter 1.3.3), namely the ligands Activin A (*INHBA*), Nodal (*NODAL*) and GDF3 (*GDF3*) (Besser, 2004; James et al., 2005; Greber et al., 2008; Levine and Brivanlou, 2006) (Figure 4-34). SMAD2/3 signaling is involved in the control of pluripotency-supporting genes by inducing expression of *NODAL* (which in turn activates SMAD2/3 signaling (Besser, 2004)), and of key transcription factors (TFs). For instance, SMAD2/3 signaling has been shown to induce expression of *NANOG* (Greber et al., 2008) by direct binding of the Activin/Nodal-responsive SMADs to its promoter (Xu et al., 2008; Vallier et al., 2009b; Brown et al., 2011). NANOG composes together with OCT4 and SOX2 the core machinery for maintaining the undifferentiated state, and all three TFs are known to regulate each other's expression (Boyer et al., 2005; Jung et al., 2010). *NANOG*, *OCT4* and *SOX2* were repressed upon treatment with all BMPs, with *SOX2* being affected at the earliest and *OCT4* at the latest (Figure 4-16). It was previously shown that BMP4-induced SMAD1/5/8 activation in hESCs represses *SOX2* (Greber et al., 2008). Similarly, *FGF2* (gene encoding bFGF) was downregulated (Figure 4-36). bFGF-mediated signaling is known to modulate TGF-β superfamily signaling in hESCs to support hESC self-renewal via supporting SMAD2/3 signaling and antagonizing competing SMAD1/5/8 signaling. This mechanism includes gene suppression of the ligand BMP4 (*BMP4*) and gene induction of the BMP antagonists Gremlin

and Cerberus (*GREM1* and *CER1*) and of the ligand Activin A (*INHBA*) (Greber et al., 2007a). In addition, FGF/MEK-ERK signaling also supports hESC self-renewal via enhancing *NANOG* promoter activity, where it synergizes with SMAD2/3 signaling (Xu et al., 2008; Greber et al., 2010; Greber et al., 2011).

The positive and negative influence on these genes as a collective transcriptional response following activation of SMAD1/5/8 signaling downstream of BMP receptors might explain why distinct BMPs induce the same differentiation fate in hESCs and hiPSCs, which is defined as trophoblast lineage in cell culture media without exogenously added bFGF:

DOWN:	**UP:**
− Key TFs that maintain the pluripotent state − Key players of competing SMAD2/3 signaling branch	− Direct inducible BMP target genes − TFs characteristic of early placenta development
→ **Exit from self-renewal**	→ **Direction towards trophoblast lineage**

5.5 Practical impact of the novel findings and outlook

5.5.1 Practical impact

This resarch project has identified with BMP5, BMP10, and to a lesser extent BMP13, three additional BMP family members suitable for use in model systems for studying trophoblast differentiation from hESCs and hiPSCs. Because to this day no true human equivalents of trophoblast stem cells have been successfully derived from the trophectoderm of blastocysts (Roberts and Fisher, 2011; Genbacev et al., 2013), such *in vitro* studies are still reliant on immortalized cytotrophoblast cells, choriocarcinoma cell lines and explants of placental chorionic villi (King et al., 2000). These cell models have the disadvantages of harboring transformed genetic backgrounds, being already mature trophoblast subtypes or having very limited proliferation capacities. The study of human placentation *in vivo* is not applicable for obvious ethical reasons, and placentation of other mammalian species significantly differs from humans, which limits the suitability of animal models (Bischof, 1997; Knipp et al., 1999; Giakoumopoulos and Golos, 2013). Thus, human pluripotent stem cells in combination with recombinant BMPs serve as a complementary alternative model system to investigate the early and late steps of trophoblast development and the molecular mechanisms involved in trophoblast cell maintenance and specification (Ezashi et al., 2012; Golos et al., 2013; Giakoumopoulos and Golos, 2013). However, it should be pointed out that evidence for an involvement of BMPs in human *in vivo* placentation is still outstanding and the observed effects of these proteins may be limited to *in vitro* conditions.

Recombinant BMPs, especially BMP4, are commonly used as cell fate inducers in differentiation protocols applying more stringent culture conditions based on human pluripotent stem cells. *Inter alia* for differentiation to definitive endoderm (Teo et al., 2012) or mesoderm (Murry and Keller, 2008; Lee et al., 2013) progenitor cells to serve as basis for further directed

differentiation steps (e.g. to hepatocytes (Song et al., 2009; Jozefczuk et al., 2011) or pancreatic cells (Van Hoof et al., 2009) through definitive endoderm), functional cardiomyocytes (Wong and Bernstein, 2010; Jinno et al., 1995), hematopoietic cells (Chadwick et al., 2003), (cardio-)vascular progenitor cells (Bai et al., 2010; Cao et al., 2013), chondrocytes (Nakagawa et al., 2009) and germ cells (Panula et al., 2011). In this regard, the present work has unveiled three additional cytokines that can be implemented into differentiation protocols. They could functionally substitute less potent BMPs or act synergistically with other cytokines and growth factors to increase the degree of differentiation efficiency. For instance, Insulin-like Growth Factor-II (IGF2) has recently been demonstrated to mimic the synergistic effect of fetal bovine serum on BMP9-induced cell response of murine MC3T3-E1 preosteoblasts, while it had no influence on BMP2 (Lauzon et al., 2014).

In particular BMP10 could be of usefulness due to its strength in activating canonical BMP signaling in hESCs and hiPSCs (Chapter 5.3). Moreover, BMP10 has proved to be insensitive to the extracellular BMP antagonist Noggin (Seemann et al., 2009). This is unlike BMP4 and numerous other ligands (e.g. BMP2, BMP5, BMP7, BMP13/GDF6 and BMP14/GDF5), which are bound and inactivated by Noggin with different affinities (reviewed by Krause et al., 2011). Noggin mRNA was significantly induced in hESCs upon treatment with BMPs (Figure 4-35). Noggin protein is known to be secreted by many cell types, such as osteoblasts, as a physiological response to constrict extensive BMP action (Gazzerro et al., 1998; Nifuji and Noda, 1999; Seemann et al., 2009). This inhibitory side effect can only be compensated by increasing the ligand concentration, leading to higher costs. Thus, supplementation with BMP10 would have enormous practical impact in cell culture medium environments containing Noggin activity. Sequence alignment of various human BMP family members elucidated that BMP10 protection against Noggin inhibition is at least partially provided by a lysine, instead of the usually highly conserved asparagine, located at a critical position (amino acid residue 82 in Figure 1-5) within overlapping receptor and antagonist interfaces (Seemann et al., 2009). In the same practical context, the knowledge of key amino acid residues that are mediating resistance to negative feedback inhibition by Noggin has been employed to engineer recombinant BMPs with superior agonist activity. This knowledge was gained from Noggin-insensitive wild-type BMPs (e.g. BMP6 (Song et al., 2010b)) or disease-associated mutant BMPs/GDFs (e.g. *GDF5* point mutations in patients with multiple synostosis syndrome (Seemann et al., 2009; Schwaerzer et al., 2012)). Today, recombinant BMPs are clinically used in regenerative medicine and tissue engineering (reviewed by Bessa et al., 2008a; Bessa et al., 2008b). Patents exist for such rationally designed BMPs with reduced antagonist sensitivity for usage as effective, low-dose therapeutics in clinical applications to induce new bone formation in long bone non-union fractures, spinal fusions, and to support the placing of dental implants.

5.5.2 Outlook

Future work should be focused on the practical application of the novel tested BMPs as tools to optimize *in vitro* differentiation strategies for the derivation of therapeutically suitable cell types. For instance, the directed differentiation of hESCs/hiPSCs to multipotent cardiac

progenitor cells and cardiomyocytes has attracted great attention in the field of regenerative medicine, as these cells are expected to restore damaged or lost tissue after myocardial infarction (reviewed by Yoshida and Yamanaka, 2011 and Yi et al., 2013). Due to the essential *in vivo* function of BMP10 in murine heart morphogenesis (Chapter 1.4.3), follow-up studies are recommended to investigate its feasibility for cardiac differentiation approaches from human pluripotent stem cells, many of which are currently involving BMP4.

The generation of hiPSCs from chorionic villi cells (Ye et al., 2009; this PhD work) or amniotic fluid cells (Ye et al., 2009; Wolfrum et al., 2010), which are obtained from early routine prenatal diagnostic procedures (chorionic villus sampling and amniocentesis, respectively (Wegner and Stumm, 2011)), offers the unique opportunity to have autologous stem cell progeny already available pre-birth. These cells could be applied for tissue engineering, which might involve recombinant human BMPs, as described in cited protocols (Chapter 5.5.1). The derived tissues could be of benefit for patient-tailored regenerative therapies or drug safety / toxicity tests. This would especially be interesting in the case of identified congenital heart defects or genetic disorders, which will require newborns to undergo surgery or continuous medication.

6   Conclusion

To date, BMP4 has served as the "standard BMP" for model studies related to human pluripotent stem cells. This research project has shown that trophoblast differentiation in hESCs and hiPSCs is also induced by members of different subgroups of the large BMP family when exogenous bFGF is absent – including BMP5, BMP10 and BMP13. The identical differentiation outcome can be explained by the conserved mechanisms in activated signal transduction pathways and resultant transcriptional responses by the distinct ligands in these cells. Individual BMPs exhibited differences in the kinetics of induced differentiation as a consequence of receptor complexity existing for BMP signaling. Canonical BMP signaling via SMAD1/5/8 downstream of activated BMP receptor complexes was revealed as the predominant trigger for the induction of trophoblast differentiation in human pluripotent stem cells. This is in contrast to the known and tested SMAD-independent pathways (via MAPKs ERK1/2, p38 and SAPK/JNK or via Akt). The same behavior of somatic-induced pluripotent stem cells and native blastocyst-derived embryonic stem cells in response to treatment with individual ligands can be explained by the comparable expression patterns of BMP-related TGF-β superfamily type-I and type-II receptor subtypes between hiPSCs and hESCs. The adaptation of receptor expression profile occurred during the reprogramming process of somatic cells to hiPSCs.

The present study, in conjunction with the results of other publications, has highlighted that the choice of the cell culture medium is a very critical aspect for BMP signaling and differentiation studies. Non-chemically-defined culture systems containing xenogeneic feeder cells and serum, or media containing pre-existing supplementation with exogenous factors such as bFGF, exert influence on BMP-mediated signal transduction. This can lead to clearly mixed cell populations, thus forming an obstacle when drawing conclusions on BMP-induced cell fate.

BMP10, a heart-specific protein, was revealed as a novel and highly potent inducer of trophoblast differentiation in hESCs and hiPSCs. Even though the tested BMP family members might be physiologically not relevant for *in vivo* placentation, they offer the opportunity to study trophoblast development from hESCs/hiPSCs *in vitro*. In addition, these cytokines can be regarded as important biomaterials for the *in vitro* manipulation of human pluripotent stem cells. Recombinant human BMP5, BMP10 and BMP13 can be implemented into various existing hESC/hiPSC differentiation protocols that require canonical BMP signaling to derive specific cell types of interest, e.g. for cell-based regenerative therapies. In particular BMP10 may be advantageous due to its insensitivity to antagonism by Noggin, which was expressed as BMP-induced feedback inhibition in these cells. This study has also highlighted the need to investigate the capability of the remaining as yet untested BMPs – in homodimeric and heterodimeric forms – with respect to the *in vitro* differentiation of human pluripotent stem cells.

7   Bibliography

Notice: Parts of my PhD work have recently been published in the peer-reviewed journal Biomaterials (http://www.journals.elsevier.com/biomaterials; authors: Björn Lichtner (first author), Prof. Dr. Petra Knaus, Prof. Dr. Hans Lehrach, Prof. Dr. James Adjaye (last and corresponding author); Lichtner et al., 2013). The writing of the manuscript by me as the first author was being performed in parallel to the writing of this dissertation. Therefore, figures and text segments of my publication also appear in my dissertation, and vice versa. This is in agreement with the copyright law of the publisher Elsevier, which leaves authors the right to use their final published article for inclusion in a thesis or dissertation.

Literature references:

Adjaye et al., 2005	Adjaye J, Huntriss J, Herwig R, BenKahla A, Brink TC, Wierling C, Hultschig C, Groth D, Yaspo ML, Picton HM, Gosden RG, Lehrach H (2005) Primary differentiation in the human blastocyst: comparative molecular portraits of inner cell mass and trophectoderm cells. Stem Cells 23(10):1514-25. PubMed PMID: 16081659
Al-Refu et al., 2009	Al-Refu K, Edward S, Ingham E, Goodfield M (2009) Expression of hair follicle stem cells detected by cytokeratin 15 stain: implications for pathogenesis of the scarring process in cutaneous lupus erythematosus. Br J Dermatol 160(6):1188-96. PubMed PMID: 19298282
Amita et al., 2013	Amita M, Adachi K, Alexenko AP, Sinha S, Schust DJ, Schulz LC, Roberts RM, Ezashi T (2013) Complete and unidirectional conversion of human embryonic stem cells to trophoblast by BMP4. Proc Natl Acad Sci U S A 110(13):E1212-21. PubMed PMID: 23493551
Andrews, 1988	Andrews PW (1988) Human teratocarcinomas. Biochim Biophys Acta 948(1):17-36. Review. PubMed PMID: 3293662
Aoki et al., 2001	Aoki H, Fujii M, Imamura T, Yagi K, Takehara K, Kato M, Miyazono K (2001) Synergistic effects of different bone morphogenetic protein type I receptors on alkaline phosphatase induction. J Cell Sci 114(Pt 8):1483-9. PubMed PMID: 11282024
Aplin et al., 2009	Aplin JD, Jones CJ, Harris LK (2009) Adhesion molecules in human trophoblast – a review. I. Villous trophoblast. Placenta 30(4):293-8. Review. PubMed PMID: 19131106
Aryee et al., 1998	Aryee DN, Petermann R, Kos K, Henn T, Haas OA, Kovar H (1998) Cloning of a novel human ELF-1-related ETS transcription factor, ELFR, its characterization and chromosomal assignment relative to ELF-1. Gene 210(1):71-8. PubMed PMID: 9524226
Ashburner et al., 2000	Ashburner M, Ball CA, Blake JA, Botstein D, Butler H, Cherry JM, Davis AP, Dolinski K, Dwight SS, Eppig JT, Harris MA, Hill DP, Issel-Tarver L, Kasarskis A, Lewis S, Matese JC, Richardson JE, Ringwald M, Rubin GM, Sherlock G (2000) Gene ontology: tool for the unification of biology. The Gene Ontology Consortium. Nat Genet 25(1):25-9. PubMed PMID: 10802651
Assou et al., 2012	Assou S, Boumela I, Haouzi D, Monzo C, Dechaud H, Kadoch IJ, Hamamah S (2012) Transcriptome analysis during human trophectoderm specification suggests new roles of metabolic and epigenetic genes. PLoS One 7(6):e39306. PubMed PMID: 22761758
Babaie et al., 2007	Babaie Y, Herwig R, Greber B, Brink TC, Wruck W, Groth D, Lehrach H, Burdon T, Adjaye J (2007) Analysis of Oct4-dependent transcriptional networks regulating self-renewal and pluripotency in human embryonic stem cells. Stem Cells 25(2):500-10. PubMed PMID: 17068183
Baczyk et al., 2004	Baczyk D, Satkunaratnam A, Nait-Oumesmar B, Huppertz B, Cross JC, Kingdom JC (2004) Complex patterns of GCM1 mRNA and protein in villous and extravillous trophoblast cells of the human placenta. Placenta 25(6):553-9. PubMed PMID: 15135239
Baczyk et al., 2009	Baczyk D, Drewlo S, Proctor L, Dunk C, Lye S, Kingdom J (2009) Glial cell missing-1 transcription factor is required for the differentiation of the human trophoblast. Cell Death Differ 16(5):719-27. PubMed PMID: 19219068
Bai et al., 2010	Bai H, Gao Y, Arzigian M, Wojchowski DM, Wu WS, Wang ZZ (2010) BMP4 regulates vascular progenitor development in human embryonic stem cells through a Smad-dependent pathway. J Cell Biochem 109(2):363-74. PubMed PMID: 19950207
Bass et al., 1997	Bass KE, Li H, Hawkes SP, Howard E, Bullen E, Vu TK, McMaster M, Janatpour M, Fisher SJ (1997) Tissue inhibitor of metalloproteinase-3 expression is upregulated during human cytotrophoblast invasion in vitro. Dev Genet 21(1):61-7. PubMed PMID: 9291581
Baum et al., 2008	Baum B, Settleman J, Quinlan MP (2008) Transitions between epithelial and mesenchymal states in development and disease. Semin Cell Dev Biol 19(3):294-308. Review. PubMed PMID: 18343170
Beck et al., 2001	Beck HN, Drahushuk K, Jacoby DB, Higgins D, Lein PJ (2001) Bone morphogenetic protein-5 (BMP-5) promotes dendritic growth in cultured sympathetic neurons. BMC Neurosci 2:12. PubMed PMID: 11580864
Becker et al., 1992	Becker T, Gerke V, Kube E, Weber K (1992) S100P, a novel Ca(2+)-binding protein from human placenta. cDNA cloning, recombinant protein expression and Ca2+ binding properties. Eur J Biochem 207(2):541-7. PubMed PMID: 1633809

Benjamini and Hochberg, 1995	Benjamini Y, Hochberg Y (1995) Controlling the false discovery rate: a practical and powerful approach to multiple testing. Journal of the Royal Statistical Society, Series B 57 (1): 289–300.
Berasi et al., 2011	Berasi SP, Varadarajan U, Archambault J, Cain M, Souza TA, Abouzeid A, Li J, Brown CT, Dorner AJ, Seeherman HJ, Jelinsky SA (2011) Divergent activities of osteogenic BMP2, and tenogenic BMP12 and BMP13 independent of receptor binding affinities. Growth Factors 29(4):128-39. PubMed PMID: 21702718
Bernardo et al., 2011	Bernardo AS, Faial T, Gardner L, Niakan KK, Ortmann D, Senner CE, Callery EM, Trotter MW, Hemberger M, Smith JC, Bardwell L, Moffett A, Pedersen RA (2011) BRACHYURY and CDX2 mediate BMP-induced differentiation of human and mouse pluripotent stem cells into embryonic and extraembryonic lineages. Cell Stem Cell 9(2):144-55. PubMed PMID: 21816365
Bessa et al., 2008a	Bessa PC, Casal M, Reis RL (2008) Bone morphogenetic proteins in tissue engineering: the road from the laboratory to the clinic, part I (basic concepts). J Tissue Eng Regen Med 2(1):1-13. Review. PubMed PMID: 18293427
Bessa et al., 2008b	Bessa PC, Casal M, Reis RL (2008) Bone morphogenetic proteins in tissue engineering: the road from laboratory to clinic, part II (BMP delivery). J Tissue Eng Regen Med 2(2-3):81-96. Review. PubMed PMID: 18383454
Besser, 2004	Besser D (2004) Expression of nodal, lefty-a, and lefty-B in undifferentiated human embryonic stem cells requires activation of Smad2/3. J Biol Chem 279(43):45076-84. PubMed PMID: 15308665
Bickmore, 2001	Bickmore WA (2001) Karyotype Analysis and Chromosome Banding. In: Encyclopedia of Life Sciences, Nature Publishing Group / John Wiley & Sons Ltd.
Bischof, 1997	Bischof P (1997) In vitro models used to study implantation, trophoblast invasion and placentation: A review. Trophoblast Research 10:67-82. Review.
Bischof et al., 2000	Bischof P, Meisser A, Campana A (2000) Paracrine and autocrine regulators of trophoblast invasion--a review. Placenta 21 Suppl A:S55-60. Review. PubMed PMID: 10831123
Bischof and Irminger-Finger, 2005	Bischof P, Irminger-Finger I (2005) The human cytotrophoblastic cell, a mononuclear chameleon. Int J Biochem Cell Biol 37(1):1-16. Review. PubMed PMID: 15381142
Blackburn, 1991	Blackburn EH (1991) Structure and function of telomeres. Nature 350(6319):569-73. Review. PubMed PMID: 1708110
Blaschitz et al., 2000	Blaschitz A, Weiss U, Dohr G, Desoye G (2000) Antibody reaction patterns in first trimester placenta: implications for trophoblast isolation and purity screening. Placenta 21(7):733-41. PubMed PMID: 10985978
Boergermann et al., 2010	Boergermann JH, Kopf J, Yu PB, Knaus P (2010) Dorsomorphin and LDN-193189 inhibit BMP-mediated Smad, p38 and Akt signalling in C2C12 cells. Int J Biochem Cell Biol 42(11):1802-7. PubMed PMID: 20691279
Bonner et al., 2011	Bonner C, Farrelly AM, Concannon CG, Dussmann H, Baqué M, Virard I, Wobser H, Kögel D, Wollheim CB, Rupnik M, Byrne MM, König HG, Prehn JH (2011) Bone morphogenetic protein 3 controls insulin gene expression and is down-regulated in INS-1 cells inducibly expressing a hepatocyte nuclear factor 1A-maturity-onset diabetes of the young mutation. J Biol Chem 286(29):25719-28. PubMed PMID: 21628466
Boyer et al., 2005	Boyer LA, Lee TI, Cole MF, Johnstone SE, Levine SS, Zucker JP, Guenther MG, Kumar RM, Murray HL, Jenner RG, Gifford DK, Melton DA, Jaenisch R, Young RA (2005) Core transcriptional regulatory circuitry in human embryonic stem cells. Cell 122(6):947-56. PubMed PMID: 16153702
Bramlage et al., 2011	Bramlage CP, Müller GA, Tampe B, Bevanda J, Maatouk I, Koziolek M, Lange K, Ahrens K, Schmid H, Cohen CD, Bramlage P, Kretzler M, Strutz F (2011) The role of bone morphogenetic protein-5 (BMP-5) in human nephrosclerosis. J Nephrol 24(5):647-55. PubMed PMID: 21319131
Brazel et al., 1988	Brazel D, Pollner R, Oberbäumer I, Kühn K (1988) Human basement membrane collagen (type IV). The amino acid sequence of the alpha 2(IV) chain and its comparison with the alpha 1(IV) chain reveals deletions in the alpha 1(IV) chain. Eur J Biochem 172(1):35-42. PubMed PMID: 3345760
Brederlau et al., 2002	Brederlau A, Faigle R, Kaplan P, Odin P, Funa K (2002) Bone morphogenetic proteins but not growth differentiation factors induce dopaminergic differentiation in mesencephalic precursors. Mol Cell Neurosci 21(3):367-78. PubMed PMID: 12498780
Brown et al., 2010	Brown K, Legros S, Artus J, Doss MX, Khanin R, Hadjantonakis AK, Foley A (2010) A comparative analysis of extra-embryonic endoderm cell lines. PLoS One 5(8):e12016. PubMed PMID: 20711519
Brown et al., 2011	Brown S, Teo A, Pauklin S, Hannan N, Cho CH, Lim B, Vardy L, Dunn NR, Trotter M, Pedersen R, Vallier L (2011) Activin/Nodal signaling controls divergent transcriptional networks in human embryonic stem cells and in endoderm progenitors. Stem Cells 29(8):1176-85. PubMed PMID: 21630377
Cao et al., 2013	Cao N, Liang H, Huang J, Wang J, Chen Y, Chen Z, Yang HT (2013) Highly efficient induction and long-term maintenance of multipotent cardiovascular progenitors from human pluripotent stem cells under defined conditions. Cell Res 23(9):1119-32. PubMed PMID: 23896987
Carlson, 2012	Carlson BM (2012) Human Embryology and Developmental Biology. Elsevier/Saunders, 5th Edition. ISBN: 9781455727971 (eBook) and 9781455727940 (Print Book).
Cavanagh et al., 2009	Cavanagh PC, Dunk C, Pampillo M, Szereszewski JM, Taylor JE, Kahiri C, Han V, Lye S, Bhattacharya M, Babwah AV (2009) Gonadotropin-releasing hormone-regulated chemokine expression in human placentation. Am J Physiol Cell Physiol 297(1):C17-27. PubMed PMID: 19369450
Cha et al., 2000	Cha SH, Sekine T, Kusuhara H, Yu E, Kim JY, Kim DK, Sugiyama Y, Kanai Y, Endou H (2000) Molecular cloning and characterization of multispecific organic anion transporter 4 expressed in the placenta. J Biol Chem 275(6):4507-12. PubMed PMID: 10660625
Chadwick et al., 2003	Chadwick K, Wang L, Li L, Menendez P, Murdoch B, Rouleau A, Bhatia M (2003) Cytokines and BMP-4 promote hematopoietic differentiation of human embryonic stem cells. Blood 102(3):906-15. PubMed PMID: 12702499
Chan et al., 2013	Chan SS, Shi X, Toyama A, Arpke RW, Dandapat A, Iacovino M, Kang J, Le G, Hagen HR, Garry DJ, Kyba

	M (2013) Mesp1 patterns mesoderm into cardiac, hematopoietic, or skeletal myogenic progenitors in a context-dependent manner. Cell Stem Cell 12(5):587-601. PubMed PMID: 23642367
Chan, 2014	Chan JK (2014) The wonderful colors of the hematoxylin-eosin stain in diagnostic surgical pathology. Int J Surg Pathol 22(1):12-32. Review. PubMed PMID: 24406626
Chen et al., 2004	Chen H, Shi S, Acosta L, Li W, Lu J, Bao S, Chen Z, Yang Z, Schneider MD, Chien KR, Conway SJ, Yoder MC, Haneline LS, Franco D, Shou W (2004) BMP10 is essential for maintaining cardiac growth during murine cardiogenesis. Development 131(9):2219-31. PubMed PMID: 15073151
Chen et al., 2013a	Chen H, Brady Ridgway J, Sai T, Lai J, Warming S, Chen H, Roose-Girma M, Zhang G, Shou W, Yan M (2013) Context-dependent signaling defines roles of BMP9 and BMP10 in embryonic and postnatal development. Proc Natl Acad Sci U S A 110(29):11887-92. PubMed PMID: 23812757
Chen et al., 2013b	Chen Y, Wang K, Chandramouli GV, Knott JG, Leach R (2013) Trophoblast lineage cells derived from human induced pluripotent stem cells. Biochem Biophys Res Commun 436(4):677-84. PubMed PMID: 23774580
Cheng et al., 2003	Cheng H, Jiang W, Phillips FM, Haydon RC, Peng Y, Zhou L, Luu HH, An N, Breyer B, Vanichakarn P, Szatkowski JP, Park JY, He TC (2003) Osteogenic activity of the fourteen types of human bone morphogenetic proteins (BMPs). J Bone Joint Surg Am 85-A(8):1544-52. Erratum in: J Bone Joint Surg Am. 2004 Jan;86-A(1):141. PubMed PMID: 12925636
Cheng et al., 2004	Cheng YH, Aronow BJ, Hossain S, Trapnell B, Kong S, Handwerger S (2004) Critical role for transcription factor AP-2alpha in human trophoblast differentiation. Physiol Genomics 18(1):99-107. PubMed PMID: 15039486
Chou et al., 2002	Chou CS, Zhu H, Shalev E, MacCalman CD, Leung PC (2002) The effects of gonadotropin-releasing hormone (GnRH) I and GnRH II on the urokinase-type plasminogen activator/plasminogen activator inhibitor system in human extravillous cytotrophoblasts in vitro. J Clin Endocrinol Metab 87(12):5594-603. PubMed PMID: 12466358
Clark et al., 2004a	Clark AT, Bodnar MS, Fox M, Rodriquez RT, Abeyta MJ, Firpo MT, Pera RA (2004) Spontaneous differentiation of germ cells from human embryonic stem cells in vitro. Hum Mol Genet 13(7):727-39. PubMed PMID: 14962983
Clark et al., 2004b	Clark AT, Rodriguez RT, Bodnar MS, Abeyta MJ, Cedars MI, Turek PJ, Firpo MT, Reijo Pera RA (2004) Human STELLAR, NANOG, and GDF3 genes are expressed in pluripotent cells and map to chromosome 12p13, a hotspot for teratocarcinoma. Stem Cells 22(2):169-79. PubMed PMID: 14990856
Cole, 1997	Cole LA (1997) Immunoassay of human chorionic gonadotropin, its free subunits, and metabolites. Clin Chem 43(12):2233-43. Review. PubMed PMID: 9439438
Cole, 2010	Cole LA (2010) Biological functions of hCG and hCG-related molecules. Reprod Biol Endocrinol 8:102. Review. PubMed PMID: 20735820
Colorado et al., 2000	Colorado PC, Torre A, Kamphaus G, Maeshima Y, Hopfer H, Takahashi K, Volk R, Zamborsky ED, Herman S, Sarkar PK, Ericksen MB, Dhanabal M, Simons M, Post M, Kufe DW, Weichselbaum RR, Sukhatme VP, Kalluri R (2000) Anti-angiogenic cues from vascular basement membrane collagen. Cancer Res 60(9):2520-6. PubMed PMID: 10811134
Constância et al., 2002	Constância M, Hemberger M, Hughes J, Dean W, Ferguson-Smith A, Fundele R, Stewart F, Kelsey G, Fowden A, Sibley C, Reik W (2002) Placental-specific IGF-II is a major modulator of placental and fetal growth. Nature 417(6892):945-8. PubMed PMID: 12087403
Copeman et al., 2000	Copeman J, Han RN, Caniggia I, McMaster M, Fisher SJ, Cross JC (2000) Posttranscriptional regulation of human leukocyte antigen G during human extravillous cytotrophoblast differentiation. Biol Reprod 62(6):1543-50. PubMed PMID: 10819754
Cormack et al., 1996	Cormack BP, Valdivia RH, Falkow S (1996) FACS-optimized mutants of the green fluorescent protein (GFP). Gene 173(1 Spec No):33-8. PubMed PMID: 8707053
Cowan et al., 2005	Cowan CA, Atienza J, Melton DA, Eggan K (2005) Nuclear reprogramming of somatic cells after fusion with human embryonic stem cells. Science 309(5739):1369-73. PubMed PMID: 16123299
Croft et al., 2011	Croft D, O'Kelly G, Wu G, Haw R, Gillespie M, Matthews L, Caudy M, Garapati P, Gopinath G, Jassal B, Jupe S, Kalatskaya I, Mahajan S, May B, Ndegwa N, Schmidt E, Shamovsky V, Yung C, Birney E, Hermjakob H, D'Eustachio P, Stein L (2011) Reactome: a database of reactions, pathways and biological processes. Nucleic Acids Res 39(Database issue):D691-7. PubMed PMID: 21067998
Cross et al., 2002	Cross JC, Anson-Cartwright L, Scott IC (2002) Transcription factors underlying the development and endocrine functions of the placenta. Recent Prog Horm Res 57:221-34. Review. PubMed PMID: 12017545
D'Amour et al., 2005	D'Amour KA, Agulnick AD, Eliazer S, Kelly OG, Kroon E, Baetge EE (2005) Efficient differentiation of human embryonic stem cells to definitive endoderm. Nat Biotechnol 23(12):1534-41. PubMed PMID: 16258519
Daniel and Smith, 2008	Daniel R, Smith JA (2008) Integration site selection by retroviral vectors: molecular mechanism and clinical consequences. Hum Gene Ther 19(6):557-68. Review. PubMed PMID: 18533894
Das et al., 2007	Das P, Ezashi T, Schulz LC, Westfall SD, Livingston KA, Roberts RM (2007) Effects of fgf2 and oxygen in the bmp4-driven differentiation of trophoblast from human embryonic stem cells. Stem Cell Res 1(1):61-74. PubMed PMID: 19194525
da Silva and Dotti, 2002	da Silva JS, Dotti CG (2002) Breaking the neuronal sphere: regulation of the actin cytoskeleton in neuritogenesis. Nat Rev Neurosci 3(9):694-704. Review. PubMed PMID: 12209118
David et al., 2007	David L, Mallet C, Mazerbourg S, Feige JJ, Bailly S (2007) Identification of BMP9 and BMP10 as functional activators of the orphan activin receptor-like kinase 1 (ALK1) in endothelial cells. Blood 109(5):1953-61. PubMed PMID: 17068149
Davis et al., 2004	Davis HE, Rosinski M, Morgan JR, Yarmush ML (2004) Charged polymers modulate retrovirus transduction via membrane charge neutralization and virus aggregation. Biophys J 86(2):1234-42. PubMed PMID: 14747357

De Coppi et al., 2007	De Coppi P, Bartsch G Jr, Siddiqui MM, Xu T, Santos CC, Perin L, Mostoslavsky G, Serre AC, Snyder EY, Yoo JJ, Furth ME, Soker S, Atala A (2007) Isolation of amniotic stem cell lines with potential for therapy. Nat Biotechnol 25(1):100-6. PubMed PMID: 17206138
Deken et al., 2000	Deken SL, Beckman ML, Boos L, Quick MW (2000) Transport rates of GABA transporters: regulation by the N-terminal domain and syntaxin 1A. Nat Neurosci 3(10):998-1003. PubMed PMID: 11017172
de Parseval and Heidmann, 2005	de Parseval N, Heidmann T (2005) Human endogenous retroviruses: from infectious elements to human genes. Cytogenet Genome Res 110(1-4):318-32. Review. PubMed PMID: 16093684
Dimri et al., 1995	Dimri GP, Lee X, Basile G, Acosta M, Scott G, Roskelley C, Medrano EE, Linskens M, Rubelj I, Pereira-Smith O, Peacocke M, Campisi J (1995) A biomarker that identifies senescent human cells in culture and in aging skin in vivo. Proc Natl Acad Sci U S A 92(20):9363-7. PubMed PMID: 7568133
Donovan et al., 2000	Donovan A, Brownlie A, Zhou Y, Shepard J, Pratt SJ, Moynihan J, Paw BH, Drejer A, Barut B, Zapata A, Law TC, Brugnara C, Lux SE, Pinkus GS, Pinkus JL, Kingsley PD, Palis J, Fleming MD, Andrews NC, Zon LI (2000) Positional cloning of zebrafish ferroportin1 identifies a conserved vertebrate iron exporter. Nature 403(6771):776-81. PubMed PMID: 10693807
Drews et al., 2012	Drews K, Jozefczuk J, Prigione A, Adjaye J (2012) Human induced pluripotent stem cells--from mechanisms to clinical applications. J Mol Med (Berl) 90(7):735-45. Review. PubMed PMID: 22643868
Dvorak et al., 2005	Dvorak P, Dvorakova D, Koskova S, Vodinska M, Najvirtova M, Krekac D, Hampl A (2005) Expression and potential role of fibroblast growth factor 2 and its receptors in human embryonic stem cells. Stem Cells 23(8):1200-11. PubMed PMID: 15955829
Ehrlich et al., 2011	Ehrlich M, Horbelt D, Marom B, Knaus P, Henis YI (2011) Homomeric and heteromeric complexes among TGF-β and BMP receptors and their roles in signaling. Cell Signal 23(9):1424-32. Review. PubMed PMID: 21515362
Eiselleova et al., 2009	Eiselleova L, Matulka K, Kriz V, Kunova M, Schmidtova Z, Neradil J, Tichy B, Dvorakova D, Pospisilova S, Hampl A, Dvorak P (2009) A complex role for FGF-2 in self-renewal, survival, and adhesion of human embryonic stem cells. Stem Cells 27(8):1847-57. PubMed PMID: 19544431
Ellis et al., 1990	Ellis SA, Palmer MS, McMichael AJ (1990) Human trophoblast and the choriocarcinoma cell line BeWo express a truncated HLA Class I molecule. J Immunol 144(2):731-5. PubMed PMID: 2295808
Ericson et al., 1997	Ericson J, Rashbass P, Schedl A, Brenner-Morton S, Kawakami A, van Heyningen V, Jessell TM, Briscoe J (1997) Pax6 controls progenitor cell identity and neuronal fate in response to graded Shh signaling. Cell 90(1):169-80. PubMed PMID: 9230312
Ezashi et al., 2012	Ezashi T, Telugu BP, Roberts RM (2012) Model systems for studying trophoblast differentiation from human pluripotent stem cells. Cell Tissue Res 349(3):809-24. Review. PubMed PMID: 22427062
Fischer et al., 2008	Fischer AH, Jacobson KA, Rose J, Zeller R (2008) Hematoxylin and eosin staining of tissue and cell sections. CSH Protoc 2008:pdb.prot4986. PubMed PMID: 21356829
Fleige and Pfaffl, 2006	Fleige S, Pfaffl MW (2006) RNA integrity and the effect on the real-time qRT-PCR performance. Mol Aspects Med 27(2-3):126-39. Review. PubMed PMID: 16469371
Floridon et al., 2000	Floridon C, Nielsen O, Holund B, Sunde L, Westergaard JG, Thomsen SG, Teisner B (2000) Localization of E-cadherin in villous, extravillous and vascular trophoblasts during intrauterine, ectopic and molar pregnancy. Mol Hum Reprod 6(10):943-50. PubMed PMID: 11006324
Fournet-Dulguerov et al., 1987	Fournet-Dulguerov N, MacLusky NJ, Leranth CZ, Todd R, Mendelson CR, Simpson ER, Naftolin F (1987) Immunohistochemical localization of aromatase cytochrome P-450 and estradiol dehydrogenase in the syncytiotrophoblast of the human placenta. J Clin Endocrinol Metab 65(4):757-64. PubMed PMID: 3308940
Fuller, 1994	Fuller RW (1994) Uptake inhibitors increase extracellular serotonin concentration measured by brain microdialysis. Life Sci 55(3):163-7. Review. PubMed PMID: 8007758
Fulwyler, 1965	Fulwyler MJ (1965) Electronic separation of biological cells by volume. Science 150(3698):910-1. PubMed PMID: 5891056
Furness and McNagny, 2006	Furness SG, McNagny K (2006) Beyond mere markers: functions for CD34 family of sialomucins in hematopoiesis. Immunol Res 34(1):13-32. Review. PubMed PMID: 16720896
Gallea et al., 2001	Gallea S, Lallemand F, Atfi A, Rawadi G, Ramez V, Spinella-Jaegle S, Kawai S, Faucheu C, Huet L, Baron R, Roman-Roman S (2001) Activation of mitogen-activated protein kinase cascades is involved in regulation of bone morphogenetic protein-2-induced osteoblast differentiation in pluripotent C2C12 cells. Bone 28(5):491-8. PubMed PMID: 11344048
Gamell et al., 2008	Gamell C, Osses N, Bartrons R, Rückle T, Camps M, Rosa JL, Ventura F (2008) BMP2 induction of actin cytoskeleton reorganization and cell migration requires PI3-kinase and Cdc42 activity. J Cell Sci 121(Pt 23):3960-70. PubMed PMID: 19001503
Gaskell et al., 2004	Gaskell TL, Esnal A, Robinson LL, Anderson RA, Saunders PT (2004) Immunohistochemical profiling of germ cells within the human fetal testis: identification of three subpopulations. Biol Reprod 71(6):2012-21. PubMed PMID: 15317684
Gasteiger et al., 2005	Gasteiger E, Hoogland C, Gattiker A, Duvaud S, Wilkins MR, Appel RD, Bairoch A (2005) Protein Identification and Analysis Tools on the ExPASy Server. (In) John M. Walker (ed): The Proteomics Protocols Handbook, Humana Press.
Gaulden and Reiter, 2008	Gaulden J, Reiter JF (2008) Neur-ons and neur-offs: regulators of neural induction in vertebrate embryos and embryonic stem cells. Hum Mol Genet 17(R1):R60-6. Review. PubMed PMID: 18632699
Gazzerro et al., 1998	Gazzerro E, Gangji V, Canalis E (1998) Bone morphogenetic proteins induce the expression of noggin, which limits their activity in cultured rat osteoblasts. J Clin Invest 102(12):2106-14. PubMed PMID: 9854046
Gazzerro and Canalis, 2006	Gazzerro E, Canalis E (2006) Bone morphogenetic proteins and their antagonists. Rev Endocr Metab Disord 7(1-2):51-65. Review. PubMed PMID: 17029022
Geens et al., 2011	Geens M, Sermon KD, Van de Velde H, Tournaye H (2011) Sertoli cell-conditioned medium induces germ cell differentiation in human embryonic stem cells. J Assist Reprod Genet 28(5):471-80. PubMed

	PMID: 21318592
Genbacev et al., 2013	Genbacev O, Lamb JD, Prakobphol A, Donne M, McMaster MT, Fisher SJ (2013) Human trophoblast progenitors: where do they reside? Semin Reprod Med. 31(1):56-61. Review. PubMed PMID: 23329637
Gentric et al., 2012	Gentric G, Desdouets C, Celton-Morizur S (2012) Hepatocytes polyploidization and cell cycle control in liver physiopathology. Int J Hepatol 2012:282430. PubMed PMID: 23150829
Gerami-Naini et al., 2004	Gerami-Naini B, Dovzhenko OV, Durning M, Wegner FH, Thomson JA, Golos TG (2004) Trophoblast differentiation in embryoid bodies derived from human embryonic stem cells. Endocrinology 145(4):1517-24. PubMed PMID: 14684604
Getsios and MacCalman, 2003	Getsios S, MacCalman CD (2003) Cadherin-11 modulates the terminal differentiation and fusion of human trophoblastic cells in vitro. Dev Biol 257(1):41-54. PubMed PMID: 12710956
Giakoumopoulos and Golos, 2013	Giakoumopoulos M, Golos TG (2013) Embryonic stem cell-derived trophoblast differentiation: a comparative review of the biology, function, and signaling mechanisms. J Endocrinol 216(3):R33-45. Review. PubMed PMID: 23291503
Gilboa et al., 2000	Gilboa L, Nohe A, Geissendörfer T, Sebald W, Henis YI, Knaus P (2000) Bone morphogenetic protein receptor complexes on the surface of live cells: a new oligomerization mode for serine/threonine kinase receptors. Mol Biol Cell 11(3):1023-35. PubMed PMID: 10712517
Girard et al., 1999	Girard JP, Baekkevold ES, Feliu J, Brandtzaeg P, Amalric F (1999) Molecular cloning and functional analysis of SUT-1, a sulfate transporter from human high endothelial venules. Proc Natl Acad Sci U S A 96(22):12772-7. PubMed PMID: 10535998
Golos et al., 2013	Golos TG, Giakoumopoulos M, Gerami-Naini B (2013) Review: Trophoblast differentiation from human embryonic stem cells. Placenta 34 Suppl:S56-61. Review. PubMed PMID: 23261342
Gordon and Blobe, 2008	Gordon KJ, Blobe GC (2008) Role of transforming growth factor-beta superfamily signaling pathways in human disease. Biochim Biophys Acta 1782(4):197-228. Review. PubMed PMID: 18313409
Greber et al., 2007a	Greber B, Lehrach H, Adjaye J (2007) Fibroblast growth factor 2 modulates transforming growth factor beta signaling in mouse embryonic fibroblasts and human ESCs (hESCs) to support hESC self-renewal. Stem Cells 25(2):455-64. PubMed PMID: 17038665
Greber et al., 2007b	Greber B, Lehrach H, Adjaye J (2007) Silencing of core transcription factors in human EC cells highlights the importance of autocrine FGF signaling for self-renewal. BMC Dev Biol 7:46. PubMed PMID: 17506876
Greber et al., 2008	Greber B, Lehrach H, Adjaye J (2008) Control of early fate decisions in human ES cells by distinct states of TGFbeta pathway activity. Stem Cells Dev 17(6):1065-77. PubMed PMID: 18393632
Greber et al., 2010	Greber B, Wu G, Bernemann C, Joo JY, Han DW, Ko K, Tapia N, Sabour D, Sterneckert J, Tesar P, Schöler HR (2010) Conserved and divergent roles of FGF signaling in mouse epiblast stem cells and human embryonic stem cells. Cell Stem Cell 6(3):215-26. PubMed PMID: 20207225
Greber, 2011	Greber B (2011) When BMP meets FGF. Cell Stem Cell 9(2):91-2. Comment. PubMed PMID: 21816358
Greber et al., 2011	Greber B, Coulon P, Zhang M, Moritz S, Frank S, Müller-Molina AJ, Araúzo-Bravo MJ, Han DW, Pape HC, Schöler HR (2011) FGF signalling inhibits neural induction in human embryonic stem cells. EMBO J 30(24):4874-84. PubMed PMID: 22085933
Greider and Blackburn, 1989	Greider CW, Blackburn EH (1989) A telomeric sequence in the RNA of Tetrahymena telomerase required for telomere repeat synthesis. Nature 337(6205):331-7. PubMed PMID: 2463488
Gropp et al., 2012	Gropp M, Shilo V, Vainer G, Gov M, Gil Y, Khaner H, Matzrafi L, Idelson M, Kopolovic J, Zak NB, Reubinoff BE (2012) Standardization of the teratoma assay for analysis of pluripotency of human ES cells and biosafety of their differentiated progeny. PLoS One 7(9):e45532. PubMed PMID: 23049812
Guicheux et al., 2003	Guicheux J, Lemonnier J, Ghayor C, Suzuki A, Palmer G, Caverzasio J (2003) Activation of p38 mitogen-activated protein kinase and c-Jun-NH2-terminal kinase by BMP-2 and their implication in the stimulation of osteoblastic cell differentiation. J Bone Miner Res 18(11):2060-8. PubMed PMID: 14606520
Guo and Wang, 2009	Guo X, Wang XF (2009) Signaling cross-talk between TGF-beta/BMP and other pathways. Cell Res 19(1):71-88. Review. PubMed PMID: 19002158
Gupta et al., 2004	Gupta AK, Holzgreve W, Huppertz B, Malek A, Schneider H, Hahn S (2004) Detection of fetal DNA and RNA in placenta-derived syncytiotrophoblast microparticles generated in vitro. Clin Chem 50(11):2187-90. PubMed PMID: 15502097
Gupta et al., 2012	Gupta R, Ezashi T, Roberts RM (2012) Squelching of ETS2 transactivation by POU5F1 silences the human chorionic gonadotropin CGA subunit gene in human choriocarcinoma and embryonic stem cells. Mol Endocrinol 26(5):859-72. PubMed PMID: 22446105
Gurdon et al., 1958	GURDON JB, ELSDALE TR, FISCHBERG M (1958) Sexually mature individuals of Xenopus laevis from the transplantation of single somatic nuclei. Nature 182(4627):64-5. PubMed PMID: 13566187
Haigh et al., 1999	Haigh T, Chen C, Jones CJ, Aplin JD (1999) Studies of mesenchymal cells from 1st trimester human placenta: expression of cytokeratin outside the trophoblast lineage. Placenta 20(8):615-25. PubMed PMID: 10527816
Hall-Stoodley et al., 2004	Hall-Stoodley L, Costerton JW, Stoodley P (2004) Bacterial biofilms: from the natural environment to infectious diseases. Nat Rev Microbiol 2(2):95-108. Review. PubMed PMID: 15040259
Hamilton et al., 1998	Hamilton GS, Lysiak JJ, Han VK, Lala PK (1998) Autocrine-paracrine regulation of human trophoblast invasiveness by insulin-like growth factor (IGF)-II and IGF-binding protein (IGFBP)-1. Exp Cell Res 244(1):147-56. PubMed PMID: 9770358
Han et al., 1996	Han VK, Bassett N, Walton J, Challis JR (1996) The expression of insulin-like growth factor (IGF) and IGF-binding protein (IGFBP) genes in the human placenta and membranes: evidence for IGF-IGFBP interactions at the feto-maternal interface. J Clin Endocrinol Metab 81(7):2680-93. PubMed PMID: 8675597
Handwerger, 2010	Handwerger S (2010) New insights into the regulation of human cytotrophoblast cell differentiation. Mol Cell Endocrinol 323(1):94-104. Review. PubMed PMID: 20036312

Hannan et al., 2009	Hannan NR, Jamshidi P, Pera MF, Wolvetang EJ (2009) BMP-11 and myostatin support undifferentiated growth of human embryonic stem cells in feeder-free cultures. Cloning Stem Cells 11(3):427-35. PubMed PMID: 19751112
Harris et al., 2009	Harris LK, Jones CJ, Aplin JD (2009) Adhesion molecules in human trophoblast – a review. II. extravillous trophoblast. Placenta 30(4):299-304. Review. PubMed PMID: 19131105
Hartung et al., 2006	Hartung A, Bitton-Worms K, Rechtman MM, Wenzel V, Boergermann JH, Hassel S, Henis YI, Knaus P (2006) Different routes of bone morphogenic protein (BMP) receptor endocytosis influence BMP signaling. Mol Cell Biol 26(20):7791-805. PubMed PMID: 16923969
Hassel et al., 2003	Hassel S, Schmitt S, Hartung A, Roth M, Nohe A, Petersen N, Ehrlich M, Henis YI, Sebald W, Knaus P (2003) Initiation of Smad-dependent and Smad-independent signaling via distinct BMP-receptor complexes. J Bone Joint Surg Am 85-A Suppl 3:44-51. PubMed PMID: 12925609
Hayflick, 1965	HAYFLICK L (1965) THE LIMITED IN VITRO LIFETIME OF HUMAN DIPLOID CELL STRAINS. Exp Cell Res 37:614-36. PubMed PMID: 14315085
Herrmann et al., 1990	Herrmann BG, Labeit S, Poustka A, King TR, Lehrach H (1990) Cloning of the T gene required in mesoderm formation in the mouse. Nature 343(6259):617-22. PubMed PMID: 2154694
Higuchi et al., 1995	Higuchi T, Kanzaki H, Nakayama H, Fujimoto M, Hatayama H, Kojima K, Iwai M, Mori T, Fujita J (1995) Induction of tissue inhibitor of metalloproteinase 3 gene expression during in vitro decidualization of human endometrial stromal cells. Endocrinology 136(11):4973-81. PubMed PMID: 7588231
Hirano et al., 1999a	Hirano T, Higuchi T, Ueda M, Inoue T, Kataoka N, Maeda M, Fujiwara H, Fujii S (1999) CD9 is expressed in extravillous trophoblasts in association with integrin alpha3 and integrin alpha5. Mol Hum Reprod 5(2):162-7. PubMed PMID: 10065872
Hirano et al., 1999b	Hirano T, Higuchi T, Katsuragawa H, Inoue T, Kataoka N, Park KR, Ueda M, Maeda M, Fujiwara H, Fujii S (1999) CD9 is involved in invasion of human trophoblast-like choriocarcinoma cell line, BeWo cells. Mol Hum Reprod 5(2):168-74. PubMed PMID: 10065873
Hollnagel et al., 1999	Hollnagel A, Oehlmann V, Heymer J, Rüther U, Nordheim A (1999) Id genes are direct targets of bone morphogenetic protein induction in embryonic stem cells. J Biol Chem 274(28):19838-45. PubMed PMID: 10391928
Hoshina et al., 1982	Hoshina M, Boothby M, Boime I (1982) Cytological localization of chorionic gonadotropin alpha and placental lactogen mRNAs during development of the human placenta. J Cell Biol 93(1):190-8. PubMed PMID: 6896058
Huang et al., 2009a	Huang DW, Sherman BT, Lempicki RA (2009) Bioinformatics enrichment tools: paths toward the comprehensive functional analysis of large gene lists. Nucleic Acids Res 37(1):1-13. PubMed PMID: 19033363
Huang et al., 2009b	Huang DW, Sherman BT, Lempicki RA (2009) Systematic and integrative analysis of large gene lists using DAVID bioinformatics resources. Nat Protoc 4(1):44-57. PubMed PMID: 19131956
Huang et al., 2012	Huang J, Elicker J, Bowens N, Liu X, Cheng L, Cappola TP, Zhu X, Parmacek MS (2012) Myocardin regulates BMP10 expression and is required for heart development. J Clin Invest 122(10):3678-91. PubMed PMID: 22996691
Huangfu et al., 2008a	Huangfu D, Maehr R, Guo W, Eijkelenboom A, Snitow M, Chen AE, Melton DA (2008) Induction of pluripotent stem cells by defined factors is greatly improved by small-molecule compounds. Nat Biotechnol 26(7):795-7. PubMed PMID: 18568017
Huangfu et al., 2008b	Huangfu D, Osafune K, Maehr R, Guo W, Eijkelenboom A, Chen S, Muhlestein W, Melton DA (2008) Induction of pluripotent stem cells from primary human fibroblasts with only Oct4 and Sox2. Nat Biotechnol 26(11):1269-75. PubMed PMID: 18849973
Hui and Perfetti, 2002	Hui H, Perfetti R (2002) Pancreas duodenum homeobox-1 regulates pancreas development during embryogenesis and islet cell function in adulthood. Eur J Endocrinol 146(2):129-41. Review. PubMed PMID: 11834421
Hulett et al., 1969	Hulett HR, Bonner WA, Barrett J, Herzenberg LA (1969) Cell sorting: automated separation of mammalian cells as a function of intracellular fluorescence. Science 166(3906):747-9. PubMed PMID: 4898615
Huppertz et al., 1998	Huppertz B, Kertschanska S, Demir AY, Frank HG, Kaufmann P (1998) Immunohistochemistry of matrix metalloproteinases (MMP), their substrates, and their inhibitors (TIMP) during trophoblast invasion in the human placenta. Cell Tissue Res 291(1):133-48. PubMed PMID: 9394051
Huppertz and Kingdom, 2004	Huppertz B, Kingdom JC (2004) Apoptosis in the trophoblast--role of apoptosis in placental morphogenesis. J Soc Gynecol Investig 11(6):353-62. Review. PubMed PMID: 15350247
Huse et al., 2011	Huse K, Bakkebø M, Oksvold MP, Forfang L, Hilden VI, Stokke T, Smeland EB, Myklebust JH (2011) Bone morphogenetic proteins inhibit CD40L/IL-21-induced Ig production in human B cells: differential effects of BMP-6 and BMP-7. Eur J Immunol 41(11):3135-45. PubMed PMID: 21898381
Hutton and Pevny, 2011	Hutton SR, Pevny LH (2011) SOX2 expression levels distinguish between neural progenitor populations of the developing dorsal telencephalon. Dev Biol 352(1):40-7. PubMed PMID: 21256837
Hyslop et al., 2005	Hyslop L, Stojkovic M, Armstrong L, Walter T, Stojkovic P, Przyborski S, Herbert M, Murdoch A, Strachan T, Lako M (2005) Downregulation of NANOG induces differentiation of human embryonic stem cells to extraembryonic lineages. Stem Cells 23(8):1035-43. PubMed PMID: 15983365
International Stem Cell Initiative, 2007	International Stem Cell Initiative (85 Collaborators) Adewumi O, Aflatoonian B, Ahrlund-Richter L, Amit M, Andrews PW, Beighton G, Bello PA, Benvenisty N, Berry LS, Bevan S, Blum B, Brooking J, Chen KG, Choo AB, Churchill GA, Corbel M, Damjanov I, Draper JS, Dvorak P, Emanuelsson K, Fleck RA, Ford A, Gertow K, Gertsenstein M, Gokhale PJ, Hamilton RS, Hampl A, Healy LE, Hovatta O, Hyllner J, Imreh MP, Itskovitz-Eldor J, Jackson J, Johnson JL, Jones M, Kee K, timeScape Marci S, King BL, Knowles BB, Lako M, Lebrin F, Mallon BS, Manning D, Mayshar Y, McKay RD, Michalska AE, Mikkola M, Mileikovsky M, Minger SL, Moore HD, Mummery CL, Nagy A, Nakatsuji N, O'Brien CM, Oh SK, Olsson C, Otonkoski T, Quietschal-Tiger, Park KY, Passier R, Patel H, Patel M, Pedersen R, Pera MF, Piekarczyk MS, Pera RA,

	Reubinoff BE, Robins AJ, Rossant J, Rugg-Gunn P, Schulz TC, Semb H, Sherrer ES, Siemen H, Stacey GN, Stojkovic M, Suemori H, Szatkiewicz J, Turetsky T, Tuuri T, van den Brink S, Vintersten K, Vuoristo S, Ward D, Weaver TA, Young LA, Zhang W (2007) Characterization of human embryonic stem cell lines by the International Stem Cell Initiative. Nat Biotechnol 25(7):803-16. PubMed PMID: 17572666
International Stem Cell Initiative Consortium, 2010	International Stem Cell Initiative Consortium (22 Collaborators) Akopian V, Andrews PW, Beil S, Benvenisty N, Brehm J, Christie M, Ford A, Fox V, Gokhale PJ, Healy L, Holm F, Hovatta O, Knowles BB, Ludwig TE, McKay RD, Miyazaki T, Nakatsuji N, Oh SK, Pera MF, Rossant J, Stacey GN, Suemori H (2010) Comparison of defined culture systems for feeder cell free propagation of human embryonic stem cells. In Vitro Cell Dev Biol Anim 46(3-4):247-58. PubMed PMID: 20186512
Itskovitz-Eldor et al., 2000	Itskovitz-Eldor J, Schuldiner M, Karsenti D, Eden A, Yanuka O, Amit M, Soreq H, Benvenisty N (2000) Differentiation of human embryonic stem cells into embryoid bodies compromising the three embryonic germ layers. Mol Med 6(2):88-95. PubMed PMID: 10859025
Itsykson et al., 2005	Itsykson P, Ilouz N, Turetsky T, Goldstein RS, Pera MF, Fishbein I, Segal M, Reubinoff BE (2005) Derivation of neural precursors from human embryonic stem cells in the presence of noggin. Mol Cell Neurosci 30(1):24-36. PubMed PMID: 16081300
James et al., 2005	James D, Levine AJ, Besser D, Hemmati-Brivanlou A (2005) TGFbeta/activin/nodal signaling is necessary for the maintenance of pluripotency in human embryonic stem cells. Development 132(6):1273-82. PubMed PMID: 15703277
Janatpour et al., 2000	Janatpour MJ, McMaster MT, Genbacev O, Zhou Y, Dong J, Cross JC, Israel MA, Fisher SJ (2000) Id-2 regulates critical aspects of human cytotrophoblast differentiation, invasion and migration. Development 127(3):549-58. PubMed PMID: 10631176
Jin et al., 2003	Jin H, Wu H, Osterhaus G, Wei J, Davis K, Sha D, Floor E, Hsu CC, Kopke RD, Wu JY (2003) Demonstration of functional coupling between gamma -aminobutyric acid (GABA) synthesis and vesicular GABA transport into synaptic vesicles. Proc Natl Acad Sci U S A 100(7):4293-8. PubMed PMID: 12634427
Jinno et al., 1995	Jinno Y, Ikeda Y, Yun K, Maw M, Masuzaki H, Fukuda H, Inuzuka K, Fujishita A, Ohtani Y, Okimoto T, Ishimaru T, Niikawa N (1995) Establishment of functional imprinting of the H19 gene in human developing placentae. Nat Genet 10(3):318-24. PubMed PMID: 7670470
Josephson et al., 2007	Josephson R, Ording CJ, Liu Y, Shin S, Lakshmipathy U, Toumadje A, Love B, Chesnut JD, Andrews PW, Rao MS, Auerbach JM (2007) Qualification of embryonal carcinoma 2102Ep as a reference for human embryonic stem cell research. Stem Cells 25(2):437-46. PubMed PMID: 17284651
Jozefczuk et al., 2011	Jozefczuk J, Prigione A, Chavez L, Adjaye J (2011) Comparative analysis of human embryonic stem cell and induced pluripotent stem cell-derived hepatocyte-like cells reveals current drawbacks and possible strategies for improved differentiation. Stem Cells Dev 20(7):1259-75. PubMed PMID: 21162674
Jozefczuk et al., 2012	Jozefczuk J, Drews K, Adjaye J (2012) Preparation of mouse embryonic fibroblast cells suitable for culturing human embryonic and induced pluripotent stem cells. J Vis Exp (64): 3854. PubMed PMID: 22760161
Juliano, 2002	Juliano RL (2002) Signal transduction by cell adhesion receptors and the cytoskeleton: functions of integrins, cadherins, selectins, and immunoglobulin-superfamily members. Annu Rev Pharmacol Toxicol 42:283-323. Review. PubMed PMID: 11807174
Jung et al., 2010	Jung M, Peterson H, Chavez L, Kahlem P, Lehrach H, Vilo J, Adjaye J (2010) A data integration approach to mapping OCT4 gene regulatory networks operative in embryonic stem cells and embryonal carcinoma cells. PLoS One 5(5):e10709. PubMed PMID: 20505756
Kanehisa and Goto, 2000	Kanehisa M, Goto S (2000) KEGG: kyoto encyclopedia of genes and genomes. Nucleic Acids Res 28(1):27-30. PubMed PMID: 10592173
Kang et al., 2009	Kang L, Wang J, Zhang Y, Kou Z, Gao S (2009) iPS cells can support full-term development of tetraploid blastocyst-complemented embryos. Cell Stem Cell 5(2):135-8. PubMed PMID: 19631602
Karatan and Watnick, 2009	Karatan E, Watnick P (2009) Signals, regulatory networks, and materials that build and break bacterial biofilms. Microbiol Mol Biol Rev 73(2):310-47. Review. PubMed PMID: 19487730
Karaulanov et al., 2004	Karaulanov E, Knöchel W, Niehrs C (2004) Transcriptional regulation of BMP4 synexpression in transgenic Xenopus. EMBO J 23(4):844-56. PubMed PMID: 14963489
Kato et al., 2008	Kato T, Sato N, Takano A, Miyamoto M, Nishimura H, Tsuchiya E, Kondo S, Nakamura Y, Daigo Y (2008) Activation of placenta-specific transcription factor distal-less homeobox 5 predicts clinical outcome in primary lung cancer patients. Clin Cancer Res 14(8):2363-70. PubMed PMID: 18413826
Kee et al., 2006	Kee K, Gonsalves JM, Clark AT, Pera RA (2006) Bone morphogenetic proteins induce germ cell differentiation from human embryonic stem cells. Stem Cells Dev 15(6):831-7. PubMed PMID: 17253946
Kim et al., 1994	Kim NW, Piatyszek MA, Prowse KR, Harley CB, West MD, Ho PL, Coviello GM, Wright WE, Weinrich SL, Shay JW (1994) Specific association of human telomerase activity with immortal cells and cancer. Science 266(5193):2011-5. PubMed PMID: 7605428
Kim et al., 2010	Kim K, Doi A, Wen B, Ng K, Zhao R, Cahan P, Kim J, Aryee MJ, Ji H, Ehrlich LI, Yabuuchi A, Takeuchi A, Cunniff KC, Hongguang H, McKinney-Freeman S, Naveiras O, Yoon TJ, Irizarry RA, Jung N, Seita J, Hanna J, Murakami P, Jaenisch R, Weissleder R, Orkin SH, Weissman IL, Feinberg AP, Daley GQ (2010) Epigenetic memory in induced pluripotent stem cells. Nature 467(7313):285-90. PubMed PMID: 20644535
King et al., 1994	King JA, Marker PC, Seung KJ, Kingsley DM (1994) BMP5 and the molecular, skeletal, and soft-tissue alterations in short ear mice. Dev Biol 166(1):112-22. PubMed PMID: 7958439
King et al., 2000	King A, Thomas L, Bischof P (2000) Cell culture models of trophoblast II: trophoblast cell lines—a workshop report. Placenta. 21 Suppl A:S113-9. PubMed PMID: 10831135
King et al., 2008	King CC, Beattie GM, Lopez AD, Hayek A (2008) Generation of definitive endoderm from human embryonic stem cells cultured in feeder layer-free conditions. Regen Med 3(2):175-80. PubMed PMID:

	[18307401](#)
Kishigami and Mishina, 2005	Kishigami S, Mishina Y (2005) BMP signaling and early embryonic patterning. Cytokine Growth Factor Rev 16(3):265-78. Review. [PubMed PMID: 15871922](#)
Kitamura et al., 2003	Kitamura T, Koshino Y, Shibata F, Oki T, Nakajima H, Nosaka T, Kumagai H (2003) Retrovirus-mediated gene transfer and expression cloning: powerful tools in functional genomics. Exp Hematol 31(11):1007-14. Review. [PubMed PMID: 14585362](#)
Kleinman et al., 1982	Kleinman HK, McGarvey ML, Liotta LA, Robey PG, Tryggvason K, Martin GR (1982) Isolation and characterization of type IV procollagen, laminin, and heparan sulfate proteoglycan from the EHS sarcoma. Biochemistry 21(24):6188-93. [PubMed PMID: 6217835](#)
Knipp et al., 1999	Knipp GT, Audus KL, Soares MJ. Nutrient transport across the placenta (1999) Adv Drug Deliv Rev 38(1):41-58. Review. [PubMed PMID: 10837745](#)
Knöfler et al., 1998	Knöfler M, Meinhardt G, Vasicek R, Husslein P, Egarter C (1998) Molecular cloning of the human Hand1 gene/cDNA and its tissue-restricted expression in cytotrophoblastic cells and heart. Gene 224(1-2):77-86. [PubMed PMID: 9931445](#)
Knöfler et al., 2002	Knöfler M, Meinhardt G, Bauer S, Loregger T, Vasicek R, Bloor DJ, Kimber SJ, Husslein P (2002) Human Hand1 basic helix-loop-helix (bHLH) protein: extra-embryonic expression pattern, interaction partners and identification of its transcriptional repressor domains. Biochem J 361(Pt 3):641-51. [PubMed PMID: 11802795](#)
Knöfler, 2010	Knöfler M (2010) Critical growth factors and signalling pathways controlling human trophoblast invasion. Int J Dev Biol 54(2-3):269-80. Review. [PubMed PMID: 19876833](#)
Krause et al., 2011	Krause C, Guzman A, Knaus P (2011) Noggin. Int J Biochem Cell Biol 43(4):478-81. Review. [PubMed PMID: 21256973](#)
Kubista et al., 2006	Kubista M, Andrade JM, Bengtsson M, Forootan A, Jonák J, Lind K, Sindelka R, Sjöback R, Sjögreen B, Strömbom L, Ståhlberg A, Zoric N (2006) The real-time polymerase chain reaction. Mol Aspects Med 27(2-3):95-125. Review. [PubMed PMID: 16460794](#)
Kuhn et al., 2004	Kuhn K, Baker SC, Chudin E, Lieu MH, Oeser S, Bennett H, Rigault P, Barker D, McDaniel TK, Chee MS (2004) A novel, high-performance random array platform for quantitative gene expression profiling. Genome Res 14(11):2347-56. [PubMed PMID: 15520296](#)
Laemmli, 1970	Laemmli UK (1970) Cleavage of structural proteins during the assembly of the head of bacteriophage T4. Nature 227(5259):680-5. [PubMed PMID: 5432063](#)
Lafond and Simoneau, 2006	Lafond J, Simoneau L (2006) Calcium homeostasis in human placenta: role of calcium-handling proteins. Int Rev Cytol 250:109-74. Review. [PubMed PMID: 16861065](#)
Lam et al., 2005	Lam C, Lim KH, Karumanchi SA (2005) Circulating angiogenic factors in the pathogenesis and prediction of preeclampsia. Hypertension 46(5):1077-85. Review. [PubMed PMID: 16230516](#)
Larman et al., 2012	Larman BW, Karolak MJ, Lindner V, Oxburgh L (2012) Distinct bone morphogenetic proteins activate indistinguishable transcriptional responses in nephron epithelia including Notch target genes. Cell Signal 24(1):257-64. [PubMed PMID: 21945409](#)
Laurent et al., 1998	Laurent A, Rouillac C, Delezoide AL, Giovangrandi Y, Vekemans M, Bellet D, Abitbol M, Vidaud M (1998) Insulin-like 4 (INSL4) gene expression in human embryonic and trophoblastic tissues. Mol Reprod Dev 51(2):123-9. [PubMed PMID: 9740319](#)
Lauzon et al., 2014	Lauzon MA, Daviau A, Drevelle O, Marcos B, Faucheux N (2014) Identification of a Growth Factor Mimicking the Synergistic Effect of Fetal Bovine Serum on BMP-9 Cell Response. Tissue Eng Part A 20(17-18):2524-35. [PubMed PMID: 24593122](#)
Lee et al., 2006	Lee BY, Han JA, Im JS, Morrone A, Johung K, Goodwin EC, Kleijer WJ, DiMaio D, Hwang ES (2006) Senescence-associated beta-galactosidase is lysosomal beta-galactosidase. Aging Cell 5(2):187-95. [PubMed PMID: 16626397](#)
Lee et al., 2010	Lee HJ, Snegovskikh VV, Park JS, Foyouzi N, Han KT, Hodgson EJ, Guller S, Norwitz ER (2010) Role of GnRH-GnRH receptor signaling at the maternal-fetal interface. Fertil Steril 94(7):2680-7. [PubMed PMID: 20400076](#)
Lee et al., 2013	Lee TJ, Jang J, Kang S, Jin M, Shin H, Kim DW, Kim BS (2013) Enhancement of osteogenic and chondrogenic differentiation of human embryonic stem cells by mesodermal lineage induction with BMP-4 and FGF2 treatment. Biochem Biophys Res Commun 430(2):793-7. [PubMed PMID: 23206696](#)
Lehmann, 2012	Lehmann R (2012) Germline stem cells: origin and destiny. Cell Stem Cell 10(6):729-39. Review. [PubMed PMID: 22704513](#)
Levenstein et al., 2006	Levenstein ME, Ludwig TE, Xu RH, Llanas RA, VanDenHeuvel-Kramer K, Manning D, Thomson JA (2006) Basic fibroblast growth factor support of human embryonic stem cell self-renewal. Stem Cells 24(3):568-74. [PubMed PMID: 16282444](#)
Levenstein et al., 2008	Levenstein ME, Berggren WT, Lee JE, Conard KR, Llanas RA, Wagner RJ, Smith LM, Thomson JA (2008) Secreted proteoglycans directly mediate human embryonic stem cell-basic fibroblast growth factor 2 interactions critical for proliferation. Stem Cells 26(12):3099-107. [PubMed PMID: 18802039](#)
Levine and Brivanlou, 2006	Levine AJ, Brivanlou AH (2006) GDF3, a BMP inhibitor, regulates cell fate in stem cells and early embryos. Development 133(2):209-16. [PubMed PMID: 16339188](#)
Li et al., 2013	Li Y, Moretto-Zita M, Soncin F, Wakeland A, Wolfe L, Leon-Garcia S, Pandian R, Pizzo D, Cui L, Nazor K, Loring JF, Crum CP, Laurent LC, Parast MM (2013) BMP4-directed trophoblast differentiation of human embryonic stem cells is mediated through a ΔNp63+ cytotrophoblast stem cell state. Development 140(19):3965-76. [PubMed PMID: 24004950](#)
Li and Chen, 2013	Li Z, Chen YG (2013) Functions of BMP signaling in embryonic stem cell fate determination. Exp Cell Res 319(2):113-9. Review. [PubMed PMID: 23051821](#)
Liang et al., 2010	Liang CY, Wang LJ, Chen CP, Chen LF, Chen YH, Chen H (2010) GCM1 regulation of the expression of syncytin 2 and its cognate receptor MFSD2A in human placenta. Biol Reprod 83(3):387-95. [PubMed PMID: 20484742](#)

Lichtner et al., 2013	Lichtner B, Knaus P, Lehrach H, Adjaye J (2013) BMP10 as a potent inducer of trophoblast differentiation in human embryonic and induced pluripotent stem cells. Biomaterials 34(38):9789-802. PubMed PMID: 24070570
Liu and Roberts, 1996	Liu L, Roberts RM (1996) Silencing of the gene for the beta subunit of human chorionic gonadotropin by the embryonic transcription factor Oct-3/4. J Biol Chem 271(28):16683-9. PubMed PMID: 8663260
Liu et al., 2006a	Liu Y, Song Z, Zhao Y, Qin H, Cai J, Zhang H, Yu T, Jiang S, Wang G, Ding M, Deng H (2006) A novel chemical-defined medium with bFGF and N2B27 supplements supports undifferentiated growth in human embryonic stem cells. Biochem Biophys Res Commun 346(1):131-9. PubMed PMID: 16753134
Liu et al., 2006b	Liu Y, Shin S, Zeng X, Zhan M, Gonzalez R, Mueller FJ, Schwartz CM, Xue H, Li H, Baker SC, Chudin E, Barker DL, McDaniel TK, Oeser S, Loring JF, Mattson MP, Rao MS (2006) Genome wide profiling of human embryonic stem cells (hESCs), their derivatives and embryonal carcinoma cells to develop base profiles of U.S. Federal government approved hESC lines. BMC Dev Biol 6:20. PubMed PMID: 16672070
Lundblad, 2000	Lundblad V (2000) DNA ends: maintenance of chromosome termini versus repair of double strand breaks. Mutat Res 451(1-2):227-40. Review. PubMed PMID: 10915875
Lunghi et al., 2007	Lunghi L, Ferretti ME, Medici S, Biondi C, Vesce F (2007) Control of human trophoblast function. Reprod Biol Endocrinol 5:6. Review. PubMed PMID: 17288592
Ma et al., 1997	Ma GT, Roth ME, Groskopf JC, Tsai FY, Orkin SH, Grosveld F, Engel JD, Linzer DI (1997) GATA-2 and GATA-3 regulate trophoblast-specific gene expression in vivo. Development 124(4):907-14. PubMed PMID: 9043071
Mahlapuu et al. 2001	Mahlapuu M, Ormestad M, Enerbäck S, Carlsson P (2001) The forkhead transcription factor Foxf1 is required for differentiation of extra-embryonic and lateral plate mesoderm. Development 128(2):155-66. PubMed PMID: 11124112
Mailhot et al., 2008	Mailhot G, Yang M, Mason-Savas A, Mackay CA, Leav I, Odgren PR (2008) BMP-5 expression increases during chondrocyte differentiation in vivo and in vitro and promotes proliferation and cartilage matrix synthesis in primary chondrocyte cultures. J Cell Physiol 214(1):56-64. PubMed PMID: 17541940
Malassiné and Cronier, 2002	Malassiné A, Cronier L (2002) Hormones and human trophoblast differentiation: a review. Endocrine 19(1):3-11. Review. PubMed PMID: 12583598
Manning and Cantley, 2007	Manning BD, Cantley LC (2007) AKT/PKB signaling: navigating downstream. Cell 129(7):1261-74. Review. PubMed PMID: 17604717
Mannucci et al., 1994	Mannucci A, Sullivan KM, Ivanov PL, Gill P (1994) Forensic application of a rapid and quantitative DNA sex test by amplification of the X-Y homologous gene amelogenin. Int J Legal Med 106(4):190-3. PubMed PMID: 8038111
Marchand et al., 2011	Marchand M, Horcajadas JA, Esteban FJ, McElroy SL, Fisher SJ, Giudice LC (2011) Transcriptomic signature of trophoblast differentiation in a human embryonic stem cell model. Biol Reprod 84(6):1258-71. PubMed PMID: 21368299
Marom at al., 2011	Marom B, Heining E, Knaus P, Henis YI (2011) Formation of stable homomeric and transient heteromeric bone morphogenetic protein (BMP) receptor complexes regulates Smad protein signaling. J Biol Chem 286(22):19287-96. PubMed PMID: 21471205
Matsumoto et al., 2012	Matsumoto Y, Otsuka F, Hino J, Miyoshi T, Takano M, Miyazato M, Makino H, Kangawa K (2012) Bone morphogenetic protein-3b (BMP-3b) inhibits osteoblast differentiation via Smad2/3 pathway by counteracting Smad1/5/8 signaling. Mol Cell Endocrinol 350(1):78-86. PubMed PMID: 22155034
Maynard et al., 2008	Maynard S, Swistowska AM, Lee JW, Liu Y, Liu ST, Da Cruz AB, Rao M, de Souza-Pinto NC, Zeng X, Bohr VA (2008) Human embryonic stem cells have enhanced repair of multiple forms of DNA damage. Stem Cells 26(9):2266-74. PubMed PMID: 18566332
Mazerbourg et al., 2004	Mazerbourg S, Klein C, Roh J, Kaivo-Oja N, Mottershead DG, Korchynskyi O, Ritvos O, Hsueh AJ (2004) Growth differentiation factor-9 signaling is mediated by the type I receptor, activin receptor-like kinase 5. Mol Endocrinol 18(3):653-65. PubMed PMID: 14684852
McDevitt and Palecek, 2008	McDevitt TC, Palecek SP (2008) Innovation in the culture and derivation of pluripotent human stem cells. Curr Opin Biotechnol 19(5):527-33. Review. PubMed PMID: 18760357
McMaster et al., 1995	McMaster MT, Librach CL, Zhou Y, Lim KH, Janatpour MJ, DeMars R, Kovats S, Damsky C, Fisher SJ (1995) Human placental HLA-G expression is restricted to differentiated cytotrophoblasts. J Immunol 154(8):3771-8. PubMed PMID: 7706718
Messam et al., 2000	Messam CA, Hou J, Major EO (2000) Coexpression of nestin in neural and glial cells in the developing human CNS defined by a human-specific anti-nestin antibody. Exp Neurol 161(2):585-96. PubMed PMID: 10686078
Mi and Thomas, 2009	Mi H, Thomas P (2009) PANTHER pathway: an ontology-based pathway database coupled with data analysis tools. Methods Mol Biol 563:123-40. PubMed PMID: 19597783
Miyama et al., 1999	Miyama K, Yamada G, Yamamoto TS, Takagi C, Miyado K, Sakai M, Ueno N, Shibuya H (1999) A BMP-inducible gene, dlx5, regulates osteoblast differentiation and mesoderm induction. Dev Biol 208(1):123-33. PubMed PMID: 10075846
Miyazono et al., 2005	Miyazono K, Maeda S, Imamura T (2005) BMP receptor signaling: transcriptional targets, regulation of signals, and signaling cross-talk. Cytokine Growth Factor Rev 16(3):251-63. Review. PubMed PMID: 15871923
Miyazono et al., 2010	Miyazono K, Kamiya Y, Morikawa M (2010) Bone morphogenetic protein receptors and signal transduction. J Biochem 147(1):35-51. PubMed PMID: 19762341
Mondello and Scovassi, 2004	Mondello C, Scovassi AI (2004) Telomeres, telomerase, and apoptosis. Biochem Cell Biol 82(4):498-507. Review. PubMed PMID: 15284903
Moore and Haig, 1991	Moore T, Haig D (1991) Genomic imprinting in mammalian development: a parental tug-of-war. Trends Genet 7(2):45-9. Review. PubMed PMID: 2035190
Moore and Best, 2001	Moore CM, Best RG (2001) Chromosome Preparation and Banding. In: Encyclopedia of Life Sciences, Nature Publishing Group / John Wiley & Sons Ltd.

Moustakas and Heldin, 2009	Moustakas A, Heldin CH (2009) The regulation of TGFbeta signal transduction. Development 136(22):3699-714. Review. PubMed PMID: 19855013
Mühlhauser et al., 1995	Mühlhauser J, Crescimanno C, Kasper M, Zaccheo D, Castellucci M (1995) Differentiation of human trophoblast populations involves alterations in cytokeratin patterns. J Histochem Cytochem 43(6):579-89. PubMed PMID: 7539466
Murphy and Polak, 2002	Murphy CL, Polak JM (2002) Differentiating embryonic stem cells: GAPDH, but neither HPRT nor beta-tubulin is suitable as an internal standard for measuring RNA levels. Tissue Eng 8(4):551-9. PubMed PMID: 12201995
Murry and Keller, 2008	Murry CE, Keller G (2008) Differentiation of embryonic stem cells to clinically relevant populations: lessons from embryonic development. Cell 132(4):661-80. Review. PubMed PMID: 18295582
Muyan and Boime, 1997	Muyan M, Boime I (1997) Secretion of chorionic gonadotropin from human trophoblasts. Placenta 18(4):237-41. Review. PubMed PMID: 9179915
Nakagawa et al., 2009	Nakagawa T, Lee SY, Reddi AH (2009) Induction of chondrogenesis from human embryonic stem cells without embryoid body formation by bone morphogenetic protein 7 and transforming growth factor beta1. Arthritis Rheum 60(12):3686-92. PubMed PMID: 19950276
Nazarenko et al., 1997	Nazarenko IA, Bhatnagar SK, Hohman RJ (1997) A closed tube format for amplification and detection of DNA based on energy transfer. Nucleic Acids Res 25(12):2516-21. PubMed PMID: 9171107
Neuhaus et al., 1999	Neuhaus H, Rosen V, Thies RS (1999) Heart specific expression of mouse BMP-10 a novel member of the TGF-beta superfamily. Mech Dev 80(2):181-4. PubMed PMID: 10072785
Nickel et al., 2009	Nickel J, Sebald W, Groppe JC, Mueller TD (2009) Intricacies of BMP receptor assembly. Cytokine Growth Factor Rev 20(5-6):367-77. Review. PubMed PMID: 19926516
Nifuji and Noda, 1999	Nifuji A, Noda M (1999) Coordinated expression of noggin and bone morphogenetic proteins (BMPs) during early skeletogenesis and induction of noggin expression by BMP-7. J Bone Miner Res 14(12):2057-66. PubMed PMID: 10620065
Niwa et al., 2005	Niwa H, Toyooka Y, Shimosato D, Strumpf D, Takahashi K, Yagi R, Rossant J (2005) Interaction between Oct3/4 and Cdx2 determines trophectoderm differentiation. Cell 123(5):917-29. PubMed PMID: 16325584
Nohe et al., 2002	Nohe A, Hassel S, Ehrlich M, Neubauer F, Sebald W, Henis YI, Knaus P (2002) The mode of bone morphogenetic protein (BMP) receptor oligomerization determines different BMP-2 signaling pathways. J Biol Chem 277(7):5330-8. PubMed PMID: 11714695
Nowrouzi et al., 2011	Nowrouzi A, Glimm H, von Kalle C, Schmidt M (2011) Retroviral vectors: post entry events and genomic alterations. Viruses 3(5):429-55. Review. PubMed PMID: 21994741
Oda, 1999	Oda Y (1999) Choline acetyltransferase: the structure, distribution and pathologic changes in the central nervous system. Pathol Int 49(11):921-37. Review. PubMed PMID: 10594838
Ohnuki et al., 2009	Ohnuki M, Takahashi K, Yamanaka S (2009) Generation and characterization of human induced pluripotent stem cells. Curr Protoc Stem Cell Biol Chapter 4:Unit 4A.2. PubMed PMID: 19536759
Okano et al., 2013	Okano H, Nakamura M, Yoshida K, Okada Y, Tsuji O, Nori S, Ikeda E, Yamanaka S, Miura K (2013) Steps toward safe cell therapy using induced pluripotent stem cells. Circ Res 112(3):523-33. Review. PubMed PMID: 23371901
Okita et al., 2007	Okita K, Ichisaka T, Yamanaka S (2007) Generation of germline-competent induced pluripotent stem cells. Nature 448(7151):313-7. PubMed PMID: 17554338
Oren-Suissa and Podbilewicz, 2007	Oren-Suissa M, Podbilewicz B (2007) Cell fusion during development. Trends Cell Biol 17(11):537-46. Review. PubMed PMID: 17981036
Pang and Xing, 2003	Pang ZJ, Xing FQ (2003) Expression profile of trophoblast invasion-associated genes in the pre-eclamptic placenta. Br J Biomed Sci 60(2):97-101. PubMed PMID: 12866918
Panula et al., 2011	Panula S, Medrano JV, Kee K, Bergström R, Nguyen HN, Byers B, Wilson KD, Wu JC, Simon C, Hovatta O, Reijo Pera RA (2011) Human germ cell differentiation from fetal- and adult-derived induced pluripotent stem cells. Hum Mol Genet 20(4):752-62. PubMed PMID: 21131292
Park and Morasso, 2002	Park GT, Morasso MI (2002) Bone morphogenetic protein-2 (BMP-2) transactivates Dlx3 through Smad1 and Smad4: alternative mode for Dlx3 induction in mouse keratinocytes. Nucleic Acids Res 30(2):515-22. PubMed PMID: 11788714
Park et al., 2008	Park IH, Zhao R, West JA, Yabuuchi A, Huo H, Ince TA, Lerou PH, Lensch MW, Daley GQ (2008) Reprogramming of human somatic cells to pluripotency with defined factors. Nature 451(7175):141-6. PubMed PMID: 18157115
Paulsen et al., 2011	Paulsen M, Legewie S, Eils R, Karaulanov E, Niehrs C (2011) Negative feedback in the bone morphogenetic protein 4 (BMP4) synexpression group governs its dynamic signaling range and canalizes development. Proc Natl Acad Sci U S A 108(25):10202-7. PubMed PMID: 21633009
Pazmany et al., 1996	Pazmany L, Mandelboim O, Valés-Gómez M, Davis DM, Reyburn HT, Strominger JL (1996) Protection from natural killer cell-mediated lysis by HLA-G expression on target cells. Science 274(5288):792-5. PubMed PMID: 8864122
Pearce and Evans, 1999	Pearce JJ, Evans MJ (1999) Mml, a mouse Mix-like gene expressed in the primitive streak. Mech Dev 87(1-2):189-92. PubMed PMID: 10495285
Peng and Payne, 2002	Peng L, Payne AH (2002) AP-2 gamma and the homeodomain protein distal-less 3 are required for placental-specific expression of the murine 3 beta-hydroxysteroid dehydrogenase VI gene, Hsd3b6. J Biol Chem 277(10):7945-54. PubMed PMID: 11773066
Peng et al., 2004	Peng L, Huang Y, Jin F, Jiang SW, Payne AH (2004) Transcription enhancer factor-5 and a GATA-like protein determine placental-specific expression of the Type I human 3beta-hydroxysteroid dehydrogenase gene, HSD3B1. Mol Endocrinol 18(8):2049-60. PubMed PMID: 15131259
Pera et al., 2004	Pera MF, Andrade J, Houssami S, Reubinoff B, Trounson A, Stanley EG, Ward-van Oostwaard D, Mummery C (2004) Regulation of human embryonic stem cell differentiation by BMP-2 and its antagonist noggin. J Cell Sci 117(Pt 7):1269-80. PubMed PMID: 14996946

143

Perrin and Ervasti, 2010	Perrin BJ, Ervasti JM (2010) The actin gene family: function follows isoform. Cytoskeleton (Hoboken) 67(10):630-4. Review. PubMed PMID: 20737541
Peters et al., 2007	Peters JL, Dufner-Beattie J, Xu W, Geiser J, Lahner B, Salt DE, Andrews GK (2007) Targeting of the mouse Slc39a2 (Zip2) gene reveals highly cell-specific patterns of expression, and unique functions in zinc, iron, and calcium homeostasis. Genesis 45(6):339-52. PubMed PMID: 17506078
Pötgens et al., 2004	Pötgens AJ, Drewlo S, Kokozidou M, Kaufmann P (2004) Syncytin: the major regulator of trophoblast fusion? Recent developments and hypotheses on its action. Hum Reprod Update 10(6):487-96. Review. PubMed PMID: 15333590
Prigione et al., 2011a	Prigione A, Hossini AM, Lichtner B, Serin A, Fauler B, Megges M, Lurz R, Lehrach H, Makrantonaki E, Zouboulis CC, Adjaye J (2011) Mitochondrial-associated cell death mechanisms are reset to an embryonic-like state in aged donor-derived iPS cells harboring chromosomal aberrations. PLoS One 6(11):e27352. PubMed PMID: 22110631
Prigione et al., 2011b	Prigione A, Lichtner B, Kuhl H, Struys EA, Wamelink M, Lehrach H, Ralser M, Timmermann B, Adjaye J (2011) Human induced pluripotent stem cells harbor homoplasmic and heteroplasmic mitochondrial DNA mutations while maintaining human embryonic stem cell-like metabolic reprogramming. Stem Cells 29(9):1338-48. PubMed PMID: 21732474
Pruitt et al., 2005	Pruitt KD, Tatusova T, Maglott DR (2005) NCBI Reference Sequence (RefSeq): a curated non-redundant sequence database of genomes, transcripts and proteins. Nucleic Acids Res 33(Database issue):D501-4. PubMed PMID: 15608248
Qiu et al., 2010	Qiu C, Ma Y, Wang J, Peng S, Huang Y (2010) Lin28-mediated post-transcriptional regulation of Oct4 expression in human embryonic stem cells. Nucleic Acids Res 38(4):1240-8. PubMed PMID: 19966271
Quinn et al., 2000	Quinn LM, Latham SE, Kalionis B (2000) The homeobox genes MSX2 and MOX2 are candidates for regulating epithelial-mesenchymal cell interactions in the human placenta. Placenta 21 Suppl A:S50-4. PubMed PMID: 10831122
Red-Horse et al., 2004	Red-Horse K, Zhou Y, Genbacev O, Prakobphol A, Foulk R, McMaster M, Fisher SJ (2004) Trophoblast differentiation during embryo implantation and formation of the maternal-fetal interface. J Clin Invest 114(6):744-54. Review. PubMed PMID: 15372095
Reubinoff et al., 2000	Reubinoff BE, Pera MF, Fong CY, Trounson A, Bongso A (2000) Embryonic stem cell lines from human blastocysts: somatic differentiation in vitro. Nat Biotechnol 18(4):399-404. PubMed PMID: 10748519
Ricard et al., 2012	Ricard N, Ciais D, Levet S, Subileau M, Mallet C, Zimmers TA, Lee SJ, Bidart M, Feige JJ, Bailly S (2012) BMP9 and BMP10 are critical for postnatal retinal vascular remodeling. Blood 119(25):6162-71. PubMed PMID: 22566602
Riley et al., 1998	Riley P, Anson-Cartwright L, Cross JC (1998) The Hand1 bHLH transcription factor is essential for placentation and cardiac morphogenesis. Nat Genet 18(3):271-5. PubMed PMID: 9500551
Rivera-Pérez and Magnuson, 2005	Rivera-Pérez JA, Magnuson T (2005) Primitive streak formation in mice is preceded by localized activation of Brachyury and Wnt3. Dev Biol 288(2):363-71. PubMed PMID: 16289026
Robb et al., 2000	Robb L, Hartley L, Begley CG, Brodnicki TC, Copeland NG, Gilbert DJ, Jenkins NA, Elefanty AG (2000) Cloning, expression analysis, and chromosomal localization of murine and human homologues of a Xenopus mix gene. Dev Dyn 219(4):497-504. PubMed PMID: 11084649
Robbins et al., 2010	Robbins JR, Skrzypczynska KM, Zeldovich VB, Kapidzic M, Bakardjiev AI (2010) Placental syncytiotrophoblast constitutes a major barrier to vertical transmission of Listeria monocytogenes. PLoS Pathog 6(1):e1000732. PubMed PMID: 20107601
Roberts, 2001	Roberts RJ (2001) PubMed Central: The GenBank of the published literature. Proc Natl Acad Sci U S A 98(2):381-2. PubMed PMID: 11209037
Roberts et al., 2002	Roberts JR, Rowe PA, Demaine AG (2002) Activation of NF-kappaB and MAP kinase cascades by hypothermic stress in endothelial cells. Cryobiology 44(2):161-9. PubMed PMID: 12151271
Roberts and Fisher, 2011	Roberts RM, Fisher SJ. Trophoblast stem cells (2011) Biol Reprod 84(3):412-21. Review. PubMed PMID: 21106963
Roberts et al., 2014	Roberts RM, Loh K, Amita M, Bernardo AS, Adachi K, Alexenko AP, Schust D, Schulz LC, Telugu B, Ezashi T, Pedersen RA (2014) Differentiation of Trophoblast Cells from Human Embryonic Stem Cells: To be or not to be? Reproduction 147(5):D1-D12. Debate. PubMed PMID: 24518070
Rodda et al., 2005	Rodda DJ, Chew JL, Lim LH, Loh YH, Wang B, Ng HH, Robson P (2005) Transcriptional regulation of nanog by OCT4 and SOX2. J Biol Chem 280(26):24731-7. PubMed PMID: 15860457
Romero-Calvo et al., 2010	Romero-Calvo I, Ocón B, Martínez-Moya P, Suárez MD, Zarzuelo A, Martínez-Augustin O, de Medina FS (2010) Reversible Ponceau staining as a loading control alternative to actin in Western blots. Anal Biochem 401(2):318-20. PubMed PMID: 20206115
Rush and Geffen, 1980	Rush RA, Geffen LB (1980) Dopamine beta-hydroxylase in health and disease. Crit Rev Clin Lab Sci 12(3):241-77. Review. PubMed PMID: 6998654
Saeed et al., 2006	Saeed AI, Bhagabati NK, Braisted JC, Liang W, Sharov V, Howe EA, Li J, Thiagarajan M, White JA, Quackenbush J (2006) TM4 microarray software suite. Methods Enzymol 411:134-93. Review. PubMed PMID: 16939790
Saiki et al., 1988	Saiki RK, Gelfand DH, Stoffel S, Scharf SJ, Higuchi R, Horn GT, Mullis KB, Erlich HA (1988) Primer-directed enzymatic amplification of DNA with a thermostable DNA polymerase. Science 239(4839):487-91. PubMed PMID: 2448875
Sansom et al., 2009	Sansom SN, Griffiths DS, Faedo A, Kleinjan DJ, Ruan Y, Smith J, van Heyningen V, Rubenstein JL, Livesey FJ (2009) The level of the transcription factor Pax6 is essential for controlling the balance between neural stem cell self-renewal and neurogenesis. PLoS Genet 5(6):e1000511. PubMed PMID: 19521500
Santos et al., 1998	Santos FR, Pandya A, Tyler-Smith C (1998) Reliability of DNA-based sex tests. Nat Genet 18(2):103. PubMed PMID: 9462733
Sapir et al., 2008	Sapir A, Avinoam O, Podbilewicz B, Chernomordik LV (2008) Viral and developmental cell fusion mechanisms: conservation and divergence. Dev Cell 14(1):11-21. Review. PubMed PMID: 18194649

Schena et al., 1995	Schena M, Shalon D, Davis RW, Brown PO (1995) Quantitative monitoring of gene expression patterns with a complementary DNA microarray. Science 270(5235):467-70. PubMed PMID: 7569999
Schmid et al., 2010	Schmid R, Baum P, Ittrich C, Fundel-Clemens K, Huber W, Brors B, Eils R, Weith A, Mennerich D, Quast K (2010) Comparison of normalization methods for Illumina BeadChip HumanHT-12 v3. BMC Genomics 11:349. PubMed PMID: 20525181
Schmierer and Hill, 2007	Schmierer B, Hill CS (2007) TGFbeta-SMAD signal transduction: molecular specificity and functional flexibility. Nat Rev Mol Cell Biol 8(12):970-82. Review. PubMed PMID: 18000526
Schmittgen and Livak, 2008	Schmittgen TD, Livak KJ (2008) Analyzing real-time PCR data by the comparative C(T) method. Nat Protoc 3(6):1101-8. PubMed PMID: 18546601
Schwaerzer et al., 2012	Schwaerzer GK, Hiepen C, Schrewe H, Nickel J, Ploeger F, Sebald W, Mueller T, Knaus P (2012) New insights into the molecular mechanism of multiple synostoses syndrome (SYNS): mutation within the GDF5 knuckle epitope causes noggin-resistance. J Bone Miner Res 27(2):429-42. PubMed PMID: 21976273
Seemann et al., 2009	Seemann P, Brehm A, König J, Reissner C, Stricker S, Kuss P, Haupt J, Renninger S, Nickel J, Sebald W, Groppe JC, Plöger F, Pohl J, Schmidt-von Kegler M, Walther M, Gassner I, Rusu C, Janecke AR, Dathe K, Mundlos S (2009) Mutations in GDF5 reveal a key residue mediating BMP inhibition by NOGGIN. PLoS Genet 5(11):e1000747. PubMed PMID: 19956691
Shao et al., 2009	Shao L, Feng W, Sun Y, Bai H, Liu J, Currie C, Kim J, Gama R, Wang Z, Qian Z, Liaw L, Wu WS (2009) Generation of iPS cells using defined factors linked via the self-cleaving 2A sequences in a single open reading frame. Cell Res 19(3):296-306. PubMed PMID: 19238173
Sharff et al., 2009	Sharff KA, Song WX, Luo X, Tang N, Luo J, Chen J, Bi Y, He BC, Huang J, Li X, Jiang W, Zhu GH, Su Y, He Y, Shen J, Wang Y, Chen L, Zuo GW, Liu B, Pan X, Reid RR, Luu HH, Haydon RC, He TC (2009) Hey1 basic helix-loop-helix protein plays an important role in mediating BMP9-induced osteogenic differentiation of mesenchymal progenitor cells. J Biol Chem 284(1):649-59. PubMed PMID: 18986983
Sherwood et al., 1988	Sherwood SW, Rush D, Ellsworth JL, Schimke RT (1988) Defining cellular senescence in IMR-90 cells: a flow cytometric analysis. Proc Natl Acad Sci U S A 85(23):9086-90. PubMed PMID: 3194411
Sieber et al., 2009	Sieber C, Kopf J, Hiepen C, Knaus P (2009) Recent advances in BMP receptor signaling. Cytokine Growth Factor Rev 20(5-6):343-55. Review. PubMed PMID: 19897402
Sievers et al., 2011	Sievers F, Wilm A, Dineen D, Gibson TJ, Karplus K, Li W, Lopez R, McWilliam H, Remmert M, Söding J, Thompson JD, Higgins DG (2011) Fast, scalable generation of high-quality protein multiple sequence alignments using Clustal Omega. Mol Syst Biol 7:539. PubMed PMID: 21988835
Smith et al., 1985	Smith PK, Krohn RI, Hermanson GT, Mallia AK, Gartner FH, Provenzano MD, Fujimoto EK, Goeke NM, Olson BJ, Klenk DC (1985) Measurement of protein using bicinchoninic acid. Anal Biochem 150(1):76-85. Erratum in: Anal Biochem 1987 May 15;163(1):279. PubMed PMID: 3843705
Solloway and Robertson, 1999	Solloway MJ, Robertson EJ (1999) Early embryonic lethality in Bmp5;Bmp7 double mutant mice suggests functional redundancy within the 60A subgroup. Development 126(8):1753-68. PubMed PMID: 10079236
Song et al., 2009	Song Z, Cai J, Liu Y, Zhao D, Yong J, Duo S, Song X, Guo Y, Zhao Y, Qin H, Yin X, Wu C, Che J, Lu S, Ding M, Deng H (2009) Efficient generation of hepatocyte-like cells from human induced pluripotent stem cells. Cell Res 19(11):1233-42. PubMed PMID: 19736565
Song et al., 2010a	Song G, Bailey DW, Dunlap KA, Burghardt RC, Spencer TE, Bazer FW, Johnson GA (2010) Cathepsin B, cathepsin L, and cystatin C in the porcine uterus and placenta: potential roles in endometrial/placental remodeling and in fluid-phase transport of proteins secreted by uterine epithelia across placental areolae. Biol Reprod 82(5):854-64. PubMed PMID: 20107207
Song et al., 2010b	Song K, Krause C, Shi S, Patterson M, Suto R, Grgurevic L, Vukicevic S, van Dinther M, Falb D, Ten Dijke P, Alaoui-Ismaili MH (2010) Identification of a key residue mediating bone morphogenetic protein (BMP)-6 resistance to noggin inhibition allows for engineered BMPs with superior agonist activity. J Biol Chem 285(16):12169-80. PubMed PMID: 20048150
Sperger et al., 2003	Sperger JM, Chen X, Draper JS, Antosiewicz JE, Chon CH, Jones SB, Brooks JD, Andrews PW, Brown PO, Thomson JA (2003) Gene expression patterns in human embryonic stem cells and human pluripotent germ cell tumors. Proc Natl Acad Sci U S A 100(23):13350-5. PubMed PMID: 14595015
Staun-Ram and Shalev, 2005	Staun-Ram E, Shalev E (2005) Human trophoblast function during the implantation process. Reprod Biol Endocrinol 3:56. Review. PubMed PMID: 16236179
Strumpf et al., 2005	Strumpf D, Mao CA, Yamanaka Y, Ralston A, Chawengsaksophak K, Beck F, Rossant J (2005) Cdx2 is required for correct cell fate specification and differentiation of trophectoderm in the mouse blastocyst. Development 132(9):2093-102. PubMed PMID: 15788452
Sudheer et al., 2012	Sudheer S, Bhushan R, Fauler B, Lehrach H, Adjaye J (2012) FGF inhibition directs BMP4-mediated differentiation of human embryonic stem cells to syncytiotrophoblast. Stem Cells Dev 21(16):2987-3000. PubMed PMID: 22724507
Takahashi et al., 2007	Takahashi K, Tanabe K, Ohnuki M, Narita M, Ichisaka T, Tomoda K, Yamanaka S (2007) Induction of pluripotent stem cells from adult human fibroblasts by defined factors. Cell 131(5):861-72. PubMed PMID: 18035408
Takamori et al., 2000	Takamori S, Rhee JS, Rosenmund C, Jahn R (2000) Identification of a vesicular glutamate transporter that defines a glutamatergic phenotype in neurons. Nature 407(6801):189-94. PubMed PMID: 11001057
Takeda et al., 2012	Takeda M, Otsuka F, Takahashi H, Inagaki K, Miyoshi T, Tsukamoto N, Makino H, Lawson MA (2012) Interaction between gonadotropin-releasing hormone and bone morphogenetic protein-6 and -7 signaling in LβT2 gonadotrope cells. Mol Cell Endocrinol 348(1):147-54. PubMed PMID: 21846488
Tam and Loebel, 2007	Tam PP, Loebel DA (2007) Gene function in mouse embryogenesis: get set for gastrulation. Nat Rev Genet 8(5):368-81. Review. PubMed PMID: 17387317
Tavernier et al., 2013	Tavernier G, Mlody B, Demeester J, Adjaye J, De Smedt SC (2013) Current methods for inducing

	pluripotency in somatic cells. Adv Mater 25(20):2765-71. Review. PubMed PMID: 23529911
Teo et al., 2012	Teo AK, Ali Y, Wong KY, Chipperfield H, Sadasivam A, Poobalan Y, Tan EK, Wang ST, Abraham S, Tsuneyoshi N, Stanton LW, Dunn NR (2012) Activin and BMP4 synergistically promote formation of definitive endoderm in human embryonic stem cells. Stem Cells 30(4):631-42. PubMed PMID: 22893457
Thomson et al., 1998	Thomson JA, Itskovitz-Eldor J, Shapiro SS, Waknitz MA, Swiergiel JJ, Marshall VS, Jones JM (1998) Embryonic stem cell lines derived from human blastocysts. Science 282(5391):1145-7. Erratum in: Science 1998 Dec 4;282(5395):1827. PubMed PMID: 9804556
Thomson, 2013	Thomson M (2013) The physiological roles of placental corticotropin releasing hormone in pregnancy and childbirth. J Physiol Biochem 69(3):559-73. Review. PubMed PMID: 23385670
Tomasz, 1995	Tomasz M (1995) Mitomycin C: small, fast and deadly (but very selective). Chem Biol 2(9):575-9. Review. PubMed PMID: 9383461
Udayashankar et al., 2011	Udayashankar R, Baker D, Tuckerman E, Laird S, Li TC, Moore HD (2011) Characterization of invasive trophoblasts generated from human embryonic stem cells. Hum Reprod 26(2):398-406. PubMed PMID: 21163855
Uehara et al., 1999	Uehara H, Nardone G, Nazarenko I, Hohman RJ (1999) Detection of telomerase activity utilizing energy transfer primers: comparison with gel- and ELISA-based detection. Biotechniques 26(3):552-8. PubMed PMID: 10090999
Umulis et al., 2009	Umulis D, O'Connor MB, Blair SS (2009) The extracellular regulation of bone morphogenetic protein signaling. Development 136(22):3715-28. Review. PubMed PMID: 19855014
UniProt Consortium, 2011	UniProt Consortium (126 Collaborators) Apweiler R, Martin MJ, O'Donovan C, Magrane M, Alam-Faruque Y, Antunes R, Barrell D, Bely B, Bingley M, Binns D, Bower L, Browne P, Chan WM, Dimmer E, Eberhardt R, Fazzini F, Fedotov A, Foulger R, Garavelli J, Castro LG, Huntley R, Jacobsen J, Kleen M, Laiho K, Legge D, Lin Q, Liu W, Luo J, Orchard S, Patient S, Pichler K, Poggioli D, Pontikos N, Pruess M, Rosanoff S, Sawford T, Sehra H, Turner E, Corbett M, Donnelly M, van Rensburg P, Xenarios I, Bougueleret L, Auchincloss A, Argoud-Puy G, Axelsen K, Bairoch A, Baratin D, Blatter MC, Boeckmann B, Bolleman J, Bollondi L, Boutet E, Quintaje SB, Breuza L, Bridge A, deCastro E, Coudert E, Cusin I, Doche M, Dornevil D, Duvaud S, Estreicher A, Famiglietti L, Feuermann M, Gehant S, Ferro S, Gasteiger E, Gateau A, Gerritsen V, Gos A, Gruaz-Gumowski N, Hinz U, Hulo C, Hulo N, James J, Jimenez S, Jungo F, Kappler T, Keller G, Lara V, Lemercier P, Lieberherr D, Martin X, Masson P, Moinat M, Morgat A, Paesano S, Pedruzzi I, Pilbout S, Poux S, Pozzato M, Redaschi N, Rivoire C, Roechert B, Schneider M, Sigrist C, Sonesson K, Staehli S, Stanley E, Stutz A, Sundaram S, Tognolli M, Verbregue L, Veuthey AL, Wu CH, Arighi CN, Arminski L, Barker WC, Chen C, Chen Y, Dubey P, Huang H, Mazumder R, McGarvey P, Natale DA, Natarajan TG, Nchoutmboube J, Roberts NV, Suzek BE, Ugochukwu U, Vinayaka CR, Wang Q, Wang Y, Yeh LS, Zhang J (2011) Ongoing and future developments at the Universal Protein Resource. Nucleic Acids Res 39(Database issue):D214-9. PubMed PMID: 21051339
Urquidi et al., 2000	Urquidi V, Tarin D, Goodison S (2000) Role of telomerase in cell senescence and oncogenesis. Annu Rev Med 51:65-79. Review. PubMed PMID: 10774453
Valera et al., 2010	Valera E, Isaacs MJ, Kawakami Y, Izpisúa Belmonte JC, Choe S (2010) BMP-2/6 heterodimer is more effective than BMP-2 or BMP-6 homodimers as inductor of differentiation of human embryonic stem cells. PLoS One 5(6):e11167. PubMed PMID: 20567515
Vallier et al., 2009a	Vallier L, Touboul T, Brown S, Cho C, Bilican B, Alexander M, Cedervall J, Chandran S, Ahrlund-Richter L, Weber A, Pedersen RA (2009) Signaling pathways controlling pluripotency and early cell fate decisions of human induced pluripotent stem cells. Stem Cells 27(11):2655-66. PubMed PMID: 19688839
Vallier et al., 2009b	Vallier L, Mendjan S, Brown S, Chng Z, Teo A, Smithers LE, Trotter MW, Cho CH, Martinez A, Rugg-Gunn P, Brons G, Pedersen RA (2009) Activin/Nodal signalling maintains pluripotency by controlling Nanog expression. Development 136(8):1339-49. PubMed PMID: 19279133
van der Flier and Sonnenberg, 2001	van der Flier A, Sonnenberg A (2001) Function and interactions of integrins. Cell Tissue Res 305(3):285-98. Review. PubMed PMID: 11572082
Van Gelder et al., 1990	Van Gelder RN, von Zastrow ME, Yool A, Dement WC, Barchas JD, Eberwine JH (1990) Amplified RNA synthesized from limited quantities of heterogeneous cDNA. Proc Natl Acad Sci U S A 87(5):1663-7. PubMed PMID: 1689846
Van Hoof et al., 2009	Van Hoof D, D'Amour KA, German MS (2009) Derivation of insulin-producing cells from human embryonic stem cells. Stem Cell Res 3(2-3):73-87. Review. PubMed PMID: 19766074
Varanou et al., 2006	Varanou A, Withington SL, Lakasing L, Williamson C, Burton GJ, Hemberger M (2006) The importance of cysteine cathepsin proteases for placental development. J Mol Med (Berl) 84(4):305-17. PubMed PMID: 16440214
Vrachnis et al., 2013	Vrachnis N, Kalampokas E, Sifakis S, Vitoratos N, Kalampokas T, Botsis D, Iliodromiti Z (2013) Placental growth factor (PlGF): a key to optimizing fetal growth. J Matern Fetal Neonatal Med 26(10):995-1002. PubMed PMID: 23330778
Vukicevic et al., 1992	Vukicevic S, Kleinman HK, Luyten FP, Roberts AB, Roche NS, Reddi AH (1992) Identification of multiple active growth factors in basement membrane Matrigel suggests caution in interpretation of cellular activity related to extracellular matrix components. Exp Cell Res 202(1):1-8. PubMed PMID: 1511725
Wagner et al., 2010	Wagner DO, Sieber C, Bhushan R, Börgermann JH, Graf D, Knaus P (2010) BMPs: from bone to body morphogenetic proteins. Sci Signal 3(107):mr1. Meeting report. PubMed PMID: 20124549
Wang et al., 2005	Wang G, Zhang H, Zhao Y, Li J, Cai J, Wang P, Meng S, Feng J, Miao C, Ding M, Li D, Deng H (2005) Noggin and bFGF cooperate to maintain the pluripotency of human embryonic stem cells in the absence of feeder layers. Biochem Biophys Res Commun 330(3):934-42. PubMed PMID: 15809086
Waseem et al., 1999	Waseem A, Dogan B, Tidman N, Alam Y, Purkis P, Jackson S, Lalli A, Machesney M, Leigh IM (1999) Keratin 15 expression in stratified epithelia: downregulation in activated keratinocytes. J Invest Dermatol 112(3):362-9. PubMed PMID: 10084315

Waters and Bassler, 2005	Waters CM, Bassler BL (2005) Quorum sensing: cell-to-cell communication in bacteria. Annu Rev Cell Dev Biol 21:319-46. Review. PubMed PMID: 16212498
Wegner and Stumm, 2011	Wegner RD, Stumm M (2011) Zytogenetische Methoden in der Pränataldiagnostik. In: Medizinische Genetik (medgen), Springer-Verlag, 23:457-462.
Wehrle-Haller, 2012	Wehrle-Haller B (2012) Structure and function of focal adhesions. Curr Opin Cell Biol 24(1):116-24. Review. PubMed PMID: 22138388
Williams et al., 1992	Williams ME, Brust PF, Feldman DH, Patthi S, Simerson S, Maroufi A, McCue AF, Veliçelebi G, Ellis SB, Harpold MM (1992) Structure and functional expression of an omega-conotoxin sensitive human N-type calcium channel. Science 257(5068):389-95. PubMed PMID: 1321501
Williams et al., 2008	Williams LA, Bhargav D, Diwan AD (2008) Unveiling the bmp13 enigma: redundant morphogen or crucial regulator? Int J Biol Sci 4(5):318-29. Review. PubMed PMID: 18797508
Williams et al., 2011	Williams PJ, Bulmer JN, Innes BA, Broughton Pipkin F (2011) Possible roles for folic acid in the regulation of trophoblast invasion and placental development in normal early human pregnancy. Biol Reprod 84(6):1148-53. PubMed PMID: 21349824
Wolfrum et al., 2010	Wolfrum K, Wang Y, Prigione A, Sperling K, Lehrach H, Adjaye J (2010) The LARGE principle of cellular reprogramming: lost, acquired and retained gene expression in foreskin and amniotic fluid-derived human iPS cells. PLoS One 5(10):e13703. PubMed PMID: 21060825
Wong and Bernstein, 2010	Wong SS, Bernstein HS (2010) Cardiac regeneration using human embryonic stem cells: producing cells for future therapy. Regen Med 5(5):763-75. Review. PubMed PMID: 20868331
Wu and Hill, 2009	Wu MY, Hill CS (2009) Tgf-beta superfamily signaling in embryonic development and homeostasis. Dev Cell 16(3):329-43. Review. PubMed PMID: 19289080
Xu et al., 2001a	Xu C, Inokuma MS, Denham J, Golds K, Kundu P, Gold JD, Carpenter MK (2001) Feeder-free growth of undifferentiated human embryonic stem cells. Nat Biotechnol 19(10):971-4. PubMed PMID: 11581665
Xu et al., 2001b	Xu P, Wang Y, Piao Y, Bai S, Xiao Z, Jia Y, Luo S, Zhuang L (2001) Effects of matrix proteins on the expression of matrix metalloproteinase-2, -9, and -14 and tissue inhibitors of metalloproteinases in human cytotrophoblast cells during the first trimester. Biol Reprod 65(1):240-6. PubMed PMID: 11420245
Xu et al., 2002	Xu RH, Chen X, Li DS, Li R, Addicks GC, Glennon C, Zwaka TP, Thomson JA (2002) BMP4 initiates human embryonic stem cell differentiation to trophoblast. Nat Biotechnol 20(12):1261-4. PubMed PMID: 12426580
Xu et al., 2008	Xu RH, Sampsell-Barron TL, Gu F, Root S, Peck RM, Pan G, Yu J, Antosiewicz-Bourget J, Tian S, Stewart R, Thomson JA (2008) NANOG is a direct target of TGFbeta/activin-mediated SMAD signaling in human ESCs. Cell Stem Cell 3(2):196-206. PubMed PMID: 18682241
Yanagita, 2005	Yanagita M (2005) BMP antagonists: their roles in development and involvement in pathophysiology. Cytokine Growth Factor Rev 16(3):309-17. Review. PubMed PMID: 15951218
Yao et al., 2006	Yao S, Chen S, Clark J, Hao E, Beattie GM, Hayek A, Ding S (2006) Long-term self-renewal and directed differentiation of human embryonic stem cells in chemically defined conditions. Proc Natl Acad Sci U S A 103(18):6907-12. PubMed PMID: 16632596
Ye et al., 2009	Ye L, Chang JC, Lin C, Sun X, Yu J, Kan YW (2009) Induced pluripotent stem cells offer new approach to therapy in thalassemia and sickle cell anemia and option in prenatal diagnosis in genetic diseases. Proc Natl Acad Sci U S A 106(24):9826-30. PubMed PMID: 19482945
Ye et al., 2012	Ye J, Coulouris G, Zaretskaya I, Cutcutache I, Rozen S, Madden TL (2012) Primer-BLAST: a tool to design target-specific primers for polymerase chain reaction. BMC Bioinformatics 13:134. PubMed PMID: 22708584
Yi et al., 2013	Yi BA, Mummery CL, Chien KR (2013) Direct cardiomyocyte reprogramming: a new direction for cardiovascular regenerative medicine. Cold Spring Harb Perspect Med 3(9):a014050. Review. PubMed PMID: 24003244
Yonemura, 2011	Yonemura S (2011) Cadherin-actin interactions at adherens junctions. Curr Opin Cell Biol 23(5):515-22. Review. PubMed PMID: 21807490
Yoshida and Yamanaka, 2011	Yoshida Y, Yamanaka S (2011) iPS cells: a source of cardiac regeneration. J Mol Cell Cardiol 50(2):327-32. Review. PubMed PMID: 21040726
Yu et al., 2002	Yu C, Shen K, Lin M, Chen P, Lin C, Chang GD, Chen H (2002) GCMa regulates the syncytin-mediated trophoblastic fusion. J Biol Chem 277(51):50062-8. PubMed PMID: 12397062
Yu et al., 2007	Yu J, Vodyanik MA, Smuga-Otto K, Antosiewicz-Bourget J, Frane JL, Tian S, Nie J, Jonsdottir GA, Ruotti V, Stewart R, Slukvin II, Thomson JA (2007) Induced pluripotent stem cell lines derived from human somatic cells. Science 318(5858):1917-20. PubMed PMID: 18029452
Yu et al., 2011	Yu P, Pan G, Yu J, Thomson JA (2011) FGF2 sustains NANOG and switches the outcome of BMP4-induced human embryonic stem cell differentiation. Cell Stem Cell 8(3):326-34. PubMed PMID: 21362572
Zhang et al., 2008	Zhang P, Li J, Tan Z, Wang C, Liu T, Chen L, Yong J, Jiang W, Sun X, Du L, Ding M, Deng H (2008) Short-term BMP-4 treatment initiates mesoderm induction in human embryonic stem cells. Blood 111(4):1933-41. PubMed PMID: 18042803
Zhang et al., 2011	Zhang W, Chen H, Wang Y, Yong W, Zhu W, Liu Y, Wagner GR, Payne RM, Field LJ, Xin H, Cai CL, Shou W (2011) Tbx20 transcription factor is a downstream mediator for bone morphogenetic protein-10 in regulating cardiac ventricular wall development and function. J Biol Chem 286(42):36820-9. PubMed PMID: 21890625
Zhou et al., 1997	Zhou Y, Fisher SJ, Janatpour M, Genbacev O, Dejana E, Wheelock M, Damsky CH (1997) Human cytotrophoblasts adopt a vascular phenotype as they differentiate. A strategy for successful endovascular invasion? J Clin Invest 99(9):2139-51. PubMed PMID: 9151786
Zhu et al., 2011	Zhu WZ, Van Biber B, Laflamme MA (2011) Methods for the derivation and use of cardiomyocytes from human pluripotent stem cells. Methods Mol Biol 767:419-31. PubMed PMID: 21822893

Appendix
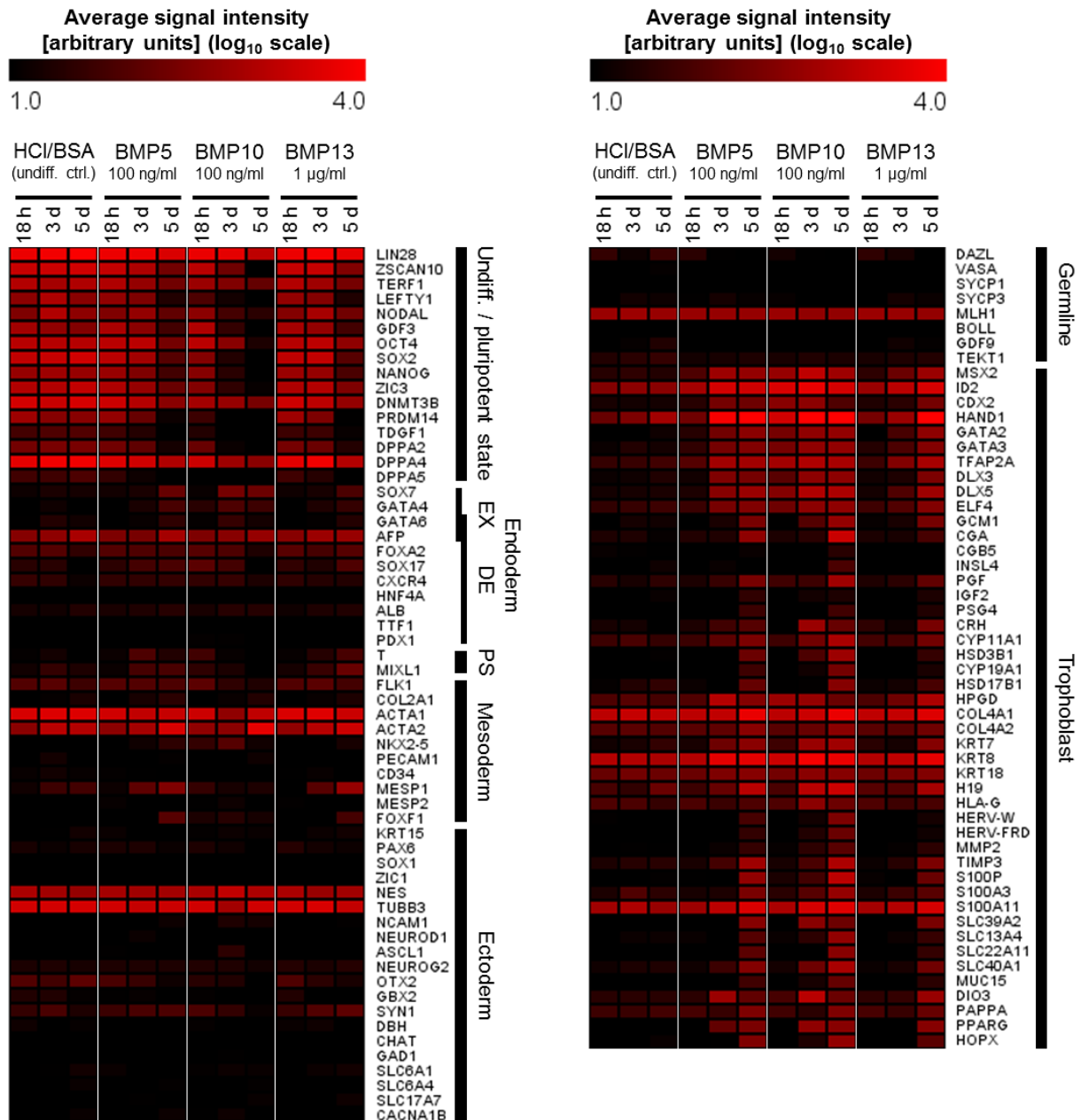
Figure A-1   Detected average signal intensities of pluripotency and differentiation marker genes expressed in H1 hESCs after exposure to different BMP family members or solvent/carrier protein for increasing periods of time (microarray raw data related to Figure 4-16).
Color-coded visualization for all samples as indicated in the heatmap (grouped biological duplicates). The defined arbitrary cut-off value of 10 ≙ 1 in $\log_{10}$ scale.
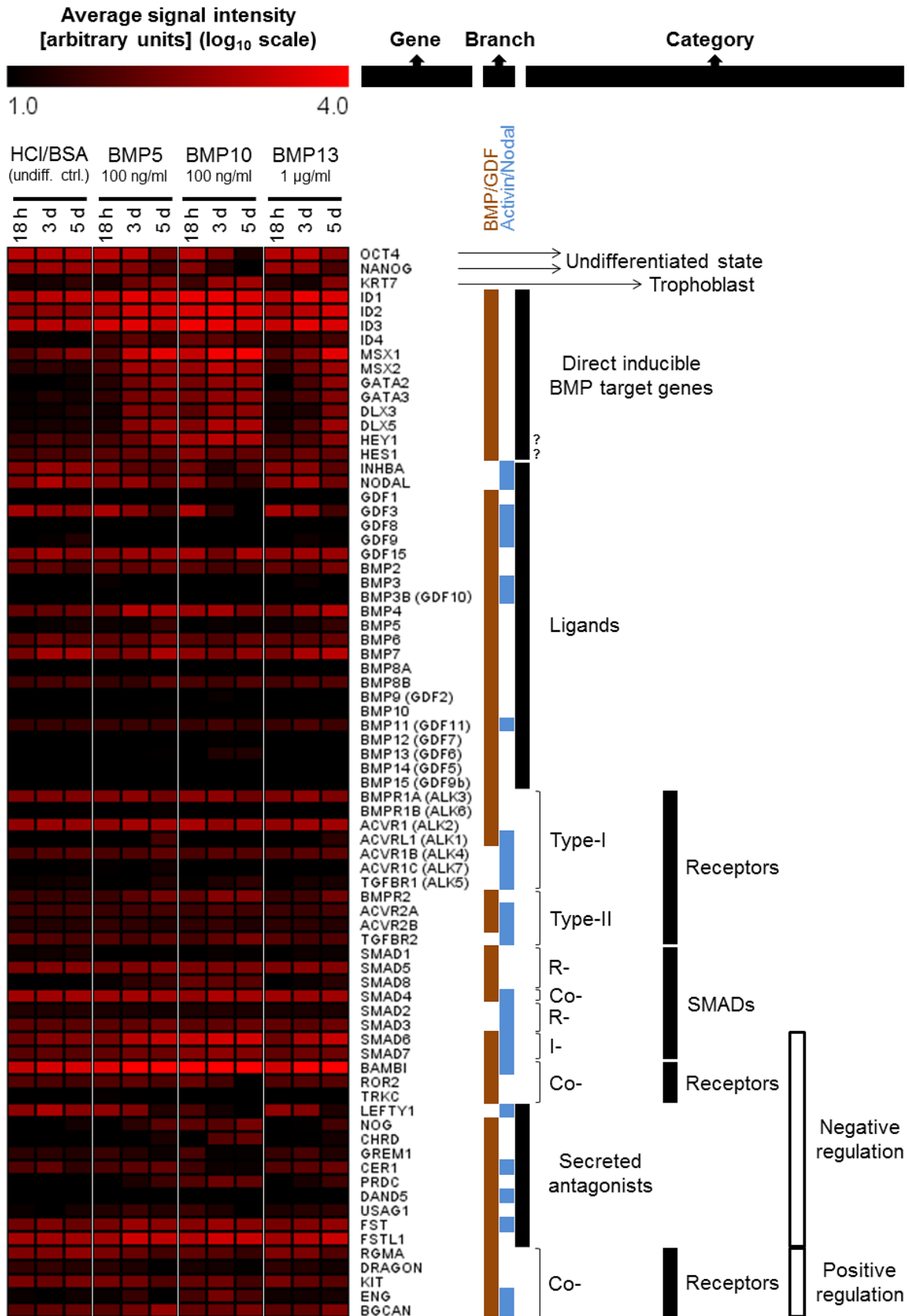
Figure A-2 **Detected average signal intensities of gene members of the TGF-β superfamily signaling network expressed in H1 hESCs after exposure to different BMP family members or solvent/carrier protein for increasing periods of time (microarray raw data related to Figure 4-34).**
Color-coded visualization for all samples as indicated in the heatmap (grouped biological duplicates). The defined arbitrary cut-off value of $10 \triangleq 1$ in $\log_{10}$ scale.

149

Table A-1   Top 100 upregulated genes in H1 hESCs after treatment with BMP5, BMP10 and BMP13 for 18 h, 3 d and 5 d.

Fold changes in gene expression as determined by microarray (ligand versus HCl/BSA reference cells of the same time point). Only significantly differentially expressed genes were considered (> 1.5-fold up, $P_{Diff} < 0.05$, $P_{Det} < 0.01$ for at least one of both samples (BMP and/or reference)).

Rank	UP at 18 h (gene, ratio) BMP5		BMP10		BMP13		UP at 3 d (gene, ratio) BMP5		BMP10		BMP13		UP at 5 d (gene, ratio) BMP5		BMP10		BMP13	
1	MSX2	2.9	LOC400578	28.3	ID2	1.8	HAND1	26.6	ACPP	125.3	TFAP2A	7.5	S100P	45.3	CGA	190.0	LOC400578	52.3
2	ID3	2.7	EBF3	27.8	ID3	1.8	FAM123A	24.1	APLNR	97.6	GATA2	7.2	CGA	40.1	S100P	147.2	MGC102966	36.0
3	ID1	2.5	MSX1	26.0	ID1	1.7	POSTN	23.9	ANKRD43	83.7	MSX2	5.1	SLC39A2	39.0	HSD3B1	61.9	DLX5	34.0
4	ID2	2.5	GATA2	24.6	GADD45GIP1	1.6	SPARCL1	23.6	HOXB8	76.1	PRKD1	5.0	CLEC1B	35.7	C8ORF4	56.5	GPR177	33.5
5	TFAP2A	2.4	LOC643700	23.2	LRAT	1.6	ATP12A	23.4	LUM	70.0	DLX5	4.6	DLX5	30.5	CCR7	54.7	ZNF750	33.2
6	BAMBI	2.3	HEY1	21.8	COCH	1.6	GATA2	22.2	DLX5	63.3	NTNG1	4.4	APLNR	30.1	DLX5	50.5	SPARCL1	31.5
7	CBLN1	2.2	CDX2	21.5	BAMBI	1.5	DIO3	21.4	ALDH1A2	62.5	BAPX1	4.3	CCR7	28.6	TRIM55	46.3	GATA2	31.3
8	COCH	2.2	MSX2	21.1	–	–	ENPEP	21.1	ENPEP	60.8	ISL2	4.3	GATA2	27.8	CDH10	46.1	APLNR	30.6
9	GADD45B	2.0	POU4F1	20.9	–	–	DLX5	20.7	HAND1	60.1	LOC389332	4.0	VTCN1	27.5	SLC40A1	41.6	CLEC1B	29.4
10	HES1	1.9	DLX5	20.9	–	–	DLX3	20.6	C8ORF4	59.6	APLNR	3.9	HOXB2	26.8	CSF3R	41.6	CCKBR	27.9
11	JAKMIP2	1.8	TFAP2A	19.9	–	–	MSX2	19.4	ISL1	59.2	LRRC3B	3.7	LOC400578	26.5	XAGE2B	41.1	SLC39A2	27.0
12	NPAS1	1.8	MGC102966	19.8	–	–	GPR177	19.0	LOC644612	58.9	C1ORF61	3.7	ZNF750	25.1	LOC644612	40.9	MSX2	26.1
13	ACTC1	1.8	KCNK13	18.9	–	–	TBC1D9	18.4	LOC729252	56.9	ID4	3.7	TIMP3	24.5	SLC22A11	40.4	CRH	25.9
14	TMEM154	1.7	BHLHE22	18.5	–	–	SPNS2	18.2	CSF1R	55.5	FAM20A	3.7	HOPX	23.8	ZNF750	40.3	HOXB2	24.7
15	CD55	1.7	GATA3	17.9	–	–	ISL1	17.8	TBC1D9	55.1	LOC643700	3.7	XAGE2B	23.8	HOPX	39.8	VTCN1	21.1
16	IGDCC3	1.7	HAND1	17.7	–	–	TFAP2A	17.5	DOK4	53.8	ID1	3.7	SLN	21.9	SLC13A4	36.9	DIO3	20.5
17	FGFR3	1.6	SMAD8	16.3	–	–	ALDH1A2	17.0	BTK	53.3	BMP4	3.6	C8ORF4	21.7	MRGPRX3	36.6	GATA3	19.9
18	C19ORF4	1.6	PRKD1	16.0	–	–	YPEL2	15.4	GATA2	50.8	ID2	3.5	MSX2	21.2	TIMP3	36.5	C8ORF4	18.7
19	SMAD6	1.6	LOC729252	15.7	–	–	ACPP	14.6	MSX2	49.0	TWIST1	3.4	CDH10	20.9	VTCN1	36.0	CDH10	18.2
20	ACP2	1.6	EFNA1	15.3	–	–	TMEM54	13.8	KANK4	48.2	ID3	3.3	MGC102966	20.5	HS.131331	35.8	ISL1	18.1
21	CXXC5	1.5	SAMD11	14.7	–	–	CDX2	13.7	DIO3	48.2	SAMD11	3.2	GPR177	19.6	GATA2	35.7	CSF1R	17.9
22	–	–	LOC389332	14.3	–	–	LOC400578	13.0	IGFBP3	47.4	COCH	3.1	ERP27	19.5	CLIC3	35.3	HS.291319	17.5
23	–	–	GATA5	14.1	–	–	HPGD	13.0	C1ORF105	46.6	SMAD6	3.0	GATA3	18.7	KRT80	34.6	TMEM88	17.3
24	–	–	ID4	13.8	–	–	DLX1	12.9	CDH10	44.6	LOX	2.9	LOC644612	18.8	GCM1	34.3	EPAS1	17.1
25	–	–	SMAD6	13.7	–	–	ZNF750	12.6	ANKRD38	42.8	SFTPD	2.9	HOXB8	18.5	GABRP	31.9	ANKRD38	16.9
26	–	–	FAM123A	13.0	–	–	IER5L	12.5	HOXB5	42.0	TMEM54	2.8	HS.19193	17.8	LOC400578	31.5	ENPEP	16.8
27	–	–	CRIP2	12.9	–	–	MSX1	12.1	GABRP	41.7	TMPRSS11E2	2.8	PMP22	17.7	CCBP2	31.3	HPGD	16.6
28	–	–	NOG	12.6	–	–	KCNK13	11.6	SLC39A2	41.5	GATA5	2.7	SVEP1	17.5	SLN	30.7	HOXB8	16.2
29	–	–	NANOS3	12.4	–	–	CAMK2N1	11.5	LOC400578	41.3	PTH1R	2.7	SVEP1	17.5	GATA3	30.2	TFAP2A	15.6
30	–	–	SHD	12.1	–	–	ANKRD43	11.0	H19	40.9	ACTG2	2.7	GABRP	17.3	CHN2	30.1	ZFHX3	15.6
31	–	–	TBX3	11.8	–	–	APLNR	10.9	LRRC32	38.9	C2ORF32	2.7	KANK4	17.2	ERVWE1	30.1	S100P	15.3
32	–	–	GRHL3	11.5	–	–	EPHB1	10.8	RGS4	38.2	BAMBI	2.6	CCKBR	16.9	NUPR1	29.9	TBX3	15.3
33	–	–	COL9A2	11.4	–	–	UPK2	10.8	MSX1	37.9	SLC2A12	2.6	HS.291319	16.9	CLEC1B	29.5	KANK4	15.1
34	–	–	C5ORF39	10.9	–	–	EFNA1	10.6	CLEC1B	37.4	IGFBP7	2.6	ODAM	16.8	MSX2	29.0	HOXB5	15.1
35	–	–	ID2	10.6	–	–	SYNPR	10.5	CRH	37.3	GRHL3	2.6	LOC728473	16.8	ANKRD38	28.5	GCM1	14.9
36	–	–	ISL1	10.5	–	–	ID4	10.4	GPR177	36.6	KCNK12	2.6	CHN2	16.6	PSD4	28.4	BTK	14.8
37	–	–	ATP12A	10.3	–	–	LRRC3B	10.4	HOXB2	35.3	SLC7A14	2.5	LEF1	16.6	CSF1R	28.3	CEBPA	14.8
38	–	–	GREM2	9.9	–	–	ZFHX3	10.1	SPARCL1	34.2	KANK2	2.5	TMEM88	16.5	IGFBP3	28.3	CCR7	14.7
39	–	–	NTF3	9.9	–	–	C8ORF4	10.0	GAS1	33.3	EFNA1	2.5	ISL1	16.5	ISL1	27.4	HAND1	14.5
40	–	–	FLJ31568	9.8	–	–	GATA5	10.0	TBX3	31.1	CENTG3	2.5	GCM1	16.4	DOK4	27.3	MYL4	14.5
41	–	–	ACADL	9.8	–	–	RHOB	10.0	SPNS2	31.0	LOC729839	2.5	TBX3	16.4	SLCO2A1	27.0	KRT80	14.5
42	–	–	RGS4	9.6	–	–	RHOBTB3	9.9	KRT7	30.7	CA12	2.5	EPAS1	16.1	TBX3	26.9	CXCR7	14.3
43	–	–	HOXD1	9.6	–	–	MGC102966	9.8	KRT16	30.7	FZD2	2.5	KRT80	16.1	C4ORF19	26.9	WNT4	14.2

Rank	UP at 18 h (gene, ratio)			UP at 3 d (gene, ratio)			UP at 5 d (gene, ratio)		
	BMP5	BMP10	BMP13	BMP5	BMP10	BMP13	BMP5	BMP10	BMP13
44	–	PITX1 9.4	–	KRT7 9.5	DLX3 30.2	TMEM90B 2.5	MYL4 15.8	C1ORF105 25.0	LOC644612 14.0
45	–	DMRTA2 9.2	–	GATA3 9.4	DLX1 29.6	HES1 2.5	HSD3B1 15.7	CYP11A1 24.1	ATP12A 13.6
46	–	BARX1 9.0	–	KRT80 9.0	MGC102966 29.3	FOXD1 2.5	RSPO2 15.6	TGFBI 23.9	CDX2 13.6
47	–	PTH1R 8.9	–	FAM20A 8.9	VTCN1 28.8	CNRIP1 2.4	HAND1 15.5	ERP27 23.8	LCP1 13.5
48	–	ZDHHC8P 8.8	–	ZDHHC8P 8.9	ADAMTS9 28.8	LOC647322 2.4	CCBP2 15.4	BTK 23.5	PSD4 13.4
49	–	ALOX5 8.7	–	HOXC13 8.8	HS.489857 27.9	LOC644276 2.4	IGFBP3 15.2	CXCR7 23.4	LEF1 13.3
50	–	HS.444855 8.6	–	BMP4 8.7	RASGRP1 26.8	CD55 2.3	AHNAK 15.1	CYP19A1 23.3	PRAC 13.2
51	–	KANK4 8.6	–	DOK4 8.7	CDX2 26.0	GLIPR1 2.3	ADAMTS9 15.1	LOC648814 22.8	AHNAK 13.0
52	–	NOTUM 8.5	–	WNT3A 8.6	LRRC4C 25.3	MLPH 2.3	HOXB5 15.0	KANK4 22.8	SPNS2 13.0
53	–	DLX1 8.4	–	FLJ31568 8.2	TMEM54 25.3	USP3 2.3	SLC40A1 14.9	EPAS1 22.6	HAPLN1 12.9
54	–	HPGD 8.2	–	SYT7 8.2	TFAP2A 25.0	CPZ 2.3	CXCR7 14.8	SVEP1 22.4	TBC1D9 12.7
55	–	DLX3 8.1	–	PRKD1 8.1	HS.19193 24.9	HABP4 2.3	HOXB7 14.6	MGC102966 22.3	FLJ31568 12.6
56	–	SGCG 8.0	–	SAMD11 8.0	CXCR7 24.5	CXCL14 2.2	RPESP 14.3	PGM5 21.9	PMP22 12.6
57	–	LRRN2 7.9	–	AHNAK 8.0	MXRA5 24.3	CRLF1 2.2	DOK4 14.3	HEY1 21.9	HS.19193 12.6
58	–	HS.291319 7.5	–	GAS1 8.0	CLSTN2 24.2	SGK1 2.2	AFAP1L2 14.1	ANXA8L2 21.6	SVEP1 12.5
59	–	FAM20A 7.4	–	LHFP 7.9	SHD 23.7	HS3ST2 2.2	SNAI2 14.0	MRGPRX1 21.4	DOK4 12.5
60	–	GPRIN3 7.3	–	OVGP1 7.7	FOXF2 23.6	SGK 2.2	WASPIP 13.9	LUM 21.3	ACPP 12.2
61	–	TMEM54 7.2	–	PLA2G2A 7.6	HOXB7 23.4	LOC730994 2.2	LRRC32 13.8	PGF 21.0	FAM89A 12.2
62	–	HES1 7.2	–	GPR56 7.6	ANXA4 23.2	HAND1 2.2	CSF1R 13.8	TRPV2 20.9	WNT5A 12.1
63	–	LOC647322 7.1	–	C1ORF61 7.5	ENG 23.1	SOCS2 2.1	CSF1R 13.7	LMO1 20.8	CAMK2N1 11.8
64	–	CA10 7.0	–	OAF 7.4	ERP27 22.4	ADM 2.1	RGS1 13.6	CXCL14 20.7	TP73L 11.8
65	–	GADD45B 7.0	–	TBX3 7.4	ODAM 22.3	CDH6 2.1	PSD4 13.6	TINAGL1 20.6	GPR56 11.8
66	–	BAPX1 6.9	–	LOC100134424 7.3	LMO1 22.1	SERPINB9 2.1	ZFHX3 13.5	DLX1 20.5	GABRP 11.8
67	–	MXRA5 6.7	–	CEBPA 7.3	TP73L 21.5	WNT5A 2.1	WNT5A 13.4	SPNS2 20.2	C4ORF19 11.7
68	–	SFTPD 6.4	–	CDH10 7.2	LEF1 21.4	MANEAL 2.1	TRPV2 13.3	HOXB2 20.0	DLX3 11.6
69	–	NOL4 6.4	–	LOC91461 7.1	ZFHX3 21.2	LRP4 2.1	ODZ4 13.2	ANKRD43 19.9	ERP27 11.3
70	–	CBLN1 6.2	–	TRIM38 7.1	CEBPA 21.0	LOC392787 2.1	HAPLN1 13.2	NLRP7 19.9	IGFBP3 11.2
71	–	ID1 6.2	–	C13ORF18 7.0	SMTNL2 21.0	TSPAN18 2.1	LOC648814 13.0	GPR56 19.8	PLA2G2A 11.2
72	–	GRM8 6.0	–	NTF3 7.0	PLA2G2A 20.9	KCNG3 2.0	NNMT 13.0	WASPIP 19.7	LOC729252 11.2
73	–	ID3 6.0	–	HS.105791 7.0	HEY1 20.5	MSX1 2.0	GPR56 12.9	TGM2 19.6	ADAMTS9 11.2
74	–	PLAC8 6.0	–	SGCG 6.9	GATA5 20.3	SAMD1 2.0	KCTD12 12.8	SLC39A2 19.6	TINAGL1 10.9
75	–	SERTAD4 6.0	–	IGFBP3 6.8	MEIS1 20.2	GADD45B 2.0	CCDC92 12.7	ZFHX3 19.3	MSX1 10.9
76	–	SCT 5.9	–	HAPLN1 6.8	YPEL2 20.0	ELF4 2.0	VGLL1 12.7	ENPEP 19.3	SNAI2 10.8
77	–	TMEM154 5.8	–	ID2 6.8	EFNA1 19.9	COMT 2.0	C1ORF105 12.6	MSX1 19.1	AFAP1L2 10.7
78	–	DOK5 5.7	–	LRRC4C 6.8	RHOBTB3 19.4	HS.570988 2.0	HEY1 12.5	GPR177 19.1	DNAH2 10.7
79	–	POSTN 5.7	–	ACADL 6.8	GREM2 19.3	SLC7A3 2.0	HOXC8 12.5	KRT7 19.0	DIO3OS 10.7
80	–	BAMBI 5.6	–	RASSF9 6.6	GATA3 19.2	STARD10 2.0	RGS4 11.9	HAND1 19.0	LOC728473 10.6
81	–	DUSP2 5.6	–	CXCR7 6.4	CAMK2N1 18.7	SERTAD2 2.0	BTK 11.9	GUCY1A3 18.6	TWIST1 10.6
82	–	NKD1 5.5	–	LOC644612 6.4	IER5L 18.5	TBL2 2.0	COL6A3 11.9	DLX3 18.4	CDX1 10.5
83	–	LRRC4C 5.4	–	PKDCC 6.2	AHNAK 18.4	LHPP 2.0	SLC22A11 11.8	C5ORF46 18.3	ODAM 10.5
84	–	LRP4 5.4	–	KANK4 6.2	WNT4 18.1	NAV2 2.0	MSX1 11.8	LCP1 18.3	LOC338758 10.5
85	–	ACTC1 5.4	–	GABRP 6.1	LOC730130 18.0	SHB 1.9	ANXA8L2 11.8	LPL 18.0	RPESP 10.4
86	–	RAI1 5.3	–	CASQ2 6.0	EPAS1 17.9	EMILIN2 1.9	ZDHHC8P 11.6	HERV–FRD 17.9	MBNL3 10.4
87	–	NR5A1 5.3	–	C1ORF88 6.0	TMEM88 17.8	LOC643778 1.9	LCP1 11.6	BHLHB2 17.8	ZDHHC8P 10.4
88	–	TMEM90B 5.3	–	C20ORF151 5.9	LOC648814 17.4	TMEM154 1.9	ENPEP 11.4	C4ORF26 17.8	HOXB7 10.3
89	–	ELF4 5.2	–	AMOT 5.9	LOC644695 17.4	METRNL 1.9	FLJ31568 11.3	TANC2 17.6	C1ORF61 10.2
90	–	KRT80 5.2	–	MEIS1 5.8	SNAI2 17.3	HPGD 1.9	C4ORF19 11.2	AHNAK 17.5	GRP 10.1
91	–	LOC644695 5.2	–	HS3ST1 5.8	ACTC1 17.1	FGFR3 1.9	CDX2 11.0	CEBPA 17.2	KAT2B 10.1

Rank	UP at 18 h (gene, ratio)			UP at 3 d (gene, ratio)			UP at 5 d (gene, ratio)		
	BMP5	BMP10	BMP13	BMP5	BMP10	BMP13	BMP5	BMP10	BMP13
92	– –	ANKRD38 5.2	– –	PTCHD1 5.8	AMOT 16.8	CBLN1 1.9	PITX2 10.9	S100A3 17.2	RHOBTB3 10.0
93	– –	FAM110B 5.2	– –	TP73L 5.7	RHOB 16.5	SYT7 1.9	TGM2 10.8	C4ORF31 17.0	COL9A2 10.0
94	– –	NTNG1 5.1	– –	LOC651921 5.7	HOXD11 16.4	LOC653506 1.9	OAF 10.7	CCKBR 17.0	LRRC32 10.0
95	– –	T 5.0	– –	ELF4 5.6	POSTN 16.3	CYR61 1.9	FAM89A 10.7	VGLL1 16.8	XAGE2B 9.9
96	– –	IER5L 5.0	– –	HS.489857 5.6	CHN2 16.2	MARK1 1.9	KRT7 10.7	SLIT3 16.7	LMO1 9.9
97	– –	CA12 4.9	– –	EPN3 5.6	ENDOD1 16.2	DHX32 1.8	SLCO2A1 10.6	CRH 16.6	WASPIP 9.9
98	– –	FURIN 4.9	– –	DLL1 5.6	HOXB6 16.1	CACNB3 1.8	LOC338758 10.5	P8 16.5	TP63 9.8
99	– –	LOC284293 4.9	– –	ADAMTS9 5.5	PSD4 16.0	MAP7D1 1.8	LUM 10.5	TFAP2A 16.5	LOC645431 9.8
100	– –	SLCO2A1 4.9	– –	C3ORF57 5.5	OAF 15.7	SERTAD4 1.8	FOXF1 10.5	HOXB7 16.0	CHN2 9.8

Table A-2   Top 100 downregulated genes in H1 hESCs after treatment with BMP5, BMP10 and BMP13 for 18 h, 3 d and 5 d.

Fold changes in gene expression as determined by microarray (ligand versus HCl/BSA reference cells of the same time point). Only significantly differentially expressed genes were considered (< 0.66-fold down, $P_{Diff} < 0.05$, $P_{Det} < 0.01$ for at least one of both samples (BMP and/or reference)).

Rank	DOWN at 18 h (gene, ratio)						DOWN at 3 d (gene, ratio)						DOWN at 5 d (gene, ratio)					
	BMP5		BMP10		BMP13		BMP5		BMP10		BMP13		BMP5		BMP10		BMP13	
1	TNIK	0.50	PRDM14	0.07	–	–	BTBD17	0.09	SOX2	0.01	BTBD17	0.16	INDO	0.02	ZSCAN10	0.00	INDO	0.02
2	HS.79881	0.54	USP44	0.10	–	–	LRAT	0.10	CAMKV	0.01	THBS2	0.20	IDO1	0.02	SOX2	0.00	IDO1	0.02
3	PRICKLE1	0.54	CXCL5	0.13	–	–	SEMG1	0.12	LEFTY1	0.02	S100A4	0.21	USP44	0.02	CAMKV	0.00	PRDM14	0.03
4	HESX1	0.58	LRAT	0.13	–	–	MYBPHL	0.13	ABHD12B	0.02	CCL26	0.24	C1ORF94	0.03	ZIC3	0.01	USP44	0.03
5	SMCR5	0.61	HESX1	0.14	–	–	ASB9	0.14	USP44	0.02	LGALS7	0.25	PRDM14	0.04	LOC643272	0.01	SOX2	0.04
6	KCNS1	0.62	PRICKLE1	0.16	–	–	C6ORF126	0.14	CHST9	0.02	C3ORF72	0.26	SOX3	0.04	HS.575696	0.01	LECT1	0.04
7	MIAT	0.62	MYH2	0.16	–	–	ABHD12B	0.15	PRDM14	0.03	LEFTY2	0.26	SOX2	0.04	HS.574590	0.01	RPRML	0.04
8	LRIG1	0.63	C15ORF27	0.17	–	–	CA4	0.15	HS.177654	0.03	OR52A1	0.26	VSNL1	0.05	LOC100132934	0.01	GALR2	0.05
9	SOX21	0.64	DPPA5	0.17	–	–	GALR2	0.16	ZIC3	0.03	GNG2	0.27	GALR2	0.05	USP44	0.01	C1ORF94	0.06
10	C3ORF72	0.66	THBS2	0.17	–	–	GLB1L3	0.17	C1ORF94	0.03	FOXJ1	0.28	GAL3ST3	0.05	PDZD4	0.02	LEFTY1	0.06
11	–	–	KAL1	0.18	–	–	NLGN1	0.17	HS.270778	0.03	KIAA1199	0.28	KLKB1	0.05	POU5F1P1	0.02	LRAT	0.06
12	–	–	PIM2	0.18	–	–	PNMA3	0.17	TIMP4	0.03	DDIT3	0.29	PDZD4	0.05	NANOG	0.02	HESX1	0.06
13	–	–	LEFTY1	0.18	–	–	INHBE	0.18	PDZD4	0.03	VCX	0.31	FLJ25404	0.06	OCT4 (POU5F1)	0.02	GAL3ST3	0.06
14	–	–	LOC283340	0.19	–	–	STK32B	0.18	INHBE	0.04	LEFTY1	0.33	SOX21	0.06	LOC645682	0.02	IGSF21	0.07
15	–	–	CH25H	0.19	–	–	C9ORF129	0.18	GLIPR1L1	0.04	FGF19	0.33	IGSF21	0.06	INDO	0.02	HS.12513	0.07
16	–	–	SOX2	0.20	–	–	HS.10862	0.18	HS.574590	0.04	HESX1	0.33	LOC100132934	0.06	CRABP1	0.02	CAMKV	0.07
17	–	–	C10ORF96	0.21	–	–	CAPN11	0.18	LOC100132934	0.04	C11ORF60	0.34	RPRML	0.06	FLJ25404	0.02	TTYH1	0.07
18	–	–	LOC157627	0.21	–	–	UTF1	0.18	THBS2	0.04	FZD7	0.37	LEFTY1	0.06	HS.177654	0.02	CXCL6	0.08
19	–	–	HS.135050	0.22	–	–	MX1	0.19	FLJ25404	0.04	TMEFF2	0.37	NPTX2	0.06	LOC642559	0.02	ZDHHC22	0.08
20	–	–	HS.519644	0.22	–	–	LSM14B	0.19	TUBA4A	0.04	PLA2G4C	0.38	C9ORF129	0.06	VSNL1	0.02	SOX21	0.08
21	–	–	TNIK	0.22	–	–	C10ORF96	0.19	NANOG	0.04	HEYL	0.39	ACTN3	0.06	GAL	0.02	LOC100132934	0.08
22	–	–	UNC5A	0.23	–	–	AK3L1	0.19	ZDHHC22	0.04	ABHD12B	0.39	LRAT	0.07	IDO1	0.02	KCND2	0.08
23	–	–	SLITRK4	0.23	–	–	VENTX	0.19	PCSK9	0.04	SHISA2	0.40	HS.574590	0.07	LEFTY1	0.02	SLC7A10	0.08
24	–	–	HS.79881	0.23	–	–	LGALS3	0.20	HAS3	0.05	TM4SF18	0.40	DPPA2	0.07	PRDM14	0.02	BTBD17	0.08
25	–	–	CCNA1	0.24	–	–	FGFBP3	0.20	HS.575696	0.05	NLGN1	0.41	HS.270778	0.07	SLC15A3	0.03	PDZD4	0.08
26	–	–	STXBP6	0.24	–	–	LOC283340	0.20	KLKB1	0.05	UTF1	0.41	TRIM22	0.07	UCA1	0.03	FAM124B	0.09
27	–	–	KLKB1	0.24	–	–	SHISA2	0.20	DPPA2	0.05	FABP7	0.41	CXCL6	0.08	SFRP2	0.03	PIPOX	0.09
28	–	–	FHOD3	0.25	–	–	FGF19	0.20	GALR2	0.05	STAMBPL1	0.42	TCEAL2	0.08	GDF3	0.03	NCRNA00153	0.09
29	–	–	VSNL1	0.25	–	–	LOC100133760	0.20	SEMG1	0.05	TFPI2	0.42	CAMKV	0.08	LRIG1	0.03	ST8SIA5	0.09
30	–	–	LOC731007	0.25	–	–	TRIB3	0.20	ATF5	0.05	AK3L1	0.43	THBS2	0.08	PTPRZ1	0.03	MIAT	0.09
31	–	–	TMEM16A	0.26	–	–	LOC644295	0.20	C9ORF129	0.05	PRTFDC1	0.43	PTPRZ1	0.08	C1ORF94	0.03	SHISA2	0.09
32	–	–	TM4SF18	0.26	–	–	CXCL6	0.21	RPRML	0.05	LOC731007	0.43	TIMP4	0.08	CHST4	0.03	HS.519644	0.09
33	–	–	KIAA0367	0.27	–	–	RPRML	0.21	NODAL	0.05	HS.10862	0.43	DDX25	0.08	CHST9	0.03	THBS2	0.09
34	–	–	RND3	0.27	–	–	TLE6	0.21	MTE	0.05	SLC39A8	0.43	FGF2	0.08	HS.270778	0.03	TIMP4	0.09
35	–	–	GLIPR1L1	0.27	–	–	C20ORF127	0.21	C6ORF126	0.06	FERMT1	0.44	RHBDL3	0.08	SYT4	0.03	TUBB4	0.09
36	–	–	SLC27A2	0.27	–	–	CXCL5	0.21	LEFTY2	0.06	DACT1	0.44	KCND2	0.08	TCEAL2	0.03	C10ORF96	0.10
37	–	–	SOX21	0.27	–	–	C1ORF94	0.21	MT1G	0.06	TCN2	0.44	ZSCAN10	0.08	ZIC2	0.03	GLS2	0.10
38	–	–	ZFPM2	0.27	–	–	KIAA1199	0.21	SHISA2	0.06	TCEAL2	0.44	HS.575696	0.08	FAM162B	0.04	UTF1	0.10
39	–	–	FGFBP3	0.28	–	–	ZDHHC22	0.21	C20ORF127	0.06	MX1	0.45	TTYH1	0.08	FAM124B	0.04	TCEAL2	0.10
40	–	–	PLD5	0.28	–	–	LOC645638	0.21	VASH2	0.06	APOB	0.45	BTBD17	0.08	NMU	0.04	DPPA2	0.10
41	–	–	PCSK9	0.28	–	–	LEFTY2	0.21	UTF1	0.06	C10ORF96	0.45	FAM124B	0.09	SOX3	0.04	PLA2G3	0.10
42	–	–	SHISA2	0.28	–	–	LOC728723	0.21	GFPT2	0.06	KAL1	0.46	ST8SIA5	0.09	SCG5	0.04	AASS	0.11
43	–	–	EDG7	0.28	–	–	HEYL	0.21	GLS2	0.06	DLL3	0.46	PIPOX	0.09	KLKB1	0.04	FLJ25404	0.11

Rank	DOWN at 18 h (gene, ratio)						DOWN at 3 d (gene, ratio)						DOWN at 5 d (gene, ratio)					
	BMP5		BMP10		BMP13		BMP5		BMP10		BMP13		BMP5		BMP10		BMP13	
44	–	–	C6ORF141	0.28	–	–	RAB17	0.22	POLR3G	0.06	C1ORF53	0.47	SLC7A10	0.09	C14ORF115	0.04	LOC157627	0.11
45	–	–	DNMT3B	0.28	–	–	PLA2G4C	0.22	MT1H	0.06	SLC38A6	0.47	MIAT	0.09	C9ORF135	0.04	UNC5D	0.11
46	–	–	SLC35D3	0.28	–	–	C6ORF150	0.22	VSNL1	0.06	TNNC2	0.47	TUBA4A	0.09	DPPA2	0.04	ANKRD24	0.11
47	–	–	LPIN1	0.29	–	–	S100A6	0.22	LOC643272	0.06	C1ORF94	0.47	HS.519644	0.09	PCSK9	0.04	NPTX2	0.11
48	–	–	HS.12513	0.29	–	–	PROK2	0.22	TRIM22	0.06	CALCB	0.48	ZIC3	0.09	SOX21	0.04	UNC5A	0.11
49	–	–	ZIC3	0.29	–	–	MYBPC2	0.22	LRAT	0.07	ASB9	0.48	MALL	0.09	PIM2	0.05	TOX3	0.11
50	–	–	LOC100131727	0.29	–	–	CHST13	0.23	LOC285016	0.07	CPSF6	0.48	LOC643272	0.09	RPRML	0.05	SEMG1	0.11
51	–	–	SOHLH2	0.29	–	–	DHDH	0.23	SYT1	0.07	GADD45G	0.48	PLA2G3	0.09	ZDHHC22	0.05	LOC100129268	0.12
52	–	–	LOC100130809	0.29	–	–	TRIM59	0.23	PIM2	0.07	HS.79881	0.49	HLA–DOA	0.09	HS.276860	0.05	PIM2	0.12
53	–	–	C13ORF30	0.29	–	–	KAL1	0.23	FGF2	0.07	STXBP6	0.49	TUBB4	0.09	VASH2	0.05	HS.270778	0.12
54	–	–	GPR176	0.30	–	–	STXBP6	0.24	HS.276860	0.07	UBE2D4	0.50	TNNI3	0.09	TUBA4A	0.05	MATK	0.12
55	–	–	ITPR1	0.30	–	–	RND1	0.24	GAL	0.07	LOC100130633	0.50	LECT1	0.09	RHBDL3	0.05	PNMA3	0.12
56	–	–	WIF1	0.30	–	–	FXYD7	0.24	MT1X	0.07	RSPO3	0.51	HESX1	0.09	PLA2G3	0.05	TMEM145	0.12
57	–	–	ABHD12B	0.30	–	–	CCL26	0.24	SLC15A3	0.07	C6ORF85	0.51	C10ORF96	0.10	GNG4	0.05	PCSK9	0.12
58	–	–	CCL26	0.30	–	–	LOC100131727	0.24	KCND2	0.07	STC1	0.51	LOC100129268	0.10	GAL3ST3	0.05	DPPA5	0.12
59	–	–	NECAB1	0.30	–	–	LAG3	0.24	RNF144B	0.07	GOLPH3L	0.51	LOC388755	0.10	TIMP4	0.05	PROK2	0.12
60	–	–	GNG2	0.30	–	–	POPDC3	0.24	CXCL5	0.07	SNX10	0.52	KCNG3	0.10	LOC388755	0.05	GPR64	0.12
61	–	–	MAPK8IP1	0.31	–	–	PRKCDBP	0.24	PIPOX	0.08	TRIB3	0.52	HS.177654	0.10	TMEM145	0.05	ZSCAN10	0.13
62	–	–	RASL11B	0.31	–	–	ABCA3	0.24	GNA14	0.08	SLC16A9	0.52	UTF1	0.10	REEP2	0.05	ACTN3	0.13
63	–	–	FZD7	0.31	–	–	LPPR4	0.24	LOC100131138	0.08	TMEM132B	0.52	HBA2	0.10	LPAR4	0.05	NANOG	0.13
64	–	–	TCF7L1	0.31	–	–	PADI4	0.24	SCGB3A2	0.08	SEMG1	0.52	NANOG	0.10	CHGA	0.06	VSNL1	0.13
65	–	–	HS.10862	0.31	–	–	LOC729378	0.24	DHDH	0.08	LOC441019	0.52	C19ORF4	0.11	TRIM22	0.06	ACAP1	0.13
66	–	–	HS.276860	0.31	–	–	KISS1R	0.25	C14ORF115	0.08	C1ORF59	0.53	MATK	0.11	HCP5	0.06	TLE6	0.13
67	–	–	KCNN2	0.31	–	–	LOC731007	0.25	FAM150B	0.08	ARHGAP22	0.53	TDGF1	0.11	POLR3G	0.06	RHBDL3	0.13
68	–	–	NCRNA00153	0.31	–	–	TIMP4	0.25	KCNF1	0.08	ESCO1	0.53	LOC157627	0.11	FZD7	0.06	TNNI3	0.13
69	–	–	TNRC9	0.31	–	–	S100A3	0.25	PARD6A	0.08	TSPAN7	0.54	CXCL5	0.11	TNNI3	0.06	HHLA2	0.13
70	–	–	C6ORF85	0.31	–	–	ECSCR	0.25	ZSCAN10	0.08	S100A6	0.54	UNC5D	0.11	VENTX	0.06	DDX25	0.13
71	–	–	LEFTY2	0.32	–	–	KCNF1	0.25	GDF3	0.08	ZNF18	0.54	GNG4	0.11	YBX2	0.06	HBA2	0.13
72	–	–	GK	0.32	–	–	THBS2	0.25	C10ORF96	0.08	HS.12513	0.54	TMEM145	0.11	GPR160	0.06	ACACB	0.13
73	–	–	DLL3	0.32	–	–	ST8SIA5	0.25	LOC100129268	0.08	TLE2	0.55	CRABP1	0.11	GALR2	0.06	GLB1L3	0.14
74	–	–	AK3L1	0.32	–	–	S100A4	0.26	RAB17	0.08	MYB	0.55	UCA1	0.11	IGSF21	0.06	HS.574590	0.14
75	–	–	SHC3	0.32	–	–	LRRC26	0.26	LOC100133609	0.08	MMP9	0.55	SFRP2	0.11	ACTN3	0.06	PPM1E	0.14
76	–	–	EID3	0.33	–	–	PLA2G3	0.26	MT1A	0.08	FLJ45337	0.55	UNC5A	0.11	DPPA4	0.06	KIAA0514	0.14
77	–	–	TMEM132B	0.33	–	–	HS.79881	0.26	INDO	0.08	TMSB4Y	0.55	ZDHHC22	0.11	C9ORF129	0.06	TDGF1	0.14
78	–	–	KCND2	0.33	–	–	CHST9	0.26	DCLK1	0.08	SLC29A1	0.56	ZDHHC19	0.11	HESX1	0.06	C9ORF129	0.14
79	–	–	LRIG1	0.33	–	–	CPEB1	0.26	LOC652097	0.09	MEGF10	0.56	CUX2	0.11	HS.66187	0.06	KISS1R	0.14
80	–	–	FOXJ1	0.33	–	–	OR52A1	0.26	NPTX2	0.09	GPRASP2	0.56	GLS2	0.11	SLC7A3	0.06	SEPT3	0.14
81	–	–	RASGRP2	0.33	–	–	SLC2A6	0.26	HCP5	0.09	PNCK	0.56	TOX3	0.11	SLC7A10	0.06	MYH2	0.14
82	–	–	CXORF57	0.33	–	–	LOC389895	0.26	LOC645638	0.09	MYBPHL	0.56	SCAMP5	0.11	MAP4K1	0.07	LOC643272	0.14
83	–	–	LOC100132934	0.33	–	–	PCSK9	0.26	LRRC26	0.09	DDX25	0.57	SEMG1	0.11	THBS2	0.07	KLKB1	0.14
84	–	–	HS.128753	0.34	–	–	FOXJ1	0.27	GAL3ST3	0.09	PRPH	0.57	RGMA	0.12	TMEM132D	0.07	TNRC9	0.14
85	–	–	TOX3	0.34	–	–	LTB	0.27	TNNC2	0.09	ZNF425	0.57	CHGA	0.12	PPM1E	0.07	TMEM132B	0.14
86	–	–	RGS17	0.34	–	–	SOX8	0.27	LOC100130769	0.09	HS.556255	0.57	STAMBPL1	0.12	NODAL	0.07	HS3ST2	0.14
87	–	–	HBQ1	0.34	–	–	CTGLF5	0.27	UCA1	0.09	CDC42EP2	0.57	HS.12513	0.12	SHISA2	0.07	PTPRZ1	0.14
88	–	–	PCDH21	0.34	–	–	CRYGD	0.27	TMEM132D	0.09	HS.270778	0.57	C14ORF115	0.12	ARHGAP22	0.07	FLJ40194	0.14
89	–	–	RNF144B	0.34	–	–	LOC339535	0.27	MT2A	0.09	HS.581690	0.57	NPAS1	0.12	DDX25	0.07	CDCA7L	0.15
90	–	–	SATB2	0.34	–	–	HS.135050	0.27	ABCA3	0.09	CCNJL	0.58	SLC15A3	0.12	MIR302C	0.07	PPP1R16B	0.15
91	–	–	LOC642342	0.34	–	–	KLHL35	0.27	DLL3	0.09	PROK2	0.58	PPP1R16B	0.12	GPR176	0.07	TOX	0.15

Rank	DOWN at 18 h (gene, ratio)						DOWN at 3 d (gene, ratio)						DOWN at 5 d (gene, ratio)					
	BMP5		BMP10		BMP13		BMP5		BMP10		BMP13		BMP5		BMP10		BMP13	
92	–	–	POLR3G	0.35	–	–	DPPA5	0.27	EFCBP1	0.09	TOX3	0.58	VASH2	0.12	SALL2	0.07	ANKRD35	0.15
93	–	–	AASS	0.35	–	–	HES6	0.27	BTBD17	0.09	AXIN2	0.58	CHST4	0.12	DLL3	0.07	SYNGR3	0.15
94	–	–	ZNF608	0.35	–	–	VAV3	0.27	KISS1R	0.09	PTPRG	0.58	DPPA5	0.12	LRAT	0.07	SCG5	0.15
95	–	–	FLJ12684	0.35	–	–	ODF3L2	0.27	PLA2G3	0.09	CYP4X1	0.58	PROK2	0.12	PMAIP1	0.07	LOC728961	0.16
96	–	–	LOC728743	0.35	–	–	LEFTY1	0.27	CHGA	0.09	BMP6	0.58	SHISA2	0.12	ANKRD35	0.07	HS.579530	0.16
97	–	–	FAM124B	0.35	–	–	LOC439949	0.27	CXCL6	0.09	JAZF1	0.59	PCSK9	0.12	CA11	0.07	C7ORF63	0.16
98	–	–	SNTB1	0.35	–	–	FILIP1	0.28	SCG5	0.09	C14ORF142	0.59	STK33	0.13	ALPL	0.07	SFRP2	0.16
99	–	–	NLGN1	0.35	–	–	FAM78B	0.28	LOC439949	0.09	DUSP6	0.59	AASS	0.13	ST8SIA5	0.07	VASH2	0.16
100	–	–	METTL7A	0.35	–	–	ZBTB3	0.28	JAZF1	0.10	ALG6	0.59	RASD2	0.13	MALL	0.07	SYT11	0.16

Curriculum Vitae

Personal information

Name	**Björn Lichtner**
Date of birth	* (*For reasons of data protection, these parts are not included in the online version.)
Place of birth	Hechingen
Citizenship	German
Address	*
Email	*

Current position

Since 05|2014	*
	*

Academic education and activities

Postgraduate training

09|2013 – 03|2014	**Clinical Research Associate | Clinical Trial Management** **PAREXEL Academic Institute, Berlin, Germany**

PhD work

09|2009 – 09|2013	**Max-Planck-Institute for Molecular Genetics, Berlin, Germany** Dept. Vertebrate Genomics | Prof. Dr. James Adjaye Title: "The Impact of Distinct Bone Morphogenetic Proteins on Self-Renewal and Differentiation of Human Embryonic and Induced Pluripotent Stem Cells"

University studies

04|2003 – 04|2009	**Biochemistry | Freie Universität Berlin, Germany** **Degree: Diploma in Biochemistry** (equivalent to MSc); grade: 1.0 (scale: 1.0 to 5.0) Minors (part two): Biophysics, Genetics and Molecular Biology Minors (part one): Biology, Organic|Inorganic|Physical Chemistry, Physics
10|2008 – 03|2009	Diploma thesis | University Medical Center Hamburg-Eppendorf, Germany Institute for Clinical Chemistry | Prof. Dr. Hartmut Schlüter Title: "Application of Displacement Chromatography for Proteome Analyses"

Research internships

02|2008 – 03|2008	Tel Aviv University, Israel Dept. Neurobiochemistry | Prof. Yoav Henis, PhD
10|2007 – 12|2007	University of California – Los Angeles, USA Dept. Microbiology, Immunology & Molecular Genetics | Prof. Benhur Lee, MD
04|2007 – 06|2007	Max-Planck-Institute for Developmental Biology, Tübingen, Germany Dept. Genetics | Prof. Dr. Christiane Nüsslein-Volhard (Nobel Prize 1995)
01|2007 – 03|2007	Robert-Koch-Institute, Berlin, Germany Dept. Infectious Diseases | Prof. Dr. Reinhard Burger

Scholarships and awards

01|2012 – 05|2013	PhD scholarship (promotion of young academics in Germany) Max Planck Society, Berlin, Germany
06|2011	Travel grant (congress participation) Dahlem Research School, Berlin, Germany
01|2010 – 01|2012	PhD scholarship (international doctoral program) Berlin-Brandenburg School for Regenerative Therapies, Berlin, Germany

Publications

Scientific journals (peer-reviewed)

2015   Mertes F, **Lichtner B**, Kuhl H, Blattner M, Otte J, Wruck W, Timmermann B, Lehrach H and Adjaye J
Combined ultra-low input mRNA and whole-genome sequencing of human embryonic stem cells.
BMC Genomics 16:925. PubMed PMID: 26564201

2015   Hossini AM*, Megges M*, Prigione A, **Lichtner B**, Toliat MR, Wruck W, Schröter F, Nuernberg P, Kroll H, Makrantonaki E, Zouboulis CC and Adjaye J (*equal contribution)
Induced pluripotent stem cell-derived neuronal cells from a sporadic Alzheimer's disease donor as a model for investigating AD-associated gene regulatory networks.
BMC Genomics 16:84. PubMed PMID: 25765079

2013   **Lichtner B**, Knaus P, Lehrach H and Adjaye J
BMP10 as a potent inducer of trophoblast differentiation in human embryonic and induced pluripotent stem cells.
Biomaterials 34(38):9789-802. PubMed PMID: 24070570

2012   Ahrends R*, **Lichtner B***, Buck F, Hildebrand D, Kotasinska M, Kohlbacher O, Kwiatkowski M, Wagner M, Trusch M and Schlüter H **(*equal contribution)**
Comparison of displacement versus gradient mode for separation of a complex protein mixture by anion-exchange chromatography.
J Chromatogr B Analyt Technol Biomed Life Sci 901:34-40. PubMed PMID: 22727752

2011   Prigione A, **Lichtner B**, Kuhl H, Struys EA, Wamelink M, Lehrach H, Ralser M, Timmermann B and Adjaye J
Human induced pluripotent stem cells harbor homoplasmic and heteroplasmic mitochondrial DNA mutations while maintaining human embryonic stem cell-like metabolic reprogramming.
Stem Cells 29(9):1338-48. PubMed PMID: 21732474

2011   Prigione A, Hossini AM, **Lichtner B**, Serin A, Fauler B, Megges M, Lurz R, Lehrach H, Makrantonaki E, Zouboulis CC and Adjaye J
Mitochondrial-associated cell death mechanisms are reset to an embryonic-like state in aged donor-derived iPS cells harboring chromosomal aberrations.
PLoS One 6(11):e27352. PubMed PMID: 22110631

2011   Mah N*, Wang Y*, Liao MC, Prigione A, Jozefczuk J, **Lichtner B**, Wolfrum K, Haltmeier M, Flöttmann M, Schaefer M, Hahn A, Mrowka R, Klipp E, Andrade-Navarro MA and Adjaye J (*equal contribution)
Molecular insights into reprogramming-initiation events mediated by the OSKM gene regulatory network.
PLoS One 6(8):e24351. PubMed PMID: 21909390

2010   Ahrends R, **Lichtner B**, Bertsch A, Kohlbacher O, Hildebrand D, Trusch M and Schlüter H
Application of displacement chromatography for the proteome analysis of a human plasma protein fraction.
J Chromatogr A 1217(19):3321-9. PubMed PMID: 19854443

2010   Trusch M, Böhlick A, Hildebrand D, **Lichtner B**, Bertsch A, Kohlbacher O, Bachmann S and Schlüter H
Application of displacement chromatography for the analysis of a lipid raft proteome.
J Chromatogr B Analyt Technol Biomed Life Sci 878(3-4):309-14. PubMed PMID: 20015709

Poster presentations (selection)

2012   **Lichtner B** and Adjaye J
BMP10, a heart-specific cytokine, induces differentiation of human pluripotent stem cells with a much higher potency than members of the BMP7 subgroup.
10th Annual Meeting of the International Society for Stem Cell Research (ISSCR)
Yokohama|Japan (13th – 16th June)

2011   **Lichtner B** and Adjaye J
The effect of distinct BMP ligands on self-renewal and differentiation of human embryonic stem cells and chorionic villi cell-derived human induced pluripotent stem cells.
9th Annual Meeting of the ISSCR
Toronto|Canada (15th – 18th June)

Statutory Declaration / Eidesstattliche Erklärung

English

I declare on oath that I have written the present PhD thesis independently, without the help from other parties, and that I have not used any other auxiliaries and sources than those specified. I further affirm that I have not submitted a PhD thesis or definitely failed a doctoral examination before, neither in Germany nor abroad. Moreover, I assure that I have not yet submitted the present work or parts of it in equal or similar form for any kind of state or other academic examination to this day.

Björn Lichtner   London, 2nd December 2015 | Berlin, 21st May 2014

Deutsch

Ich erkläre eidesstattlich, dass ich die vorliegende Doktorarbeit selbständig und ohne fremde Hilfe angefertigt und keine anderen als die angegebenen Hilfsmittel und Quellen verwendet habe. Ferner erkläre ich, dass ich bisher weder in Deutschland noch im Ausland eine Doktorarbeit eingereicht oder eine Doktorprüfung endgültig nicht bestanden habe. Außerdem versichere ich, dass ich die vorliegende Arbeit oder Teile davon in gleicher oder ähnlicher Form noch nicht als Prüfungsarbeit für eine staatliche oder andere wissenschaftliche Prüfung eingereicht habe.

Björn Lichtner   London, 2. Dezember 2015 | Berlin, 21. Mai 2014